UNIVERSITÀ DEGLI STUDI DI PALERMO

Dottorato di Ricerca in Scienze Molecolari e Biomolecolari

Dipartimento di Scienze e Tecnologie Biologiche Chimiche e Farmaceutiche (STEBICEF)

S. S. D. – CHIM/06

Hybrid materials based on carbon nanostructures/poly ionic liquids as catalytic platforms

Materiali Ibridi a base di carbonio nanostrutturato/poli liquidi ionici come piattaforme catalitiche

---

PhD STUDENT   COORDINATOR

LAURA VALENTINO   **GIOVANNA PITARRESI**

TUTOR   CO-TUTOR

FRANCESCO GIACALONE   **MICHELANGELO GRUTTADAURIA**

CICLO XXXVI

2024

TABLE OF CONTENTS

Preface

Catalysis is the heart of most chemical processes, as it facilitates and accelerates reaction kinetics and increases the efficiency of desired reaction pathways.[1] Over the past decade, researchers have focused on the concept of sustainable catalysis. The utilization of catalysts has the potential to significantly decrease energy consumption, reduce the production of sub-products and minimize waste generation. In the context of sustainability, Green Chemistry undoubtedly assumes a crucial role. Among the *Twelve Principles of Green Chemistry* initially proposed by Anastas and Warner in 1998, the ninth principle centres on catalysis.[2-3] This principle serves to validate the global commitment to sustainability by enhancing processes in both the academic realm and the chemical industry, rendering them more efficient and benign.[4] The benefits of employing catalytic processes derive from the intrinsic characteristics of the catalyst, defined as a sub-stoichiometric substance that can adequately decrease the activation energy resulting in an increase in reaction rate. At the end, the catalysts are found chemically unaltered and ready to be reused in a further chemical process.

The development of more environmentally friendly catalytic protocols occurs through the rational design of new catalysts, both homogeneous and heterogeneous. These catalysts are specifically designed to achieve two primary objectives: to possess outstanding performance in terms of selectivity toward the desired product, to achieve high turnover numbers and turnover frequency values, and to reduce negative impacts on human health and environment. Heterogeneous catalysis is more in line with the principles of sustainability than homogeneous catalysis.[5] This is mainly attributed to the simple separation of catalysts from the reaction mixture, which results in their reuse for consecutive runs. Therefore, the possibility of easily recycling the catalyst increases the economic interest in heterogeneous catalysis compared to the homogeneous one.[6-9] Although excellent yields and selectivity can be achieved in homogeneous catalysis, its main drawback lies specifically in the challenging process of separating and recovering the catalyst from the reaction mixture. This complication frequently hinders the translation of scientific achievements into industrial applications. One of the most exploited routes to develop a heterogeneous catalyst consists in immobilizing a molecular moieties on an inert support. The immobilization of the organic species can be performed by means of two approaches: a) covalent immobilization and b) non-covalent (**Figure 1**).
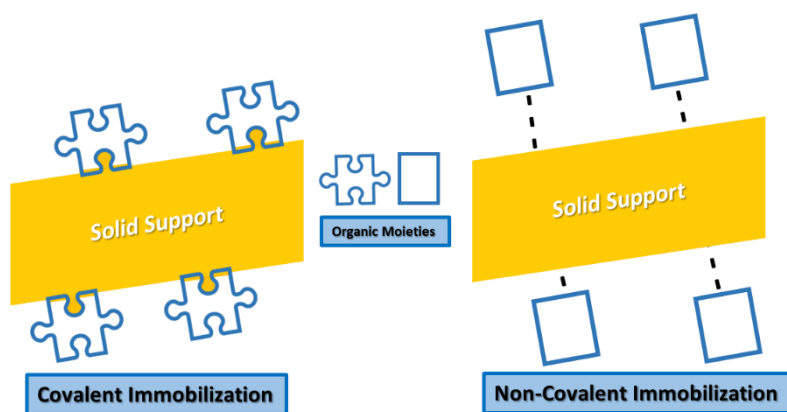
Figure 1. Schematic representation of non-covalent and covalent immobilization.

This PhD dissertation focuses on the design of heterogeneous catalysts for the conversion of carbon dioxide into cyclic carbonates, using a combination of ionic liquid/metalloporphyrin or deep eutectic solvents (DES)-based hybrid materials on multi-walled carbon nanotubes (MWCNTs) (**Figure 2a**). This topic is explored in Chapters III, IV, V and VI. A new material derived from dopamine covalently linked on single-walled carbon nanotubes (SWCNTs) has been prepared to serve as catalytic support for palladium nanoparticles. The effectiveness of the resulting metal-phenolic network was examined in the reduction of nitro compounds to anilines and in Heck's C–C cross coupling reaction, as detailed in Chapter VII (**Figure 2b-c**).
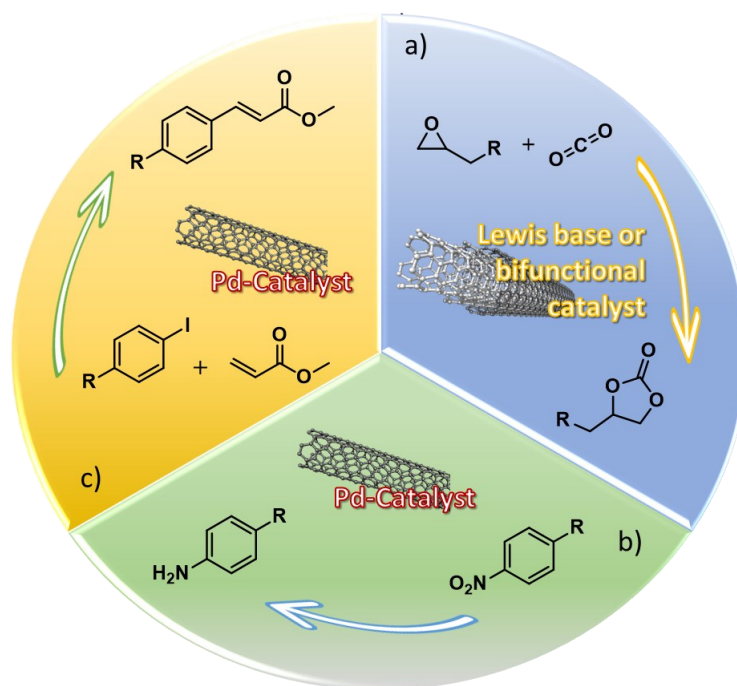
Figure 2. a) CO_2 cycloaddition reaction, b) nitro group reduction reaction and of c) Heck reaction mediated by modified carbon nanotubes-based catalysts.

CHAPTER I

General Introduction

CHAPTER I

General Introduction

1.1 Carbon Nanoforms

Nanocarbon-based materials, a family of carbon allotropes, have attracted the scientific community's interest since their discovery. Thanks to their unique characteristics, applications can be found in a wide range of research fields, from electronics to nanomedicine.[10-16] The intrinsic features of this class of nanomaterials are influenced by the sp^2/sp^3 ratio, morphology, structure and the presence of defects.[17] More specifically, the properties include high surface area, high chemical inertness under many conditions, thermal stability and mechanical strength.

Also referred to as Carbon Nanoforms (CNFs), to this exotic class belong zero-dimensional (0D), one-dimensional (1D), two-dimensional (2D), and three-dimensional (3D) structures. The most notable and extensively studied members of this family are fullerenes, closed carbon cages with spherical (C_{60} as the most abundant) or elliptical shape (C_{70} and other giant fullerenes), carbon nanotubes (CNTs), rolled-up seamless graphene cylinders, nanohorns, conical carbon nanostructures made up of single rolled graphene sheets, graphene, formed by one atom-thick flat sheets of carbon and, among the other ones diamonds (**Figure 3**).

fullerenes　　*SWCNTs*　　*MWCNTs*　　*graphene*　　*nanohorns*
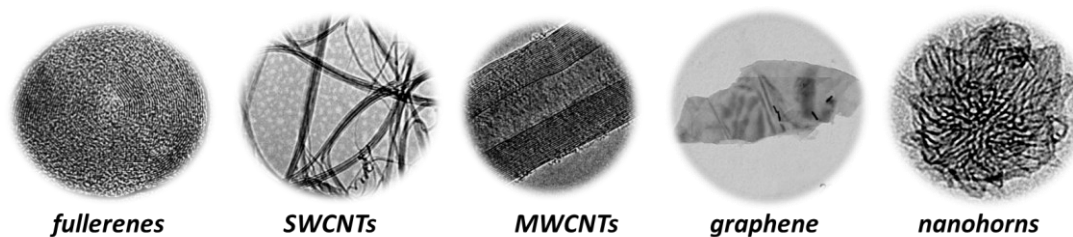
Figure 3. TEM pictures of different carbon nanoforms.

In heterogeneous catalysis, the use of this family of carbon nanostructures is constantly evolving. Due to their peculiar and advantageous features, nanocarbon-based materials showed to be suitable supports for heterogeneous catalysis.[18-29] Furthermore, another aspect that makes CNFs interesting catalytic supports is their possible participation in a given catalytic process through various interactions between the catalytic active site and surface functionalities (e.g., acid groups) and/or through electronic interactions of the support itself (e.g., π-π interactions).[30-31] By this way, CNFs no longer act as a classic inert, but can

determine the outcome of a process. However, the chemical modification of CNFs is essential to obtain catalytic materials, where the distribution of active sites is uniform overall. At the same time, modified CNFs show less aggregation than the pristine form, thus gaining in dispersibility and improving catalytic performance. The lack of dispersibility of CNFs makes their application difficult. The strong long-range van der Waals forces of attraction cause them to aggregate and extremely hard to disperse because of their stable structures.[32] To overcome this problem and take full advantage of CNFs, functionalization is employed, which involves two main types of approach: covalent and non-covalent (**Figure 4**).[29,33]
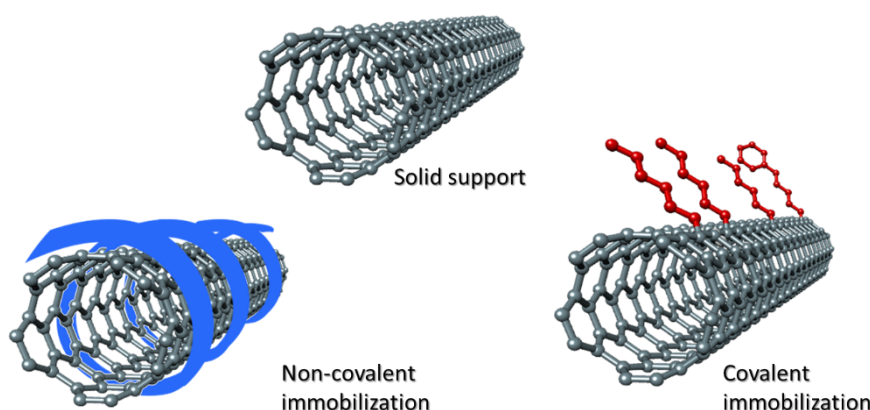
Figure 4. Covalent and non-covalent functionalization of carbon nanostructures.

Through spontaneous and reversible interactions, supramolecular modification offers the possibility of absorbing various groups onto the solid matrix while preserving the original carbon sp^2 structure and meanwhile the electronic and optical properties of the CNFs. The driving forces behind this approach are van der Waals forces and $\pi-\pi$ stacking forces. Due to the high surface area, high mechanical and chemical stability carbon nanotubes or graphene are also excellent support materials for the deposition of metal nanoparticles (MNPs). Several methods are reported in the literature for depositing MNPs onto CNFs and each of which offering a different degree of control over the size of nanoparticles and their distribution.[34]

The covalent functionalization involves a structural modification that leads to the saturation of some of the C–C double bonds. This results in a more or less severe disruption of the π-network with the rehybridization from sp^2 to the sp^3 configuration of the carbon atoms involved in the functionalization process. While the partial loss of π-conjugation constitutes a detrimental event that can affect the mechanical, electrical and thermal properties of CNFs, at the same time the attachment of molecular fragments, through covalent bonds formation, allows the formation of stable and fine dispersions in both aqueous solutions and organic

solvents. This makes possible overcoming van der Waals and π−π stacking interactions, otherwise responsible for the formation of aggregates in bundles and chords that make CNFs poorly dispersible. In addition, it is evident that this approach results in a limitation of the leaching phenomenon, i.e. the loss of catalytic active sites, which would lead to a consequent decrease in catalytic activity, contamination of the product and loss of the catalyst.

1.1.1 Carbon Nanotubes

Among the different Carbon Nanoforms, carbon nanotubes emerged as attractive materials due to their unique chemical and physical properties. Discovered by Iijima in 1991[35], CNTs are tubular structures, consisting of carbon atoms with a diameter between 0.7 and 30-50 nm and a length between hundreds of nm and several μm, which, depending on atomic rearrangement, have electronic properties similar to metals or semiconductors. These carbon allotropes possess high chemical and thermal stability, large specific surface area, and mechanical strength, which enable them to have a wide range of uses. The most popular types of nanotubes are single-walled carbon nanotubes (SWCNTs) with a diameter of 1-2 nm, formed by rolling up a single graphenic sheet, and multi-walled carbon nanotubes (MWCNTs), consisting of multiple graphite layers rolled-up in a concentric fashion, of which the simplest one is the double-walled carbon nanotube. These concentric cylinders are arranged around a common core hollow, which has a layer spacing of 0.34 to 0.39 nm between the layers.[36-37] The features of CNTs, such as diameter, wall number and length, depend on the exact method and conditions of production. CNTs are generally produced using three main techniques: arc discharge[38-40] with pure or metal-doped carbon electrodes, laser ablation[41-42] and chemical vapor deposition (CVD),[43] in which carbon-containing molecules such as ethane, methane, or carbon monoxide are decomposed on supported metal nanoparticles that serve as catalysts for carbon nanotube growth. Despite sharing similar properties, SWCNTs and MWCNTs are generated through distinct production conditions. Confirmation of this concept is demonstrated by the pioneering work of Iijima and Ichihashi[35] and by the research of Bethune *et al.*[44] In their investigations of the electric arc discharge method for the production of carbon nanotubes, they separately observed that the introduction of elements such as Fe and Co as dopants into one of the electrodes produced exclusively SWCNTs, without the formation of MWCNTs.

A significant impediment that continues to hinder the effective integration of CNTs into various technological applications is the inherent tendency of produced CNTs to aggregate

into bundles comprising from 50 to several hundred individual CNTs. These bundles are held together by remarkably strong van der Waals interactions.[45] To overcome these difficulties and, at the same time, harnessing the distinctive characteristics of CNTs, one strategy entails chemically modifying CNTs with suitable functional groups.[46] As to functionalization, it is important to mention the reactivity of this carbon nanoforms, which results from the nonplanar structure of the nanotube. Indeed, the non-planar nature of double bonds in the nanotube structure, combined with their intrinsic bond tension, amplifies their reactivity, making them more favourable to functionalisation processes. This characteristic is particularly evident in small-diameter tubes, which are intrinsically more reactive.

As mentioned above, to act as support, CNTs generally require chemical modification. Focusing attention on the covalent functionalization of CNTs, the oxidative pre-treatment and the subsequent post-modification of such materials is surely the most employed method that provides access to a wide range of functionalities, covalently grafted onto their surface. Other procedures include the possibility of cutting the nanotube, using very severe oxidation conditions.[47] Ozonolysis has been employed on single-walled carbon nanotubes at both -78 °C and room temperature, resulting in the formation of primary CNT-ozonides.[48-50] Pristine SWCNTs were subjected to cleavage through chemical treatment with hydrogen peroxide or sodium borohydride, leading to a significant presence of carboxylic acid/ester, ketone/aldehyde, and alcohol groups on the nanotube surface. This process adorned the sidewalls and tips of the nanotubes with active moieties, significantly broadening the chemical reactivity of these carbon nanostructures. The chemical reactivity in this sidewall addition reaction, as observed by Banerjee *et al.*,[49] depends on the diameter of the nanotubes, with smaller diameter nanotubes exhibiting greater strain energy per carbon atom due to increased curvature and higher rehybridization energy.

One alternative is to proceed with the direct covalent functionalization of pristine CNTs by means of different routes, avoiding any oxidative pre-treatment. Margrave *et al.* pioneered the fluorination of carbon nanotubes.[51] Typically, this process involves treating CNTs with molecular fluorine at temperatures ranging from 150 to 600 °C, with varying degrees of fluorination achieved depending on the reaction temperature. Fluorinated nanotubes were reported to have a moderate solubility in alcoholic solvents.[52] An advantageous aspect of fluorination is its facilitation of further nucleophilic substitutions (**Figure 5**).[53] Studies have shown that Grignard or organolithium reagents can be employed to replace fluorine atoms with alkyl groups.[54-55] Alkylated CNTs exhibit good dispersion in common organic solvents like THF and can be fully dealkylated by heating to 500 °C under inert atmosphere, thereby

restoring pristine CNTs. Furthermore, nucleophilic substitution reactions with various diamines or diols have been reported to react with fluoro-nanotubes (**Figure 5**).[56-57] Aminoalkylated CNTs, featuring terminal amine groups, demonstrate solubility in dilute acids and water. Additionally, primary amines have been utilized to bind biomolecules to the sidewalls of CNTs for diverse biological applications.
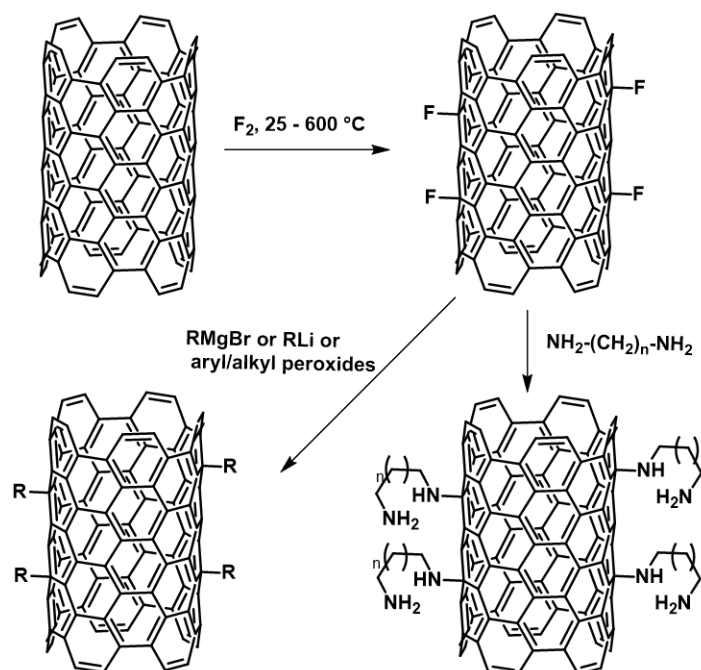
Figure 5. Fluorination and further post-derivatization of nanotubes.

Hydrogenated carbon nanotubes were produced through the Birch reduction method, involving the reduction of pristine CNTs with lithium metal and methanol dissolved in liquid ammonia.[58]

Prato *et al.* reported the [3+2] cycloaddition of azomethine ylides on the sidewalls of CNTs (**Figure 6**).[59-60] This specific method of functionalization results in high solubility of the products in water and various organic solvents such as chloroform, acetone, and methanol. The notable advantage of this reaction lies in the facile attachment of pyrrolidine rings, featuring diverse chemical functionalities, to the sidewalls of carbon nanotubes. This capability opens avenues for constructing novel materials with a broad spectrum of applications.
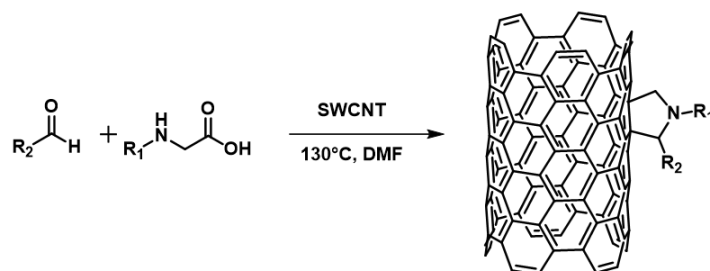
Figure 6. [3+2] Cycloaddition of azomethine ylides on CNTs (Prato reaction).

Carbon nanotubes have been subjected to functionalization with aryl compounds through the radical addition of various substituted aryl diazonium salts, either electrochemically or under standard conditions at room temperature (**Figure 7**).[61-62] However, these moieties can be eliminated by heating in an argon atmosphere. According to Tour *et al.*, both direct treatment of single-walled carbon nanotubes with aryl diazonium tetrafluoroborate salts in solution and in situ generation of diazonium with an alkyl nitrite are effective methods of functionalization.[61-62] In some cases, direct treatment with preformed diazonium salts proves effective at moderate or even room temperature. However, in situ generation of diazonium species is advantageous because it eliminates the need to isolate and store unstable and light-sensitive aryl diazonium salts.
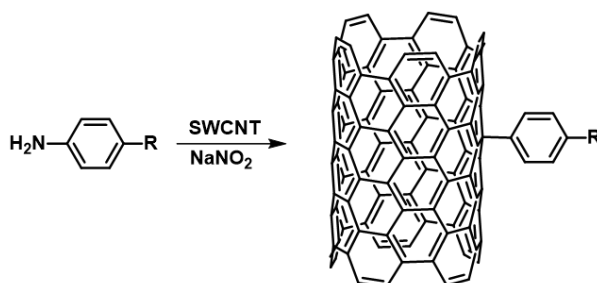
Figure 7. Tour reaction.

Another efficient strategy is the radical polymerization of organic units in the presence of CNTs. This synthetic strategy makes possible obtaining a heterogeneous and robust material in which waste production is limited. This approach also demonstrates significant benefits as it involves minimal alteration of the π-network. This outcome can be attributed to the development of only a few anchor points in the polymer network surrounding the nanotube. Consequently, the ratio of anchor points to the load is reduced, minimizing the disruption of the interconnected network structure. Another interesting route is [1+2] cycloadditions onto CNTs sidewall, in which the π-conjugated electronic structure of the CNTs is preserved by splitting the bonds between adjacent carbons of the sidewall, recovering the sp^2 hybridization

and properties of the pristine CNTs. In the initial step of this reaction, a p-electron pair of the carbon structure undergoes a conversion to a covalent bridge, forming a three-membered ring (closed configuration). This is followed by a subsequent rehybridization process, which relieves the tension of the C-C bond underlying the bridge. As a result, the two carbon atoms return to the sp^2 state, restoring the aromatic nature of the system (open configuration) (**Figure 8**). Adeli, Haag and Reich[63] initially demonstrated the validation of this hypothesis. In their work, they achieved the covalent functionalization of single-walled carbon nanotubes (SWCNTs) through a nitrene [2+1] cycloaddition reaction, utilizing an electron-poor monoazido-dichloro-triazine compound. This innovative approach allowed for the incorporation of enduring functional groups onto the sidewalls of SWCNTs, while limiting the alteration of the π−network.
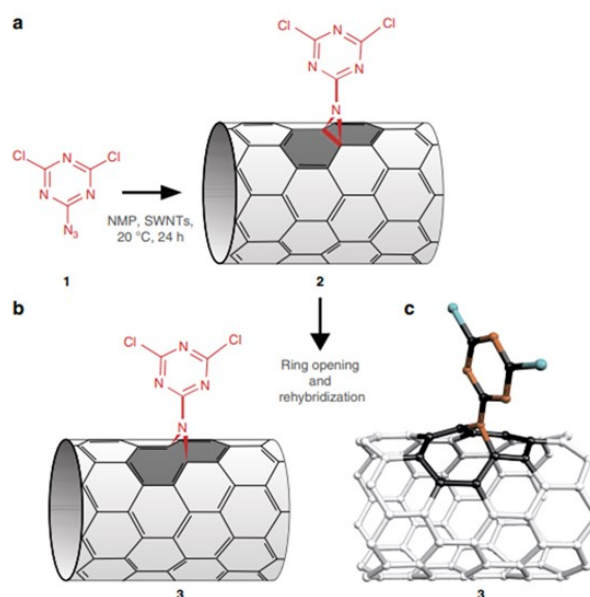
Figure 8. One-pot functionalization of carbon nanotubes by heterocyclic [2 + 1] cycloaddition reaction. (a) The initially formed bridge between monoazido-dichloro-triazine **1** and SWNTs, (b) the cycloaddition product (**2**) undergoes ring opening and rehybridization of the C atoms underlying the bridge and is converted into the form (**3**) with regenerated p-conjugation. (c) Quantum chemically optimized molecular configuration of the triazine on an nanotube.[63]

1.2 Ionic Liquids

The study of Ionic Liquids (ILs) began in 1914, with Paul Walden who defined them as "materials composed of anions and cations, which melt around 100 °C or at arbitrarily lower temperatures". Such substances have attracted increasing interest, becoming an alternative to traditional organic solvents due to some of their peculiar properties. The very low vapour pressure at room temperature makes these materials extremely non-flammable and

consequently very exploitable. In addition, this class of solvent can have a wide liquid phase range (as high as 300 °C), excellent solvent capacity for organic, inorganic and polymeric materials, high ionic conductivity, excellent thermal and chemical stability. These features make ILs very interesting in several fields such as synthesis and catalysis,[64-65] biotechnology,[66] separation science,[67] energy storage[68-69] and electrochemistry,[70-71] among others. The scope of application of ILs can be further extended by the introduction of specific functional moieties leading to the so-called task specific ionic liquids (TSILs).[72-74] In particular, Davis described the design of TSILs as "the covalent tethering of a functional group to one or both of the ions of an otherwise ordinary ionic liquid can imbue the resulting salt with a capacity to interact with dissolved substrates in specific ways".[75] The cationic structures forming ILs are based on aromatic or aliphatic moieties. Some of the most common cations are imidazolium, thiazolium, pyridinium, ammonium, and phosphonium. They can be easily prepared by quaternization of the heterocycle, amine or phosphate core. Among the most used anions in ionic liquids, it is possible to find chloride, bromide, iodide, tetrafluoroborate, and hexafluorophosphate (**Figure 9**).
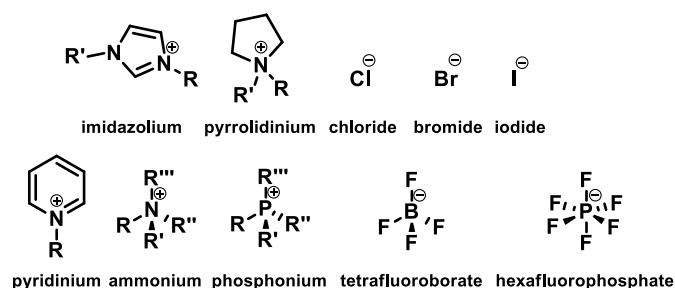
Figure 9. Some of the cations and anions present in ionic liquids (ILs).

In the field of catalysis several types of ILs immobilized onto different support materials have been developed. The supported ionic liquids (SIL) can be divided in two major classes: supported ionic liquid phase (SILP) and supported ionic liquid-like phase (SILLP) (**Figure 10a-b**). To the first category belong ILs physically absorbed on the support, in which the properties of ILs are transferred to the final material. The first example of SILP was described by Fehrmann who immobilized rhodium complexes in the ILs phase for application in continuous fixed-bed gas phase hydroformylation.[76-78] Davis and his supported aqueous-phase catalysts inspired him.[79] The preference for ionic liquids (ILs) over water as the catalytic phase stems from the distinctive attributes of ILs. Specifically, ILs possess a low vapour pressure that enables them to maintain a liquid state on the support material under reaction conditions, facilitating their utilization in both liquid and gas-phase applications.[80] However, the SILP

systems are preferentially used in gas phase rather than in liquid phase conditions owing to the high level of ILs leaching that might occur in the latter case.
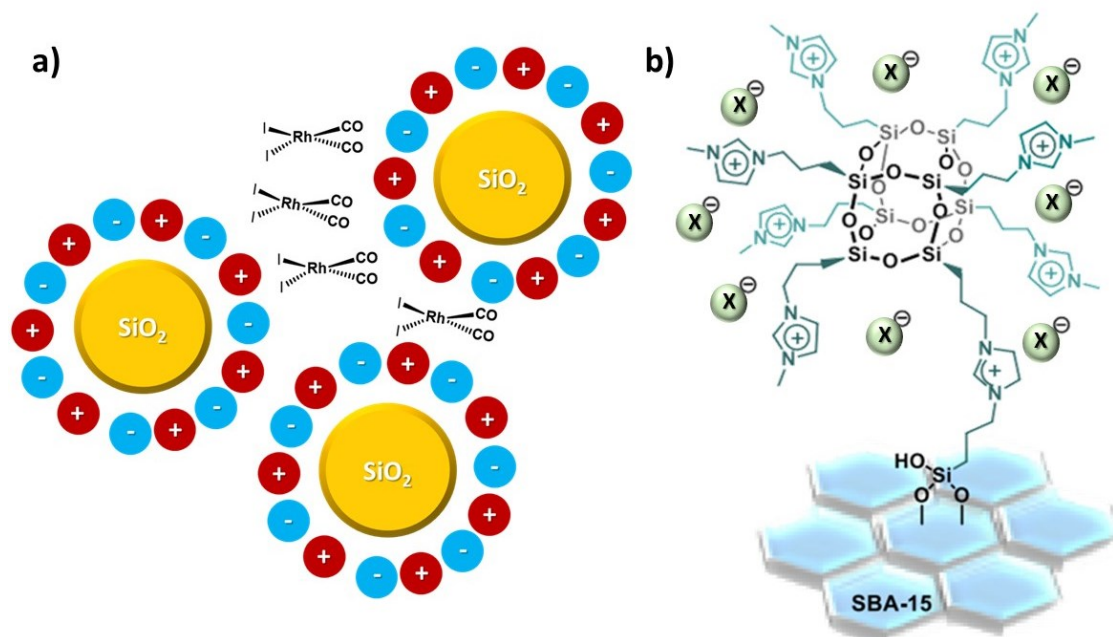
Figure 10. (a) Supported ionic liquid phase (SILP)[78] and (b) covalently supported ionic liquid-like phase (SILLP).[81]

Conversely, in the SILLP class, ILs and support material are covalently bound. This class is strictly related to supported ionic liquid catalysis (SILC) concept, developed by Mehnert.[82-83] This covalent strategy offers attractive advantages. In such a way, the obtained heterogeneous material is easy to recover from the reaction media, owing to a limited use of ILs and to the absence or limitation of ILs leaching. In addition, the physicochemical properties of ILs are transferred to the final material.

Imidazolium-based SILs materials have been employed as support for organocatalysts, as catalysts themselves, and as stabilizing support for metal-based catalysts. Among the numerous applications of ILs, their use for CO_2 adsorption and conversion has aroused a great interest in the scientific community. In particular, imidazolium salts have been widely used and studied as catalysts in the conversion of CO_2 and epoxide into cyclic carbonates. The imidazolium counterions, halide ions ($Cl^- < Br^- \leq I^-$), play a crucial role in the reaction mechanism by promoting the epoxide ring opening followed by the CO_2 insertion.[84-85] The order of catalytic activity of the halides is related to the ability of the halide to act as a nucleophile as well as a leaving group. Linkers in the imidazolium moieties have also a central role in the catalytic cycle. Indeed, since the nucleophilic attack by halide ions is likely to occur in the proximity of the cationic moieties, a too short linker implicates a very congested series

of active sites that could not exert simultaneously their catalytic activity. On the other hand, a too long linker implies a lower concentration of catalytic sites. Imidazolium-based ILs have a very wide chemical and thermal stability window, good electrical conductivity, and especially high counter anion mobility due to the delocalized positive charge in the 5-membered ring. In addition, CO_2 is very soluble in these salts, which makes it possible to increase the compatibility and affinity between epoxide substrates and active sites.

A crucial factor to obtain an efficient heterogeneous catalyst is to ensure easy access of reagents to the active sites. The highly cross-linked nature of the prepared hybrid generates a material with a low surface area, which could drastically reduce the rate of diffusion of reagents to the active sites, ultimately causing a lowering of catalytic activity. A support material is for needed on which the polymer network can be evenly distributed.[85]

1.3 Metalloporphyrin

Porphyrin is a natural pigment with a unique chemical structure that consists of four pyrrolic rings and four bridging carbon atoms in a circular 18π-aromatic macrocyclic system (**Figure 11**).
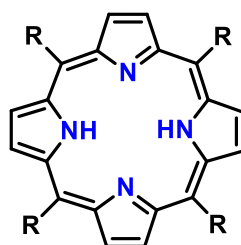
Figure 11. A meso-substituted porphyrin 18π-aromatic macrocycle.

The porphyrin structure is found in nature in the form of different chlorophylls and heme. Chlorophylls are essential components of photosynthesis and function both as light-harvesting antennae and as systems for charge-separation reactions. Heme, on the other hand, play a crucial role as biocatalysts and transporters of oxygen in the blood. Porphyrins are so fundamental that life as we know it would not be possible without them on Earth. In the field of chemistry, porphyrins and their metalized derivatives have fascinated organic and inorganic chemists through their aesthetically pleasing molecular structures. The remarkably symmetrical D_{4h} planar arrangement of metalloporphyrins has inspired numerous synthetic chemists. Beyond aesthetics, porphyrin is a functional molecule that takes a central role in various fields of scientific exploration due to its unique electronic and optical properties. These macrocycles

can also be harnessed through the introduction of functional groups, thereby rendering these molecules suitable for different applications. Porphyrin can be synthesized from pre-functionalized aldehydes or pyrroles, or alternatively, substituents can be incorporated subsequent to the assembly of the porphyrin macrocycles (**Figure 12**).[86]
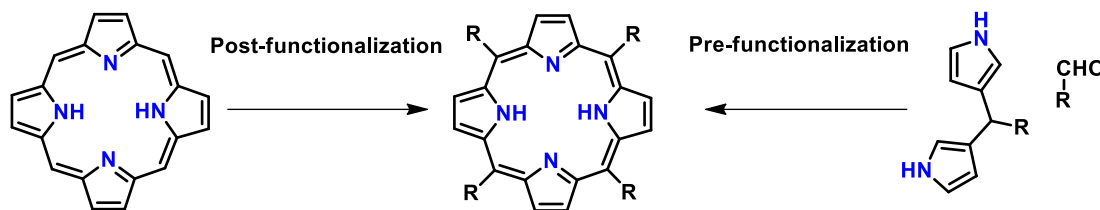
Figure 12. Post- and pre-functionalization of porphyrins.

The pyrrolic macrocycle has the benefit of having two nitrogen donors. The quartet of pyrrolic nitrogen atoms can act as efficient, dianionic ligands, interacting with a range of metal ions for the formation of metalloporphyrins, which play essential roles as catalysts in significant synthetic reactions.[87-90] One of the notable synthetic approaches utilizing metalloporphyrins involves the conversion of CO_2 into cyclic carbonates through the reaction with epoxides.[20,91-97] This process necessitates the careful selection of a highly reactive substrate, the epoxide, along with a catalyst that can effectively lower the activation energy required for the desired transformation. In this context, catalysts based on metals often exhibit enhanced catalytic efficiency and enable the CO_2-involved reaction to proceed under milder conditions compared to traditional organic catalysts. The mechanism of the metal-catalyzed CO_2-epoxide coupling reaction centers around the opening of the epoxide ring, which generally serves as the step determining the overall rate of the reaction. The activation of the epoxide ring is facilitated by the coordination between the electrophilic center of the metal catalyst and the nucleophilic oxygen atom present within the epoxide molecule. The schematic representation in **Figure 13** illustrates the dual activation of epoxides over metal-based catalyst systems.
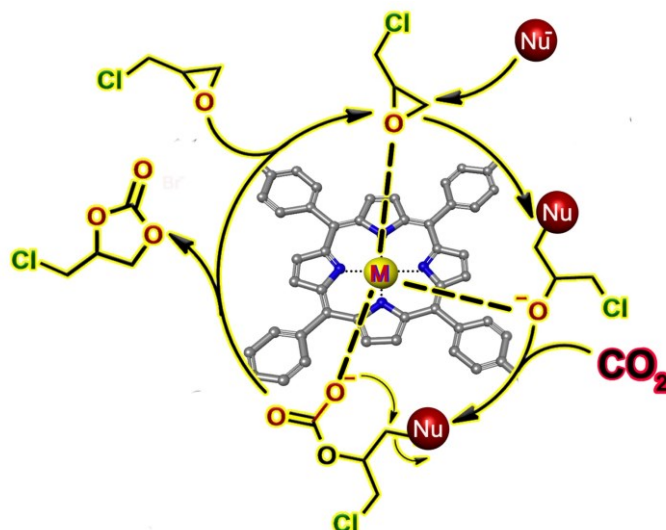
Figure 13. Proposed mechanism for the reaction between epoxides and CO_2 catalyzed by nucleophilic species and co-catalyzed by Lewis acid species.

When investigating the utility of metalloporphyrins as Lewis acids in CO_2 cycloaddition reactions, researchers have developed various catalysts that incorporate these metal complexes within bifunctional or binary catalytic systems. Certainly, the most appealing challenge is to design a bifunctional material, which contains both Lewis acid sites, responsible for epoxide activation, and Lewis base sites, which serve as nucleophilic entities, in close proximity. This arrangement ensures robust stability and the potential for repeated use under operational conditions. In the field of bifunctional heterogeneous catalysts, metal-organic frameworks (MOFs), porous organic polymers (POPs), silica-supported catalysts and covalent organic frameworks (COFs) have been widely used in recent years.[97-108] In porous organic polymers (POPs), which are generally amorphous materials with disordered porosity, the inclusion of the metalloporphyrin component serves a dual function. Indeed, the metalloporphyrin acts both as a co-catalyst, facilitating the conversion of cyclic carbonates and as a "covalent swelling agent", contributing to the expansion of the material's surface area.[109]

1.4 Deep Eutectic Solvents

Deep eutectic solvents (DESs) have gained significant interest over the last twenty years as a new category of environment friendly solvents, similar to ionic liquids (ILs). This heightened attention follows a study by Abbott *et al.*,[110-111] which observed an unusually pronounced reduction in melting points at the eutectic composition of specific hydrogen bond donors (HBDs) and acceptors (HBAs) (**Figure 14**).

Hydrogen bond donors (HBDs)

acetamide   1-methylurea   1,3-dimethylurea

urea   thiourea   pyrocatechol   propane-1,2,3-triol

Hydrogen bond acceptors (HBAs)

choline chloride   tetramethylammonium chloride

methyltriphenylphosphonium bromide   tetrabutylammoniumbromide
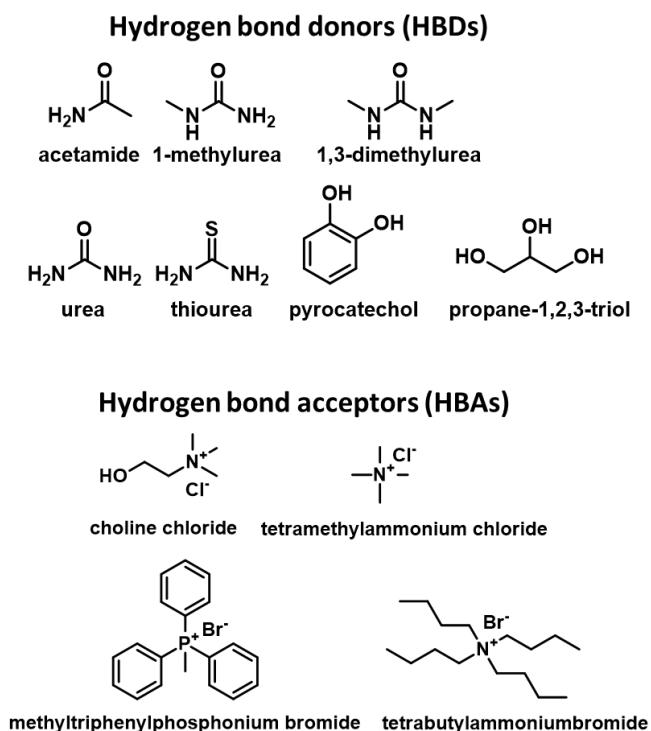
Figure 14. Examples of common HBDs and HBAs constituents of DES.

In his research, it is shown that combinations of substituted quaternary ammonium salts, such as choline chloride in conjunction with urea, generate eutectic solutions that remain in a liquid state at room temperatures, showcasing distinctive solvent properties. This phenomenon becomes particularly evident when a 1:2 molar ratio blend of powdered choline chloride (with a melting point, Tm ≈ 302 °C) is mixed with crystalline urea (with a melting point, Tm ≈ 133 °C), resulting in a liquid state under room temperature conditions (melting point of the mixture at eutectic composition, $T_{eutectic}$ = 12 °C). Termed a "deep eutectic mixture", this liquid state was labelled to capture the observed phenomenon. These mixtures exhibit sufficiently low melting points, allowing for economical utilization as solvents and/or electrolytes in both new and established chemical applications. Since the defining characteristics of these liquids are of primary interest, the commonly adopted term "deep eutectic solvent" (DES) has become the inclusive description for this diverse array of materials. Current viewpoints suggest that the creation of DES is a result of self-associated intermolecular interactions, likely stemming from mixing entropy, van der Waals forces, hydrogen bonding, and/or ionic bonding.[112-114] However, the exact nature of these interactions remains somewhat unclear, underscoring the need for more in-depth exploration into the fundamental aspects of this class. DES are frequently recognized as a subclass of ionic liquids due to their shared fundamental traits, encompassing notable thermal stability, minimal volatility, low vapour pressures, and modifiable polarity. These characteristics position DES as promising

contenders for potentially substituting volatile organic compounds (VOCs) that are widely utilized across research and industry. Nevertheless, ILs are often burdened with high costs, limited biodegradability, and elevated toxicity, in contrast to DES which generally exhibit affordability, biodegradability, non-toxicity, and relative ease of preparation compared to ILs.[115-118] The prevailing method commonly used to produce DES involves heating and stirring their components under an inert atmosphere until a uniform liquid mixture is generated. This eliminates the need for additional solvents and avoids traditional procedures. As a result, the requirement for purification steps is eliminated, emphasizing their potential as cost-effective alternatives to established organic solvents and ILs. Other techniques for DES preparation include vacuum evaporation, grinding, and freeze-drying. In the evaporation process, components dissolve in water, and subsequent vacuum evaporation at 49 °C effectively removes the majority of the water content, resulting in a final mixture stored within a desiccator with silica gel until a consistent weight is achieved. The grinding method involves combining solid components within a mortar and grinding them until a clear and uniform liquid is produced.[115] This is often conducted within a nitrogen-filled environment and/or within a controlled setting like a glovebox. In the freeze-drying procedure, both HBDs and HBAs are dissolved in around 5 wt% of water. These solutions are mixed, frozen, and then subjected to freeze-drying, ultimately leading to the creation of a transparent and homogeneous liquid state.

DESs have a wide range of potential applications. In particular, a significant area is their application in metallurgy.[119-122] This interest has been sparked by the discovery that DES can facilitate high solubilities and electrical conductivities for metals and metal salts, making them favourable contenders for activities such as solution metal extraction and recycling, or refining, and electroplating. Furthermore, DESs have emerged as excellent candidates for potential electrolytes for lithium-ion batteries (LIBs) due to their low flammability, wide liquidity range, and high conductivity.[89,123-124] Separation processes represent a pivotal facet of industrial chemical procedures, encompassing the physical segregation of two or more components from each other. The exploration of DESs in the context of liquid-liquid extraction for azeotropic mixtures is of particular interest. In a related field, advancements in carbon dioxide capture hold universal significance across various scientific domains. DESs have demonstrated intriguing properties that could prove advantageous in addressing specific aspects of carbon capture.[125-127] Traditional CO_2 scrubbing methods employ absorbent fluids like aqueous amines; however, the degradation, volatility, and corrosive nature of amine solvents prompt the exploration of alternative solutions. Certainly DESs are very promising

due to their notable CO_2 solubilities, low vapour pressures, and heightened thermal stabilities when compared to conventional aqueous amines.

Exploiting DES in a dual role is an attractive option, as it involves its use both as a reaction solvent and as an active participant through one of its two components.[128] One example is the use of DESs not only as solvents for polymerization processes but also as reactive components. This emerging category of polymerizable deep eutectics, referred to as deep eutectic monomers (DEM), is characterized by the dual role of solvent and an integral part of the polymerization process. This dual role arises from the incorporation of polymerizable units, mainly within the hydrogen bond donor or acceptor components. Mota-Morales *et al.* pioneered the application of frontal polymerization in deep eutectic solvents by employing combinations of acrylic acid or methacrylic acid with choline chloride.[129] These DESs were characterized by the inclusion of a polymerizable acrylate group within the hydrogen donor unit. Furthermore, they explored frontal polymerization using DESs consisting of various ammonium salts and hydrogen bond donors containing acrylic acids and acrylamides.[130] Within this context, the front polymerization is a phenomenon arising when a monomer undergoes transformation into a polymer in a localized reaction zone.[131-132] The utilization of DESs in front polymerization introduces an intriguing dimension and paves the way for captivating prospects within the materials domain. This potential arises not only from the cost-effective and facile nature of preparing DES but also from the virtually boundless spectrum of attainable compositions achievable through diverse combinations of compounds mixed at varying molar ratios.

1.6 CO_2 Cycloaddition

The transformation of carbon dioxide into valuable chemicals is an issue of growing interest because of its potential to convert industrial waste into a cheap, non-toxic, environmentally safe and sustainable carbon resource.[133-139] Carbon dioxide is essential in the production of a broad range of widely used chemical compounds including organic carbonates, urea derivatives, carboxylic acids, alcohols, and alkylamines (**Figure 15**).[140-142]
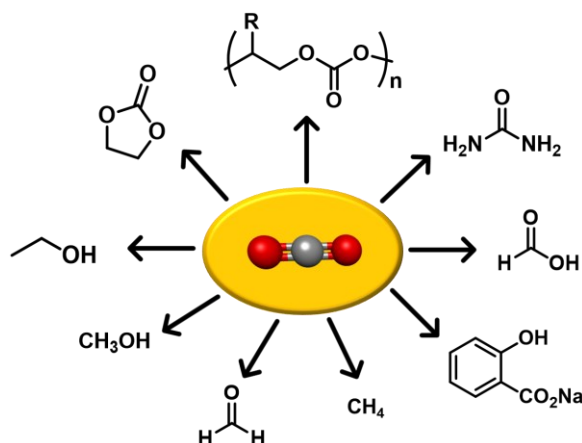
Figure 15. Organic synthesis using CO_2 as C1 feedstock.

Due to the highly oxidized state of the carbon atom in CO_2, its molecular reactivity is inherently low. To address this problem, highly energetic substances, such as small cyclic ethers, are used along with a catalyst that can reduce the activation energy required for the desired reaction. A convenient route to exploiting CO_2 is its cycloaddition into epoxides for the production of cyclic carbonates,[143-144] which have found wide applications as polar aprotic solvents, electrolytes in lithium-ion batteries, fuel cells and intermediates in pharmaceutical chemistry.[145-146] This process is one of the most effective and promising synthetic routes in Green Chemistry, displaying an atom economy of 100%, as all reactants are incorporated in the product and can be carried out effectively without requiring a solvent. In addition, CO_2 can also replace toxic and flammable species such as phosgene, which is used industrially in the transesterification of polyols to obtain cyclic carbonates.[147] The transformation of epoxides into cyclic carbonates involves the participation of nucleophilic species as catalysts, which induce the epoxide ring opening. In addition, the presence of Lewis acid catalysts in the system offers an advantage, as they can activate the ring-opening process. The two species can either be present in separate systems, known as binary catalysts, or can be incorporated into the structure of a bifunctional catalyst. The decision between utilizing metal-based or organocatalysts for CO_2 fixation entails a careful consideration of their respective advantages and limitations. Metal-based catalysts offer distinct strengths, such as enabling milder reaction conditions, including lower temperatures and reduced catalytic loading. This capability arises from their capacity to activate and stabilize substrates or intermediate species through coordination interactions. This feature contributes to enhanced reaction efficiency. Conversely, organocatalysts present themselves as attractive and safer options when designing sustainable processes. They possess several favorable attributes, including affordability, non-toxic properties, and robust stability. Furthermore, organocatalysts exhibit enhanced resistance towards moisture and air, strengthening their utility in various practical applications. These

qualities collectively position organocatalysts as environmentally friendly alternatives, aligning well with the principles of sustainability. The choice between metal-based and organocatalysts for CO_2 fixation hinges upon a trade-off between reaction conditions, catalytic performance, and environmental considerations. Each category of catalyst offers unique benefits that can be leveraged based on the specific goals and requirements of the synthetic process.

Several catalytic systems, both homogeneous and heterogeneous, have been proposed for the conversion of CO_2 into cyclic carbonates by reaction with epoxides. Many organocatalysts and metallic complexes have been developed as homogeneous catalysts.[148-158] Even though homogeneous catalysts have high activity and catalytic efficiency, their recovery/recycling is quite complicated, making the purification of cyclic carbonates obtained highly tedious and energy intensive. To avoid these drawbacks and meet the needs of sustainable development and environmental protection, there is a paramount interest in the preparation and use of recyclable catalytic systems. In this context, heterogeneous catalysis represent a viable alternative to homogeneous one. The easy separation, recovery and possible reusability of such catalysts make them a sustainable and green alternative to their homogeneous counterparts. Widely used in recent years are metal-organic frameworks (MOFs), porous organic polymers (POPs), silica-supported catalysts, and covalent organic frameworks (COFs).[159-163] However, in most of the metal-based catalytic systems, the nucleophilic species is used as a co-catalyst under homogeneous conditions, often in large amount with respect to metal catalyst, leading to incorrect TOF values and usually not recovered.[164] In such a way, both the electrophilic/Lewis acid and the nucleophilic/Lewis base centers can simultaneously cooperate contributing to improve the catalytic efficiency. However, if on the one hand the use of a nucleophilic additive can enhances the performance towards the conversion of CO_2, on the other hand the presence of an external component could cause a detrimental effect in terms of complexity of the reaction mixture and difficulty of the purification process of cyclic carbonates.[165] Thus, a plausible remedy for this challenge could be provided through the development of heterogeneous bifunctional catalysts. Compared to materials with a nucleophilic component only,[24,26,166-169] these bifunctional materials display catalytic activity even under mild reaction conditions. Furthermore, heterogeneous bifunctional catalysts[97-108] are interesting owing to their possible synergistic features. Among the metal complexes used as co-catalyst in the cycloaddition of CO_2 with epoxides, metalloporphyrins have raised considerable interest.[109,170-171] This is due to the possibility of incorporating various metal ions as Ni, Al, Zn, Co and Mg in the core of the porphyrin ring.

1.7 Catalytic activity of Pd Nanoparticles

Transition metal nanoparticles (NPs) have attracted considerable interest over the past decades because of their promising potential as catalysts. Their main characteristics include a high surface area to volume ratio, which allows higher reaction rates under milder conditions and at low catalyst loadings.[172] In this context, we will focus on the importance of palladium nanoparticles-based catalysts in facilitating C–C cross-coupling reactions such as the Heck-Mizoroki reaction and the reduction of nitro compounds.

The reduction of nitro compounds to anilines is a key reaction in the production of pigments, agrochemicals and pharmaceuticals.[173] Historically, this procedure relied on the use of metallic iron as a catalyst, but generated a significant waste stream. On an industrial level, the simplest aromatic amine, aniline, used to be synthesized by treating nitrobenzene with iron and a small amount of hydrochloric acid. This process, referred to as the Béchamp reduction, was initially employed for the production of aniline and iron oxide pigments.[114] As a more sustainable alternative, hydrogenation of nitroarenes facilitated by transition metals has become the preferred technique for achieving efficient aniline production. The conversion of nitroaromatic compounds through hydrogenation into valuable organic chemical intermediates, such as anilines and azo-aromatic compounds, has attracted an increasing interest.[174] This interest stems from its applicability under mild reaction conditions, particularly in an aqueous environment, and in particular offers the potential to transform substances considered hazardous to the environment because of their high toxicity, stability, and resistance to biodegradation, thus raising ecological concerns.[175] This reaction involves the use of a metal catalyst to activate the nitro compound, along with reducing agents such as hydrogen, sodium borohydride, formic acid, and hydrazine hydrate. The synergistic use of these metal catalysts and reducing agents forms a suitable combination to effectively transform nitro groups. Homogeneous catalysts, while showing remarkable efficiency in the reduction of nitroaromatics, have instability problems when exposed to water or alcohol reaction solvents, and this makes them not reusable for subsequent chemical processes.[176] Considerable efforts have been made in recent decades to create immobilized metal or metal oxide catalysts for the heterogeneous reduction of nitroaromatics. These efforts include various support materials, including carbon-based materials,[177-178] porous molecular sieves[179] and polymers.[180]

Heck's cross-coupling is a powerful technique for the formation of new C–C bonds through the catalytic reaction between aryl/alkenyl halides and alkenes. This revolutionary discovery, independently revealed by Mizoroki and Heck, has evolved into a versatile milestone in

organic chemistry. Heck-type reactivity, which is a key aspect of palladium-driven catalytic cycles, results from the inherent ability of Pd(0) species to participate in oxidative addition to various C–X bonds. Subsequently, the resulting R–Pd–X intermediates are ready for addition to unsaturated bonds. This reaction offers one of the most straightforward routes to acquiring a diverse array of substituted olefins, dienes, and other unsaturated compounds.[181] Furthermore, the reaction's relevance extends to polymerization chemistry, enabling the production of conjugated polymers that have potential applications as innovative materials in optoelectronic devices, among other uses. The catalytic species that demonstrates efficiency in this reaction is Pd(0). However, in several instances, a Pd(II) complexes undergoes in situ reduction to Pd(0). Notably, the alkene itself is deemed a reducing agent. The Pd(II) complex is accompanied by ligands like phosphines or amines, which serve the purpose of coordinating with the metallic Pd and maintaining it in a dissolved state. The catalytic cycle of the Heck reaction unfolds in five distinct stages (**Figure 16**). In the first step, the PdL_2 (0) catalyst undergoes oxidative insertion into the aryl/alkenyl halide R-X. This process results in the formation of a Pd(II) complex in which both the R and X groups are coordinated to the palladium center. The generated complex engages in further coordination with the alkene, leading to the creation of a π-complex.
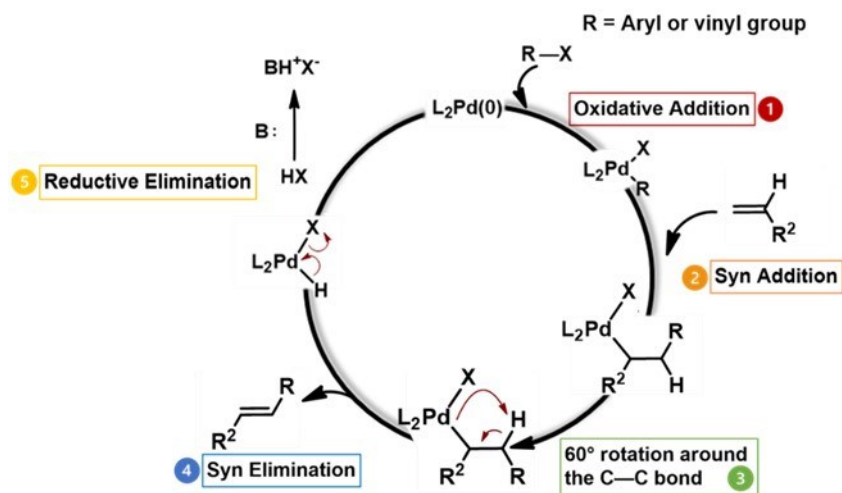
Figure 16. General mechanism for Heck reaction.

Subsequently, this complex mediates the syn addition (**Step 2**) of the alkene. Owing to the steric hindrance posed by the R group, the palladium becomes bonded to the most substituted carbon atom. At stage 3, the intermediate molecule undergoes an internal rotation around the central single C–C bond. This movement leads to the arrangement of PdL_2X and a hydrogen atom in a synchronous orientation. In the next step, hydrogen β-elimination occurs, leading to the formation of an alkene and a Pd(II)–H complex (**Step 4**). This complex proceeds in the

fifth step through a reductive elimination facilitated by the presence of a base. This reductive elimination leads to regeneration of the Pd(0) complex.

At the beginning, the reaction involved the use of palladium complexes with or without phosphine bonds (phosphine-assisted or phosphine-free catalysis).[182] Phosphine bonds play a key role in maintaining palladium in its zero oxidation state, manifesting as stable entities such as PdL_4 or PdL_3. The phosphine-assisted method is the traditional and widely accepted approach, providing outstanding results in a wide range of cases. However, this approach is not sustainable for several compelling reasons, stemming from both economic and chemical considerations. Phosphoric ligands are expensive, have toxicity issues, and cannot be easily recovered. In particular, in larger industrial and semi-industrial applications, the economic impact of using phosphine could exceed that of palladium itself. Moreover, the utilization of soluble complexes gives rise to a pertinent inquiry regarding the eventual recovery of these soluble entities upon the conclusion of the reaction.[183-185] Despite the documentation of Pd-based catalytic species being recaptured, it remains crucial to garner additional substantiation of this "release and capture" mechanism, thus comprehensively unraveling the broad applicability of this phenomenon.[186] To circumvent the challenges of separating homogeneous catalysts and the use of phosphine-based complexes, strategies involving the immobilization of palladium nanoparticles on various supports, including silica,[81,187] alumina, zeolites, organic polymers,[188-189] magnetic nanoparticles,[190-191] and carbon nanotubes,[19,23,27] have been devised. Among these various supports, carbon nanoforms have demonstrated significant potential for the deposition of palladium nanoparticles due to their ability to be tailored to specific needs. In particular, carbon nanotubes stand out for their inherent characteristics that make them outstanding materials for catalytic applications. These characteristics include exceptional mechanical and chemical stability, adequate pore size, and relatively high specific surface area. These qualities make CNTs excellent candidates for supporting the immobilization of metal nanoparticles. Pristine CNTs have been successfully used to immobilize palladium, facilitating C–C coupling reactions.[192-193] However, materials based on pristine or oxidized CNTs often result in the formation of larger palladium nanoparticles (PdNPs) with a broad size distribution, and are often faced with the challenge of significant leaching. Furthermore, pristine carbon nanotubes have a tendency to aggregate and form bundles, which reduces their exposed surface area. It becomes essential to chemically functionalize CNTs to prevent bundling and enhance their dispersion in solvents, ultimately leading to improved catalytic performance.[194] In these cases, both multi-walled carbon nanotubes and single-walled carbon nanotubes have been chemically modified using various

approaches. These modifications are designed to optimize the interactions between the metal nanoparticles and the support. Regarding polymer modifications, it's noteworthy that polymers play a pivotal role in stabilizing metal nanoparticles.[172] Firstly, their physical size imparts stability by preventing NPs from clustering together. Secondly, polymers establish weak bonds with the NP surface through heteroatoms, similar to ligand behavior. This twofold stabilization approach synergistically enhances the overall stability of the system.

1.7 References

1. Crabtree, R. H., Homogeneous Catalysts and Catalysis. In *Encyclopedia of Catalysis*, Horváth, I., Ed. John Wiley & Sons: Wiley Online Books, **2011**.

2. Anastas, P.; Eghbali, N., Green Chemistry: Principles and Practice. *Chem. Soc. Rev.* **2010**, *39*, 301-312.

3. Anastas, P. T.; Kirchhoff, M. M., Origins, Current Status, and Future Challenges of Green Chemistry. *Acc. Chem. Res.* **2002**, *35*, 686-694.

4. Kaneda, K.; Mizugaki, T.; Mitsudome, T., Green Catalysis. In *Encyclopedia of Catalysis*, Horváth, I., Ed. John Wiley & Sons: Wiley Online Books, **2010**.

5. Rothenberg, G., Heterogeneous Catalysis. In *Catalysis: Conceptsand Green Applications*, Rothenberg, G., Ed. Wiley-VCH: Weinheim, Germany, **2008**; pp 127-187.

6. Schmal, M., Introduction. In *Heterogeneous Catalysis and its Industrial Applications*, Schmal, M., Ed. Springer Nature: Cham, Switzerland, **2016**; pp 1-4.

7. de Vries, J. G.; Jackson, S. D., Homogeneous and heterogeneous catalysis in industry. *Catal. Sci. Technol.* **2012**, *2*, 2009-2009.

8. Friend, C. M.; Xu, B., Heterogeneous Catalysis: A Central Science for a Sustainable Future. *Acc. Chem. Res.* **2017**, *50*, 517-521.

9. Fechete, I.; Wang, Y.; Védrine, J. C., The past, present and future of heterogeneous catalysis. *Catal. Today* **2012**, *189*, 2-27.

10. Janas, D.; Koziol, K. K., Carbon nanotube fibers and films: synthesis, applications and perspectives of the direct-spinning method. *Nanoscale* **2016**, *8*, 19475-19490.

11. Janas, D.; Koziol, K. K., A review of production methods of carbon nanotube and graphene thin films for electrothermal applications. *Nanoscale* **2014**, *6*, 3037-3045.

12. Noor, A.; Khalid, H.; Aslam, M.; Hayat, A.; Khan, A. F.; Nasir, M.; Chaudhry, A. A.; Nawaz, M. H., Graphene oxide reinforced silk fibroin nanocomposite as an electroactive interface for the estimation of dopamine. *RSC Adv.* **2022**, *12*, 29319-29328.

13. Moskvitina, E.; Kuznetsov, V.; Moseenkov, S.; Serkova, A.; Zavorin, A., Antibacterial Effect of Carbon Nanomaterials: Nanotubes, Carbon Nanofibers, Nanodiamonds, and Onion-like Carbon. *Materials* **2023**, *16*, 957.

14. Liu, L.; Niu, Z.; Chen, J., Unconventional supercapacitors from nanocarbon-based electrode materials to device configurations. *Chem. Soc. Rev.* **2016**, *45*, 4340-4363.

15. Zhu, S.; Xu, G., Single-walled carbon nanohorns and their applications. *Nanoscale* **2010**, *2*, 2538-2549.

16. Martín, N., Carbon Nanoforms for Photovoltaics: Myth or Reality? *Adv. Energy Mater.* **2017**, *7*, 1601102.

17. Bittencourt, C.; Van Tendeloo, G., Carbon Nanoforms. In *Handbook of Nanoscopy*, G. Van Tendeloo; D. Van Dyck, S.; Pennycoo, J., Eds. Wiley-VCH: Weinheim, Germany, **2012**; pp 995-1070.

18. Ziccarelli, I.; Mancuso, R.; Giacalone, F.; Calabrese, C.; La Parola, V.; De Salvo, A.; Della Ca, N.; Gruttadauria, M.; Gabriele, B., Heterogenizing palladium tetraiodide catalyst for carbonylation reactions. *J. Catal.* **2022**, *413*, 1098-1110.

19. Mercadante, A.; Campisciano, V.; Morena, A.; Valentino, L.; La Parola, V.; Aprile, C.; Gruttadauria, M.; Giacalone, F., Catechol-Functionalized Carbon Nanotubes as Support for Pd Nanoparticles: a Recyclable System for the Heck Reaction. *Eur. J. Org. Chem.* **2022**, *2022*, e202200497.

20.   Campisciano, V.; Valentino, L.; Morena, A.; Santiago-Portillo, A.; Saladino, N.; Gruttadauria, M.; Aprile, C.; Giacalone, F., Carbon nanotube supported aluminum porphyrin-imidazolium bromide crosslinked copolymer: A synergistic bifunctional catalyst for CO2 conversion. *J. CO2 Util.* **2022**, *57*, 101884.

21.   Morena, A.; Campisciano, V.; Comès, A.; Liotta, L. F.; Gruttadauria, M.; Aprile, C.; Giacalone, F., A Study on the Stability of Carbon Nanoforms–Polyimidazolium Network Hybrids in the Conversion of CO2 into Cyclic Carbonates: Increase in Catalytic Activity after Reuse. *Nanomaterials* **2021**, *11*, 2243.

22.   Campisciano, V.; Burger, R.; Calabrese, C.; Liotta, L. F.; Lo Meo, P.; Gruttadauria, M.; Giacalone, F., Straightforward preparation of highly loaded MWCNT–polyamine hybrids and their application in catalysis. *Nanoscale Adv.* **2020**, *2*, 4199-4211.

23.   Giacalone, F.; Campisciano, V.; Calabrese, C.; La Parola, V.; Syrgiannis, Z.; Prato, M.; Gruttadauria, M., Single-Walled Carbon Nanotube–Polyamidoamine Dendrimer Hybrids for Heterogeneous Catalysis. *ACS Nano* **2016**, *10*, 4627-4636.

24.   Buaki-Sogó, M.; Vivian, A.; Bivona, L. A.; García, H.; Gruttadauria, M.; Aprile, C., Imidazolium functionalized carbon nanotubes for the synthesis of cyclic carbonates: reducing the gap between homogeneous and heterogeneous catalysis. *Catal. Sci. Technol.* **2016**, *6*, 8418-8427.

25.   Beejapur, H. A.; Campisciano, V.; Giacalone, F.; Gruttadauria, M., Catalytic Synergism in a C60IL10TEMPO2 Hybrid in the Efficient Oxidation of Alcohols. *Adv. Synth. Catal.* **2015**, *357*, 51-58.

26.   Calabrese, C.; Liotta, L. F.; Carbonell, E.; Giacalone, F.; Gruttadauria, M.; Aprile, C., Imidazolium-Functionalized Carbon Nanohorns for the Conversion of Carbon Dioxide: Unprecedented Increase of Catalytic Activity after Recycling. *ChemSusChem* **2017**, *10*, 1202-1209.

27.   Campisciano, V.; Calabrese, C.; Liotta, L. F.; La Parola, V.; Spinella, A.; Aprile, C.; Gruttadauria, M.; Giacalone, F., Templating effect of carbon nanoforms on highly cross-linked imidazolium network: Catalytic activity of the resulting hybrids with Pd nanoparticles. *Appl. Organomet. Chem.* **2019**, *33*, e4848.

28.   Campisciano, V.; Gruttadauria, M.; Giacalone, F., Modified Nanocarbons as Catalysts in Organic Processes. In *Catalyst Immobilization*, Benaglia, M.; Puglisi, A., Eds. Wiley-VCH: Weinheim, Germany, **2020**; pp 77-113.

29.   Campisciano, V.; Gruttadauria, M.; Giacalone, F., Modified Nanocarbons for Catalysis. *ChemCatChem* **2019**, *11*, 90-133.

30.   Gutiérrez López, M. Á.; Tan, M.-L.; Renno, G.; Jozeliūnaitė, A.; Nué-Martinez, J. J.; Lopez-Andarias, J.; Sakai, N.; Matile, S., Anion–π catalysis on carbon allotropes. *Beilstein J. Org. Chem.* **2023**, *19*, 1881-1894.

31.   Schaetz, A.; Zeltner, M.; Stark, W. J., Carbon Modifications and Surfaces for Catalytic Organic Transformations. *ACS Catal.* **2012**, *2*, 1267-1284.

32.   Chen, Q.; Saltiel, C.; Manickavasagam, S.; Schadler, L. S.; Siegel, R. W.; Yang, H., Aggregation behavior of single-walled carbon nanotubes in dilute aqueous suspension. *J. Colloid Interface Sci.* **2004**, *280*, 91-97.

33.   Dubey, R.; Dutta, D.; Sarkar, A.; Chattopadhyay, P., Functionalized carbon nanotubes: synthesis, properties and applications in water purification, drug delivery, and material and biomedical sciences. *Nanoscale Adv.* **2021**, *3*, 5722-5744.

34.   Olivares, F.; Peón, F.; Henríquez, R.; del Río, R. S., Strategies for area-selective deposition of metal nanoparticles on carbon nanotubes and their applications: a review. *J. Mater. Sci.* **2022**, *57*, 2362-2387.

35.   Iijima, S.; Ichihashi, T., Single-shell carbon nanotubes of 1-nm diameter. *Nature* **1993**, *363*, 603-605.

36.   Prasek, J.; Drbohlavova, J.; Chomoucka, J.; Hubalek, J.; Jasek, O.; Adam, V.; Kizek, R., Methods for carbon nanotubes synthesis—review. *J. Mater. Chem.* **2011**, *21*, 15872-15884.

37.   Zhou, W.; Bai, X.; Wang, E.; Xie, S., Synthesis, Structure, and Properties of Single-Walled Carbon Nanotubes. *Adv. Mater.* **2009**, *21*, 4565-4583.

38.   Arora, N.; Sharma, N. N., Arc discharge synthesis of carbon nanotubes: Comprehensive review. *Diam. Relat. Mater.* **2014**, *50*, 135-150.

39.   Janas, D., Perfectly imperfect: a review of chemical tools for exciton engineering in single-walled carbon nanotubes. *Mater. Horiz.* **2020**, *7*, 2860-2881.

40.   Mubarak, N. M.; Abdullah, E. C.; Jayakumar, N. S.; Sahu, J. N., An overview on methods for the production of carbon nanotubes. *J. Ind. Eng. Chem.* **2014**, *20*, 1186-1197.

41.   Szabó, A.; Perri, C.; Csató, A.; Giordano, G.; Vuono, D.; Nagy, J. B., Synthesis Methods of Carbon Nanotubes and Related Materials. *Materials* **2010**, *3*, 3092-3140.

42.   Golnabi, H., Carbon nanotube research developments in terms of published papers and patents, synthesis and production. *Sci. Iran* **2012**, *19*, 2012-2022.

43.   Kumar, M.; Ando, Y., Chemical Vapor Deposition of Carbon Nanotubes: A Review on Growth Mechanism and Mass Production. *J. Nanosci. Nanotechnol.* **2010**, *10*, 3739-3758.

44.   Bethune, D. S.; Kiang, C. H.; de Vries, M. S.; Gorman, G.; Savoy, R.; Vazquez, J.; Beyers, R., Cobalt-catalysed growth of carbon nanotubes with single-atomic-layer walls. *Nature* **1993**, *363*, 605-607.

45.   Herranz, M. Á.; Martín, N., Polymers Based on Carbon Nanotubes. In *Fullerene Polymers*, Martín, N.; Giacalone, F., Eds. John Wiley & Sons, Inc: Weinheim, Germany, **2009**; pp 271-303.

46.   Hirsch, A., Functionalization of Single-Walled Carbon Nanotubes. *Angew. Chem. Int. Ed.* **2002**, *41*, 1853-1859.

47.   Ziegler, K. J.; Gu, Z.; Peng, H.; Flor, E. L.; Hauge, R. H.; Smalley, R. E., Controlled Oxidative Cutting of Single-Walled Carbon Nanotubes. *J. Am. Chem. Soc.* **2005**, *127*, 1541-1547.

48.   Mawhinney, D. B.; Naumenko, V.; Kuznetsova, A.; Yates, J. T.; Liu, J.; Smalley, R. E., Infrared Spectral Evidence for the Etching of Carbon Nanotubes: Ozone Oxidation at 298 K. *J. Am. Chem. Soc.* **2000**, *122*, 2383-2384.

49.   Banerjee, S.; Wong, S. S., Rational Sidewall Functionalization and Purification of Single-Walled Carbon Nanotubes by Solution-Phase Ozonolysis. *J. Phys. Chem. B* **2002**, *106*, 12144-12151.

50.   Fu, K.; Kitaygorodskiy, A.; Rao, A. M.; Sun, Y.-P., Deuterium Attachment to Carbon Nanotubes in Solution. *Nano Lett.* **2002**, *2*, 1165-1168.

51.   Mickelson, E. T.; Huffman, C. B.; Rinzler, A. G.; Smalley, R. E.; Hauge, R. H.; Margrave, J. L., Fluorination of single-wall carbon nanotubes. *Chem. Phys. Lett.* **1998**, *296*, 188-194.

52.   Kelly, K. F.; Chiang, I. W.; Mickelson, E. T.; Hauge, R. H.; Margrave, J. L.; Wang, X.; Scuseria, G. E.; Radloff, C.; Halas, N. J., Insight into the mechanism of sidewall

functionalization of single-walled nanotubes: an STM study. *Chem. Phys. Lett.* **1999**, *313*, 445-450.

53.   Khabashesku, V. N.; Billups, W. E.; Margrave, J. L., Fluorination of single-wall carbon nanotubes and subsequent derivatization reactions. *Acc. Chem. Res.* **2002**, *35*, 1087-95.

54.   Saini, R. K.; Chiang, I. W.; Peng, H.; Smalley, R. E.; Billups, W. E.; Hauge, R. H.; Margrave, J. L., Covalent Sidewall Functionalization of Single Wall Carbon Nanotubes. *J. Am. Chem. Soc.* **2003**, *125*, 3617-3621.

55.   Boul, P. J.; Liu, J.; Mickelson, E. T.; Huffman, C. B.; Ericson, L. M.; Chiang, I. W.; Smith, K. A.; Colbert, D. T.; Hauge, R. H.; Margrave, J. L.; Smalley, R. E., Reversible sidewall functionalization of buckytubes. *Chem. Phys. Lett.* **1999**, *310*, 367-372.

56.   Zhang, L.; Kiny, V. U.; Peng, H.; Zhu, J.; Lobo, R. F. M.; Margrave, J. L.; Khabashesku, V. N., Sidewall Functionalization of Single-Walled Carbon Nanotubes with Hydroxyl Group-Terminated Moieties. *Chem. Mater.* **2004**, *16*, 2055-2061.

57.   Stevens, J. L.; Huang, A.; Peng, H.; Chiang, I. W.; Khabashesku, V. N.; Margrave, J. L., Sidewall Amino-Functionalization of Single-Walled Carbon Nanotubes through Fluorination and Subsequent Reactions with Terminal Diamines. *Nano Lett.* **2003**, *3*, 331-336.

58.   Pekker, S.; Salvetat, J. P.; Jakab, E.; Bonard, J.-M.; Forró, L., Hydrogenation of carbon nanotubes and graphite in liquid ammonia. *J. Phys. Chem. B* **2001**, *105*, 7938-7943.

59.   Georgakilas, V.; Kordatos, K.; Prato, M.; Guldi, D. M.; Holzinger, M.; Hirsch, A., Organic Functionalization of Carbon Nanotubes. *J. Am. Chem. Soc.* **2002**, *124*, 760-761.

60.   Tagmatarchis, N.; Prato, M., Functionalization of carbon nanotubes via 1,3-dipolar cycloadditions. *J. Mater. Chem.* **2004**, *14*, 437-439.

61.   and, J. L. B.; Tour, J. M., Highly Functionalized Carbon Nanotubes Using in Situ Generated Diazonium Compounds. *Chem. Mater.* **2001**, *13*, 3823-3824.

62.   Bahr, J. L.; Yang, J.; Kosynkin, D. V.; Bronikowski, M. J.; Smalley, R. E.; Tour, J. M., Functionalization of carbon nanotubes by electrochemical reduction of aryl diazonium salts: a bucky paper electrode. *J. Am. Chem. Soc.* **2001**, *123*, 6536-42.

63.   Setaro, A.; Adeli, M.; Glaeske, M.; Przyrembel, D.; Bisswanger, T.; Gordeev, G.; Maschietto, F.; Faghani, A.; Paulus, B.; Weinelt, M.; Arenal, R.; Haag, R.; Reich, S., Preserving π-conjugation in covalently functionalized carbon nanotubes for optoelectronic applications. *Nat. Commun.* **2017**, *8*, 14281.

64.   Ganesan, K., Perspective Chapter: Applications of Novel Ionic Liquids as Catalyst. In *Industrial Applications of Ionic Liquids*, Fabrice, M., Ed. IntechOpen: London, United Kingdom, **2022**; pp 1-14.

65.   Wasserscheid, P.; Keim, W., Ionic Liquids—New "Solutions" for Transition Metal Catalysis. *Angew. Chem. Int. Ed.* **2000**, *39*, 3772-3789.

66.   Berton, P.; Shamshina, J. L., Ionic Liquids as Tools to Incorporate Pharmaceutical Ingredients into Biopolymer-Based Drug Delivery Systems. *Pharmaceuticals* **2023**, *16*, 272.

67.   Berthod, A.; Ruiz-Ángel, M. J.; Carda-Broch, S., Recent advances on ionic liquid uses in separation techniques. *J. Chromatogr. A* **2018**, *1559*, 2-16.

68.   Martins, V. L.; Torresi, R. M., Ionic liquids in electrochemical energy storage. *Curr. Opin. Electrochem.* **2018**, *9*, 26-32.

69.   Watanabe, M.; Thomas, M. L.; Zhang, S.; Ueno, K.; Yasuda, T.; Dokko, K., Application of Ionic Liquids to Energy Storage and Conversion Materials and Devices. *Chem. Rev.* **2017**, *117*, 7190-7239.

70.   MacFarlane, D. R.; Forsyth, M.; Howlett, P. C.; Pringle, J. M.; Sun, J.; Annat, G.; Neil, W.; Izgorodina, E. I., Ionic Liquids in Electrochemical Devices and Processes: Managing Interfacial Electrochemistry. *Acc. Chem. Res.* **2007**, *40*, 1165-1173.

71.   Liu, H.; Liu, Y.; Li, J., Ionic liquids in surface electrochemistry. *Phys. Chem. Chem. Phys.* **2010**, *12*, 1685-1697.

72.   Yue, C.; Fang, D.; Liu, L.; Yi, T.-F., Synthesis and application of task-specific ionic liquids used as catalysts and/or solvents in organic unit reactions. *J. Mol. Liq.* **2011**, *163*, 99-121.

73.   Müller, T. E., Supported Ionic Liquids as Part of a Building-Block System for Tailored Catalysts. In *Supported Ionic Liquids*, Fehrmann, R.; Riisager, A.; Haumann, M., Eds. John Wiley & Sons, Inc: Weinheim, Germany, **2014**; pp 209-232.

74.   Meijboom, R.; Haumann, M.; Müller, T. E.; Szesni, N., Synthetic Methodologies for Supported Ionic Liquid Materials. In *Supported Ionic Liquids*, R. Fehrmann; Riisager, A.; Haumann, M., Eds. John Wiley & Sons, Inc: Weinheim, Germany, **2014**; pp 75-94.

75.   MacFarlane, D. R.; Tachikawa, N.; Forsyth, M.; Pringle, J. M.; Howlett, P. C.; Elliott, G. D.; Davis, J. H.; Watanabe, M.; Simon, P.; Angell, C. A., Energy applications of ionic liquids. *Energy Environ. Sci.* **2014**, *7*, 232-250.

76.   Riisager, A.; Wasserscheid, P.; van Hal, R.; Fehrmann, R., Continuous fixed-bed gas-phase hydroformylation using supported ionic liquid-phase (SILP) Rh catalysts. *J. Catal.* **2003**, *219*, 452-455.

77.   Riisager, A.; Eriksen, K. M.; Hjortkjær, J.; Fehrmann, R., Propene hydroformylation by supported aqueous-phase Rh-NORBOS catalysts. *J. Mol. Catal. A Chem.* **2003**, *193*, 259-272.

78.   Riisager, A.; Jørgensen, B.; Wasserscheid, P.; Fehrmann, R., First application of supported ionic liquid phase (SILP) catalysis for continuous methanol carbonylation. *Chem. Commun.* **2006**, 994-996.

79.   Arhancet, J. P.; Davis, M. E.; Merola, J. S.; Hanson, B. E., Hydroformylation by supported aqueous-phase catalysis: a new class of heterogeneous catalysts. *Nature* **1989**, *339*, 454-455.

80.   García-Verdugo, E.; Altava, B.; Burguete, M. I.; Lozano, P.; Luis, S. V., Ionic liquids and continuous flow processes: a good marriage to design sustainable processes. *Green Chem.* **2015**, *17*, 2693-2713.

81.   Calabrese, C.; Campisciano, V.; Siragusa, F.; Liotta, L. F.; Aprile, C.; Gruttadauria, M.; Giacalone, F., SBA-15/POSS-Imidazolium Hybrid as Catalytic Nanoreactor: the role of the Support in the Stabilization of Palladium Species for C−C Cross Coupling Reactions. *Adv. Synth. Catal.* **2019**, *361*, 3758-3767.

82.   Mehnert, C. P.; Cook, R. A.; Dispenziere, N. C.; Afeworki, M., Supported Ionic Liquid Catalysis − A New Concept for Homogeneous Hydroformylation Catalysis. *J. Am. Chem. Soc.* **2002**, *124*, 12932-12933.

83.   Mehnert, C. P.; Mozeleski, E. J.; Cook, R. A., Supported ionic liquid catalysis investigated for hydrogenation reactions. *Chem. Commun.* **2002**, 3010-3011.

84.   Giacalone, F.; Gruttadauria, M., Covalently Supported Ionic Liquid Phases: An Advanced Class of Recyclable Catalytic Systems. *ChemCatChem* **2016**, *8*, 664-684.

85.   Campisciano, V.; Giacalone, F.; Gruttadauria, M., Supported Ionic Liquids: A Versatile and Useful Class of Materials. *Chem. Rec.* **2017**, *17*, 918-938.

86. Hiroto, S.; Miyake, Y.; Shinokubo, H., Synthesis and Functionalization of Porphyrins through Organometallic Methodologies. *Chem. Rev.* **2017**, *117*, 2910-3043.

87. Collman, J. P.; Denisevich, P.; Konai, Y.; Marrocco, M.; Koval, C.; Anson, F. C., Electrode catalysis of the four-electron reduction of oxygen to water by dicobalt face-to-face porphyrins. *J. Am. Chem. Soc.* **1980**, *102*, 6027-6036.

88. Zhang, P.; Hu, J.; Liu, B.; Yang, J.; Hou, H., Recent advances in metalloporphyrins for environmental and energy applications. *Chemosphere* **2019**, *219*, 617-635.

89. De Sloovere, D.; Vanpoucke, D. E. P.; Paulus, A.; Joos, B.; Calvi, L.; Vranken, T.; Reekmans, G.; Adriaensens, P.; Eshraghi, N.; Mahmoud, A.; Boschini, F.; Safari, M.; Van Bael, M. K.; Hardy, A., Deep Eutectic Solvents as Nonflammable Electrolytes for Durable Sodium-Ion Batteries. *Adv. Energy Sustainability Res.* **2022**, *3*, 2100159.

90. Gotico, P.; Halime, Z.; Aukauloo, A., Recent advances in metalloporphyrin-based catalyst design towards carbon dioxide reduction: from bio-inspired second coordination sphere modifications to hierarchical architectures. *Dalton Trans.* **2020**, *49*, 2381-2396.

91. Morena, A.; Campisciano, V.; Santiago-Portillo, A.; Gruttadauria, M.; Giacalone, F.; Aprile, C., POSS-Al-porphyrin-imidazolium cross-linked network as catalytic bifunctional platform for the conversion of CO_2 with epoxides. *Fuel* **2022**, 126819.

92. Valentino, L.; Campisciano, V.; Célis, C.; Lemaur, V.; Lazzaroni, R.; Gruttadauria, M.; Aprile, C.; Giacalone, F., Highly cross-linked bifunctional magnesium porphyrin-imidazolium bromide polymer: Unveiling the key role of co-catalysts proximity for CO2 conversion into cyclic carbonates. *J. Catal.* **2023**, *428*, 115143.

93. Valentino, L.; Célis, C.; Campisciano, V.; Gruttadauria, M.; Aprile, C.; Giacalone, F., Phosphonium Salt/Al-Porphyrin Copolymer as Bifunctional Heterogeneous Catalyst for CO2 Conversion to Cyclic Carbonates. *ChemCatChem* **2024**, e202301428.

94. Ema, T.; Miyazaki, Y.; Taniguchi, T.; Takada, J., Robust porphyrin catalysts immobilized on biogenous iron oxide for the repetitive conversions of epoxides and CO2 into cyclic carbonates. *Green Chem.* **2013**, *15*, 2485-2492.

95. Wang, S.; Song, K.; Zhang, C.; Shu, Y.; Li, T.; Tan, B., A novel metalporphyrin-based microporous organic polymer with high CO2 uptake and efficient chemical conversion of CO2 under ambient conditions. *J. Mater. Chem. A* **2017**, *5*, 1509-1515.

96. Chen, A.; Zhang, Y.; Chen, J.; Chen, L.; Yu, Y., Metalloporphyrin-based organic polymers for carbon dioxide fixation to cyclic carbonate. *J. Mater. Chem. A* **2015**, *3*, 9807-9816.

97. Wang, W.; Wang, Y.; Li, C.; Yan, L.; Jiang, M.; Ding, Y., State-of-the-Art Multifunctional Heterogeneous POP Catalyst for Cooperative Transformation of CO2 to Cyclic Carbonates. *ACS Sustain. Chem. Eng.* **2017**, *5*, 4523-4528.

98. Luo, R.; Zhang, W.; Yang, Z.; Zhou, X.; Ji, H., Synthesis of cyclic carbonates from epoxides over bifunctional salen aluminum oligomers as a CO2-philic catalyst: Catalytic and kinetic investigation. *J. CO2 Util.* **2017**, *19*, 257-265.

99. Liu, L.; Jayakumar, S.; Chen, J.; Tao, L.; Li, H.; Yang, Q.; Li, C., Synthesis of Bifunctional Porphyrin Polymers for Catalytic Conversion of Dilute CO2 to Cyclic Carbonates. *ACS Appl. Mater. Interfaces* **2021**, *13*, 29522-29531.

100. Su, Z.; Ma, L.; Wei, J.; Bai, X.; Wang, N.; Li, J., A zinc porphyrin polymer as efficient bifunctional catalyst for conversion of CO2 to cyclic carbonates. *Appl. Organomet. Chem.* **2024**, e6632.

101. Bai, X.; Su, Z.; Wei, J.; Ma, L.; Duan, S.; Wang, N.; Zhang, X.; Li, J., Zinc(II)porphyrin-Based Porous Ionic Polymers (PIPs) as Multifunctional Heterogeneous Catalysts for the Conversion of CO2 to Cyclic Carbonates. *Ind. Eng. Chem. Res.* **2022**, *61*, 5093-5102.

102. Wu, Q.-J.; Mao, M.-J.; Chen, J.-X.; Huang, Y.-B.; Cao, R., Integration of metalloporphyrin into cationic covalent triazine frameworks for the synergistically enhanced chemical fixation of CO2. *Catal. Sci. Technol.* **2020**, *10*, 8026-8033.

103. He, H.; Zhu, Q.-Q.; Zhang, W.-W.; Zhang, H.-W.; Chen, J.; Li, C.-P.; Du, M., Metal and Co-Catalyst Free CO2 Conversion with a Bifunctional Covalent Organic Framework (COF). *ChemCatChem* **2020**, *12*, 5192-5199.

104. Chen, Y.; Luo, R.; Xu, Q.; Jiang, J.; Zhou, X.; Ji, H., Charged Metalloporphyrin Polymers for Cooperative Synthesis of Cyclic Carbonates from CO2 under Ambient Conditions. *ChemSusChem* **2017**, *10*, 2534-2541.

105. Luo, R.; Chen, Y.; He, Q.; Lin, X.; Xu, Q.; He, X.; Zhang, W.; Zhou, X.; Ji, H., Metallosalen-Based Ionic Porous Polymers as Bifunctional Catalysts for the Conversion of CO2 into Valuable Chemicals. *ChemSusChem* **2017**, *10*, 1526-1533.

106. Li, H.; Li, C.; Chen, J.; Liu, L.; Yang, Q., Synthesis of a Pyridine–Zinc-Based Porous Organic Polymer for the Co-catalyst-Free Cycloaddition of Epoxides. *Chem. Asian J.* **2017**, *12*, 1095-1103.

107. Ma, D.; Li, B.; Liu, K.; Zhang, X.; Zou, W.; Yang, Y.; Li, G.; Shi, Z.; Feng, S., Bifunctional MOF heterogeneous catalysts based on the synergy of dual functional sites for efficient conversion of CO2 under mild and co-catalyst free conditions. *J. Mater. Chem. A* **2015**, *3*, 23136-23142.

108. Liu, J.; Zhao, G.; Cheung, O.; Jia, L.; Sun, Z.; Zhang, S., Highly Porous Metalloporphyrin Covalent Ionic Frameworks with Well-Defined Cooperative Functional Groups as Excellent Catalysts for CO₂ Cycloaddition. *Chem. Eur. J.* **2019**, *25*, 9052-9059.

109. Luo, R.; Chen, M.; Zhou, F.; Zhan, J.; Deng, Q.; Yu, Y.; Zhang, Y.; Xu, W.; Fang, Y., Synthesis of metalloporphyrin-based porous organic polymers and their functionalization for conversion of CO2 into cyclic carbonates: recent advances, opportunities and challenges. *J. Mater. Chem. A* **2021**, *9*, 25731-25749.

110. Abbott, A. P.; Boothby, D.; Capper, G.; Davies, D. L.; Rasheed, R. K., Deep Eutectic Solvents Formed between Choline Chloride and Carboxylic Acids: Versatile Alternatives to Ionic Liquids. *J. Am. Chem. Soc.* **2004**, *126*, 9142-9147.

111. Abbott, A. P.; Capper, G.; Davies, D. L.; Rasheed, R. K.; Tambyrajah, V., Novel solvent properties of choline chloride/urea mixtures. *Chem. Commun.* **2003**, 70-71.

112. Mjalli, F. S.; Ahmed, O. U., Characteristics and intermolecular interaction of eutectic binary mixtures: Reline and Glyceline. *Korean J. Chem. Eng.* **2016**, *33*, 337-343.

113. Schaeffer, N.; Martins, M. A. R.; Neves, C. M. S. S.; Pinho, S. P.; Coutinho, J. A. P., Sustainable hydrophobic terpene-based eutectic solvents for the extraction and separation of metals. *Chem. Commun.* **2018**, *54*, 8104-8107.

114. Francisco, M.; van den Bruinhorst, A.; Kroon, M. C., Low-Transition-Temperature Mixtures (LTTMs): A New Generation of Designer Solvents. *Angew. Chem. Int. Ed.* **2013**, *52*, 3074-3085.

115. Hansen, B. B.; Spittle, S.; Chen, B.; Poe, D.; Zhang, Y.; Klein, J. M.; Horton, A.; Adhikari, L.; Zelovich, T.; Doherty, B. W.; Gurkan, B.; Maginn, E. J.; Ragauskas, A.; Dadmun,

M.; Zawodzinski, T. A.; Baker, G. A.; Tuckerman, M. E.; Savinell, R. F.; Sangoro, J. R., Deep Eutectic Solvents: A Review of Fundamentals and Applications. *Chem. Rev.* **2021**, *121*, 1232-1285.

116. Zhang, Q.; De Oliveira Vigier, K.; Royer, S.; Jérôme, F., Deep eutectic solvents: syntheses, properties and applications. *Chem. Soc. Rev.* **2012**, *41*, 7108-7146.

117. Smith, E. L.; Abbott, A. P.; Ryder, K. S., Deep Eutectic Solvents (DESs) and Their Applications. *Chem. Rev.* **2014**, *114*, 11060-11082.

118. Aroso, I. M.; Paiva, A.; Reis, R. L.; Duarte, A. R. C., Natural deep eutectic solvents from choline chloride and betaine – Physicochemical properties. *J. Mol. Liq.* **2017**, *241*, 654-661.

119. Malaquias, J. C.; Steichen, M.; Thomassey, M.; Dale, P. J., Electrodeposition of Cu–In alloys from a choline chloride based deep eutectic solvent for photovoltaic applications. *Electrochim. Acta* **2013**, *103*, 15-22.

120. Migliorati, V.; Sessa, F.; D'Angelo, P., Deep eutectic solvents: A structural point of view on the role of the cation. *Chem. Phys. Lett.* **2019**, *737*, 100001.

121. Abbott, A. P.; Capper, G.; McKenzie, K. J.; Ryder, K. S., Electrodeposition of zinc–tin alloys from deep eutectic solvents based on choline chloride. *J. Electroanal. Chem.* **2007**, *599*, 288-294.

122. Söldner, A.; Zach, J.; König, B., Deep eutectic solvents as extraction media for metal salts and oxides exemplarily shown for phosphates from incinerated sewage sludge ash. *Green Chem.* **2019**, *21*, 321-328.

123. Millia, L.; Dall'Asta, V.; Ferrara, C.; Berbenni, V.; Quartarone, E.; Perna, F. M.; Capriati, V.; Mustarelli, P., Bio-inspired choline chloride-based deep eutectic solvents as electrolytes for lithium-ion batteries. *Solid State Ion.* **2018**, *323*, 44-48.

124. Boisset, A.; Menne, S.; Jacquemin, J.; Balducci, A.; Anouti, M., Deep eutectic solvents based on N-methylacetamide and a lithium salt as suitable electrolytes for lithium-ion batteries. *Phys. Chem. Chem. Phys.* **2013**, *15*, 20054-20063.

125. Makarov, D. M.; Fadeeva, Y. A.; Golubev, V. A.; Kolker, A. M., Designing deep eutectic solvents for efficient CO2 capture: A data-driven screening approach. *Sep. Purif. Technol.* **2023**, *325*, 124614.

126. Trivedi, T. J.; Lee, J. H.; Lee, H. J.; Jeong, Y. K.; Choi, J. W., Deep eutectic solvents as attractive media for CO2 capture. *Green Chem.* **2016**, *18*, 2834-2842.

127. Sarmad, S.; Mikkola, J.-P.; Ji, X., Carbon Dioxide Capture with Ionic Liquids and Deep Eutectic Solvents: A New Generation of Sorbents. *ChemSusChem* **2017**, *10*, 324-352.

128. Carriazo, D.; Serrano, M. C.; Gutiérrez, M. C.; Ferrer, M. L.; del Monte, F., Deep-eutectic solvents playing multiple roles in the synthesis of polymers and related materials. *Chem. Soc. Rev.* **2012**, *41*, 4996-5014.

129. Mota-Morales, J. D.; Gutiérrez, M. C.; Sanchez, I. C.; Luna-Bárcenas, G.; del Monte, F., Frontal polymerizations carried out in deep-eutectic mixtures providing both the monomers and the polymerization medium. *Chem. Commun.* **2011**, *47*, 5328-5330.

130. Mota-Morales, J. D.; Gutiérrez, M. C.; Ferrer, M. L.; Sanchez, I. C.; Elizalde-Peña, E. A.; Pojman, J. A.; Monte, F. D.; Luna-Bárcenas, G., Deep eutectic solvents as both active fillers and monomers for frontal polymerization. *J. Polym. Sci. A Polym. Chem.* **2013**, *51*, 1767-1773.

131.   Ajino, K.; Torii, A.; Ogawa, H.; Mori, H., Synthesis of ion-conductive polymers by radical polymerization of deep eutectic monomers bearing quaternary ammonium groups with urea. *Polymer* **2020**, *204*, 122803.

132.   Mota-Morales, J. D.; Gutiérrez, M. C.; Ferrer, M. L.; Jiménez, R.; Santiago, P.; Sanchez, I. C.; Terrones, M.; Del Monte, F.; Luna-Bárcenas, G., Synthesis of macroporous poly(acrylic acid)–carbon nanotube composites by frontal polymerization in deep-eutectic solvents. *J. Mater. Chem. A* **2013**, *1*, 3970-3976.

133.   Sakakura, T.; Choi, J.-C.; Yasuda, H., Transformation of Carbon Dioxide. *Chem. Rev.* **2007**, *107*, 2365-2387.

134.   Wu, X.; Chen, C.; Guo, Z.; North, M.; Whitwood, A. C., Metal- and Halide-Free Catalyst for the Synthesis of Cyclic Carbonates from Epoxides and Carbon Dioxide. *ACS Catal.* **2019**, *9*, 1895-1906.

135.   Dibenedetto, A.; Angelini, A.; Stufano, P., Use of carbon dioxide as feedstock for chemicals and fuels: homogeneous and heterogeneous catalysis. *J. Chem. Technol. Biotechnol.* **2014**, *89*, 334-353.

136.   Aresta, M.; Dibenedetto, A.; Angelini, A., Catalysis for the Valorization of Exhaust Carbon: from CO_2 to Chemicals, Materials, and Fuels. Technological Use of CO_2. *Chem. Rev.* **2014**, *114*, 1709-1742.

137.   Lu, X.-B.; Darensbourg, D. J., Cobalt catalysts for the coupling of CO2 and epoxides to provide polycarbonates and cyclic carbonates. *Chem. Soc. Rev.* **2012**, *41*, 1462-1484.

138.   Qin, Z.; Thomas, C. M.; Lee, S.; Coates, G. W., Cobalt-Based Complexes for the Copolymerization of Propylene Oxide and CO2: Active and Selective Catalysts for Polycarbonate Synthesis. *Angew. Chem. Int. Ed.* **2003**, *42*, 5484-5487.

139.   Mota-Morales, J. D.; Sánchez-Leija, R. J.; Carranza, A.; Pojman, J. A.; del Monte, F.; Luna-Bárcenas, G., Free-radical polymerizations of and in deep eutectic solvents: Green synthesis of functional materials. *Prog. Polym. Sci.* **2018**, *78*, 139-153.

140.   Huang, K.; Zhang, J.-Y.; Liu, F.; Dai, S., Synthesis of Porous Polymeric Catalysts for the Conversion of Carbon Dioxide. *ACS Catal.* **2018**, *8*, 9079-9102.

141.   Maeda, C.; Miyazaki, Y.; Ema, T., Recent progress in catalytic conversions of carbon dioxide. *Catal. Sci. Technol.* **2014**, *4*, 1482-1497.

142.   Quadrelli, E. A.; Centi, G.; Duplan, J.-L.; Perathoner, S., Carbon Dioxide Recycling: Emerging Large-Scale Technologies with Industrial Potential. *ChemSusChem* **2011**, *4*, 1194-1215.

143.   North, M.; Pasquale, R.; Young, C., Synthesis of cyclic carbonates from epoxides and CO2. *Green Chem.* **2010**, *12*, 1514-1539.

144.   Shaikh, R. R.; Pornpraprom, S.; D'Elia, V., Catalytic Strategies for the Cycloaddition of Pure, Diluted, and Waste CO2 to Epoxides under Ambient Conditions. *ACS Catal.* **2018**, *8*, 419-450.

145.   Sakakura, T.; Kohno, K., The synthesis of organic carbonates from carbon dioxide. *Chem. Commun.* **2009**, 1312-1330.

146.   Schäffner, B.; Schäffner, F.; Verevkin, S. P.; Börner, A., Organic Carbonates as Solvents in Synthesis and Catalysis. *Chem. Rev.* **2010**, *110*, 4554-4581.

147.   Mujmule, R. B.; Chung, W.-J.; Kim, H., Chemical fixation of carbon dioxide catalyzed via hydroxyl and carboxyl-rich glucose carbonaceous material as a heterogeneous catalyst. *Chem. Eng. J.* **2020**, *395*, 125164.

148. Castro-Osma, J. A.; Lamb, K. J.; North, M., Cr(salophen) Complex Catalyzed Cyclic Carbonate Synthesis at Ambient Temperature And Pressure. *ACS Catal.* **2016**, *6*, 5012-5025.

149. De la Cruz-Martínez, F.; Castro-Osma, J. A.; Lara-Sánchez, A., Carbon dioxide fixation into cyclic carbonates at room temperature catalyzed by heteroscorpionate aluminum complexes. *Green Chem. Eng.* **2022**, 280-287.

150. de la Cruz-Martínez, F.; Martínez, J.; Gaona, M. A.; Fernández-Baeza, J.; Sánchez-Barba, L. F.; Rodríguez, A. M.; Castro-Osma, J. A.; Otero, A.; Lara-Sánchez, A., Bifunctional Aluminum Catalysts for the Chemical Fixation of Carbon Dioxide into Cyclic Carbonates. *ACS Sustain. Chem. Eng.* **2018**, *6*, 5322-5332.

151. Faizan, M.; Srivastav, N.; Pawar, R., Azaboratrane as an exceptionally potential organocatalyst for the activation of CO_2 and coupling with epoxide. *Mol. Catal.* **2022**, *521*, 112201.

152. la Cruz-Martínez, F. d.; Sarasa Buchaca, M. M. d.; Fernández-Baeza, J.; Sánchez-Barba, L. F.; Rodríguez, A. M.; Alonso-Moreno, C.; Castro-Osma, J. A.; Lara-Sánchez, A., Heteroscorpionate Rare-Earth Catalysts for the Low-Pressure Coupling Reaction of CO_2 and Cyclohexene Oxide. *Organometallics* **2021**, *40*, 1503-1514.

153. Lei, Y.; Gunaratne, H. Q. N.; Jin, L., Design and synthesis of pyridinamide functionalized ionic liquids for efficient conversion of carbon dioxide into cyclic carbonates. *J. CO2 Util.* **2022**, *58*, 101930.

154. Li, M.-R.; Zhang, M.-C.; Yue, T.-J.; Lu, X.-B.; Ren, W.-M., Highly efficient conversion of CO_2 to cyclic carbonates with a binary catalyst system in a microreactor: intensification of "electrophile–nucleophile" synergistic effect. *RSC Adv.* **2018**, *8*, 39182-39186.

155. Liu, Y.; Cao, Z.; Zhou, Z.; Zhou, A., Imidazolium-based deep eutectic solvents as multifunctional catalysts for multisite synergistic activation of epoxides and ambient synthesis of cyclic carbonates. *J. CO2 Util.* **2021**, *53*, 101717.

156. Qu, L.; del Rosal, I.; Li, Q.; Wang, Y.; Yuan, D.; Yao, Y.; Maron, L., Efficient CO2 transformation under ambient condition by heterobimetallic rare earth complexes: Experimental and computational evidences of a synergistic effect. *J. CO2 Util.* **2019**, *33*, 413-418.

157. Saptal, V. B.; Bhanage, B. M., Bifunctional Ionic Liquids Derived from Biorenewable Sources as Sustainable Catalysts for Fixation of Carbon Dioxide. *ChemSusChem* **2017**, *10*, 1145-1151.

158. Whiteoak, C. J.; Martin, E.; Belmonte, M. M.; Benet-Buchholz, J.; Kleij, A. W., An Efficient Iron Catalyst for the Synthesis of Five- and Six-Membered Organic Carbonates under Mild Conditions. *Adv. Synth. Catal.* **2012**, *354*, 469-476.

159. Luo, R.; Chen, M.; Liu, X.; Xu, W.; Li, J.; Liu, B.; Fang, Y., Recent advances in CO2 capture and simultaneous conversion into cyclic carbonates over porous organic polymers having accessible metal sites. *J. Mater. Chem. A* **2020**, *8*, 18408-18424.

160. Pal, T. K.; De, D.; Bharadwaj, P. K., Metal-organic frameworks as heterogeneous catalysts for the chemical conversion of carbon dioxide. *Fuel* **2022**, *320*, 123904.

161. Siddig, L. A.; Alzard, R. H.; Nguyen, H. L.; Göb, C. R.; Alnaqbi, M. A.; Alzamly, A., Hexagonal Layer Manganese Metal–Organic Framework for Photocatalytic CO2 Cycloaddition Reaction. *ACS Omega* **2022**, *7*, 9958-9963.

162. Tapiador, J.; Leo, P.; Rodríguez-Diéguez, A.; Choquesillo-Lazarte, D.; Calleja, G.; Orcajo, G., A novel Zn-based-MOF for efficient CO_2 adsorption and conversion under mild conditions. *Catal. Today* **2022**, *390-391*, 230-236.

163. Wang, W.; Li, C.; Jin, J.; Yan, L.; Ding, Y., Mg–porphyrin complex doped divinylbenzene based porous organic polymers (POPs) as highly efficient heterogeneous catalysts for the conversion of CO2 to cyclic carbonates. *Dalton Trans.* **2018**, *47*, 13135-13141.

164. Campisciano, V.; Calabrese, C.; Giacalone, F.; Aprile, C.; Lo Meo, P.; Gruttadauria, M., Reconsidering TOF calculation in the transformation of epoxides and CO2 into cyclic carbonates. *J. CO2 Util.* **2020**, *38*, 132-140.

165. Singh Dhankhar, S.; Ugale, B.; Nagaraja, C. M., Co-Catalyst-Free Chemical Fixation of CO2 into Cyclic Carbonates by using Metal-Organic Frameworks as Efficient Heterogeneous Catalysts. *Chem. Asian J.* **2020**, *15*, 2403-2427.

166. Agrigento, P.; Al-Amsyar, S. M.; Sorée, B.; Taherimehr, M.; Gruttadauria, M.; Aprile, C.; Pescarmona, P. P., Synthesis and high-throughput testing of multilayered supported ionic liquid catalysts for the conversion of CO2 and epoxides into cyclic carbonates. *Catal. Sci. Technol.* **2014**, *4*, 1598-1607.

167. Aprile, C.; Giacalone, F.; Agrigento, P.; Liotta, L. F.; Martens, J. A.; Pescarmona, P. P.; Gruttadauria, M., Multilayered Supported Ionic Liquids as Catalysts for Chemical Fixation of Carbon Dioxide: A High-Throughput Study in Supercritical Conditions. *ChemSusChem* **2011**, *4*, 1830-1837.

168. Calabrese, C.; Liotta, L. F.; Giacalone, F.; Gruttadauria, M.; Aprile, C., Supported Polyhedral Oligomeric Silsesquioxane-Based (POSS) Materials as Highly Active Organocatalysts for the Conversion of CO2. *ChemCatChem* **2019**, *11*, 560-567.

169. Bivona, L. A.; Fichera, O.; Fusaro, L.; Giacalone, F.; Buaki-Sogo, M.; Gruttadauria, M.; Aprile, C., A polyhedral oligomeric silsesquioxane-based catalyst for the efficient synthesis of cyclic carbonates. *Catal. Sci. Technol.* **2015**, *5*, 5000-5007.

170. Gao, W.-Y.; Chrzanowski, M.; Ma, S., Metal–metalloporphyrin frameworks: a resurging class of functional materials. *Chem. Soc. Rev.* **2014**, *43*, 5841-5866.

171. Tashiro, K.; Aida, T., Metalloporphyrin hosts for supramolecular chemistry of fullerenes. *Chem. Soc. Rev.* **2007**, *36*, 189-197.

172. Astruc, D., Transition-metal Nanoparticles in Catalysis: From Historical Background to the State-of-the Art. In *Nanoparticles and Catalysis*, Astruc, D., Ed. **2007**; pp 1-48.

173. Goksu, H.; Sert, H.; Kilbas, B.; Sen, F., Recent Advances in the Reduction of Nitro Compounds by Heterogenous Catalysts. *Curr. Org. Chem.* **2017**, *21*, 794-820.

174. Orlandi, M.; Brenna, D.; Harms, R.; Jost, S.; Benaglia, M., Recent Developments in the Reduction of Aromatic and Aliphatic Nitro Compounds to Amines. *Org. Process. Res. Dev.* **2018**, *22*, 430-445.

175. Zhao, W.; Wang, T.; Wang, B.; Wang, R.; Xia, Y.; Liu, M.; Tian, L., Controllable synthesis of oxygenated carbon supported palladium nanodendrites for highly efficient nitroaromatics reduction. *Colloids Surf. A Physicochem. Eng. Asp.* **2023**, *658*, 130677.

176. Hareesh, H. N.; Minchitha, K. U.; Venkatesh, K.; Nagaraju, N.; Kathyayini, N., Environmentally benign selective hydrogenation of α,β-unsaturated aldehydes and reduction of aromatic nitro compounds using Cu based bimetallic nanoparticles supported on multiwalled carbon nanotubes and mesoporous carbon. *RSC Adv.* **2016**, *6*, 82359-82369.

177. Lu, Y.-M.; Zhu, H.-Z.; Li, W.-G.; Hu, B.; Yu, S.-H., Size-controllable palladium nanoparticles immobilized on carbon nanospheres for nitroaromatic hydrogenation. *J. Mater. Chem. A* **2013**, *1*, 3783-3788.

178. Ding, R.; Chen, Q.; Luo, Q.; Zhou, L.; Wang, Y.; Zhang, Y.; Fan, G., Salt template-assisted in situ construction of Ru nanoclusters and porous carbon: excellent catalysts toward hydrogen evolution, ammonia-borane hydrolysis, and 4-nitrophenol reduction. *Green Chem.* **2020**, *22*, 835-842.

179. Sadeghi, S.; Karimi, M.; Radfar, I.; Gavinehroudi, R. G.; Saberi, D.; Heydari, A., Efficient strategy for interchangeable roles in a green and sustainable redox catalytic system: IL/PdII-decorated SBA-15 as a mesoporous nanocatalyst. *New J. Chem.* **2021**, *45*, 6682-6692.

180. Yadav, D.; Awasthi, S. K., A Pd confined hierarchically conjugated covalent organic polymer for hydrogenation of nitroaromatics: catalysis, kinetics, thermodynamics and mechanism. *Green Chem.* **2020**, *22*, 4295-4303.

181. Paul, D.; Das, S.; Saha, S.; Sharma, H.; Goswami, R. K., Intramolecular Heck Reaction in Total Synthesis of Natural Products: An Update. *Eur. J. Org. Chem.* **2021**, *2021*, 2057-2076.

182. Beletskaya, I. P.; Cheprakov, A. V., The Heck Reaction as a Sharpening Stone of Palladium Catalysis. *Chem. Rev.* **2000**, *100*, 3009-3066.

183. Burguete, M. I.; García-Verdugo, E.; Garcia-Villar, I.; Gelat, F.; Licence, P.; Luis, S. V.; Sans, V., Pd catalysts immobilized onto gel-supported ionic liquid-like phases (g-SILLPs): A remarkable effect of the nature of the support. *J. Catal.* **2010**, *269*, 150-160.

184. Köhler, K.; Kleist, W.; Pröckl, S. S., Genesis of Coordinatively Unsaturated Palladium Complexes Dissolved from Solid Precursors during Heck Coupling Reactions and Their Role as Catalytically Active Species. *Inorg. Chem.* **2007**, *46*, 1876-1883.

185. Sans, V.; Gelat, F.; Karbass, N.; Burguete, M. I.; García-Verdugo, E.; Luis, S. V., Polymer Cocktail: A Multitask Supported Ionic Liquid-Like Species to Facilitate Multiple and Consecutive C-C Coupling Reactions. *Adv. Synth. Catal.* **2010**, *352*, 3013-3021.

186. Gruttadauria, M.; Giacalone, F.; Noto, R., "Release and catch" catalytic systems. *Green Chem.* **2013**, *15*, 2608-2618.

187. Pavia, C.; Giacalone, F.; Bivona, L. A.; Salvo, A. M. P.; Petrucci, C.; Strappaveccia, G.; Vaccaro, L.; Aprile, C.; Gruttadauria, M., Evidences of release and catch mechanism in the Heck reaction catalyzed by palladium immobilized on highly cross-linked-supported imidazolium salts. *J. Mol. Catal. A Chem.* **2014**, *387*, 57-62.

188. Buscemi, R.; Giacalone, F.; Orecchio, S.; Gruttadauria, M., Cross-Linked Imidazolium Salts as Scavengers for Palladium. *ChemPlusChem* **2014**, *79*, 421-426.

189. Agrigento, P.; Beier, M. J.; Knijnenburg, J. T. N.; Baiker, A.; Gruttadauria, M., Highly cross-linked imidazolium salt entrapped magnetic particles – preparation and applications. *J. Mater. Chem.* **2012**, *22*, 20728-20735.

190. Li, P.; Wang, L.; Zhang, L.; Wang, G.-W., Magnetic Nanoparticles-Supported Palladium: A Highly Efficient and Reusable Catalyst for the Suzuki, Sonogashira, and Heck Reactions. *Adv. Synth. Catal.* **2012**, *354*, 1307-1318.

191. Wang, J.; Xu, B.; Sun, H.; Song, G., Palladium nanoparticles supported on functional ionic liquid modified magnetic nanoparticles as recyclable catalyst for room temperature Suzuki reaction. *Tetrahedron Lett.* **2013**, *54*, 238-241.

192. Siamaki, A. R.; Lin, Y.; Woodberry, K.; Connell, J. W.; Gupton, B. F., Palladium nanoparticles supported on carbon nanotubes from solventless preparations: versatile catalysts for ligand-free Suzuki cross coupling reactions. *J. Mater. Chem. A* **2013**, *1*, 12909-12918.

193. Cano, M.; Benito, A. M.; Maser, W. K.; Urriolabeitia, E. P., One-step microwave synthesis of palladium–carbon nanotube hybrids with improved catalytic performance. *Carbon* **2011**, *49*, 652-658.

194. Zhang, B.; Shao, L.; Zhang, W.; Sun, X.; Pan, X.; Su, D. S., Interaction between Palladium Nanoparticles and Surface-Modified Carbon Nanotubes: Role of Surface Functionalities. *ChemCatChem* **2014**, *6*, 2607-2612.

CHAPTER II

Bifunctional Heterogeneous Catalysts in CO_2 Conversion: An Introduction to Chapters III, IV and V

CHAPTER II

Bifunctional Heterogeneous Catalysts in CO_2 Conversion: An Introduction to Chapters III, IV and V

2.1 Introduction

The high concentration of carbon dioxide (CO_2) in the atmosphere is responsible for the greenhouse effect and the consequent changes to the global climate. This increased emission is mainly due to fossil fuel combustion for energy production, transportation, and industrial processes. Against this background, the scientific community is committed to seeking alternative energy sources and developing systems for the chemical utilization of CO_2.[1] A viable strategy that enables the reduction of CO_2 emissions is the carbon capture and storage (CCS).[2-3] The CCS has emerged as a tangible process that aims to reduce negative impacts on humans and environment. On the other hand, carbon dioxide is an interesting raw material for the production of valuable chemicals.[4] Indeed, it is possible to consider this molecule as a source of renewable feedstock rather than as a "waste" product. Furthermore, it should be emphasized that this renewable source of carbon is abundant, economical, non-toxic and non-flammable. However, because of its low reactivity, processes that could use carbon dioxide as a sustainable resource requires the use of highly energetic starting materials such as hydrogen, epoxides, and amines employed in conjunction with a catalyst that can adequately decrease the activation energy of the selected reaction. A significant transformation is the incorporation of CO_2 into epoxides to generate cyclic carbonates.[3,5-9] It is because of their interesting features, such as low vapor pressure, high boiling point, low toxicity, and biodegradability, cyclic carbonates find applications in both industry and academia. Their uses include those as polar solvents with a high boiling point, electrolytes solvents for lithium ion batteries, precursors for polymeric materials, and additives for fuels.[5,10] Furthermore, organic carbonates are considered a green alternative to replace various toxic chemical reagents.[11-13] From the point of view of Green Chemistry and sustainability, the relevance of the synthesis of five-membered cyclic carbonates, from carbon dioxide and epoxides, lies in the transformation of a renewable source into a valuable chemical product, as well as in the possibility of carrying out the process under solvent-free conditions. In addition, the process exhibits 100% atomic economy and the use of an easily recoverable heterogeneous catalyst can improve the greenness of the reaction.[14-15] Heterogeneous catalysts are often at the forefront of the chemical industry, as the

possibility of recycling the material in a very simple way allows for a more economical process, increasing the turnover number of the process.[16] In this context, there is growing interest in the design of catalytic systems that include Lewis acid sites for electrophilic activation of the epoxy substrate and nucleophilic species for promoting epoxide ring opening. Indeed, catalysis with Lewis acids coupled to halogen anions has been shown to be efficient compared with the use of organocatalysts. This is due to the possibility of synergy/cooperation that is created between the two active sites, which greatly increases the activity of the catalyst. Arai *et al.* were the first to state that the activity of ionic liquids, such as imidazolium salts, is greatly enhanced by the addition in homogenous conditions of Lewis acid compounds of metal halides or metal complexes that by themselves have no or little activity (**Figure 1**).[17]
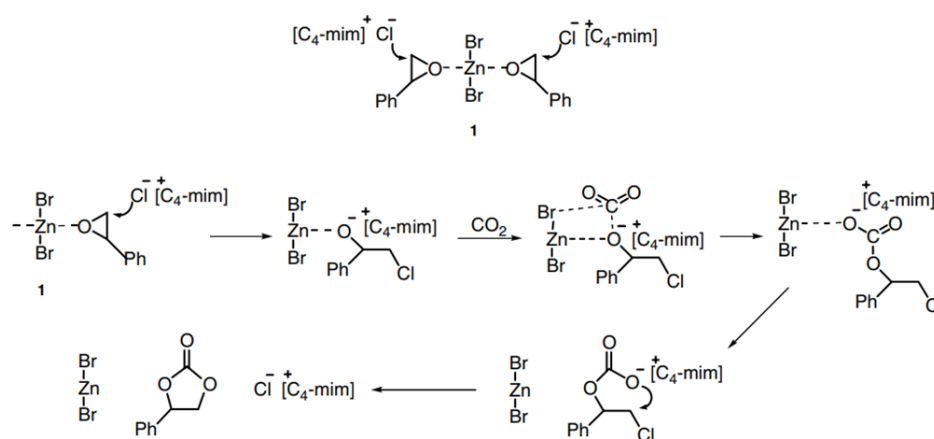

Figure 1. Proposed mechanism for the synthesis of styrene carbonate from styrene oxide and CO_2 with $ZnBr_2$/[C_4-mim]Cl catalyst by Ari *et al.*[17]

The use of polymeric Lewis acid catalysts in combination with ammonium halide salts as co-catalysts has been also largely employed. In **Figure 2**, an example of aluminium porphyrin-based hyper-cross linked polymer (0.25 mol%) was used in the presence of TBAB (2 mol%) under mild conditions to give quantitative conversion of propylene oxide. Under such conditions, aluminium polymer alone or TBAB alone did not give conversion.[18]
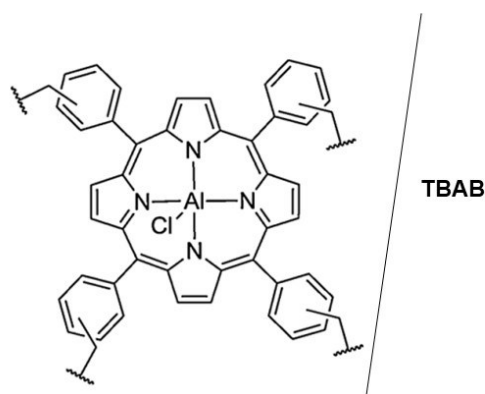

Figure 2. Aluminium porphyrin-based hyper-cross linked polymer and TBAB as co-catalyst.

Xiong and coworkers[19] demonstrated the synergistic effect between the two active sites by designing different polymers based on phosphonium salts and homogeneously incorporating different metalloporphyrins. They showed that the most active combination was CoTPP/Ph$_3$PHexBr for the cycloaddition reaction of CO_2 and epoxide at temperature (50 °C) and pressure (1 atm CO_2).

In these binary systems, the formation of cyclic carbonates in terms of TOF values is calculated by considering only the amount of Lewis acid catalyst, even when the amount of Lewis base is used in large amounts relative to Lewis acid, which in turn does not catalyze the reaction when used alone. Moreover, although homogeneous catalysts achieve high efficiency in the cycloaddition reaction of CO_2, the decision to rely on a heterogeneous bifunctional catalyst is probably more attractive than using a homogeneous catalytic system consisting of two separate components (binary systems). This point could be advantageous in terms of environmental impact and cost-effectiveness. Indeed, when employing homogeneous catalysts, the recovery and recycling of the catalyst, along with the laborious purification process of cyclic carbonates, result in a significant consumption of time and energy.[20]

In this context, a rational design of the heterogeneous bifunctional catalyst at the molecular scale is of paramount importance. For this purpose, metalloporphyrin complexes represent ideal molecular scaffolds since the porphyrin core can be properly functionalized in order to improve the activity of the final catalyst. The high versatility of these complexes, together with that of another highly exploited class of complex, namely Salen-based metal complexes, is witnessed by their widespread use in the cycloaddition of CO_2 with epoxides.[21-27] Various complexes based on many metals, such as Zn, Al, Mg, Ni, Cr, and Co have been incorporated in the structure of different heterogeneous bifunctional catalysts used for this aim.[28-40]

In the last years, several heterogeneous catalytic systems, such as polymeric matrix, covalent organic frameworks (COFs), porous organic polymers (POPs), porous ionic polymers (PIPs), have been developed with the goal of having the two active sites in the same structure.[22,27,34,41-46]

In our research group, Morena *et al.*[43] developed a bifunctional heterogeneous catalyst based on aluminum porphyrin and imidazolium salt supported on polyhedral octavinylsilsesquioxane (POSS) (**Figure 3**). POSS-TSP-AlCl-imiBr leads to a catalyst with high catalytic performance due to the synergistic effects exerted by the metal centers and halide ions. The hybrid catalyst showed high catalytic activity with a range of different epoxides, with TON and TOF values of up to 16,000 and 5,000, respectively.
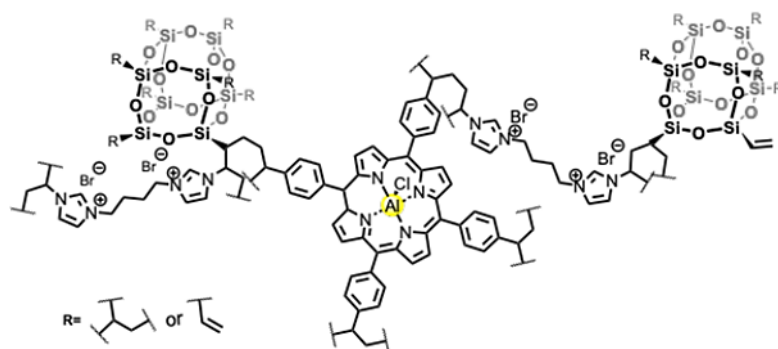
Figure 3. Suggested structure for the random co-polymer POSS-TSP-AlCl-imiBr.

In this PhD dissertations, we analyze the effect of Al or Mg porphyrin as the Lewis acid center and bromide ions as the counterion of imidazolium or phosphonium moieties when covalently bonded, focusing on the role played by the proximity between the two (co)catalysts on the overall catalytic performance. These bifunctional systems have been designed to be supported or unsupported onto MWCNTs (Chapter III-V). These innovative organo-catalytic systems demonstrate an efficient approach towards catalysis, integrating green chemistry concepts into their design.

2.2 References

1. Inhaber, H., Why wind power does not deliver the expected emissions reductions. *Renew. Sust. Energ. Rev.* **2011** *15*, 2557–2562.

2. Adamu, A.; Russo-Abegão, F.; Boodhoo, K., Process intensification technologies for CO2 capture and conversion – a review. *BMC Chem. Eng.* **2020**, *2*, 2.

3. North, M.; Pasquale, R.; Young, C., Synthesis of cyclic carbonates from epoxides and CO2. *Green Chem.* **2010**, *12*, 1514-1539.

4. Song, Q.-W.; Zhou, Z.-H.; He, L.-N., Efficient, selective and sustainable catalysis of carbon dioxide. *Green Chem.* **2017**, *19*, 3707-3728.

5. Sakakura, T.; Kohno, K., The synthesis of organic carbonates from carbon dioxide. *Chem. Commun.* **2009**, 1312-1330.

6. Yan, S.; Li, W.; He, D.; He, G.; Chen, H., Recent research progress of metal-organic frameworks (MOFs) based catalysts for CO2 cycloaddition reaction. *Mol. catal.* **2023**, *550*, 113608.

7. Ma, H.; Liu, S.; Wang, H.; Li, G.; Zhao, K.; Cui, X.; Shi, F., In situ CO2 capture and transformation into cyclic carbonates using flue gas. *Green Chem.* **2023**, *25*, 2293-2298.

8. Urbani, D.; Rovegno, C.; Massi, A.; Leblebici, M. E.; Kayahan, E.; Polo, E.; Dambruoso, P., Efficiency in CO2-utilization strategies: The case of styrene carbonate synthesis in microdroplets conditions. *J. CO2 Util.* **2023**, *67*, 102328.

9. Valverde-González, A.; Borrallo-Aniceto, M. C.; Díaz, U.; Maya, E. M.; Gándara, F.; Sánchez, F.; Iglesias, M., Nitrogen-rich cobalt (II) MOFs as efficient bifunctional catalysts for single or tandem oxidation and CO2 conversion reactions. *J. CO2 Util.* **2023**, *67*, 102298.

10. Li, Q.; Chen, J.; Fan, L.; Kong, X.; Lu, Y., Progress in electrolytes for rechargeable Li-based batteries and beyond. *Green Energy Environ.* **2016**, *1*, 18-42.

11. Parker, H. L.; Sherwood, J.; Hunt, A. J.; Clark, J. H., Cyclic Carbonates as Green Alternative Solvents for the Heck Reaction. *ACS Sustain. Chem. Eng.* **2014**, *2*, 1739-1742.

12. Duval, A.; Avérous, L., Cyclic Carbonates as Safe and Versatile Etherifying Reagents for the Functionalization of Lignins and Tannins. *ACS Sustain. Chem. Eng.* **2017**, *5*, 7334-7343.

13. Pyo, S.-H.; Park, J. H.; Chang, T.-S.; Hatti-Kaul, R., Dimethyl carbonate as a green chemical. *Curr. Opin. Green Sustain. Chem.* **2017**, *5*, 61-66.

14. Anastas, P.; Eghbali, N., Green Chemistry: Principles and Practice. *Chem. Soc. Rev.* **2010**, *39*, 301-312.

15. Calabrese, C.; Giacalone, F.; Aprile, C., Hybrid Catalysts for CO2 Conversion into Cyclic Carbonates. *Catalysis* **2019**, *9*, 325.

16. de Vries, J. G.; Jackson, S. D., Homogeneous and heterogeneous catalysis in industry. *Catal. Sci. Technol.* **2012**, *2*, 2009-2009.

17. Sun, J.; Fujita, S.-i.; Arai, M., Development in the green synthesis of cyclic carbonate from carbon dioxide using ionic liquids. *J. Organomet. Chem.* **2005**, *690*, 3490-3497.

18. Chen, Y.; Luo, R.; Xu, Q.; Zhang, W.; Zhou, X.; Ji, H., State-of-the-Art Aluminum Porphyrin-based Heterogeneous Catalysts for the Chemical Fixation of CO2 into Cyclic Carbonates at Ambient Conditions. *ChemCatChem* **2017**, *9*, 767-773.

19. Wang, K.; Liu, Y.; Wang, S.; Dai, Z.; Xiong, Y., Synergistic catalysis of metalloporphyrins and phosphonium ionic liquids for the efficient transformation of CO2 under ambient conditions. *J. CO2 Util.* **2021**, *48*, 101519.

20.   Singh Dhankhar, S.; Ugale, B.; Nagaraja, C. M., Co-Catalyst-Free Chemical Fixation of CO2 into Cyclic Carbonates by using Metal-Organic Frameworks as Efficient Heterogeneous Catalysts. *Chem. Asian J.* **2020**, *15*, 2403-2427.

21.   Kuznetsova, S. A.; Rulev, Y. A.; Larionov, V. A.; Smol'yakov, A. F.; Zubavichus, Y. V.; Maleev, V. I.; Li, H.; North, M.; Saghyan, A. S.; Belokon, Y. N., Self-Assembled Ionic Composites of Negatively Charged Zn(salen) Complexes and Triphenylmethane Derived Polycations as Recyclable Catalysts for the Addition of Carbon Dioxide to Epoxides. *ChemCatChem* **2019**, *11*, 511-519.

22.   Liu, T.-T.; Liang, J.; Huang, Y.-B.; Cao, R., A bifunctional cationic porous organic polymer based on a Salen-(Al) metalloligand for the cycloaddition of carbon dioxide to produce cyclic carbonates. *Chem. Commun.* **2016**, *52*, 13288-13291.

23.   Luo, R.; Zhang, W.; Yang, Z.; Zhou, X.; Ji, H., Synthesis of cyclic carbonates from epoxides over bifunctional salen aluminum oligomers as a CO2-philic catalyst: Catalytic and kinetic investigation. *J. CO2 Util.* **2017**, *19*, 257-265.

24.   Carvalho, P. A.; Comerford, J. W.; Lamb, K. J.; North, M.; Reiss, P. S., Influence of Mesoporous Silica Properties on Cyclic Carbonate Synthesis Catalysed by Supported Aluminium(Salen) Complexes. *Adv. Synth. Catal.* **2019**, *361*, 345-354.

25.   Luo, R.; Chen, Y.; He, Q.; Lin, X.; Xu, Q.; He, X.; Zhang, W.; Zhou, X.; Ji, H., Metallosalen-Based Ionic Porous Polymers as Bifunctional Catalysts for the Conversion of CO2 into Valuable Chemicals. *ChemSusChem* **2017**, *10*, 1526-1533.

26.   Li, J.; Han, Y.; Lin, H.; Wu, N.; Li, Q.; Jiang, J.; Zhu, J., Cobalt–Salen-Based Porous Ionic Polymer: The Role of Valence on Cooperative Conversion of CO2 to Cyclic Carbonate. *ACS Appl. Mater. Interfaces* **2020**, *12*, 609-618.

27.   Seo, Y. H.; Hyun, Y. B.; Lee, H. J.; Lee, H. C.; Lee, J. H.; Jeong, S. M.; Lee, B. Y., CO2/Propylene Oxide Copolymerization with a Bifunctional Catalytic System Composed of Multiple Ammonium Salts and a Salen Cobalt Complex Containing Sulfonate Anions. *Macromol. Res.* **2021**, *29*, 855-863.

28.   Jayakumar, S.; Li, H.; Tao, L.; Li, C.; Liu, L.; Chen, J.; Yang, Q., Cationic Zn-Porphyrin Immobilized in Mesoporous Silicas as Bifunctional Catalyst for CO2 Cycloaddition Reaction under Cocatalyst Free Conditions. *ACS Sustain. Chem. Eng.* **2018**, *6*, 9237-9245.

29.   Liu, L.; Jayakumar, S.; Chen, J.; Tao, L.; Li, H.; Yang, Q.; Li, C., Synthesis of Bifunctional Porphyrin Polymers for Catalytic Conversion of Dilute CO2 to Cyclic Carbonates. *ACS Appl. Mater. Interfaces* **2021**, *13*, 29522-29531.

30.   Sharma, N.; Dhankhar, S. S.; Nagaraja, C. M., Environment-friendly, co-catalyst- and solvent-free fixation of CO2 using an ionic zinc(ii)–porphyrin complex immobilized in porous metal–organic frameworks. *Sustain. Energy Fuels* **2019**, *3*, 2977-2982.

31.   Chen, Y.; Luo, R.; Ren, Q.; Zhou, X.; Ji, H., Click-Based Porous Ionic Polymers with Intercalated High-Density Metalloporphyrin for Sustainable CO2 Transformation. *Ind. Eng. Chem. Res.* **2020**, *59*, 20269-20277.

32.   Liu, X.; Zhou, F.; Chen, M.; Xu, W.; Liu, H.; Zhong, J.; Luo, R., Synergistically Converting Carbon Dioxide into Cyclic Carbonates by Metalloporphyrin-Based Cationic Polymers with Imidazolium Functionality. *ChemistrySelect* **2021**, *6*, 583-588.

33.   Chen, Y.; Ren, Q.; Zeng, X.; Tao, L.; Zhou, X.; Ji, H., Sustainable synthesis of multifunctional porous metalloporphyrin polymers for efficient carbon dioxide transformation under mild conditions. *Chem. Eng. Sci.* **2021**, *232*, 116380.

34. Ema, T.; Miyazaki, Y.; Taniguchi, T.; Takada, J., Robust porphyrin catalysts immobilized on biogenous iron oxide for the repetitive conversions of epoxides and CO2 into cyclic carbonates. *Green Chem.* **2013**, *15*, 2485-2492.

35. Yi, Q.; Liu, T.; Wang, X.; Shan, Y.; Li, X.; Ding, M.; Shi, L.; Zeng, H.; Wu, Y., One-step multiple-site integration strategy for CO2 capture and conversion into cyclic carbonates under atmospheric and cocatalyst/metal/solvent-free conditions. *Appl. Catal. B Env.* **2021**, *283*, 119620.

36. Chen, Y.; Luo, R.; Xu, Q.; Jiang, J.; Zhou, X.; Ji, H., Charged Metalloporphyrin Polymers for Cooperative Synthesis of Cyclic Carbonates from CO2 under Ambient Conditions. *ChemSusChem* **2017**, *10*, 2534-2541.

37. Jayakumar, S.; Li, H.; Chen, J.; Yang, Q., Cationic Zn–Porphyrin Polymer Coated onto CNTs as a Cooperative Catalyst for the Synthesis of Cyclic Carbonates. *ACS Appl. Mater. Interfaces* **2018**, *10*, 2546-2555.

38. Chen, Y.; Luo, R.; Xu, Q.; Jiang, J.; Zhou, X.; Ji, H., Metalloporphyrin Polymers with Intercalated Ionic Liquids for Synergistic CO2 Fixation via Cyclic Carbonate Production. *ACS Sustain. Chem. Eng.* **2018**, *6*, 1074-1082.

39. Liu, J.; Zhao, G.; Cheung, O.; Jia, L.; Sun, Z.; Zhang, S., Highly Porous Metalloporphyrin Covalent Ionic Frameworks with Well-Defined Cooperative Functional Groups as Excellent Catalysts for CO$_2$ Cycloaddition. *Chem. Eur. J.* **2019**, *25*, 9052-9059.

40. Wang, W.; Wang, Y.; Li, C.; Yan, L.; Jiang, M.; Ding, Y., State-of-the-Art Multifunctional Heterogeneous POP Catalyst for Cooperative Transformation of CO2 to Cyclic Carbonates. *ACS Sustain. Chem. Eng.* **2017**, *5*, 4523-4528.

41. Wang, W.; Li, C.; Yan, L.; Wang, Y.; Jiang, M.; Ding, Y., Ionic Liquid/Zn-PPh3 Integrated Porous Organic Polymers Featuring Multifunctional Sites: Highly Active Heterogeneous Catalyst for Cooperative Conversion of CO2 to Cyclic Carbonates. *ACS Catal.* **2016**, *6*, 6091-6100.

42. Naveen, K.; Ji, H.; Kim, T. S.; Kim, D.; Cho, D.-H., C3-symmetric zinc complexes as sustainable catalysts for transforming carbon dioxide into mono- and multi-cyclic carbonates. *Appl. Catal. B Env.* **2021**, *280*, 119395.

43. Morena, A.; Campisciano, V.; Santiago-Portillo, A.; Gruttadauria, M.; Giacalone, F.; Aprile, C., POSS-Al-porphyrin-imidazolium cross-linked network as catalytic bifunctional platform for the conversion of CO2 with epoxides. *Fuel* **2023**, *336*, 126819.

44. Campisciano, V.; Valentino, L.; Morena, A.; Santiago-Portillo, A.; Saladino, N.; Gruttadauria, M.; Aprile, C.; Giacalone, F., Carbon nanotube supported aluminum porphyrin-imidazolium bromide crosslinked copolymer: A synergistic bifunctional catalyst for CO2 conversion. *J. CO2 Util.* **2022**, *57*, 101884.

45. Wang, W.; Wang, Y.; Li, C.; Yan, L.; Jiang, M.; Ding, Y., State-of-the-Art Multifunctional Heterogeneous POP Catalyst for Cooperative Transformation of CO2 to Cyclic Carbonates. *ACS Sustain. Chem. Eng.* **2017**, *5*, 4523-4528.

46. Dai, Z.; Tang, Y.; Zhang, F.; Xiong, Y.; Wang, S.; Sun, Q.; Wang, L.; Meng, X.; Zhao, L.; Xiao, F.-S., Combination of binary active sites into heterogeneous porous polymer catalysts for efficient transformation of CO2 under mild conditions. *Chinese J. Catal.* **2021**, *42*, 618-626.

CHAPTER III

Carbon Nanotube Supported Aluminum Porphyrin-Imidazolium Bromide Crosslinked Copolymer: A Synergistic Bifunctional Catalyst for CO$_2$ Conversion
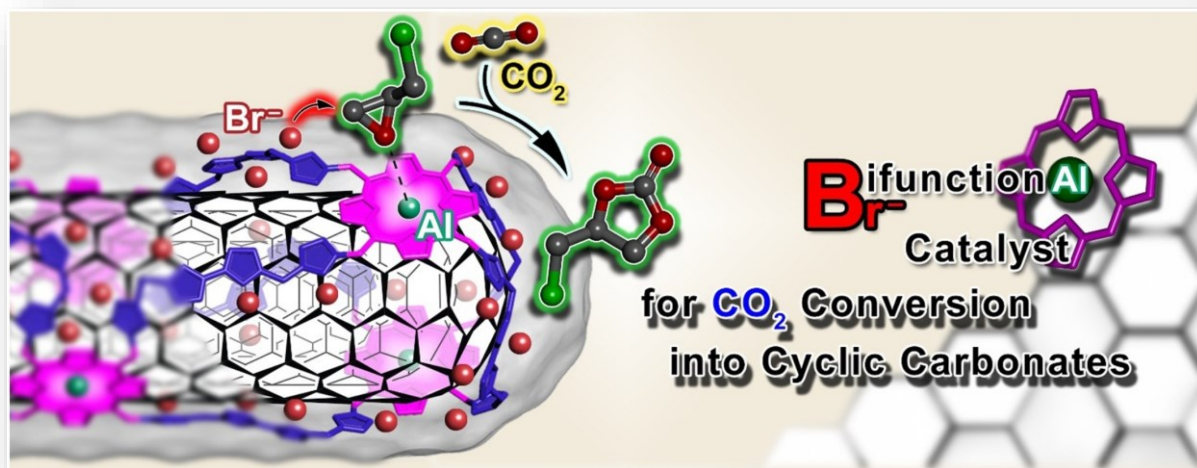

This chapter is based on:

CHAPTER III

Carbon Nanotube Supported Aluminum Porphyrin-Imidazolium Bromide Crosslinked Copolymer: A Synergistic Bifunctional Catalyst for CO₂ Conversion

3.1 Abstract

The increased awareness of the catastrophic consequences caused by the accumulation of greenhouse gases into the atmosphere has generated a large mobilization aimed at CO_2 mitigation. Herein, in the spirit of the transformation of a waste as CO_2 into value added products, we propose an efficient preparation of two different hybrid systems based on aluminum chloride tetrastyrylporphyrin (**TSP-Al-Cl**) and 1,4-butanediyl-3,3'-bis-1-vinylimidazolium dibromide copolymerized in the presence (**MWCNT-TSP-AlCl-imi**) and in absence (**TSP-AlCl-imi**) of multi-walled carbon nanotubes(MWCNTs) for the CO_2 utilization in the synthesis of cyclic carbonates. The so-prepared materials have been thoroughly characterized by means of several spectroscopic and analytical techniques. The **MWCNT-TSP-AlCl-imi** heterogenous catalyst enabled the highly efficient chemical transformation of CO_2 and epoxides into cyclic carbonates with high turnover number (TON) and frequency (TOF) values at low temperature down to 30 °C in solvent-free conditions. **MWCNT-TSP-AlCl-imi** proved to be a very stable and reusable heterogeneous catalyst in consecutive cycles without the need of any reactivation procedure and no leaching phenomena. Furthermore, the optimal morphology of **MWCNT-TSP-AlCl-imi**, with the crosslinked polymer uniformly distributed onto MWCNTs backbone, resulted in a more active catalyst with a TON double than the unsupported one. The enhanced activity of **MWCNT-TSP-AlCl-imi** can be ascribed to its higher surface area that permits fully accessible catalytic sites. Interestingly, **MWCNT-TSP-AlCl-imi** also showed a catalytic activity comparable to a reference homogeneous catalytic system, proving that synergism occurred between the metal centers and the nucleophilic sites due to their close proximity.

3.2 Results and discussion

The formylation of the Grignard reagent arising from 4-bromostyrene **1** gave rise to 4-vinylbenzaldehyde **2** (78%) that was reacted with pyrrole in propionic acid to obtain tetrastyrylporphyrin (**TSP**, 29%). The following reaction of **TSP** with Et$_2$AlCl led to the formation of tetrastyrylporphyrin aluminum chloride (**TSP-AlCl**, 47%) complex. **TSP-AlCl** was afterwards copolymerized with the bis-vinylimidazolium salt **bis-imi** to produce the copolymer **TSP-AlCl-imi**, or **MWCNT-TSP-AlCl-imi** when MWCNTs were used as support material (**Scheme 1**).
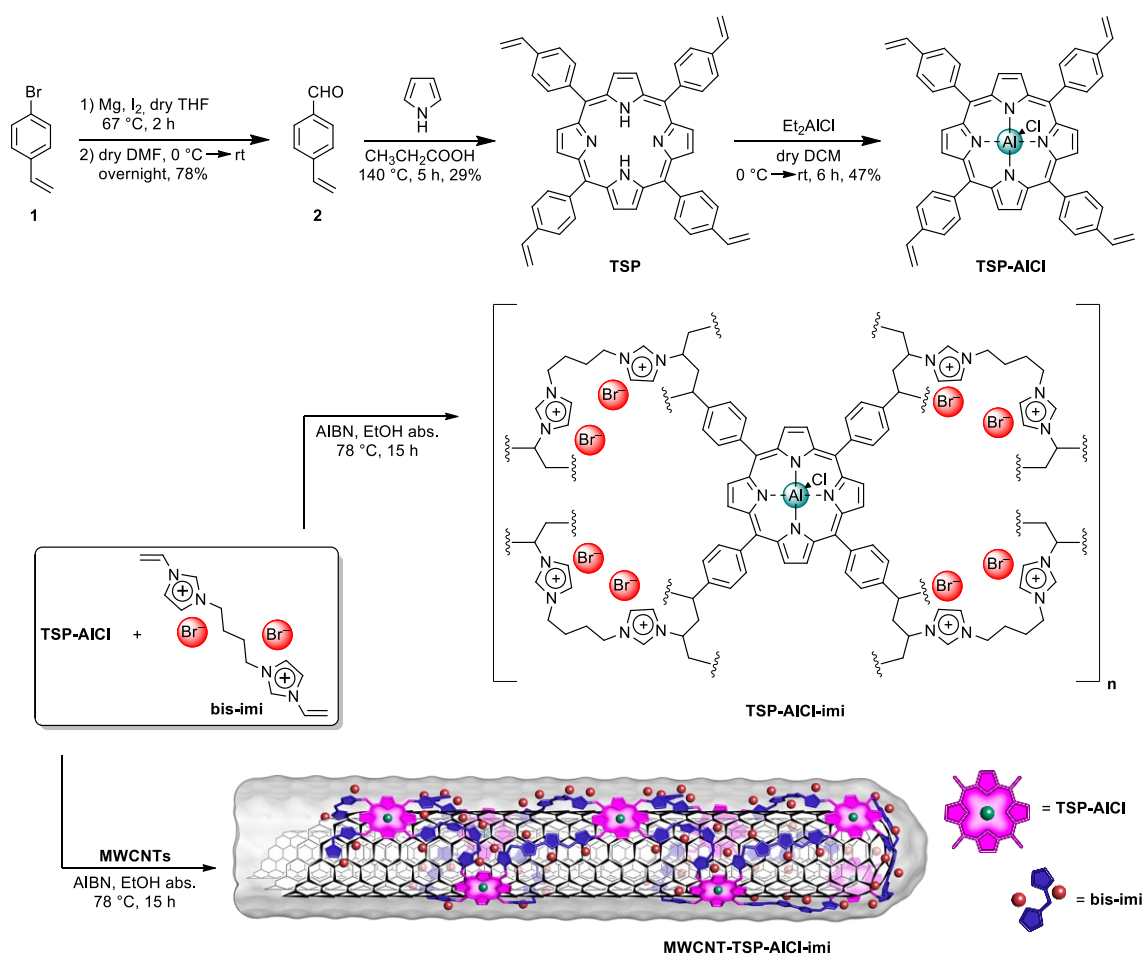
Scheme 1. Procedure for the preparation of **TSP-AlCl-imi** and **MWCNT-TSP-AlCl-imi**.

TSP and **TSP-AlCl** were firstly analyzed by means of FT-IR spectroscopy (**Figure 1**). The spectrum of **TSP** (**Figure 1**, black line) shows the typical bands associated with the free base porphyrin derivatives,[1-3] including the weak band centered at 3328 cm^{-1} ascribed to the N–H stretching, two bands at 1602 and 1557 cm^{-1} due to the pyrrole rings stretching vibrations, a band of medium intensity at 1471 cm^{-1} generated by the C–N–C bending, two bands at 987 and 966 cm^{-1} due to the asymmetric breathing motions of the pyrrole rings, and a strong absorption band at 803 cm^{-1} attributed to the N–H *out-of-plane* bending vibration mode. The

disappearance of these absorptions in the **TSP-AlCl** spectrum and the presence of a new strong absorption centered at 1012 cm^{-1} due to the porphyrin ring vibration in the metal complex (**Figure 1**, red line) confirmed the aluminum insertion into the porphyrin ring.
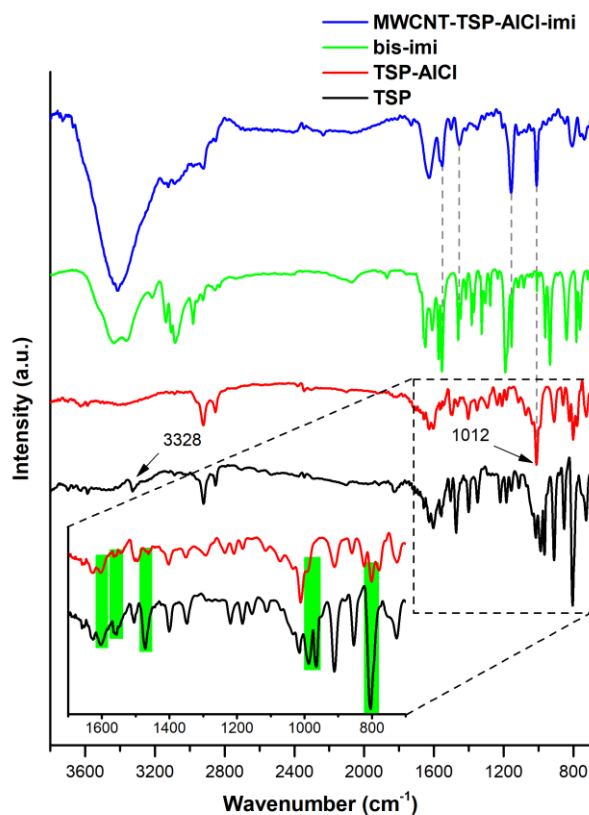

Figure 1. FT-IR spectra of **TSP** (black line), **TSP-AlCl** (red line), **bis-imi** (green line), and **MWCNT-TSP-AlCl-imi** (KBr pellet; blue line).

UV-Vis spectrum of the free-base **TSP** (**Figure 2**, dashed black line) exhibits a series of bands in the 370-450 nm and 480-680 nm regions due to π- π^* transitions. The absorption at 420 nm is associated with the Soret band ($S_0{\rightarrow}S_2$), whereas the Q-bands ($S_0{\rightarrow}S_1$) are shown in the magnification of **Figure 2** at 517, 553, 591, and 647 nm.[4] The complexation of the metal center resulted in a slightly red-shifted Soret band of **TSP-AlCl** at 422 nm (**Figure 2**, red line). However, as previously reported for similar Al(III)porphyrin derivatives,[5] the UV-Vis spectrum of **TSP-AlCl** was still characterized by the presence of four Q-bands but with different relative intensities (**Figure 2**).
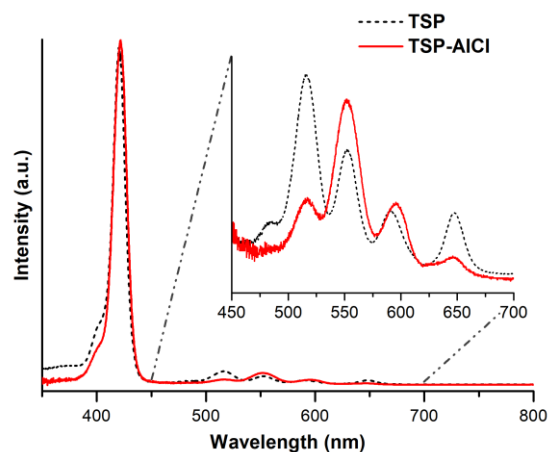
Figure 2. UV-Vis spectra of **TSP** (dashed black line), and **TSP-AlCl** (red line) in CHCl₃.

In addition, further evidence of the successful insertion of Al center into tetrastyrylporphyrin was provided by NMR spectroscopy (**Figures 3a-b**).
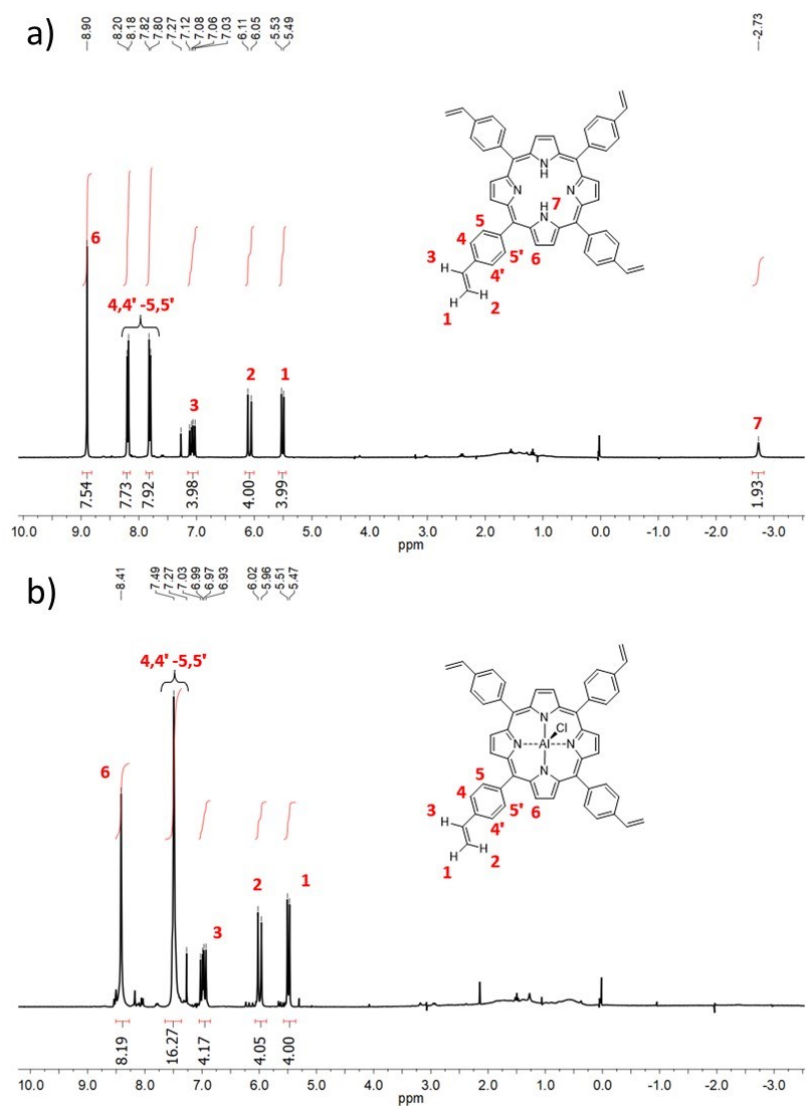

Figure 3. ¹H NMR (300 MHz, CDCl₃) of a) tetrastyrylporphyrin and b) tetrastyrylporphyrin aluminum chloride complex (**TSP-AlCl**).

In particular, the comparison of **TSP** and **TSP-AlCl** ^{1}H NMR spectra shows the disappearance of the pyrrolic protons resonating at -2.73 ppm after the complexation step (**Figure 3a** and **3b**).

As stated before, the copolymerization of **TSP-AlCl** with **bis-imi** gave **TSP-AlCl-imi**, whereas **MWCNT-TSP-AlCl-imi** was obtained when the copolymerization was carried out in the presence of MWCNTs as support. Both materials **TSP-AlCl-imi** and **MWCNT-TSP-AlCl-imi** were fully characterized by means of different techniques.

Once again, FT-IR spectroscopy has proved to be a useful tool for providing the first evidence of the successful copolymerization process, and the comparison of **MWCNT-TSP-AlCl-imi** spectrum (**Figure 1**, blue line), with those of **TSP-AlCl-imi** (red line) and **bis-imi** (green line) confirmed the presence of the Al porphyrin complex and bis-vinylimidazolium salt in the material **MWCNT-TSP-AlCl-imi**. The strong absorption at 1012 cm^{-1}, which is typical of **TSP-AlCl**, and the medium intensity absorptions at 1551, 1454, and 1157 cm^{-1}, associated with the imidazolium ring stretching vibration modes,[6-7] can be detected in the FT-IR spectrum of **MWCNT-TSP-AlCl-imi** (**Figure 1**, compare blue line with red and green lines). The high hygroscopicity of the copolymerized imidazolium-based salt causes the presence of the very strong and broad absorption band at 3415 cm^{-1} due to the O–H stretch, and the medium absorption at 1628 cm^{-1} generated by the H–O–H bending of the adsorbed water.

Materials **MWCNT-TSP-AlCl-imi** and **TSP-AlCl-imi** were further characterized by means of ^{13}C cross-polarization magic angle spinning (^{13}C CPMAS) NMR spectroscopy (**Figure 4**). Both spectra show the signals attributed to the resonance of the carbon atoms of the porphyrin core along with those of the imidazolium moieties in the 115-150 ppm region, whereas the signals ascribed to the aliphatic carbon atoms resonate in the upfield part of the spectra (20−60 ppm). Further proof of the good outcome of the polymerization was provided by the absence of any signal in the 100-115 ppm region where carbon atoms of vinyl group resonate.
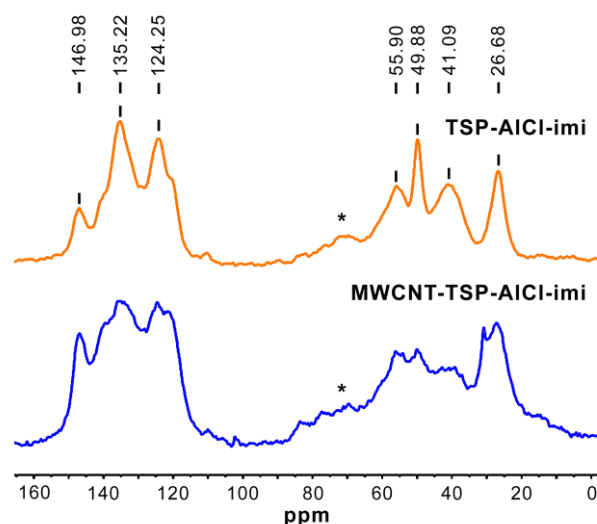
Figure 4. ^{13}C CP-MAS NMR of **TSP-AlCl-imi** (orange line) and **MWCNT-TSP-AlCl-imi** (blue line). Asterisks indicate spinning side bands.

X-ray photoelectron spectroscopy (XPS) analysis was used to analyze the outer surface of materials **MWCNT-TSP-AlCl-imi** and **TSP-AlCl-imi** (**Figure 5**). The survey spectrum of **MWCNT-TSP-AlCl-imi** (**Figure 5a**) confirms the presence of Al and Br arising from the **TSP-AlCl** and **bis-imi** monomers, respectively. The high-resolution XPS spectra of the N1s region of **MWCNT-TSP-AlCl-imi** (**Figure 5b**) can be deconvoluted into two peaks at 399.1 and 401.3 eV with atomic percentages of 34.4% and 65.6% corresponding to the nitrogen atoms of the porphyrin ring coordinated with aluminum (Al–N)[8] and the nitrogen atoms of the imidazolium rings,[9] respectively. The atomic percentages of the two different nitrogen atoms in **TSP-AlCl-imi** correspond to 18.0% and 82.0% for Al–N and imidazolium-N, respectively (**Figure 5c**).

Thermogravimetric analysis of **MWCNT-TSP-AlCl-imi** and **TSP-AlCl-imi** under nitrogen atmosphere was used to assess the good thermal stability of the materials. With the exception of the initial weight loss between room temperature and 100 °C due to the adsorbed moisture, the materials proved to be very stable up to 250 °C (**Figure 6**), at which temperature they start to degrade with a first weight loss centered at about 320 °C for both materials, and a second degradation peak centered at 438 and 462 °C for **MWCNT-TSP-AlCl-imi** and **TSP-AlCl-imi**, respectively. Conversely, TGA under nitrogen of pristine MWCNT showed only a 3% weight loss at 700 °C (**Figure 6**, black line).

The Al content of **MWCNT-TSP-AlCl-imi** (0.251 mmol/g) and **TSP-AlCl-imi** (0.444 mmol/g) was determined by means of inductively coupled plasma atomic emission spectroscopy (ICP-OES) analysis.
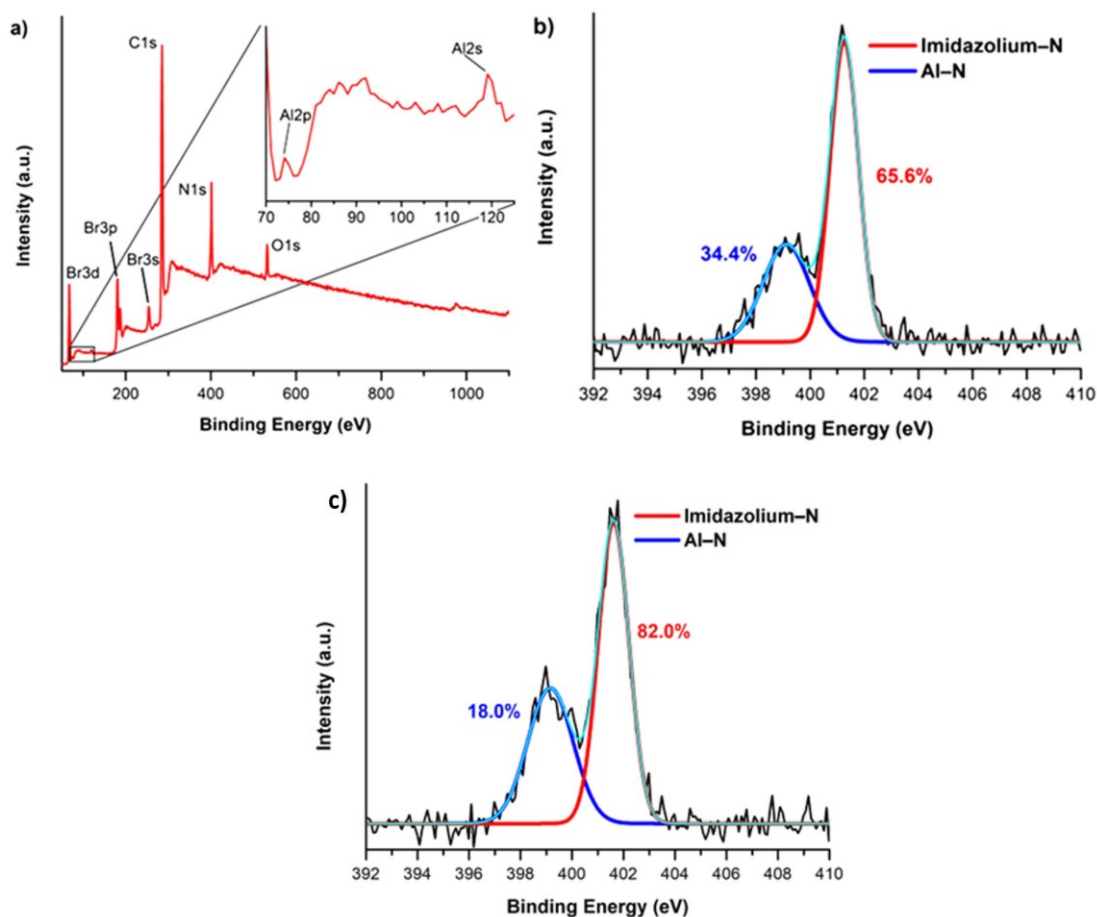
Figure 5. a) XPS survey spectrum of **MWCNT-TSP-AlCl-imi**, b) high-resolution N1s region **MWCNT-TSP-AlCl-imi** and c) high-resolution N1s region **TSP-AlCl-imi.**

Transmission electron microscopy (TEM) was used to investigate the morphology of **TSP-AlCl-imi** and **MWCNT-TSP-AlCl-imi** (**Figure 7**). TEM micrographs (**Figure 7a-c**) show that **TSP-AlCl-imi** forms a series of compact and large aggregates. In contrast, in the case of **MWCNT-TSP-AlCl-imi** (**Figure 7e, f**), MWCNTs offer a framework for the formation of individual nanoobject. Therefore, the comparison between the TEM images of the two different systems highlights how MWCNTs behave as suitable support material since they result uniformly wrapped by the copolymeric coverage along their whole surface. This is of particular importance for the properties of **MWCNT-TSP-AlCl-imi**, especially in term of surface area and accessibility of the reagents to active sites.

The first evidences highlighted by the TEM images analysis were corroborated by the nitrogen adsorption/desorption measurements carried out on pristine MWCNTs, **TSP-AlCl-imi**, and **MWCNT-TSP-AlCl-imi**. Specific surface area (SSA), estimated using the Brunauer-Emmett-Teller (BET) equation,[10] showed that **TSP-AlCl-imi** possess a very low SSA (<1 m^2/g). On the contrary, the immobilization of the copolymeric matrix onto MWCNTs to obtain

MWCNT-TSP-AlCl-imi, allowed to reach a higher SSA of 216 m^2/g, being 238 m^2/g the SSA of pristine MWCNTs.
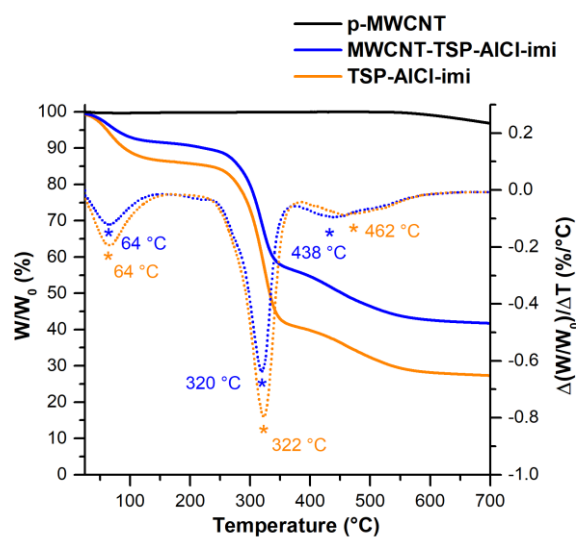

Figure 6. TGA (solid lines) under N$_2$ flow and DTG (dotted lines) of pristine MWCNT (black line), **TSP-AlCl-imi** (orange lines) and **MWCNT-TSP-AlCl-imi** (blue lines).

Once characterized, both **TSP-AlCl-imi** and **MWCNT-TSP-AlCl-imi** materials were tested in the conversion of carbon dioxide into cyclic carbonates using styrene oxide as target epoxide under solvent free conditions and without the addition of any co-catalytic species. The comparison of their catalytic activities was studied using an equal mass amount of both materials as illustrated in **Scheme 2**. Conversions of 49% and 55% into the corresponding cyclic carbonate were obtained using **TSP-AlCl-imi** and **MWCNT-TSP-AlCl-imi**, respectively.
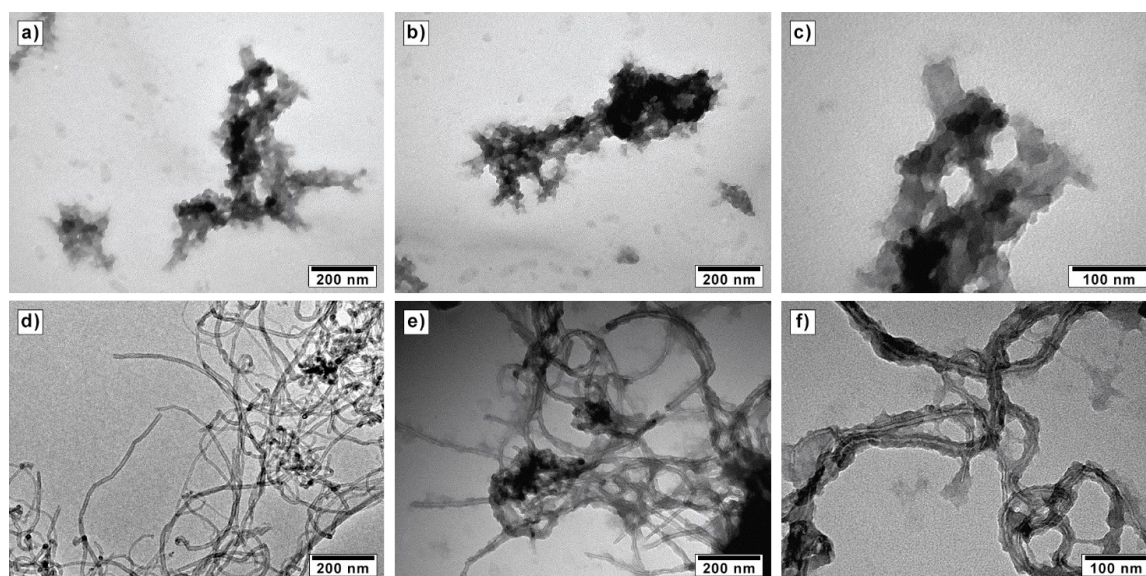

Figure 7. TEM micrographs of a-c) **TSP-AlCl-imi**, d) pristine MWCNTs, and e, f) **MWCNT-TSP-AlCl-imi**.

However, due to the different content of active species in the two materials, a more accurate comparison of the performances of **TSP-AlCl-imi** and **MWCNT-TSP-AlCl-imi** catalytic systems was carried out taking into account the turnover number (TON$_{Al}$; defined as moles of epoxide converted/moles of Al active sites) and turnover frequency (TOF$_{Al}$; TON$_{Al}$/reaction time in hours) values. The results, reported in **Scheme 2**, showed that **MWCNT-TSP-AlCl-imi** possesses higher catalytic activity than **TSP-AlCl-imi** in the conversion of styrene oxide. TON$_{Al}$ and TOF$_{Al}$ values (7649, and 2550 h^{-1}) of **MWCNT-TSP-AlCl-imi** are about twice as high as those of **TSP-AlCl-imi** (3868 and 1289 h^{-1}). These findings further emphasize the importance of the use of MWCNTs as support material for the performance improvement of the catalytic material. The optimal morphology of **MWCNT-TSP-AlCl-imi,** which possesses a high surface area and fully accessible catalytic sites, can be ascribed as the reason of its higher activity. Conversely, the unsupported copolymer **TSP-AlCl-imi** revealed to be a less active catalyst due to its low surface area that hinders the access of the reactants to the catalytic centers.
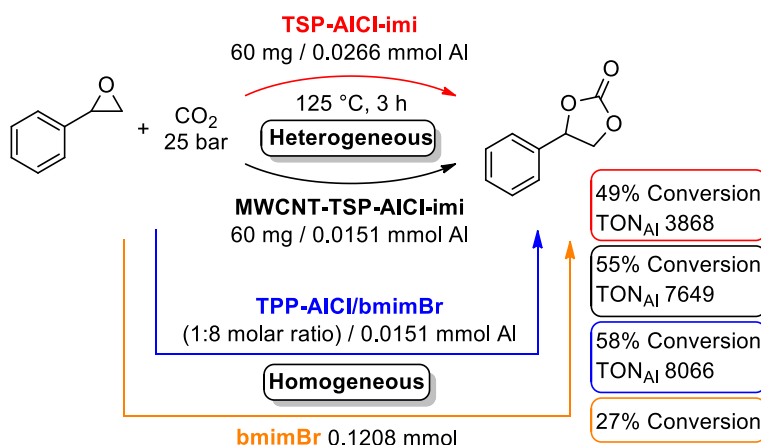
Scheme 2. Comparison of the activity between the heterogenous catalysts **TSP-AlCl-imi** and **MWCNT-TSP-AlCl-imi**, and the homogenous system **TPP-AlCl/bmimBr** and **bmimBr** in the reaction of styrene oxide with CO$_2$. Reaction conditions: styrene oxide (217 mmol), catalyst (0.0266 or 0.0151 mmol Al), 25 bar CO$_2$, 125 °C, 3 h, 500 rpm.

Two additional experiments in which tetraphenylporphyrin aluminum chloride complex **TPP-AlCl** with the addition of 1-butyl-3-methylimidazolium bromide (bmimBr) as source of Br⁻ (Al/Br⁻ molar ratio 1:8) or only **bmimBr** were used as homogeneous catalytic systems were carried out (**Scheme 2**). The aluminum loading used for the reaction in homogenous conditions was the same employed in the case of **MWCNT-TSP-AlCl-imi**, namely 0.0151 mmol. Interestingly, **MWCNT-TSP-AlCl-imi** showed an activity comparable to that of **TPP-AlCl/bmimBr** homogeneous system with conversion values of 55% and 58%, respectively. On the contrary, the reaction catalyzed by the Lewis base species alone

(**bmimBr**) reached a much lower conversion of 27%. For the sake of completeness, a blank test with just MWCNTs has been also carried out showing no conversion of the epoxide. The outstanding performance of **MWCNT-TSP-AlCl-imi** could be ascribed to the fine control achieved over the relative position of the two different catalytic sites (aluminum and bromide ions) which is missing in the case of the homogeneous **TPP-AlCl/bmimBr** mixture, that represent a more disordered system. The structure of the supported polymeric network formed by the linkage between the porphyrin core and the bis-vinylimidazolium salt ensures the close proximity between the metal centers and the bromide ions, which are able to cooperate and exert a synergistic effect during the catalytic cycle for the formation of the cyclic carbonate, as depicted in **Scheme 3**. In the step A, the oxygen atom of the epoxide interacts with the Lewis acidic aluminum site of the porphyrin core with the formation of a coordination complex, which is attacked by the nucleophile (Br$^-$) on the less-hindered side of epoxide to afford the Al-coordinated bromo alkoxide (step B). Subsequently, the insertion of CO_2 into the Al–O bond gave rise to a metal coordinated carbonate (step C), which undergoes an intramolecular SN_2 cyclization with the release of a bromide ion, which regenerate the catalyst, and the concomitant formation of the cyclic carbonate (step D). Therefore, **MWCNT-TSP-AlCl-imi** has proved to be a promising catalyst both from the point of view of its morphology, which ensures a high accessibility to the reactants, and of its molecular structure, which leads to an increase of the catalytic activity thank to the cooperation/synergism between the electrophilic and nucleophilic sites.
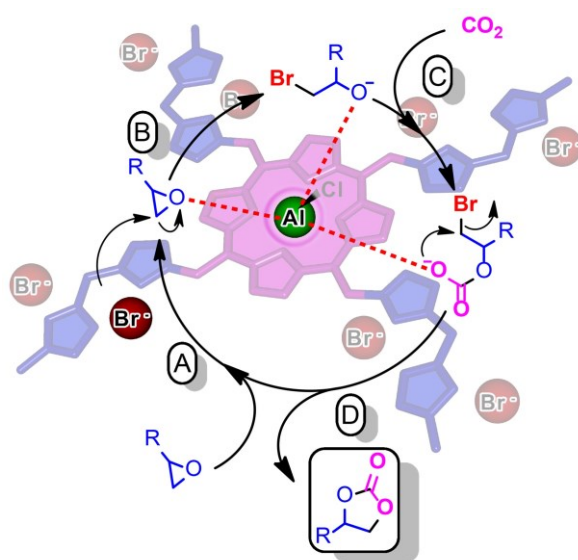
Scheme 3. Representation of the synergy between the Lewis acid and the bromide ion in the prepared bifunctional catalysts for the synthesis of cyclic carbonates.

The recyclability of both heterogeneous catalysts in the styrene oxide conversion was studied. Five consecutive runs were carried out and after each cycle the materials were easily recovered

by centrifugation and washed with toluene, ethanol, and diethyl ether without any additional activation treatment. The results, showed in **Figure 8a-b**, highlighted that both catalysts revealed to be robust and able to be used for multiple cycles without any decrease in catalytic activity.
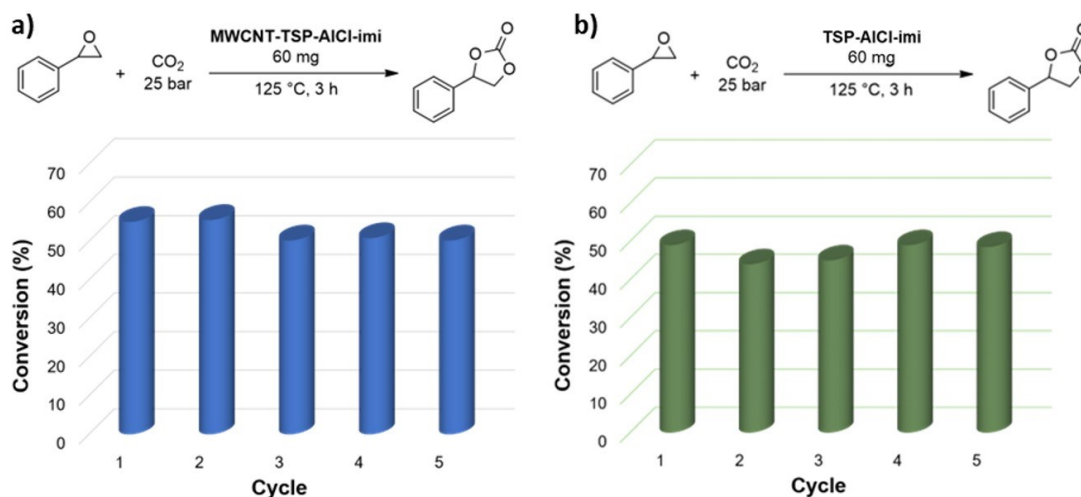
Figure 8. Recycling test of **MWCNT-TSP-AlCl-Imi** and **TSP-AlCl-Imi**. Reaction conditions: styrene oxide (210 mmol), 60 mg **MWCNT-TSP-AlCl-Imi** (0.0151 mmol Al) or 60 mg **TSP-AlCl-Imi** (0.0266 mmol Al), 25 bar CO_2, 3 h, 500 rpm.

Interestingly, the high-resolution XPS spectrum of the N1s region of the used **MWCNT-TSP-AlCl-imi** after the recycling tests showed that the catalyst was not affected by any notable alteration since the atomic percentages of the two different nitrogen atoms remained almost unchanged with respect to the fresh **MWCNT-TSP-AlCl-imi** (**Figures 4b** and **Figure 9**).
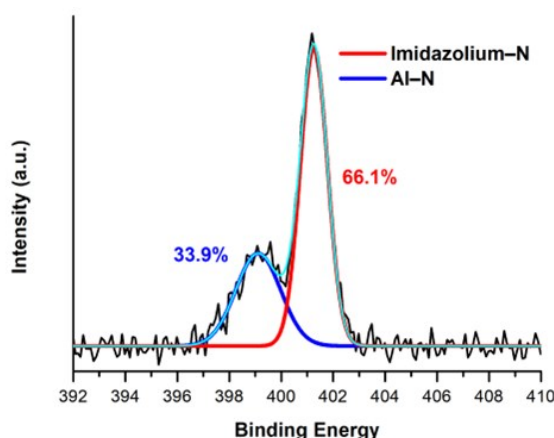
Figure 9. High-resolution XPS spectrum of the N1s region of used **MWCNT-TSP-AlCl-Imi** after five cycles.

More in-depth studies to exclude the presence in solution of catalytically active species at the end of the reaction were undertaken. The more active **MWCNT-TSP-AlCl-imi** catalyst was

subjected to a leaching test in the reaction of CO_2 with styrene oxide. At the end of the reaction, the material was removed by centrifugation and the liquid phase was again reacted in the same reaction conditions. The graph of the variation of CO_2 pressure during the reaction time showed that an almost constant pressure of carbon dioxide was maintained during the reaction. This finding was also confirmed by ^{1}H NMR analysis of the reaction mixture that showed only a 1.5% increase in the conversion of the styrene oxide into styrene carbonate confirming the absence of leached species in solution.

Once verified both the recyclability and the absence of any leaching, the substrate scope of **MWCNT-TSP-AlCl-imi** catalyst was further explored using, in addition to styrene oxide, a series of epoxides including epichlorohydrin, glycidol, and 1,4-butanediol diglycidyl ether (**Table 1**, **entries 1-12**).

Some of the catalytic tests were repeated thus confirming the good reproducibility of the experiments and indicating that the error associated to the catalytic data can be estimated in the range of +/- 2%. As shown in **Scheme 2** styrene oxide was transformed into the corresponding cyclic carbonate with a conversion of 55% when **MWCNT-TSP-AlCl-imi** (0.0151 mmol Al) was employed at 125 °C and with a reaction time of 3 h (entry 1). However, the reduction of the catalytic loading by half (0.0075 mmol Al) and the extension of the reaction time up to 20 h resulted in the increase of the conversion of styrene oxide up to 84 % with a TON value of 23400 (entry 2). In addition, full conversion (>95%) was reached in 18 h by increasing the reaction temperature up to 150 °C affording a TON value of 26800 (entry 3). The reactivity of epichlorohydrin was explored at three different temperatures, namely 50, 80, and 100 °C (entries 4-6), applying a reaction time of 3 h and a catalytic loading of 0.0151 mmol Al. The conversion values ranged from 18% at 50 °C to >95% when the temperature was increased up to 100 °C. Moderate conversion values of the more reactive glycidol was obtained at 30 °C in 3 h, with only small differences when an initial CO_2 pressure of 25 bar or a constant pressure of 10 bar was applied (entries 7 and 8). Conversely, the increase of the temperature up to 50 °C with the same reaction time gave rise to 62% conversion of glycidol (entry 9). A longer reaction time (5 h) allowed to obtain a higher conversion of 83% into the corresponding cyclic carbonate (entry 10). However, a longer reaction time (10 h) produced only a little increase of the conversion up to 91% (entry 11), indicating that the kinetic of this reaction strongly decreased with the increasing conversion. 1,4-butanediol diglycidyl ether was successfully converted into the corresponding cyclic carbonate at 125 °C after 20 h (entry 12).

Table 1. Cyclic carbonates synthesis catalyzed by **MWCNT-TSP-AlCl-imi**.

Entry	Substrate	t (h)	T (°C)	Conversion (%)[a]	TON_{Al}[b]	TOF_{Al} (h^{-1})[b]
1		3	125	55	7650	2550
2[c]	(210 mmol)	20		84	23400	1170
3[c]		18	150	>95	26800	1490
4			50	18	3650	1210
5	(306 mmol)	3	80	83	16820	5610
6			100	>95	20260	6750
7[d]			30	31	6280	2090
8[d,e]		3	30	26	5270	1750
9[f]	(306 or 379 mmol)		50	62	15560	5190
10[f]		5	50	83	20830	4160
11[f]		10	50	91	22840	2280
12	(131 mmol)	20	125	>95	16500	824
13[g]	(237 mmol)	24	150	71[h]	3350	140

Reaction conditions: CO_2 (25 bar), catalyst 60 mg (0.0151 mmol Al), 500 rpm. [a] Determined by ^{1}H NMR. [b] TON and TOF values calculated on the basis of the Al content obtained from ICP analysis. [c] Catalyst 30 mg (0.0075 mmol Al). [d] 306 mmol of glycidol were used. [e] CO_2 constant pressure 10 bar. [f] 379 mmol of glycidol were used. [g] Catalyst 200 mg (0.0502 mmol Al). [h] Selectivity toward cyclic carbonates 74% (*cis/trans* ratio 65:35).

The outstanding results obtained encouraged us to test **MWCNT-TSP-AlCl-imi** with the less reactive cyclohexene oxide. Cyclohexene oxide displayed a 71% conversion when the reaction was carried out at 150 °C for 24 h (entry 13). However, the *cis*-cyclohexene carbonate was not the only product obtained and poly(cyclohexene carbonate) and *trans*-cyclohexene carbonate, the latter formed by back-biting reaction that can occur at the end of the growing polymer chain,[11-12] were also detected. ^{1}H NMR spectrum of the reaction mixture (**Figure 10**) allowed to calculate the selectivity toward the cyclic carbonates products by integrating the signals attributed to the methylene groups of the different products.
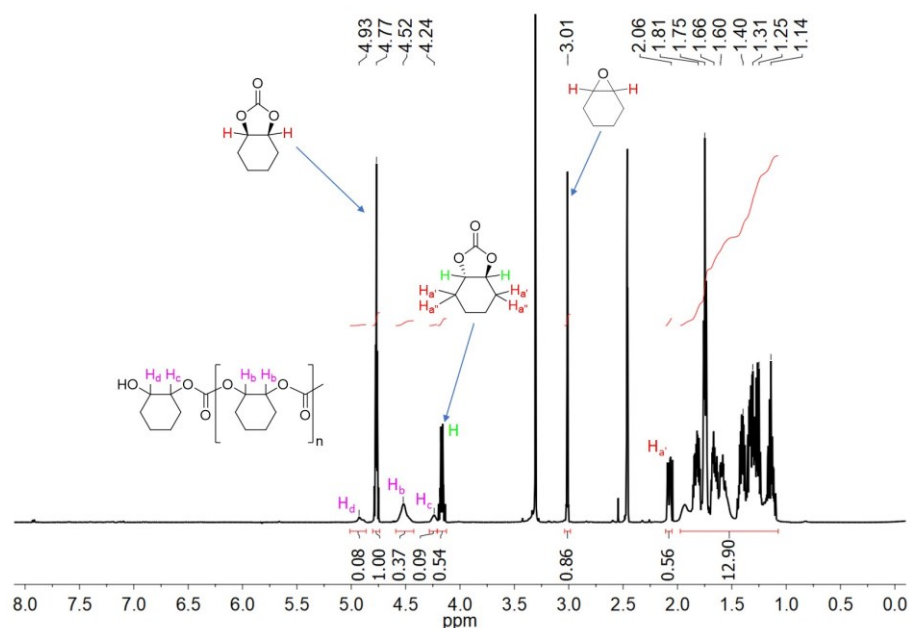
Figure 10. ^{1}H NMR (DMSO-d$_6$) **Table 1**, entry 13.

Finally, the remarkable catalytic activity of **MWCNT-TSP-AlCl-imi** is among the highest achieved by heterogeneous bifunctional (Lewis acid/X⁻) catalysts in the cyclic carbonate synthesis.[13-35] In particular, **Table 2** compares the activity of previously reported heterogeneous bifunctional porphyrin-based catalytic systems with **MWCNT-TSP-AlCl-imi**, which proved to be highly competitive with other systems.

Table 2. Selected data for the reaction between epichlorohydrin and CO_2 in the presence of porphyrin-M-based heterogeneous bi-functional catalytic systems.

Entry	Catalyst	Yield (%)	TOF (h^{-1})	P[a]	P/h (h^{-1})	Conditions	Ref.
1	MWCNT-TSP-AlCl-imi	>99	6755	696	232	3 h, 100 °C, 2.5 MPa	Chapter III
2	Al-iPOP-2	>99	167	89	15	6 h, 40 °C, 1.0 MPa	21
3	BIO-1c	91	910	11	11	1 h, 120 °C, 1.7 MPa	29
4	ZnTPy-BIM4/CNTs-3	98	528 (1842)[b]	10	4	2.5 h, 120 °C, 1.5 MPa	20
5	SYSU-Zn@IL2	>99	52	34	3	12 h, 80 °C, 1.0 MPa	19
6	Zn-CIF2-C$_2$H$_4$	98	136	30	7	4 h, 120 °C, 2.5 MPa	16
7	Mg-por/pho@POP	67	13400	293	293	1 h, 140 °C, 3.0 MPa	15
8	ZnTPP/QA-azo-PiP$_1$	>99	33	29	2	12 h, 80 °C, 1.0 MPa	30
9	ZnPor-CP	93	73	38	2	16 h, 100 °C, 1.0 MPa	31
10	CoTPP-PiP(Br)	>99	42	64	5	12 h, 80 °C, 1.0 MPa	32
11	[Zn(II)NMeTPyP]$^{4+}$[I$^-$]$_4$@PCN-224	>99	35	27	1	24 h, 90 °C, 0.8 MPa	33
12	PP-Br-Zn-0.09	94	528 (4080)[c]	23	12	2 h, 100 °C, 1.5 MPa	34
13	SBA-Zn-TPy$^+$PBr$^-$$_{DMF}$	>99	286 (685)[d]	25	7	3.5 h, 120 °C, 1.5 MPa	35

[a] Productivity: calculated as $g_{carbonate}/g_{catalyst}$. [b] TOF was calculated with the conversion below 35% and S/C = 7100. [c] TOF was calculated with the conversion below 35%. [d] TOF was calculated with the conversion below 35% and S/C = 2000.

3.3 Conclusions

Aluminum chloride tetrastyrylporphyrin (**TSP-Al-Cl**) and 1,4-butanediyl-3,3'-bis-1-vinylimidazolium dibromide have been subjected to AIBN-mediated radical polymerization in the presence (**MWCNT-TSP-AlCl-imi**) and in absence (**TSP-AlCl-imi**) of multi-walled carbon nanotubes (MWCNTs). The corresponding crosslinked materials have been thoroughly characterized by means of several spectroscopic and analytic techniques such as TGA, ICP-OES, FT-IR, XPS, TEM, solid state NMR, porosimetry. The hybrid materials have been employed as heterogeneous catalysts in the cycloaddition reaction of CO_2 to epoxides to afford the corresponding cyclic carbonates under solvent-free conditions, resulting **MWCNT-TSP-AlCl-imi** the most active with TON and TOF double than those obtained with the unsupported one. The enhanced activity of the nanocarbon-based catalyst can be ascribed to its higher surface area that permits fully accessible catalytic sites, in comparison with the very

low SSA of **TSP-AlCl-imi** (<1 m^2/g). Moreover, the heterogeneous **MWCNT-TSP-AlCl-imi** system displays a catalytic activity very similar to that of a reference homogeneous catalytic mixture comprised of aluminum tetraphenylporphyrin and **bmimBr**. This outstanding performance could be ascribed to the fine control achieved over the relative position of the catalytic sites given that the direct covalent linking between the porphyrin core and the bis-vinylimidazolium salt ensures the close proximity between the metal centers and the bromide ions, which are able to cooperate and exert a synergistic effect during the catalytic cycle. The hybrid catalyst showed an excellent catalytic activity, among the highest ever reported for a bifunctional material, with a set of different epoxides, with TON and TOF values of up to 26800 and 6750, respectively. **MWCNT-TSP-AlCl-imi** was easily recoverable and recyclable for at least five cycles with unchanged activity, and no leaching phenomena have been observed during the performed tests. This promising material pave the way toward the setting up of a family of robust and recyclable catalysts to be used both in batch and in flow systems. Most performing materials could be prepared by changing both the kind of metalloporphyrin as well as the anion of the poly-ionic liquid network.

3.4 Experimental Sections

Materials and methods. Styrene oxide, epichlorohydrin and cyclohexene oxide were purchased from TCI. Glycidol, limonene oxide, 1,4-butanediol diglycidyl ether and 2,2'-Azobis(2-methylpropionitrile) (AIBN) were purchased from Sigma-Aldrich. These chemicals were used without further purification. Transmission electron microscopy (TEM) images were obtained using a Philips Tecnai 10 microscope operating at 80 kV. The samples were prepared by dispersion of a small quantity of the material in absolute ethanol and deposited into a copper grid. X-ray photoelectron spectroscopy (XPS) analysis were carried out in a ThermoFisher ESCALAB 250Xi instrument. Inductively coupled plasma optical emission spectroscopy (ICP-OES) were performed in an Optima 8000 ICP-OES Spectrometer. Nitrogen adsorption analysis were carried out in a Micromeritics Tristar 3000 and ASAP 2000. The material was pre-treated at 150 ºC for 16 h under reduced pressure. The Brunauer-Emmett-Teller (BET) method as applied in the 0.05-0.30 p/p_0 range to calculate the specific surface area. Thermogravimetric analysis was performed under nitrogen flow from 25 to 900 ºC with a heating rate of 10 ºC/min in a Mettler Toledo TGA STAR system. Chemical combustion analysis was performed on a Perkin-Elmer 2400 Serie 2 analyzer. ^{1}H and ^{13}C NMR spectra were recorded on a Bruker 300 MHz spectrometer. Solid state ^{13}C NMR spectra

were recorded at room temperature on a Bruker Avance-500 spectrometer operating at 11.7 T using a 4.0 mm probe and spinning frequencies of 8 and 10 kHz.

Synthetic procedures

Synthesis of bisvinylimidazolium salt (bis-imi). In a 10 mL round bottom flask, a solution of 1,4-dibromobutane (950 µL, 7.88 mmol) and 1-vinylimidazole (1.5 mL, 16.24 mmol) in methanol (2 mL) was stirred in the dark and under Ar atmosphere at 65 °C for 13 h. The solution was transferred in a 100 mL round bottom flask and the volume was reduced under vacuum before adding Et_2O (70 mL). After sonication and vigorous stirring, a white precipitate was obtained and the supernatant was removed by simple decantation. Afterwards, methanol (2 mL) was added and gently warmed to solubilize the solid obtaining a yellowish viscous oil, which again after the addition of diethyl ether and sonication gave rise to a white precipitate. Diethyl ether was then removed and the whole procedure of solubilization in methanol and precipitation with diethyl ether was repeated twice. The obtained white solid was dried under vacuum at 40 °C. **bis-imi** was obtained as a white solid (3.128 g; 98%).

Synthesis of 4-vinylbenzaldehyde (2). 4-Vinylbenzaldehyde was synthesized according to a reported procedure.[36] In a 100 mL two-neck round-bottom flask, under Ar atmosphere, Mg (550 mg, 22.63 mmol), a catalytic amount of I_2 and dry THF (28 mL) were transferred. The mixture was allowed to stir at 30 °C for 30 minutes before the dropwise addition of 4-bromostyrene 1 (2 mL, 14.53 mmol). The temperature was gradually increased up to 67 °C and the reaction mixture was reacted at this temperature for 2 h. Dry DMF (3.4 mL) was added at 0 °C and stirred at room temperature overnight. The reaction mixture was quenched with a saturated NH_4Cl solution (15 mL), filtered to remove any insoluble residue, and extracted with ethyl acetate. The combined organic phases were dried over $MgSO_4$, filtered, concentrated under vacuum (at room temperature to avoid the polymerization of 4-vinylbenzaldehyde), and purified by column chromatography on silica gel (hexane/ethyl acetate (v/v): 30/1). The 4-vinylbenzaldehyde was obtained as a yellowish oil (1.496 g; 78%). ^{1}H NMR (300 MHz, $CDCl_3$, δ): 7.86 (d, J = 8.2 Hz, 2H), 7.57 (d, J = 8.2 Hz, 2H), 6.79 (dd, J = 17.6, 10.9 Hz, 1H), 5.93 (d, J = 17.6 Hz, 1H), 5.46 (d, J = 10.9 Hz, 1H) ppm.

Synthesis of tetrastyrylporphyrin (TSP). Tetrastyrylporphyrin (**TSP**) was synthesized according to a reported procedure.[37] In a 250 mL two-neck round-bottom flask propionic acid (104 mL) was heated to 140 °C in air before adding fresh distilled pyrrole (795 µL, 11.34 mmol) and 4-vinylbenzaldehyde (1.496 g, 11.32 mmol). After 5 h the reaction mixture was

allowed to reach room temperature and then the two-neck round-bottom flask was placed in an ice bath before filtering and washing with methanol and ethyl acetate. After drying, the tetrastyrylporphyrin was obtained as purple crystals (600 mg, 29%). ^{1}H NMR (300 MHz, CDCl$_3$, δ): 8.90 (s, 8H), 8.19 (d, J = 7.9 Hz, 8H), 7.81 (d, J = 8.0 Hz, 8H), 7.07 (dd, J = 17.6, 10.9 Hz, 4H), 6.08 (d, J = 17.6 Hz, 4H), 5.51 (d, J = 10.9 Hz, 4H), -2.73 (s, 2H) ppm. ^{13}C NMR (75 MHz, CDCl$_3$, δ): 141.69, 136.94, 136.71, 134.83, 124.61, 119.90, 114.67 ppm. FT-IR (film): 3328, 2920, 2853, 1827, 1627, 1602, 1557, 1504, 1471, 1401, 1349, 1219, 1185, 1154, 1112, 1017, 987, 966, 911, 854, 803, 727 cm^{-1}. UV−vis: (CHCl$_3$) λ max (ε) = 420 (379950), 517 (14900), 553 (9375), 591 (4825), 647 (4700) nm.

Synthesis of tetrastyrylporphyrin aluminum chloride (TSP-AlCl). In a 50 mL two-neck round-bottom flask, under Ar atmosphere, tetrastyrylporphyrin (570 mg, 0.79 mmol), and dry DCM (11.4 mL) were charged. The mixture was cooled to 0 °C by means of an ice bath and then a solution of diethylaluminum chloride (25 wt% solution in toluene, 490 μL, 0.90 mmol) was slowly added. Then the reaction mixture was allowed to reach the room temperature and stirred for 6 h before transferring it in a centrifuge tube and adding methanol. Four centrifugations with methanol were carried out and the combined supernatants were evaporated under vacuum. The residue was taken up with DCM and all the insoluble residues were removed by filtration. The filtrate was concentrated under vacuum and TSP-AlCl was obtained as purple powder (293 mg, 47%). ^{1}H NMR (300 MHz, CDCl$_3$, δ): 8.41 (s, 8H), 7.49 (s, 16H), 6.98 (dd, J = 17.6, 11.0 Hz, 4H), 5.99 (d, J = 17.7 Hz, 4H), 5.49 (d, J = 10.9 Hz, 4H) ppm. ^{13}C NMR (75 MHz, CDCl$_3$, δ): 146.72, 140.77, 136.70, 136.62, 134.32, 131.12, 124.38, 119.33, 114.62 ppm. FT-IR (film): 2922, 2853, 1627, 1496, 1402, 1351, 1293, 1236, 1209, 1012, 911, 801, 726 cm^{-1}. UV−vis: (CHCl$_3$) λ max (ε) = 422 (138250), 517 (2075), 552 (4675), 595 (1900), 646 (525) nm.

Preparation of MWCNT-TSP-AlCl-imi. In a 25 mL two-neck round-bottom flask, MWCNTs (97 mg), **TSP-AlCl** (146 mg, 0.19 mmol), bis-vinylimidazolium salt **bis-imi** (303 mg, 0.75 mmol), and absolute ethanol (9.7 mL) were transferred and sonicated for 20 minutes. Then, under Ar atmosphere, AIBN (51 mg, 0.31 mmol) was added and Ar was bubbled in the reaction mixture while stirring for 30 minutes at room temperature. The temperature was gradually increased up to 78 °C and the reaction mixture was allowed to react at this temperature for 15 h. The dark viscous residue obtained was transferred in a centrifuge tube adding a mixture of methanol/Et$_2$O (v/v) 2/1. The residue was subjected to centrifugation, three times using the methanol/Et$_2$O (v/v) 2/1 mixture, one time with a methanol/Et$_2$O

(v/v) 1/1 mixture, and three additional times with pure Et_2O. The residue was recovered and dried under vacuum at 40 °C. **TSP-AlCl-imi-MWCNT** was obtained as a dark powder (463 mg). FT-IR (KBr pellet): 3417, 3123, 3085, 2920, 2850, 1627, 1552, 1454, 1157, 1011, 807, 738, 653 cm^{-1}. CHN analysis (%): C 59.7; H 4.9; N 8.6.

Preparation of TSP-AlCl-imi. In a 25 mL two-neck round-bottom flask, under Ar atmosphere, TSP-AlCl (250 mg, 0.32 mmol), bis-vinylimidazolium salt **bis-imi** (518 mg, 1.28 mmol), AIBN (21 mg, 0.13 mmol), and absolute ethanol (5.0 mL) were transferred. Then, Ar was bubbled in the reaction mixture while stirring for 20 minutes at room temperature. The temperature was gradually increased up to 78 °C and the reaction mixture was allowed to react at this temperature for 15 h. The solvent was removed und er vacuum and the residue was washed by soxhlet extraction with methanol overnight. After oven-drying at 60 °C, **TSP-AlCl-imi** was obtained as dark powder (576 mg). FT-IR (KBr pellet): 3403, 3132, 3085, 2933, 2868, 1627, 1553, 1501, 1451, 1351, 1208, 1157, 1011, 859, 805, 748 cm^{-1}. CHN analysis (%): C 50.5; H 5.6; N 10.5.

Synthesis of tetraphenylporphyrin (TPP). Tetraphenylporphyrin (**TPP**) was synthesized according to a reported procedure.[8] In a 250 mL two-neck round-bottom flask propionic acid (90 mL) was heated to 140 °C in air before adding fresh distilled pyrrole (650 μL, 9.27 mmol) and 4-vinylbenzaldehyde (950 μL, 9.25 mmol). After 5 h the reaction mixture was allowed to reach room temperature and then the two-neck round-bottom flask was placed in an ice bath before filtering and washing with methanol and ethyl acetate. After drying, the tetraphenylporphyrin was obtained as purple crystals (299 mg, 21%). Spectroscopic data are in accordance with those reported in literature.[8]

Synthesis of tetraphenylporphyrin aluminum chloride (TPP-AlCl) complex. Tetraphenylporphyrin aluminum chloride (**TPP-AlCl**) complex was synthesized according to a reported procedure.[8] in a 50 mL two-neck round-bottom flask, under Ar atmosphere, tetraphenylporphyrin (90 mg, 0.15 mmol), and dry DCM (2.1 mL) were charged. The mixture was cooled to 0 °C by means of an ice bath and then a solution of diethylaluminum chloride (25 wt% solution in toluene, 90 μL, 0.16 mmol) was slowly added. Then the reaction mixture was allowed to reach the room temperature and stirred for 6 h before transferring it in a centrifuge tube and adding methanol. Four centrifugations with methanol were carried out and the combined supernatants were evaporated under vacuum. The residue was further purified by a short column chromatography on silica gel (DCM/methanol (v/v): 10/1). The

TPP-AlCl was obtained as purple powder (48 mg, 47%). Spectroscopic data are in accordance with those reported in literature.[8]

Catalytic experiments. Catalytic experiments were performed in a Cambridge Design Bullfrog batch reactor with temperature control and mechanical stirring. In this reactor, also pressure can be monitored. Before each experiment, the material was dried overnight in a vacuum oven at 60 °C. In each test, the catalyst was added to 24 mL of epoxide in a Teflon vial under solvent free conditions. After closing the reactor, the mixture was stirred at 500 rpm. The system was then purged for 10 min with N_2 before the addition of 25 bar of CO_2. After this, the system was heated to the required temperature with a rate of 5 °C/min. The reaction mixture was kept to the required temperature during the reaction time. When needed a refill of CO_2 was performed during the experiment to preserve the amount of reactant required for the reaction. In any case the pressure of CO_2 added overpasses the initial pressure reached at the temperature of the experiment. After this time, the reactor was cooled down to room temperature and then it was depressurized. The catalyst was separated from the reaction mixture via centrifugation during 30 min at 4500 rpm and the supernatant was analyzed by ^{1}H NMR in $(CD_3)_2SO$.

Recycling test. Recycling test were carried out in the reaction of styrene oxide with CO_2. At the end of the reaction, the material was recovered by centrifugation and washed several times with 45 mL of toluene, ethanol and one time with diethyl ether. Moreover, each time the catalyst was previously sonicated with the washing solvent. Then, before the next cycle, the catalyst was dried overnight in a vacuum oven at 60 °C. After drying, the catalyst was reused in the same reaction maintaining the ratio between moles of catalyst and moles of epoxides.

Leaching test. Leaching test was performed in the reaction of styrene oxide with CO_2. Once the reaction time passed, the reactor was cooled down to room temperature and then it was depressurized. As usually, the catalyst was separated from the reaction mixture via centrifugation during 30 min at 4500 rpm and the supernatant was analyzed by ^{1}H NMR in $(CD_3)_2SO$. Then, the remaining supernatant (without catalyst) was introduced again into the reactor. As in a normal reaction, the system was then purged for 10 min with N_2 before the addition of 25 bar of CO_2 and the increase of the temperature with a rate of 5 °C/min. The reaction mixture was kept to the selected temperature for the required time. During the reaction time, no decrease of the CO_2 pressure was observed and no further conversion was detected by ^{1}H NMR analysis.

3.5 References

1.   Li, X. Y.; Zgierski, M. Z., Porphine force field: in-plane normal modes of free-base porphine; comparison with metalloporphines and structural implications. *J. Phys. Chem.* **1991**, *95*, 4268-4287.

2.   Zhang, Y.-H.; Ruan, W.-J.; Li, Z.-Y.; Wu, Y.; Zheng, J.-Y., DFT study on the influence of meso-phenyl substitution on the geometric, electronic structure and vibrational spectra of free base porphyrin. *Chem. Phys.* **2005**, *315*, 201-213.

3.   Alben, J. O.; Choi, S. S.; Adler, A. D.; Caughey, W. S., Infrared Spectroscopy of Porphyrins. *Ann. N. Y. Acad. Sci.* **1973**, *206*, 278-295.

4.   Mitchell-Koch, J. T.; Padden, K. M.; Borovik, A. S., Modification of immobilized metal complexes toward the design and synthesis of functional materials for nitric oxide delivery. *J. Polym. Sci. A Polym. Chem.* **2006**, *44*, 2282-2292.

5.   Qin, Y.; Guo, H.; Sheng, X.; Wang, X.; Wang, F., An aluminum porphyrin complex with high activity and selectivity for cyclic carbonate synthesis. *Green Chem.* **2015**, *17*, 2853-2858.

6.   Tait, S.; Osteryoung, R. A., Infrared study of ambient-temperature chloroaluminates as a function of melt acidity. *Inorg. Chem.* **1984**, *23*, 4352-4360.

7.   Campisciano, V.; Burger, R.; Calabrese, C.; Liotta, L. F.; Lo Meo, P.; Gruttadauria, M.; Giacalone, F., Straightforward preparation of highly loaded MWCNT–polyamine hybrids and their application in catalysis. *Nanoscale Adv.* **2020**, *2*, 4199-4211.

8.   Chen, Y.; Luo, R.; Xu, Q.; Zhang, W.; Zhou, X.; Ji, H., State-of-the-Art Aluminum Porphyrin-based Heterogeneous Catalysts for the Chemical Fixation of CO2 into Cyclic Carbonates at Ambient Conditions. *ChemCatChem* **2017**, *9*, 767-773.

9.   Lovelock, K. R. J.; Villar-Garcia, I. J.; Maier, F.; Steinrück, H.-P.; Licence, P., Photoelectron Spectroscopy of Ionic Liquid-Based Interfaces. *Chem. Rev.* **2010**, *110*, 5158-5190.

10.   Brunauer, S.; Emmett, P. H.; Teller, E., Adsorption of Gases in Multimolecular Layers. *J. Am. Chem. Soc.* **1938**, *60*, 309-319.

11.   Cozzolino, M.; Melchionno, F.; Santulli, F.; Mazzeo, M.; Lamberti, M., Aldimine-Thioether-Phenolate Based Mono- and Bimetallic Zinc Complexes as Catalysts for the Reaction of CO2 with Cyclohexene Oxide. *Eur. J. Inorg. Chem.* **2020**, 1645-1653.

12.   Pescarmona, P. P.; Taherimehr, M., Challenges in the catalytic synthesis of cyclic and polymeric carbonates from epoxides and CO2. *Catal. Sci. Technol.* **2012**, *2*, 2169-2187.

13.   Dai, Z.; Tang, Y.; Zhang, F.; Xiong, Y.; Wang, S.; Sun, Q.; Wang, L.; Meng, X.; Zhao, L.; Xiao, F.-S., Combination of binary active sites into heterogeneous porous polymer catalysts for efficient transformation of CO2 under mild conditions. *Chinese J. Catal.* **2021**, *42*, 618-626.

14.   Li, J.; Han, Y.; Lin, H.; Wu, N.; Li, Q.; Jiang, J.; Zhu, J., Cobalt–Salen-Based Porous Ionic Polymer: The Role of Valence on Cooperative Conversion of CO2 to Cyclic Carbonate. *ACS Appl. Mater. Interfaces* **2020**, *12*, 609-618.

15.   Wang, W.; Wang, Y.; Li, C.; Yan, L.; Jiang, M.; Ding, Y., State-of-the-Art Multifunctional Heterogeneous POP Catalyst for Cooperative Transformation of CO2 to Cyclic Carbonates. *ACS Sustain. Chem. Eng.* **2017**, *5*, 4523-4528.

16.   Liu, J.; Zhao, G.; Cheung, O.; Jia, L.; Sun, Z.; Zhang, S., Highly Porous Metalloporphyrin Covalent Ionic Frameworks with Well-Defined Cooperative Functional Groups as Excellent Catalysts for CO2 Cycloaddition. *Chem. Eur. J.* **2019**, *25*, 9052-9059.

17. Luo, R.; Chen, Y.; He, Q.; Lin, X.; Xu, Q.; He, X.; Zhang, W.; Zhou, X.; Ji, H., Metallosalen-Based Ionic Porous Polymers as Bifunctional Catalysts for the Conversion of CO2 into Valuable Chemicals. *ChemSusChem* **2017**, *10*, 1526-1533.

18. Liu, T.-T.; Liang, J.; Huang, Y.-B.; Cao, R., A bifunctional cationic porous organic polymer based on a Salen-(Al) metalloligand for the cycloaddition of carbon dioxide to produce cyclic carbonates. *Chem. Commun.* **2016**, *52*, 13288-13291.

19. Chen, Y.; Luo, R.; Xu, Q.; Jiang, J.; Zhou, X.; Ji, H., Metalloporphyrin Polymers with Intercalated Ionic Liquids for Synergistic CO2 Fixation via Cyclic Carbonate Production. *ACS Sustain. Chem. Eng.* **2018**, *6*, 1074-1082.

20. Jayakumar, S.; Li, H.; Chen, J.; Yang, Q., Cationic Zn–Porphyrin Polymer Coated onto CNTs as a Cooperative Catalyst for the Synthesis of Cyclic Carbonates. *ACS Appl. Mater. Interfaces* **2018**, *10*, 2546-2555.

21. Chen, Y.; Luo, R.; Xu, Q.; Jiang, J.; Zhou, X.; Ji, H., Charged Metalloporphyrin Polymers for Cooperative Synthesis of Cyclic Carbonates from CO2 under Ambient Conditions. *ChemSusChem* **2017**, *10*, 2534-2541.

22. Puthiaraj, P.; Ravi, S.; Yu, K.; Ahn, W.-S., CO2 adsorption and conversion into cyclic carbonates over a porous ZnBr2-grafted N-heterocyclic carbene-based aromatic polymer. *Appl. Catal. B* **2019**, *251*, 195-205.

23. Naveen, K.; Ji, H.; Kim, T. S.; Kim, D.; Cho, D.-H., C3-symmetric zinc complexes as sustainable catalysts for transforming carbon dioxide into mono- and multi-cyclic carbonates. *Appl. Catal. B* **2021**, *280*, 119395.

24. Kuznetsova, S. A.; Rulev, Y. A.; Larionov, V. A.; Smol'yakov, A. F.; Zubavichus, Y. V.; Maleev, V. I.; Li, H.; North, M.; Saghyan, A. S.; Belokon, Y. N., Self-Assembled Ionic Composites of Negatively Charged Zn(salen) Complexes and Triphenylmethane Derived Polycations as Recyclable Catalysts for the Addition of Carbon Dioxide to Epoxides. *ChemCatChem* **2019**, *11*, 511-519.

25. Carvalho, P. A.; Comerford, J. W.; Lamb, K. J.; North, M.; Reiss, P. S., Influence of Mesoporous Silica Properties on Cyclic Carbonate Synthesis Catalysed by Supported Aluminium(Salen) Complexes. *Adv. Synth. Catal.* **2019**, *361*, 345-354.

26. Yi, Q.; Liu, T.; Wang, X.; Shan, Y.; Li, X.; Ding, M.; Shi, L.; Zeng, H.; Wu, Y., One-step multiple-site integration strategy for CO2 capture and conversion into cyclic carbonates under atmospheric and cocatalyst/metal/solvent-free conditions. *Appl. Catal. B* **2021**, *283*, 119620.

27. Luo, R.; Zhang, W.; Yang, Z.; Zhou, X.; Ji, H., Synthesis of cyclic carbonates from epoxides over bifunctional salen aluminum oligomers as a CO2-philic catalyst: Catalytic and kinetic investigation. *J. CO2 Util.* **2017**, *19*, 257-265.

28. Martín, C.; Whiteoak, C. J.; Martin, E.; Martínez Belmonte, M.; Escudero-Adán, E. C.; Kleij, A. W., Easily accessible bifunctional Zn(salpyr) catalysts for the formation of organic carbonates. *Catal. Sci. Technol.* **2014**, *4*, 1615-1621.

29. Ema, T.; Miyazaki, Y.; Taniguchi, T.; Takada, J., Robust porphyrin catalysts immobilized on biogenous iron oxide for the repetitive conversions of epoxides and CO2 into cyclic carbonates. *Green Chem.* **2013**, *15*, 2485-2492.

30. Chen, Y.; Ren, Q.; Zeng, X.; Tao, L.; Zhou, X.; Ji, H., Sustainable synthesis of multifunctional porous metalloporphyrin polymers for efficient carbon dioxide transformation under mild conditions. *Chem. Eng. Sci.* **2021**, *232*, 116380.

31. Liu, X.; Zhou, F.; Chen, M.; Xu, W.; Liu, H.; Zhong, J.; Luo, R., Synergistically Converting Carbon Dioxide into Cyclic Carbonates by Metalloporphyrin-Based Cationic Polymers with Imidazolium Functionality. *ChemistrySelect* **2021**, *6*, 583-588.

32. Chen, Y.; Luo, R.; Ren, Q.; Zhou, X.; Ji, H., Click-Based Porous Ionic Polymers with Intercalated High-Density Metalloporphyrin for Sustainable CO2 Transformation. *Ind. Eng. Chem. Res.* **2020**, *59*, 20269-20277.

33. Sharma, N.; Dhankhar, S. S.; Nagaraja, C. M., Environment-friendly, co-catalyst- and solvent-free fixation of CO2 using an ionic zinc(ii)–porphyrin complex immobilized in porous metal–organic frameworks. *Sustain. Energy Fuels* **2019**, *3*, 2977-2982.

34. Liu, L.; Jayakumar, S.; Chen, J.; Tao, L.; Li, H.; Yang, Q.; Li, C., Synthesis of Bifunctional Porphyrin Polymers for Catalytic Conversion of Dilute CO2 to Cyclic Carbonates. *ACS Appl. Mater. Interfaces* **2021**, *13*, 29522-29531.

35. Jayakumar, S.; Li, H.; Tao, L.; Li, C.; Liu, L.; Chen, J.; Yang, Q., Cationic Zn-Porphyrin Immobilized in Mesoporous Silicas as Bifunctional Catalyst for CO2 Cycloaddition Reaction under Cocatalyst Free Conditions. *ACS Sustain. Chem. Eng.* **2018**, *6*, 9237-9245.

36. Jiang, J.; Yoon, S., A Metalated Porous Porphyrin Polymer with [Co(CO)4]− Anion as an Efficient Heterogeneous Catalyst for Ring Expanding Carbonylation. *Sci. Rep.* **2018**, *8*, 13243.

37. Dai, Z.; Sun, Q.; Liu, X.; Bian, C.; Wu, Q.; Pan, S.; Wang, L.; Meng, X.; Deng, F.; Xiao, F.-S., Metalated porous porphyrin polymers as efficient heterogeneous catalysts for cycloaddition of epoxides with CO2 under ambient conditions. *J. Catal.* **2016**, *338*, 202-209.

CHAPTER IV

Highly cross-linked bifunctional magnesium porphyrin-imidazolium bromide polymer: Unveiling the key role of co-catalysts proximity for CO₂ conversion into cyclic carbonates
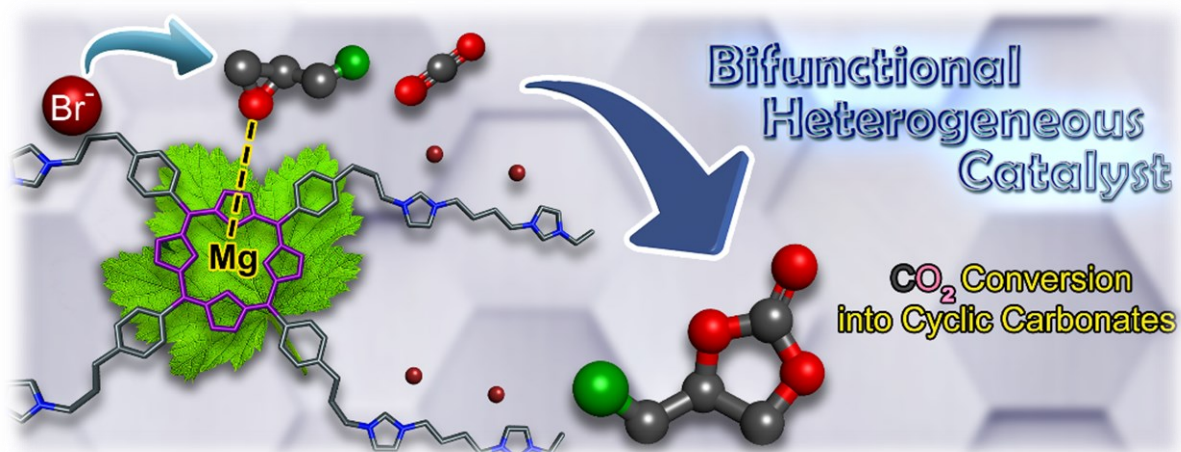

This chapter is based on:

CHAPTER IV

Highly cross-linked bifunctional magnesium porphyrin-imidazolium bromide polymer: Unveiling the key role of co-catalysts proximity for CO_2 conversion into cyclic carbonates

4.1 Abstract

Highly cross-linked materials containing an imidazolium salt and magnesium porphyrin, either in the absence (**TSP-Mg-imi**) or in the presence (**7a** and **7b**) of multi-walled carbon nanotubes (MWCNTs), were synthesized and used as heterogeneous bifunctional catalysts for the conversion of CO_2 into cyclic carbonates. The metalloporphyrin moiety acts both as a "covalent swelling agent", generating hybrids with high surface area, and as a Lewis acid co-catalytic species. **TSP-Mg-imi** produced excellent conversion and TON_{Mg} values, under solvent-free conditions, even at room temperature and with low catalytic loading (0.003 mol%). In terms of conversion and TON_{Mg}, **TSP-Mg-imi** exhibited better catalytic performance compared to a reference homogeneous system, demonstrating that the proximity between the metal centers and the nucleophilic site results in a synergistic effect during the catalytic cycle. The results of the computational study confirmed both the cooperative function and the significance of incorporating a co-catalytic species into the system.

4.2 Results and discussion

New hybrid materials **TSP-Mg-imi 6** and **7a** were designed and prepared to be applied as heterogeneous catalysts for the synthesis of cyclic carbonates from the addition of carbon dioxide to various epoxides (**Scheme 1**). Initially, the synthesis of **TSP-Mg 2** was achieved through the complexation of TSP **1** with magnesium bromide ethyl etherate (MgBr$_2$•OEt$_2$), whereas bis(vinyl)imidazolium **5** was quantitatively obtained by reaction of 1-vinylimidazole **3** and 1,4-dibromobutane **4**. Afterward, **TSP-Mg-imi 6** and **7a** were easily prepared by the radical copolymerization of bis(vinyl)imidazolium **5** and **TSP-Mg** mediated by thermal decomposition of azobis(isobutyronitrile) (AIBN) in refluxing DMF. In the case of **7a**, the radical polymerization was performed in the presence of MWCNTs as a support and templating material. The objective behind this approach was to improve the final specific surface area of the polyimidazolium copolymer, thereby enhancing the availability of active sites. Previous studies have indicated that unsupported polyimidazolium cross-linked networks exhibit significantly low specific surface areas. [1-3] In addition, monomer **5** was also polymerized to give **Homopolymer 8**, in order to compare the catalytic activity of the two hybrids. Catalyst **7b** was prepared with a different **TSP-Mg**/**Bis-imi** ratio (1:12) as a consequence of the results obtained with **TSP-Mg-imi 6** and **7a** and will be discussed below. To investigate the structures and morphologies of the obtained materials, several analytical and spectroscopic characterization techniques were used. The morphological properties of **TSP-Mg-imi** and **7a**, in terms of specific surface area (BET), were determined by N$_2$ adsorption/ desorption measurements (**Figure 1**). According to the IUPAC classification, both co-polymeric cross-linked networks exhibit a type II isotherm typical of macroporous adsorbent with H3 hysteresis loop. [4] The supported copolymer **7a** (**Figure 1b**) has a very low specific surface area (36 m^2/g) compared to **TSP-Mg-imi,** which displays a much higher value (216 m^2/g).
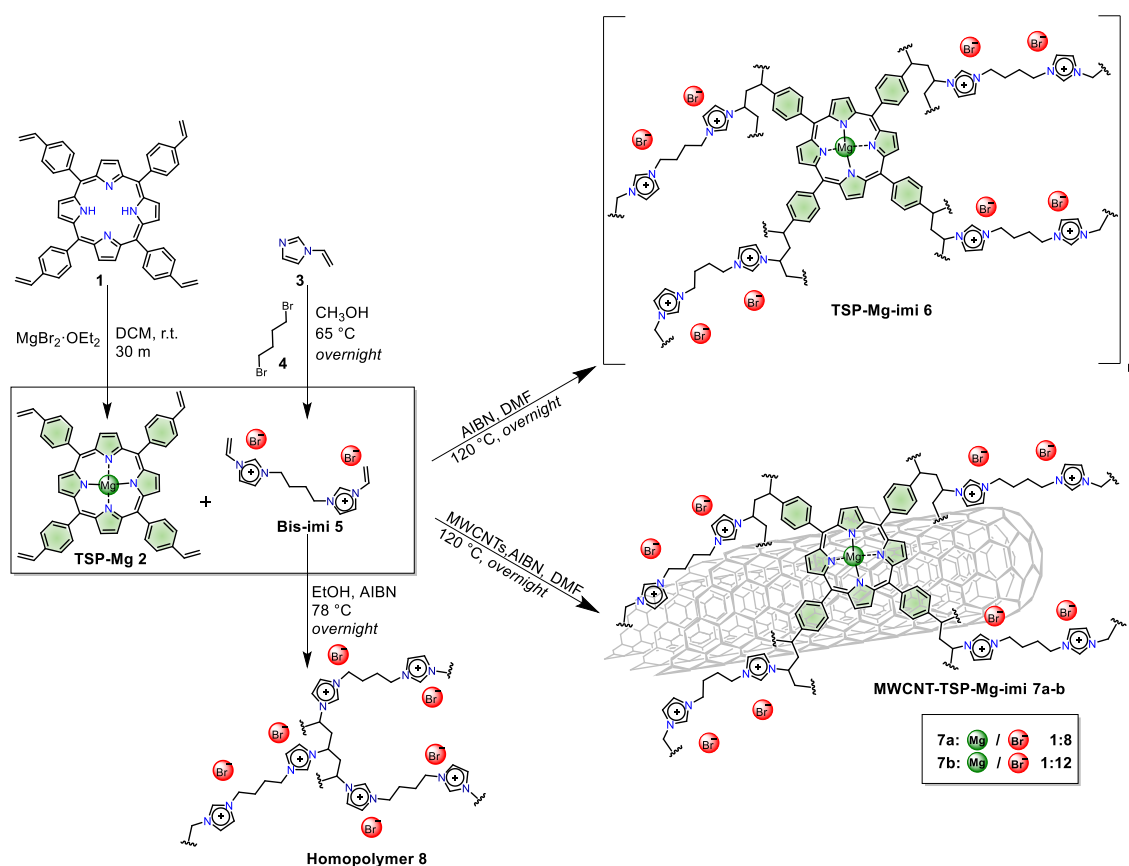
Scheme 1. Synthetic procedure for the preparation of **TSP-Mg-imi 6** and **7a-b**.

This value is surprisingly high, compared to almost all poly(ionic liquid)s, including **Homopolymer 8**, which are mostly non-porous or have a low-specific surface area.[1-3,5-7] The difference could be ascribed to the presence of magnesium porphyrin, which probably plays a role of swelling agent. Indeed, the presence of the porphyrin structure allows obtaining a more flexible polymer network in which the catalytic active sites are more accessible. In the case of **7a**, the effect of swelling agent by porphyrin is not observed, resulting in a material with a low specific surface area. To better understand this discrepancy, additional studies were conducted on the morphology of the two materials.
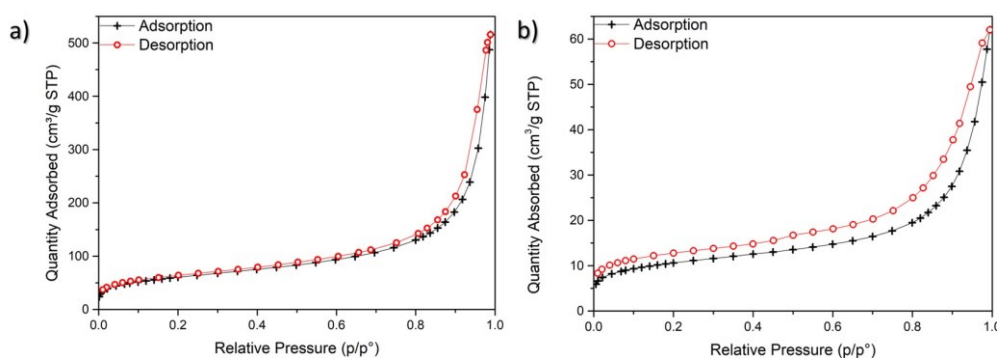

Figure 1. Nitrogen adsorption-desorption isotherms of (a) **TSP-Mg-imi**, and (b) **7a**.

The characterization *via* transmission electron microscopy (TEM) of **TSP-Mg-imi** confirms the above hypothesis (**Figure 2**): **TSP-Mg-imi** is a self-condensed polymeric material with an open network constituted by non-ordered macroporosity (thus displaying potential highly accessible catalytic active sites) (**Figure 2a-c**). In contrast, **7a** forms a physical mixture consisting of supported and not supported copolymer (**Figure 2e-f**). In this case, a limited templating effect of the MWCNTs can be noticed in comparison with our previous findings.[3,8-10] Overall, TEM micrographs reflect the difference between the two materials in terms of specific surface area.
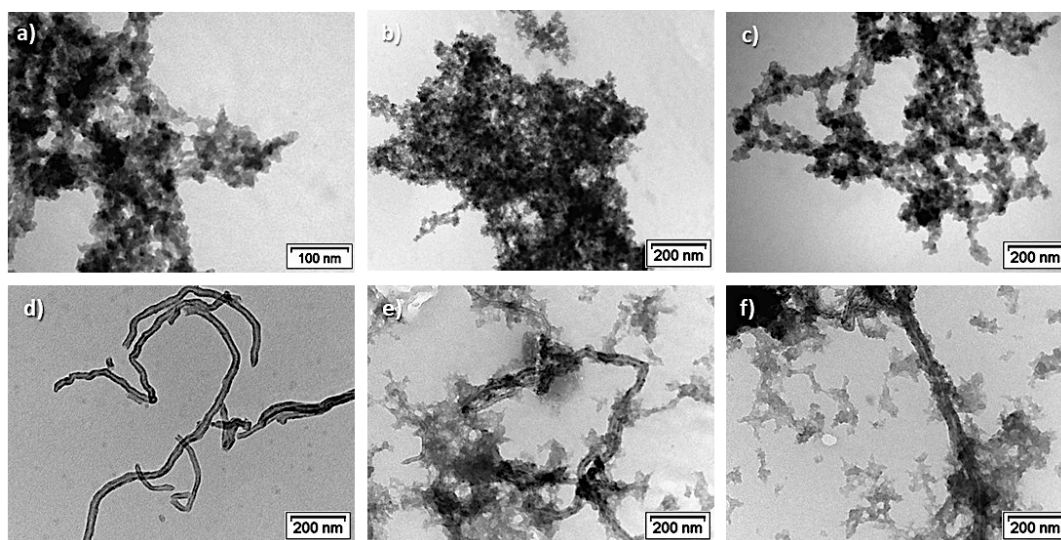
Figure 2. TEM micrographs of **TSP-Mg-imi** (a-c), pristine-MWCNT (d) and **7a** (e-f).

Scanning electron microscopy with energy dispersive X-ray spectroscopy (SEM/EDX) has been used to investigate the chemical composition of **TSP-Mg-imi** (**Figure 3**). In particular, the presence in the **TSP-Mg-imi** network of both active sites, magnesium and bromide, is verified with EDX-mapping and no significant separate domains are observed (**Figure 3e** and **3c**).
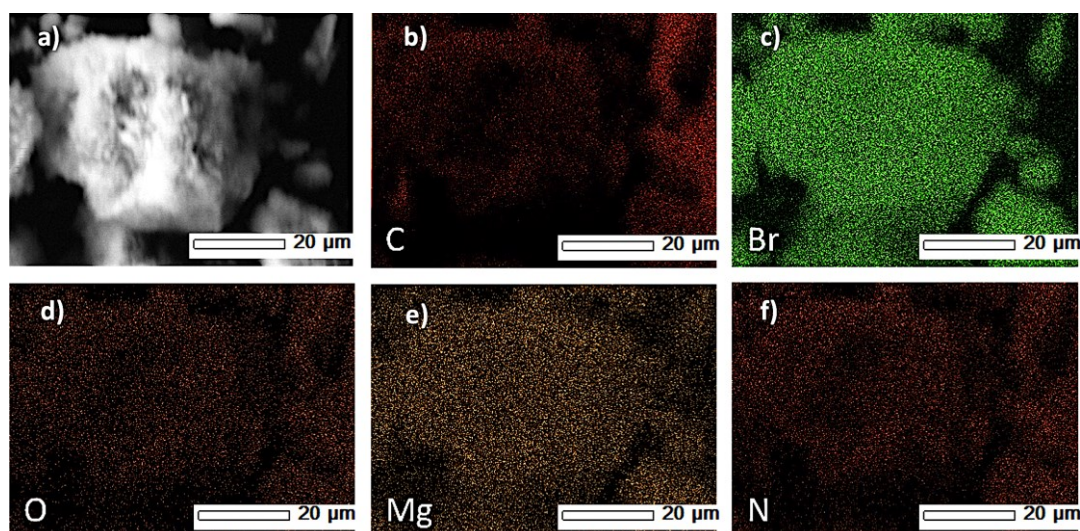
Figure 3. (a) SEM image of **TSP-Mg-imi**, (b-f) EDX elemental-mapping images of **TSP-Mg-imi**.

Solid-state ^{13}C NMR spectroscopy was carried out using the Cross-Polarization Magic Angle Spinning Total Suppression of spinning side bands technique (CP-MAS-TOSS ^{13}C NMR) (**Figure 4**). The spectra for both materials confirmed the success of the polymerization as evidenced by the absence of signals around 110 ppm corresponding to the vinyl groups, which are now present as methylene signals in the range between 20 and 60 ppm. The aliphatic carbons that form the linker between the imidazolium rings also resonate in this region. In addition, at low field (110–150 ppm), the signals referring to the aromatic carbon atoms of the porphyrin and imidazolium moieties are present.

Figure 4. ^{13}C CP-MAS-TOSS NMR of **TSP-Mg-imi** (blue line) and **7a** (green line).

The thermal behavior of the new hybrid materials was investigated using thermogravimetric analysis - TGA (**Figure 5**). Under nitrogen flow, **TSP-Mg-imi** and **7a** (yellow and green

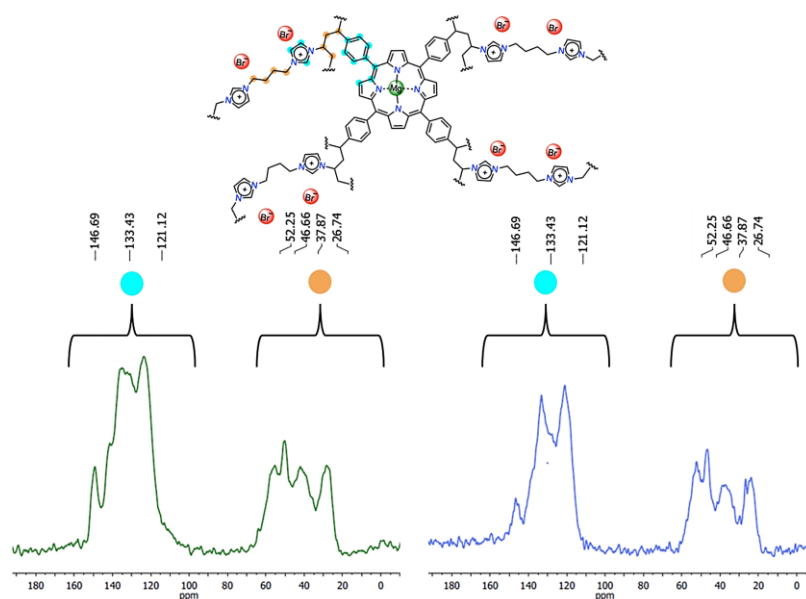curves) show a good thermal stability, with decomposition of the organic backbone beginning around 250 °C (**Figure 5a**). In addition, the TGA profile under air flow of **TSP-Mg-imi** (**Figure 5b**) confirms the thermal robustness of the material, which is promising for its possible repeated use under heating conditions. TGA in air also allows estimating the Mg content (1.4%, as MgO) from the residual weight percentage at 800 °C, corresponding to a Mg(II) loading of 0.35 mmol/g. On the contrary, the Mg content in **7a** cannot be estimated using this technique, as the fixed residue is made of both magnesium in the form of MgO and MWCNTs (**Figure 5b**). The Mg content of **7a** (0.39 mmol/g) was determined using inductively coupled plasma atomic emission spectroscopy (ICP-OES) analysis; the corresponding value for **TSP-Mg-imi** (0.33 mmol/g) is very similar to the one evaluated via TGA.
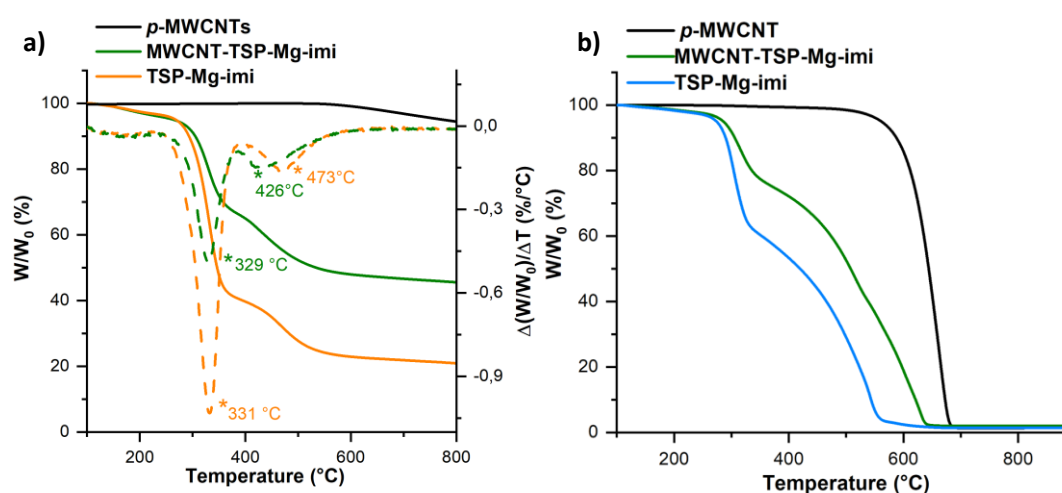
Figure 5. a) TGA (sold lines) analysis under N_2 and DGT (dotted lines) flow of pristine MWCNTs (black line), **MWCNT-TSP-Mg-imi 7a** (green line) and **TSP-Mg-imi** (yellow line). b) TGA analysis under air flow of pristine MWCNT (black lines), **MWCNT-TSP-Mg-imi 7a** (green lines) and **TSP-Mg-imi** (blue lines).

Furthermore, both materials **TSP-Mg-imi** and **7a** were subjected to XPS analysis to evaluate the presence of the active sites Mg/Br⁻ (**Figure 6**). The survey spectrum of **TSP-Mg-imi** (**Figure 6a**) confirms the signatures of the metal at 1305 eV (Mg1s) and of the nucleophilic sites of the catalyst at 254, 180 and 67 eV, respectively (Br3s, Br3p and Br3d). In addition, the high-resolution N 1s spectra display three peaks with distinct binding energies that can be attributed to the nitrogen of the imidazolium moieties at 401.3 eV and the nitrogen of the porphyrin at 400 and 398 eV (**Figure 6b**). The splitting in two peaks for the metalloporphyrin is not surprising and has already been described in the literature; it is due to the partial demetallation of the **TSP-Mg** during its prolonged exposure to X-ray.[11-13] Hence, an approximate 1:4 ratio between the areas of the peaks of Mg–N (green and blue lines) and

imidazolium–N (red line) was determined by XPS analysis (**Figure 6b**). This value agrees with the Mg/Br⁻ stoichiometric ratio of 1:8. On the contrary, in **7a** this ratio is not respected; the atomic percentages of the two different nitrogen atoms are 39% and 61% for Mg–N and imidazolium–N, corresponding to 1/1.5 ratio (**Figure 6c**).
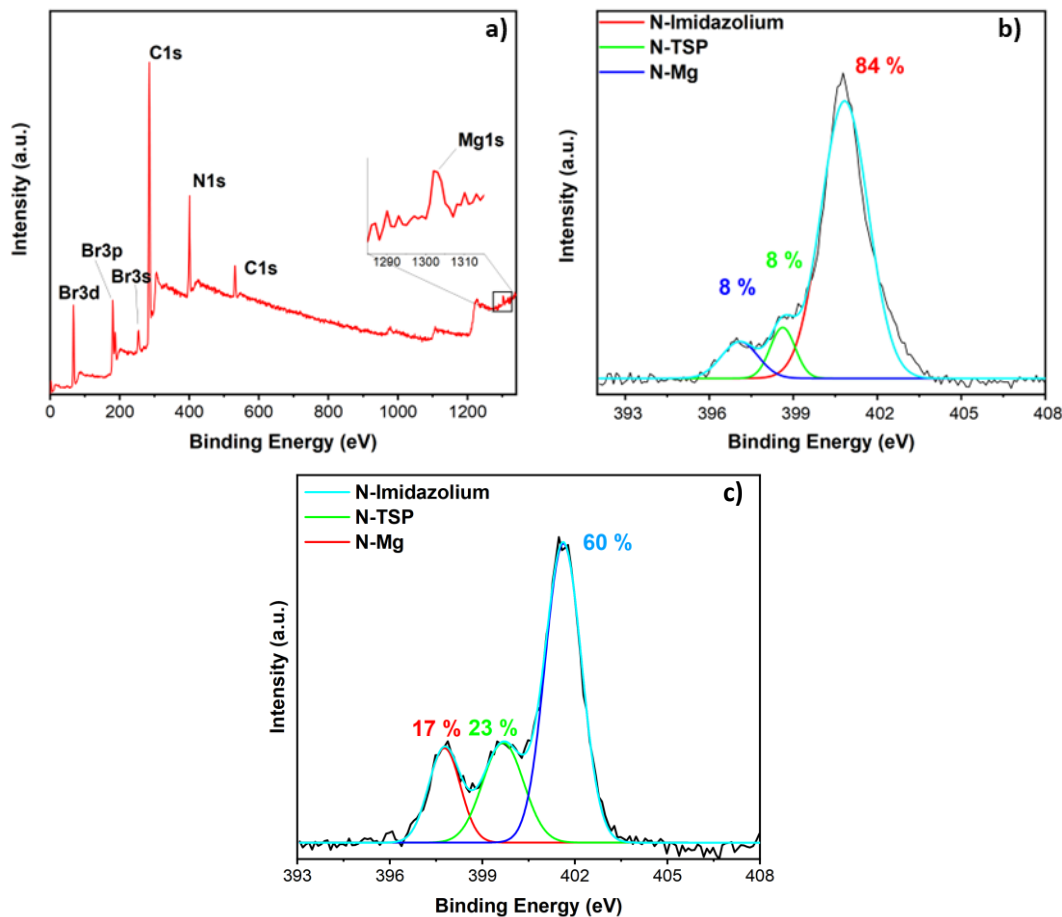
Figure 6. XPS Survey spectrum of **TSP-Mg-imi** (a), high-resolution N1s region (b) and high-resolution N 1s region of **7a**.

The nitrogen content of **TSP-Mg-imi** was also estimated by combustion chemical analysis (C 49%, H 6 %, N 12%).

In order to investigate the role of **TSP-Mg-imi** and **7a** as heterogeneous catalysts, both hybrids were studied in the synthesis of cyclic carbonates under solvent-free conditions. The catalytic performances were evaluated in terms of turnover number (TON_{Mg}, calculated as moles of epoxide converted/moles of Mg active sites), turnover frequency (TOF_{Mg} = TON_{Mg}/reaction time in hours), productivity (P, calculated as grams of cyclic carbonates obtained *per* grams of catalyst). and recyclability. All catalytic tests were performed in a batch-type reactor operating with large amounts of epoxide (200 mmol, *ca.* 20–25 mL) leaving a headspace over the liquid surface of ∼25 mL. Therefore, in our case, the use of high pressures not only allows significant volume reduction, since atmospheric CO_2 would require

significantly more volume than the pressurized gas but, most importantly, allowed us to have enough CO_2 to convert the epoxide. In addition, the conditions adopted here are particularly relevant because they are similar to those normally used on an industrial scale, and thus only minor adjustments would be needed to move the preparations reported here to a larger scale.

The reaction between carbon dioxide and epichlorohydrin was selected for a preliminary investigation (**Figure 7**). The recycling efficiency of the hybrid solids was evaluated over four catalytic runs at 60 °C. At the end of each catalytic cycle, the catalyst was recovered from the reaction mixture by centrifugation and washed with toluene, ethanol, and diethyl ether without any additional activation treatment.
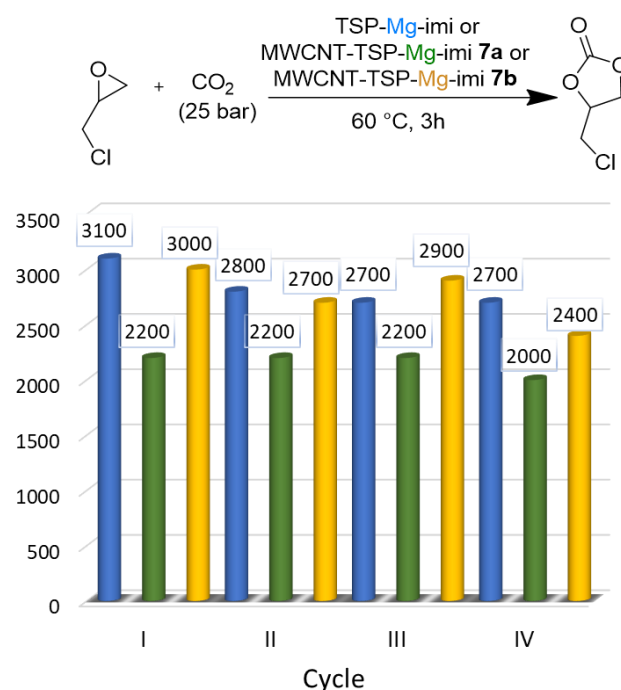
Figure 7. Comparison of the TON_{Mg} values for **TSP-Mg-imi** (blue), **7a** (green) and **7b** (yellow) over four catalytic cycles in the reaction of epichlorohydrin with CO_2. Reaction conditions: epichlorohydrin (382 mmol), catalyst (**TSP-Mg-imi** 0.039 mmol Mg or **7a** 0.045 mmol Mg or **7b** 0.022 mmol Mg), 25 bar CO_2, 60 °C, 3 h, 500 rpm.

The results illustrated in **Figure 7**, show that: (i) both the **TSP-Mg-imi** and **7a** catalysts can be reused in multiple catalytic cycles without any considerable decrease of the catalytic activity, and (ii) the TON_{Mg} performance of **TSP-Mg-imi** is significantly better than that of the supported hybrid solid. At this stage, it is not possible to discern whether the lower activity of **7a** is due to a possible negative influence of the nanotubes, or if it is a consequence of the lower specific surface area of the material or if it is caused by a non-optimal Mg/Br⁻ ratio, as highlighted by XPS analyses.

To address those questions, a second MWCNTs hybrid material, called **7b,** was prepared by changing the porphyrin/bis imidazolium salt ratio (Mg/Br⁻) in the feed from 1:8 to 1:12, in order to obtain a catalyst with a Mg/Br⁻ ratio closer to 1:8, as in **TSP-Mg-imi**. The

morphological analysis of **7b** (**Figure 8a**) reveals that the cross-linked polymer now covers the nanotubes, resulting also in an enhancement of the specific surface area to 174 m^2/g.
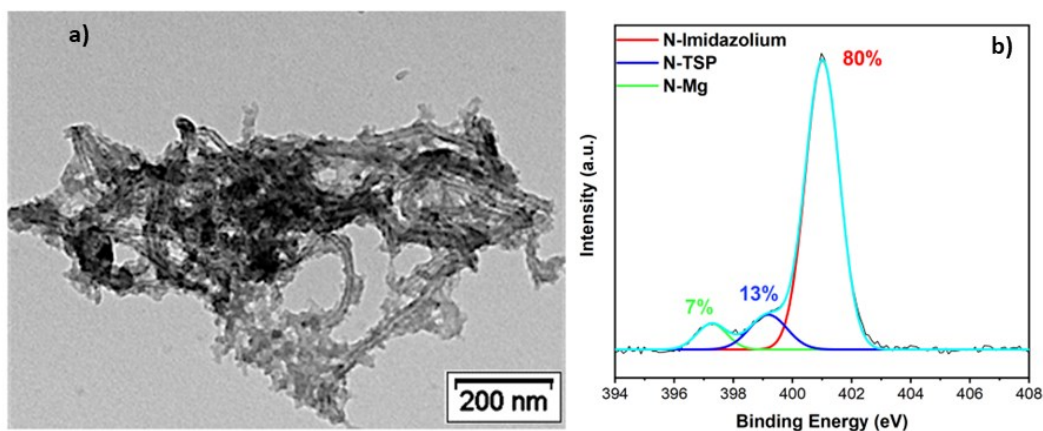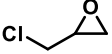
Figure 8. a)TEM micrograph of **MWCNT-TSP-Mg-imi 7b** and b) XPS high-resolution N 1s region of **MWCNT-TSP-Mg-imi 7b**.

XPS analysis confirmed that the selected feed stoichiometry was appropriate since a 1:8 Mg/Br$^-$ ratio has been achieved in the final material (**Figure 8b**). Subsequently, the new catalyst **7b** was tested under the same reaction conditions and a clear enhancement compared with **7a** has been achieved (**Figure 7**). This marked difference can be now explained by the homogeneity of the new hybrid, uniformly supported on the MWCNTs, the resulting increase in surface area and a more adequate Mg/Br$^-$ ratio. The new hybrid material **7b** and the copolymer **TSP-Mg-imi** exhibit a quite similar catalytic activity. Nevertheless, considering the excellent performance of the unsupported copolymer, it was decided to focus the study on this hybrid material. Indeed, **TSP-Mg-imi** results more appealing from an economic and environmental point of view, since this bifunctional catalyst has been designed and prepared using only two components, without any waste. From a morphological point of view, its porous structure and the unexpected high surface area allow excellent dispersion of the active sites, as well as good diffusion of reactants during the reaction process. The catalytic performance of **TSP-Mg-imi** was then studied at different temperatures, again choosing epichlorohydrin as benchmark substrate.

Table 1. Epichlorohydrin carbonate synthesis catalyzed by **TSP-Mg-imi**[a]

| Entry	Substrate	t (h)	T (°C)	Conversion (%)[b]	TON_{Mg}[c]	TOF_{Mg} (h^{-1})[c]	Productivity[d]
1[f,e]		24	30	24	2400	100	100
2[f,e]		3	60	32	3100	1000	100
3	Cl⌒△O	3	80	65	10500	3500	400
4	306 or 382 mmol	3	100	95	15300	5100	700
5		1	100	70	11300	11300	500
6[g,h]		3	100	66	20400	6800	900
7[g,i]		3	100	80	24700	8200	1100

[a] Reaction conditions: CO_2 (25 bar), epichlorohydrin (306 mmol), catalyst 60 mg (0.019 mmol Mg), 500 rpm. [b] Determined by ^{1}H-NMR. [c] TON_{Mg} and TOF_{Mg} values calculated based on the Mg content obtained from ICP analysis. [d] productivity (P, calculated as grams of cyclic carbonates obtained *per* grams of catalyst). [e] Epichlorohydrin 382 mmol. [f] Catalyst 120 mg (0.039 mmol Mg). [g] Catalyst 30 mg (0.009 mmol Mg). [h] CO_2 constant pressure 10 bar. [i] CO_2 constant pressure 25 bar.

As shown in **Table 1**, the conversion values of epichlorohydrin range from 24% at room temperature to 95% when the temperature is increased up to 100 °C. These values show the good catalytic activity of **TSP-Mg-imi** even at room temperature. Indeed, the conversion increases from 24% at room temperature (24 h) to 32% at 60 °C (3 h) with 120 mg of catalyst corresponding to 0.010 mol% (entries 1 and 2). The effect of the temperature on the conversion is clear when the title reaction has been carried out at 80 °C with half the amount of catalyst (0.006 mol%) yielding an 80% conversion (entry 3) and almost total conversion (>95%) when the temperature was further increased up to 100 °C (entry 4), achieving a TON of 15300. When the reaction was conducted in one hour, epichlorohydrin was converted into the cyclic carbonate with a conversion of 70% (entry 5). Finally, considering the excellent results obtained at 100 °C, two additional tests were conducted aimed to further reduce the amount of catalyst to 30 mg, 0.003 mol% (entry 6). Although the catalytic loading has been decreased, a very good conversion of 66% with a TON_{Mg} value of 20,400 has been obtained, when the system was maintained with a constant pressure of CO_2 (10 bar). A further improvement in terms of conversion and TON_{Mg} has been achieved by increasing and maintaining the working pressure of CO_2 at 25 bar, allowing to reach 80% conversion into the corresponding cyclic carbonate, which resulted in a TON_{Mg} of 24,700 (entry 7).

A more detailed study of the catalytic activity of **TSP-Mg-imi** was carried out by performing additional tests. **Scheme 2** shows the synthesis of epichlorohydrin carbonate at 80 °C for 3 h using different catalytic systems. **Homopolymer 8**, synthesized via polymerization of **Bis-imi 5**, and **Bis-imi 5** itself were used as the source of Br⁻ as heterogeneous and homogeneous systems, respectively (**Scheme 2**). Three different systems were tested using **TSP-Mg** as Lewis acid: (a) **TSP-Mg** alone; (b) a combination of **TSP-Mg** and **Homopolymer**; (c) a combination of **TSP-Mg** and **Bis-imi**. For each test performed, the amount of catalyst was based on the Mg loading of the catalyst in the reference reaction, **TSP-Mg-imi** (19 μmol). The **Homopolymer** as well as the [**Homopolymer**+**TSP-Mg**] system, under the title conditions, display no catalytic activity (reactions 1–2). This result can be attributed to the low value (<1 m²/g) of the specific surface area of the homopolymer. Also, **TSP-Mg** alone shows no conversion of epoxide (reaction 3). Under homogeneous conditions **Bis-imi** alone gave a low conversion (12%), whereas when the co-catalyst **TSP-Mg** is added, the conversion is boosted, reaching 60% (reactions 4–5). These results show the importance of the co-catalyst in the system. Finally, the catalytic test with **TSP-Mg-imi** was repeated (**Table 1**, entry 4), thus confirming the good reproducibility of the hybrid material (reaction 6).

Comparing the homogeneous [**Bis-imi**+**TSP-Mg**] system with the heterogeneous catalyst, TON_{Mg} values are quite similar (reactions 5–6) but with the clear advantage of easy recovery and reuse of the heterogeneous catalyst through a simple filtration and, considering the mass transfer limitations for heterogeneous catalysis. It can be hypothesized that the improved catalytic performance shown by the bifunctional polymeric catalyst stems from the direct linking between the two active parts, namely the porphyrin core and the bis(vinyl)imidazolium salt. This ensures the spatial proximity between the metal centers and the bromide ions, which can cooperate more efficiently, resulting in a synergistic effect during the catalytic cycle for the formation of the cyclic carbonates. To support this hypothesis a catalytic test, in which the proper amount of **Bis-imi** was added to **7a**, was performed. In this way, the optimal Mg/Br⁻ ratio, such as that found in **7b**, was reached. This addition of the homogeneous bromide source, namely **Bis-imi**, showed no improvement concerning the previously obtained TON_{Mg} value (**Figure 7**), further indicating that covalently linked co-catalytic moieties behave more efficiently than the homogeneous counterpart.
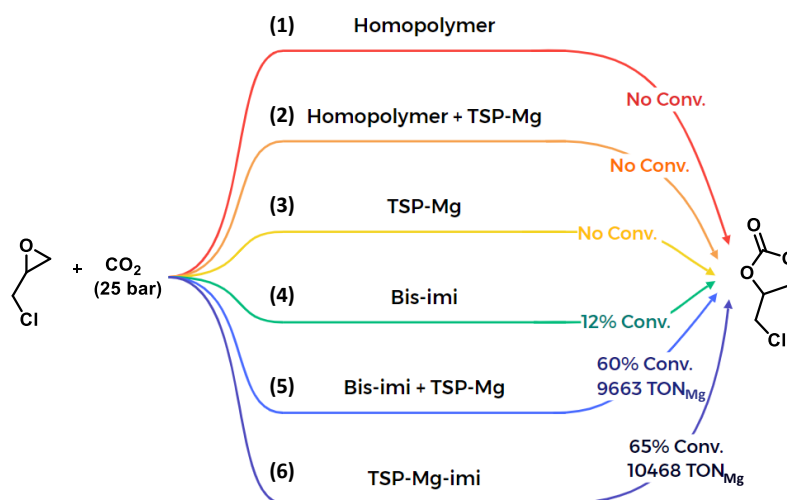
Scheme 2. Comparison of the catalytic activity between the heterogeneous system **TSP-Mg-imi**, **Homopolymer** and **Homopolymer + TSP-Mg** and the homogenous systems **Bis-imi, Bis-imi + TSP-Mg** and **TSP-Mg** in the reaction of epichlorohydrin with CO_2. Reaction conditions of tests 1-6 are reported in Experimental Section.

To verify this hypothesis, the energetics of two different catalytic routes have been estimated at the quantum-chemical level (M062X/6-311G*/GD3BJ), see details in the Materials and Methods section. On one hand (route 1, see **Figure 9**), tetraphenyl porphyrin, TPP-Mg, is first activating epichlorohydrin; as a result, the oxygen atom is clearly interacting with the metal center, the Mg-O distance being about 2.13 Å. On the other hand (route 2), it is CO_2 that first interacts with TPP-Mg. In that case, the CO_2 molecule is found to bend slightly (O–C–O angle of 178.1°) and gets nonsymmetric upon interaction with TPP-Mg: the C–O bond involving the activated oxygen becomes longer (1.163 Å *versus* 1.148 Å). In that complex, the closest Mg–O contact is 2.350 Å. Comparing the first step in the two routes, our calculations clearly point to more stabilizing interactions of TPP-Mg with epichlorohydrin, the complexation energies being 23.1 kcal/mol and 8.9 kcal/mol for epichlorohydrin and CO_2, respectively. Once the second reactant, i.e., either CO_2 (route 1) or epichlorohydrin (route 2), is added to the systems, the more stable complex (-7.9 kcal/mol) is still when epichlorohydrin is interacting primarily with TPP-Mg. The CO_2 molecule is getting even more nonsymmetric in route 2 in the presence of epichlorohydrin (O–C–O angle of 177.3°, C–O bonds of 1.167 Å and 1.146 Å), whereas it remains symmetric but bends in route 1 (O–C–O angle of 177.1°). The more stable complex (epichlorohydrin-TPP-Mg) points up the importance of synthesizing a material in which the two active catalytic sites are covalently linked. Indeed, the close spatial proximity between the porphyrin ring and the imidazole group, as well as the presence of bromide ions, result in a material with significantly improved catalytic efficiency.
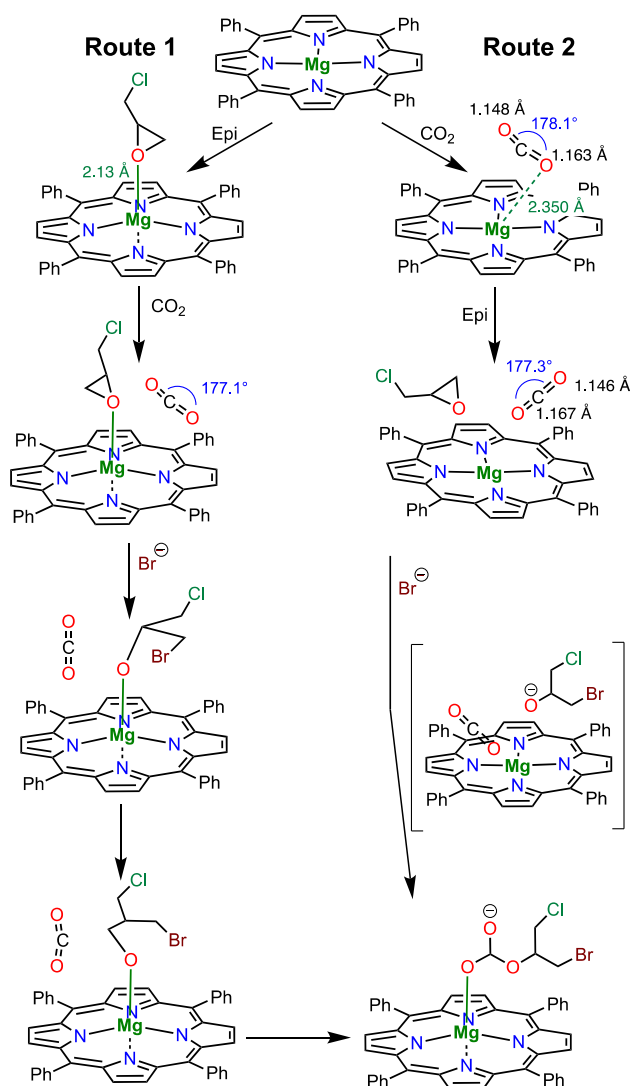
Figure 9. Representation of the two catalytic routes investigated at the quantum-chemical level (M062X/6-311G*/GD3BJ). The structure between brackets is a representation of the intermediate formed upon the bromide anion nucleophilic attack but does not correspond to a stable energy minimum. Epi stands for epichlorohydrin.
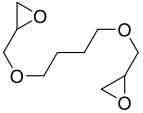
The computational results also show that, once the bromide ion is reacting with epichlorohydrin (see details in the Materials and Methods section), the three-membered ring opens and the resulting activated oxygen spontaneously attacks the carbon atom of CO_2 when the latter is interacting with TPP-Mg (route 2). In route 1, the opened epichlorohydrin also reacts with CO_2 but this requires crossing an energy barrier. Even in route 1 for which epichlorohydrin is initially in interaction with the Mg atom, the reaction with CO_2 leads to a rearrangement of the epichlorohydrin-CO_2 complex in such a way that the reaction ends up with the same product as in route 2. We thus believe that the complex shown at the bottom right of **Figure 9** reliably represents the species appearing upon reaction between epichlorohydrin and CO_2 in the presence of TPP-Mg and bromide ions.

Finally, the overall versatility of **TSP-Mg-imi** was explored using other epoxides such as 1,4-butanediol diglycidyl ether, propylene oxide or the more challenging cyclohexene oxide, styrene oxide and oxetane (**Table 2**).

In all the catalytic tests, good conversions to the corresponding cyclic carbonates were achieved, as well as good TON and productivities. Due to the high steric hindrance of the reactant, reaction with cyclohexene oxide required a longer reaction time (24 h) at 150 °C (entry 1). **TSP-Mg-imi** showed full selectivity toward the corresponding cyclic carbonate with a conversion of 75%. In addition, a *cis/trans*-cyclohexene carbonate ratio of 94:6 was detected by ^{1}H NMR. Styrene oxide was converted at 56% into the corresponding carbonate after 3 h (entry 2). The reaction with 1,4-butanediol diglycidyl ether was run at 125 °C affording quantitative conversion into the corresponding cyclic carbonate in 20 h (entry 3). The reactivity of propylene oxide was explored at 100 °C, with a reaction time of 3 h and applying a catalytic loading of 0.019 mmol Mg. Overall, a good conversion of 32% was obtained with a TON_{Mg} value of 6000 (entry 4). Using oxetane as a substrate, 70% of conversion was achieved, with very high selectivity toward the polycyclic carbonate product (entry 5). This value can be attributed to the combination of the high operating temperature and the presence of Mg, which plays a coordinating effect during the catalytic process.[14]

Even though the comparison of different catalysts is always a hard task because of the heterogeneity of reaction conditions, the results highlight that **TSP-Mg-imi** possesses excellent catalytic activity if compared with several previously reported heterogeneous bifunctional metalloporphyrin-based catalysts (**Table 3**).

Table 2. Cyclic carbonates synthesis catalyzed by **TSP-Mg-imi**.[a]
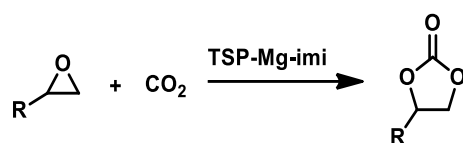
Entry	Substrate	t(h)	T (° C)	Conv (%)[b]	TON_{Mg}[c]	TOF_{Mg} (h^{-1})[c]	Productivity[d]
1[e,f]	237 mmol	24	150	75	2300	95	100
2	210 mmol	3	125	56	6200	2100	300
3	131 mmol	20	125	95	13100	660	1200
4	355 mmol	3	100	32	6000	2000	200
5[g]	231 mmol	24	150	70	8500	360	300

[a] Reaction conditions: CO_2 (25 bar), catalyst 60 mg (0.019 mmol Mg), 500 rpm. [b] Determined by ^{1}H-NMR. [c] TON_{Mg} and TOF_{Mg} values calculated based on the Mg content obtained from ICP analysis. [d] productivity (P, calculated as grams of cyclic carbonates obtained *per* grams of catalyst. [e] Catalyst 240 mg (0.079 μmol Mg). [f] Selectivity toward cyclic carbonates 96% (*cis/trans* ratio 94:6). [g] Selectivity toward polycarbonates 90%.

Table 3. Selected data for the reaction between epoxides and CO_2 in the presence of different heterogeneous bifunctional catalysts based on metalloporphyrin.

Entry	Catalyst	Substrate[a]	Conv (%)	TON_M[b]	TON_x[c]	P[d]	Conditions	Ref.
1	TSP-Mg-imi	SO	56	6180	590	322	25 bar; 3h; 125 °C	Chapter IV
2	TSP-AlCl-imi	SO	49	3868	1983	281	25 bar; 3h; 125 °C	8
3	MWCNT-TSP-AlCl-imi	SO	55	7649	4025	316	25 bar; 3h; 125 °C	8
4	POSS_TSP_AlCl_imiBr	SO	53	5849	3749	304	25 bar; 3h; 125 °C	15
5	Mg-por/pho@POP	SO	36	7200		188	3 Mpa; 1h; 140 °C	16
6	POP-PBnCl-TPPMg-12	SO	74	1480		38	1 bar; 48h; 80 °C	17
7	Mg-Por\DVB(1:20)@POPs+TBAB(homog.)	SO	96	19200	690	255	3 Mpa; 5h; 120 °C	18
8	[ZnPy+CPP-BTA]I⁻	SO	63	1260		109	0.5 Mpa; 8h; 80 °C	19
9	Zn-CIF2-C2H4	SO	95	527	133	28	2.5 MPa; 4 h; 120 °C	20
10	TSP-Mg-imi	ECH	>95	15300	1457	658	25 bar; 3h; 100 °C	Chapter IV
11	MWCNT-TSP-AlCl-imi	ECH	>95	20265	10665	661	25 bar; 3h; 100 °C	8
12	POSS_TSP_AlCl_imiBr	ECH	91	14656	9394	634	25 bar; 3h; 100 °C	15
13	Mg-por/pho@POP	ECH	67	13400		293	3 Mpa; 1h; 120 °C	16
14	Mg-Por\DVB(1:20)@POPs+TBAB(homog.)	ECH	97	19400	700	214	3 Mpa; 5h; 120 °C	18
15	[ZnPy+CPP-BTA]I⁻	ECH	91	1820		130	1.0 MPa; 16 h; 100 C	19
16	Zn-CIF2-C2H4	ECH	98	540	136	30	2.5 MPa; 4 h; 120 °C	20

[a] SO equal to styrene oxide and ECH equal to epichlorohyrin, [b]TON_M values calculated based on the metal content obtained from ICP analysis; [c]TON_x values calculated based on the halide content; [d] Productivity(P)= grams of product/grams catalyst.

Moreover, considering that the reaction conditions can be easily adapted to obtain full conversion with a selectivity higher than 95%, and that the process takes place under solvent free conditions, in the presence of a reusable heterogeneous catalyst, the overall process is highly sustainable (with an E-factor close to zero). The reaction conditions used here to convert CO_2 required a temperature range of 30–150 °C, using a pressure of 25 bar for each run. These conditions may appear as not mild, but one must consider that our reactor operates with large amounts of epoxide (usually more than 200 mmol). The use of only one equivalent of CO_2 at atmospheric pressure would require the filling of a volume of almost 5 L at room temperature, hence the high pressure used instead. One of the goals of the process

intensification[21] is the reduction in the size and/or volume of all the process plant components. High CO_2 pressures make it possible to significantly reduce the reactor volume. For instance, the industrial production of propylene carbonate can be carried out within a reactor operating at high pressures (20 bar) at 180 °C in the presence of a homogeneous catalyst. [22]

4.3 Conclusions

In the present work, magnesium tetrastyrylporphyrin (**TSP-Mg**) and bis(vinyl)imidazolium salt **5** have been polymerized in the presence (**7a** and **7b**) or in the absence (**TSP-Mg-imi**) of multi-walled carbon nanotubes. The corresponding highly cross-linked materials have been characterized by means of several spectroscopic and analytical techniques such as TGA, TEM, SEM-EDX, ICP-OES, XPS, solid state NMR, porosimetry. **TSP-Mg-imi** possesses a high specific surface area for this kind of cross-linked materials resulting in good performances as heterogeneous catalyst in the cycloaddition reaction of CO_2 to epoxides to afford the corresponding cyclic carbonates under solvent-free conditions. In the same conditions, the nanotube-based analogue **7a** displayed poor performances. An improvement in the catalytic activity has been achieved with the hybrid **7b** with a 1:8 Mg/Br⁻ ratio in the final material. However, the unsupported material **TSP-Mg-imi** has been elected as the catalyst of choice due to its easier preparation and cheaper cost, resulting in highly active in the formation of cyclic carbonates and recyclable for at least four cycles. Additional tests proved a superior activity for **TSP-Mg-imi** under heterogeneous catalysis conditions compared to the corresponding [**Bis-imi**+T**SP-Mg**] homogeneous system. The enhanced activity of the bifunctional catalyst can be ascribed to its high surface area, which permits full access to the catalytic sites, combined with the proximity between the metal centers and the bromide ions due to the covalent link between the porphyrin core and the bis(vinyl)imidazolium salt, enabling a strong cooperation that results in a synergistic effect during the catalytic cycle, as also highlighted by the computational results. The metalloporphyrin moiety acts both as a sort of "covalent swelling agent" giving rise to a higher surface area and as a Lewis acid co-catalytic species.

4.4 Experimental Section

Materials and methods. Chemicals and solvents were purchased from commercial suppliers to be used without further purification. Thermogravimetric analysis (TGA) was performed in a Mettler Toledo TGA STAR system with a heating rate of 10 °C/min, either under oxygen flow from 100 to 1000 °C or under nitrogen flow from 25 to 900 °C. Transmission electron microscopy (TEM) images were recorded using a Philips Tecnai 10 microscope operating at 80-100 kV. Nitrogen adsorption-desorption analyses were carried out at 77 K in a Micromeritics ASAP 2420 volumetric adsorption analyzer. Before the analysis the sample was pre-treated at 150 °C for 8 h under reduced pressure (0.1 mbar). The Brunauer-Emmett-Teller (BET) method was applied in the $0.05-0.30$ p/p_0 range to calculate the specific surface area. X-ray photoelectron spectroscopy (XPS) analyses were carried out in a ThermoFisher ESCALAB 250Xi instrument equipped with a monochromatic Al Kα X-ray source (1486.6 eV) and a hemispherical deflector analyzer (SDA) working at constant pass energy (CAE) allowing to obtain a constant energy resolution on the whole spectrum. The experiments were performed using a 200 μm diameter X-ray spot. The charge neutralization of the sample was achieved with a flood gun using low energy electrons and argon ions. The pressure in the analysis chamber was in the range of 10^{-8} Torr during data collection. Survey spectra were recorded with a 200 eV pass energy, whereas high-resolution individual spectra were collected with a 50 eV pass energy. Analyses of the peaks were carried out with the Thermo Avantage software, based on the non-linear squares fitting program using a weighted sum of Lorentzian and Gaussian component curves after background subtraction according to Shirley and Sherwood. Inductively coupled plasma optical emission spectroscopy (ICP-OES) was employed in an Optima 8000 Spectrometer. ^{1}H NMR spectra were recorded on a Bruker 400 MHz spectrometer. Solid state ^{13}C NMR spectra were recorded at room temperature on a JEOL ECZ-R spectrometer operating at 11.7 T using a 3.2 mm AUTOMAS probe and spinning frequencies of 10 kHz. FT-IR measurements were performed in absorbance mode using a Perkin Elmer two DEP. Chemical combustion analysis was performed on a Perkin-Elmer 2400 Serie 2 analyzer.

Synthetic procedures

Synthesis of magnesium bromide ethyl etherate.[16] In a 25 mL two-neck round-bottom flask, under Ar atmosphere, magnesium turnings (194 mg, 7.98 mmol) and diethyl ether (12.0 mL) were transferred. The mixture was allowed to stir at 35 °C before the dropwise addition of

1,2-dibromoethane (705 µL, 8.18 mmol). Then the reaction mixture was left at this temperature until the end of gas evolution. Afterwards the volume was reduced under a stream of argon and the obtained white solid was dried under vacuum (0.200 mg; 100%).

Synthesis of tetrastyrylporphyrin of magnesium (TSP-Mg). The procedure was similar to that reported previously with minor changes.[16] In a 25 mL round-bottom flask, tetrastyrylporphyrin (200 mg, 0.282 mmol) and DCM (14 mL) were charged. The mixture was allowed to stir at room temperature before the addition of triethylamine (800 µL, 5.60 mmol) and magnesium bromide ethyl etherate (723 mg, 2.80 mmol). After 15 minute the volume of the reaction mixture was diluted with CHCl$_3$ and the mixture was washed with NaHCO$_3$ (3 × 50 mL). Then the organic layers were dried over MgSO$_4$, filtered, concentrated under vacuum and purified by celite plug (DCM) to remove any insoluble residue. The filtrate was concentrated under vacuum and **TSP-Mg** was obtained as purple powder (207 mg; 100%). 1 H NMR (300 MHz, CDCl$_3$, δ): 8.41 (s, 8 H), 7.49 (s, 16 H), 6.98 (dd, J = 17.6, 11.0 Hz, 4 H), 5.99 (d, J = 17.7 Hz, 4 H), 5.49 (d, J = 10.9 Hz, 4 H) ppm

Synthesis of highly cross-linked imidazolium salt. In a 25 mL two neck round-bottom flask, under Ar atmosphere, bis(vinyl)imidazolium salt (250 mg, 0.618 mmol), azobis(isobutyronitrile) (AIBN) (5 mol%) and dry ethanol (1.5 mL) were charged. The reaction mixture, magnetically stirred, was degassed by bubbling argon for 10 minutes. Then the temperature was gradually increased up to 78 °C and the mixture was kept reacting at this temperature overnight. Once a white precipitate was obtained, the system was brought to room temperature, and the homopolymer was washed using methanol and diethyl ether. The residue was finally dried under vacuum at 60 °C to give the final material (0.18 g; 74%).

Synthesis of highly cross-linked TSP-Mg-imi (6). Under argon atmosphere, bis(vinyl)imidazolium salt **5** (327 mg, 0.809 mmol) and **TSP-Mg** (150 mg, 0.202 mmol) were transferred to a two-necked round bottom flask and dissolved in dry dimethylformamide (DMF) (5.6 mL). After the addition of azobis(isobutyronitrile) (AIBN) (5 wt%), argon was bubbled into the mixture for 20 min, which was then refluxed and stirred at 120 °C overnight. The hybrid solid material was recovered by centrifugation and washed several times with DMF, chloroform and methanol. Before each centrifugation, the catalyst was sonicated for 10 min in the washing solvent. The last washing was done with diethyl ether. The green-colored catalyst was recovered and dried under vacuum at 60 °C (437 mg, 91%).

Synthesis of MWCNT-TSP-Mg-imi 1:8 (7a) and MWCNT-TSP-Mg-imi 1:12 (7b). In a two-neck round-bottom flask, bis(vinyl)imidazolium sal **5** (0.809 or 0.809 mmol), **TSP-Mg** (0.202 or 0.135 mmol), MWCNTs (100 or 50 mg) and dry DMF (10 or 5 mL) were transferred and sonicated for 20 min, under argon atmosphere. AIBN (5 wt%) was added to the reaction mixture, which was bubbled argon for 20 min. The mixture was then refluxed and stirred at 120 °C overnight. The solid was recovered by centrifugation and washed several times with DMF, chloroform and methanol. Before each centrifugation, the catalyst was sonicated for 10 min in the washing solvent. After drying under vacuum at 60 °C, **MWCNT-TSP-Mg-imi** was obtained as a green solid (555 mg, 96% for **7a**; 450 mg, 94% for **7b**).

General procedure for the conversion of CO_2. The catalytic tests were carried out in a Cambridge Design Bullfrog batch reactor, with temperature control, pressure monitoring and mechanical stirring. In each test, a fine dispersion of the catalyst was added into the selected epoxide under solvent-free conditions. Once the reactor was closed, the mechanical stirring speed was set at 500 rpm. The mixture was purged with N_2 for 10 min and then pressurized with 25 bar of CO_2. After this, the temperature was increased with a ramp of 5 °C/min and kept to the required temperature during the reaction time. In selected case, a refill of CO_2 was carried out during the experiment to maintain the quantity of reagent required for the reaction. At the end of the reaction time, the reactor was cooled down to room temperature and slowly depressurized. The separation of the catalyst from the reaction mixture was easily performed by centrifugation (15 min, 4500 rpm). The supernatant solution was analyzed by ^{1}H NMR spectroscopy in $(CD_3)_2SO$ or in $CDCl_3$.

General recycling procedure for the conversion of CO_2. The stability of the materials was tested in the reaction between epichlorohydrin and CO_2. After each catalytic test, the catalyst was recovered by centrifugation and washed with toluene (4x40 mL), ethanol (4x40 mL) and diethyl ether. To get a good dispersion, before each centrifugation, the catalyst was previously sonicated in the washing solvent for 15 min. Then, the solid was dried under vacuum at 60 °C. Once dried, the catalyst was reused for the next cycle keeping the ratio between moles of catalyst and moles of epoxides constant. The conversion of epichlorohydrin into cyclic carbonate was estimated by ^{1}H NMR analysis.

Reaction conditions of Scheme 2. The catalytic experiments of **Scheme 2** were performed in a Teflon vial, under solvent-free conditions. In each test, the same amount of epichlorohydrin (24 mL, 306 mmol) was added. The comparison of the catalytic activity of the six systems was studied considering the Mg loading (0.019 mmol) and consequently the mass amount used of **TSP-Mg-imi 6** (60 mg). Therefore, the electrophilic center component

(**TSP-Mg**) inserted was 15 mg, while the nucleophilic component (**Homopolymer** and **Bis-imi 5**) was 45 mg. After closing the reactor, the mixture was stirred at 500 rpm. The system was then purged for 10 min with N_2 before the addition of 25 bar of CO_2. After this, the system was heated to 80 °C with a heating rate of 5 °C/min. The conversion of epichlorohydrin into cyclic carbonate was estimated by ^1H NMR analysis.

Quantum-chemical calculations. All the quantum-chemical calculations have been performed in the Density Functional Theory (DFT) formalism with the Gaussian16 package using the M062X functional and the 6-311G* basis set. In all cases, the dispersion interactions were corrected with the D3 version of Grimme's dispersion with Becke-Johnson damping.[23] The complexation energies are estimated as the energy difference between the product and isolated reactants taking into account the correction for the basis set superposition error.[24] To simulate the nucleophilic attack of Br⁻, a bromide anion has been bound in four different ways on the two carbons of the epoxy ring. The geometry of those species has then been first optimized while keeping the C–Br⁻ bond fixed at 1.96 Å before performing a full optimization of the complexes. In route 1 (**Figure 9**), the results point to the opening of the epichlorohydrin upon addition of the bromide anion, but the resulting activated oxygen does not react spontaneously with CO_2; an additional activation energy barrier has to be crossed. Determining the height of this activation energy barrier is beyond the scope of this study. Instead, we put CO_2 in closer contact (distance of 1.42 Å) with epichlorohydrin and reoptimized the assembly.

4.5 References

1.   García-López, E. I.; Campisciano, V.; Giacalone, F.; Liotta, L. F.; Marcì, G., Supported Poly(Ionic Liquid)-Heteropolyacid Based Materials for Heterogeneous Catalytic Fructose Dehydration in Aqueous Medium. *Molecules* **2022**, *27*, 4722.

2.   Buscemi, R.; Giacalone, F.; Orecchio, S.; Gruttadauria, M., Cross-Linked Imidazolium Salts as Scavengers for Palladium. *ChemPlusChem* **2014**, *79*, 421-426.

3.   Morena, A.; Campisciano, V.; Comès, A.; Liotta, L. F.; Gruttadauria, M.; Aprile, C.; Giacalone, F., A Study on the Stability of Carbon Nanoforms–Polyimidazolium Network Hybrids in the Conversion of CO2 into Cyclic Carbonates: Increase in Catalytic Activity after Reuse. *Nanomaterials* **2021**, *11*, 2243.

4.   Thommes, M.; Kaneko, K.; Neimark, A. V.; Olivier, J. P.; Rodriguez-Reinoso, F.; Rouquerol, J.; Sing, K. S. W., Physisorption of gases, with special reference to the evaluation of surface area and pore size distribution (IUPAC Technical Report). *Pure Appl. Chem.* **2015**, *87*, 1051-1069.

5.   Pavia, C.; Ballerini, E.; Bivona, L. A.; Giacalone, F.; Aprile, C.; Vaccaro, L.; Gruttadauria, M., Palladium Supported on Cross-Linked Imidazolium Network on Silica as Highly Sustainable Catalysts for the Suzuki Reaction under Flow Conditions. *Adv. Synth. Catal.* **2013**, *355*, 2007-2018.

6.   Song, H.; Wang, Y.; Xiao, M.; Liu, L.; Liu, Y.; Liu, X.; Gai, H., Design of Novel Poly(ionic liquids) for the Conversion of CO2 to Cyclic Carbonates under Mild Conditions without Solvent. *ACS Sustain. Chem. Eng.* **2019**, *7*, 9489-9497.

7.   Yuan, J.; Mecerreyes, D.; Antonietti, M., Poly(ionic liquid)s: An update. *Prog. Polym. Sci* **2013**, *38*, 1009-1036.

8.   Campisciano, V.; Valentino, L.; Morena, A.; Santiago-Portillo, A.; Saladino, N.; Gruttadauria, M.; Aprile, C.; Giacalone, F., Carbon nanotube supported aluminum porphyrin-imidazolium bromide crosslinked copolymer: A synergistic bifunctional catalyst for CO2 conversion. *J CO2 Util* **2022**, *57*, 101884.

9.   Calabrese, C.; Liotta, L. F.; Carbonell, E.; Giacalone, F.; Gruttadauria, M.; Aprile, C., Imidazolium-Functionalized Carbon Nanohorns for the Conversion of Carbon Dioxide: Unprecedented Increase of Catalytic Activity after Recycling. *ChemSusChem* **2017**, *10*, 1202-1209.

10.   Campisciano, V.; Calabrese, C.; Liotta, L. F.; La Parola, V.; Spinella, A.; Aprile, C.; Gruttadauria, M.; Giacalone, F., Templating effect of carbon nanoforms on highly cross-linked imidazolium network: Catalytic activity of the resulting hybrids with Pd nanoparticles. *Appl. Organomet. Chem.* **2019**, *33*, e4848.

11.   Muralidharan, S.; Hayes, R., Intense satellites in the N 1s X-ray photoelectron spectra of certain metalloporphyrins. *J. Am. Chem. Soc.* **1980**, *102*, 5106-5107.

12.   Karweik, D. H.; Winograd, N., Nitrogen charge distributions in free-base porphyrins, metalloporphyrins, and their reduced analogs observed by x-ray photoelectron spectroscopy. *Inorg. Chem.* **1976**, *15*, 2336-2342.

13.   Zhang, J.; Zhang, P.; Zhang, Z.; Wei, X., Spectroscopic and Kinetic Studies of Photochemical Reaction of Magnesium Tetraphenylporphyrin with Oxygen. *J. Phys. Chem. A* **2009**, *113*, 5367-5374.

14. Huang, J.; Jehanno, C.; Worch, J. C.; Ruipérez, F.; Sardon, H.; Dove, A. P.; Coulembier, O., Selective Organocatalytic Preparation of Trimethylene Carbonate from Oxetane and Carbon Dioxide. *ACS Catal.* **2020**, *10*, 5399-5404.

15. Morena, A.; Campisciano, V.; Santiago-Portillo, A.; Gruttadauria, M.; Giacalone, F.; Aprile, C., POSS-Al-porphyrin-imidazolium cross-linked network as catalytic bifunctional platform for the conversion of CO_2 with epoxides. *Fuel* **2022**, 126819.

16. Wang, W.; Wang, Y.; Li, C.; Yan, L.; Jiang, M.; Ding, Y., State-of-the-Art Multifunctional Heterogeneous POP Catalyst for Cooperative Transformation of CO2 to Cyclic Carbonates. *ACS Sustain. Chem. Eng.* **2017**, *5*, 4523-4528.

17. Dai, Z.; Tang, Y.; Zhang, F.; Xiong, Y.; Wang, S.; Sun, Q.; Wang, L.; Meng, X.; Zhao, L.; Xiao, F.-S., Combination of binary active sites into heterogeneous porous polymer catalysts for efficient transformation of CO2 under mild conditions. *Chinese J. Catal.* **2021**, *42*, 618-626.

18. Wang, W.; Li, C.; Jin, J.; Yan, L.; Ding, Y., Mg–porphyrin complex doped divinylbenzene based porous organic polymers (POPs) as highly efficient heterogeneous catalysts for the conversion of CO2 to cyclic carbonates. *Dalton Trans.* **2018**, *47*, 13135-13141.

19. Su, Z.; Ma, L.; Wei, J.; Bai, X.; Wang, N.; Li, J., A zinc porphyrin polymer as efficient bifunctional catalyst for conversion of CO2 to cyclic carbonates. *Appl. Organomet. Chem.* **2024**, e6632.

20. Liu, J.; Zhao, G.; Cheung, O.; Jia, L.; Sun, Z.; Zhang, S., Highly Porous Metalloporphyrin Covalent Ionic Frameworks with Well-Defined Cooperative Functional Groups as Excellent Catalysts for CO2 Cycloaddition. *Chem. Eur. J.* **2019**, *25*, 9052-9059.

21. Reay, D.; Ramshaw, C.; Harvey, A., *Process intensification: Engineering for efficiency, sustainability and flexibility*. Butterworth-Heinemann: Oxford, United Kingdom, **2013**.

22. Lange, J. P. Process for the preparation of propylene carbonate. US patent 7,728,164 B2, 2010.

23. Grimme, S.; Ehrlich, S.; Goerigk, L., Effect of the damping function in dispersion corrected density functional theory. *J. Comp. Chem.* **2011**, *32*, 1456-65.

24. Simon, S.; Duran, M.; Dannenberg, J. J., How does basis set superposition error change the potential surfaces for hydrogen-bonded dimers? *J. Chem. Phys.* **1996**, *105*, 11024-11031.

CHAPTER V

Phosphonium salt/Al-porphyrin copolymer as bifunctional heterogeneous catalyst for CO₂ conversion to cyclic carbonates
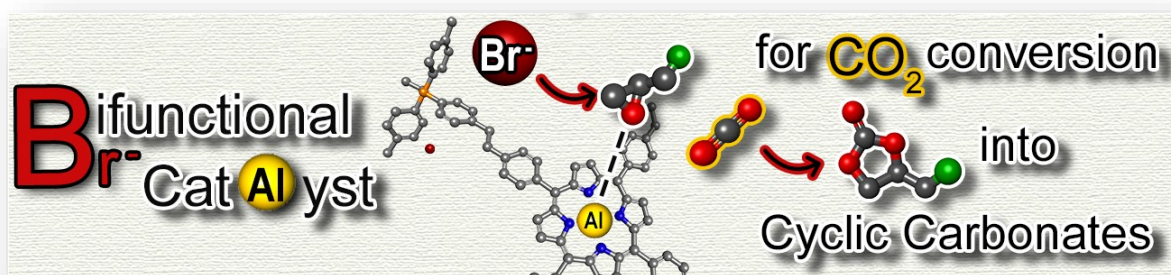
This chapter is based on:

CHAPTER V

Phosphonium salt/Al-porphyrin copolymer as bifunctional heterogeneous catalyst for CO_2 conversion to cyclic carbonates

5.1 Abstract

The effective chemical valorization of CO_2 by means of its conversion into valuable products is now more than ever a topic of considerable interest. It is on that basis that herein we have chosen the conversion of CO_2 and epoxides to cyclic carbonates as a convenient route to achieve this goal. A new bifunctional (Lewis acid/nucleophile) heterogeneous material, **TSP-AlCl-PhospBr**, was designed in order to guarantee a close proximity between the two active sites that can cooperate to the activation and opening of the epoxide ring. The prepared copolymer has been extensively characterized using various spectroscopic and analytical techniques. As a heterogeneous catalyst, it enables efficient chemical conversion of CO_2 and epoxides, even at low temperatures, down to 30 °C, without the use of solvents. In particular, the catalyst demonstrates high turnover numbers (TON) and frequency values (TOF). Recyclability studies on **TSP-AlCl-PhospBr** have shown its stability and reusability for consecutive cycles without the need of reactivation procedures.

5.2 Results and discussion

An aluminium porphyrin based ionic porous cross-linked polymer was designed and prepared to be applied as heterogeneous bifunctional catalytic system in the conversion of CO_2 and epoxides into cyclic carbonates. The copolymer **TSP-AlCl-PhospBr** was obtained following a simple one-pot radical polymerization by mixing the thermal radical initiator 2,2'-azobis(2-methylpropionitrile) (AIBN) and the two building blocks: aluminium porphyrin (TSP-AlCl) **1** and vinyl-functionalized quaternary phosphonium salt monomer **2** (**Scheme 1**).
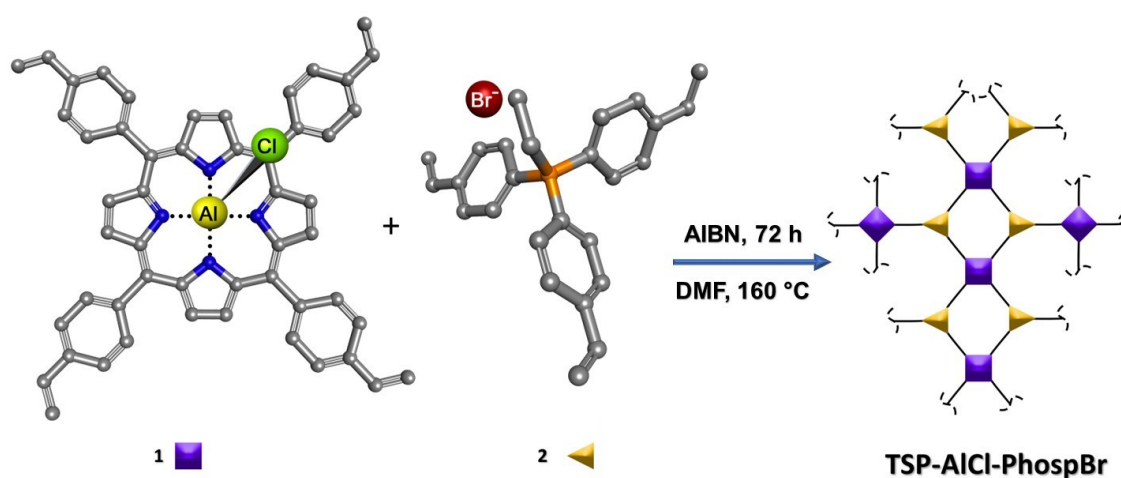
Scheme 1. Schematic representation of the synthesis of **TSP-AlCl-PhospBr**.

This simple approach allows an easy and effective synthesis of a material containing two active sites, the nucleophile species (catalyst) and the Lewis acid species (co-catalyst). This synthetic strategy is highly performing, as demonstrated by the excellent yield (96%). In order to study the thermal behaviour of the cross-linked material, thermogravimetric analysis (TGA) was performed under nitrogen flow (**Figure 1a**). TGA profile of **TSP-AlCl-PhospBr** indicates good thermal stability of the solid up to 300 °C; above this temperature the degradation of the organic moieties with a first weight loss centred at 347 °C will start along with a second decomposition peak at 466 °C. In this regard, it should be highlighted that the good thermal stability of the solid represents a promising feature for its repeated use under heating conditions. Moreover, through the TGA thermogram under oxygen, the thermal stability of the copolymer was also corroborated under oxidizing conditions, as shown by the TGA profile under air, which exhibits a marked weight loss only after 300 °C (**Figure 1b**).
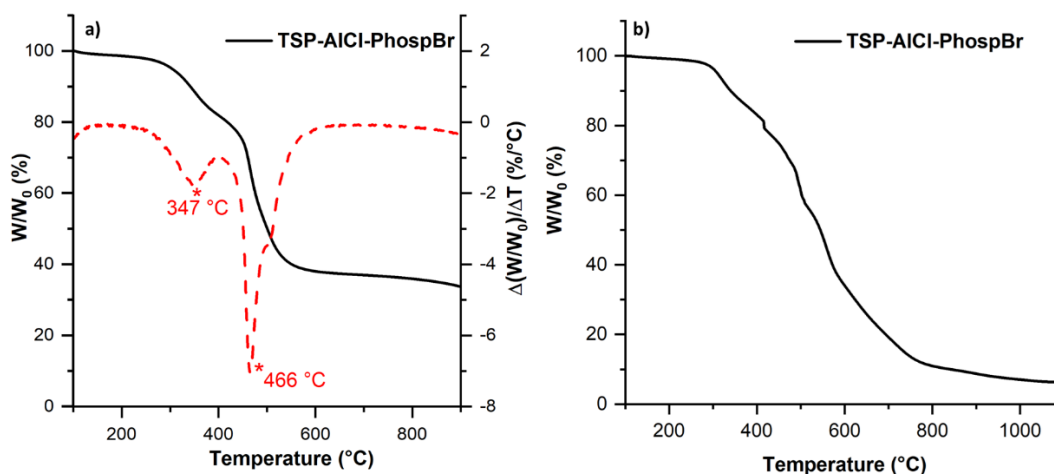
Figure 1. TGA profile a) under N_2 flow (solid line) and derivative thermogravimetry (dotted line) of **TSP-AlCl-PhospBr** and b) under air flow.

The morphology of the bifunctional material was investigated by transmission electron microscopy (TEM). TEM analysis revealed that the copolymer forms a series of compact and large aggregates (**Figure 2**).
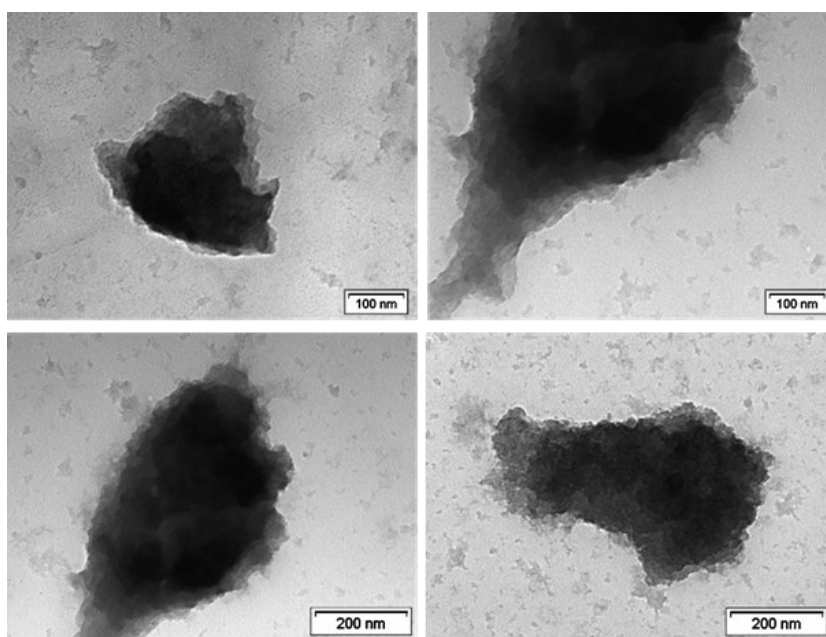
Figure 2. TEM micrographs of **TSP-AlCl-PhospBr**.

Through the use of TEM-EDX, the presence of both catalytic active sites, aluminium and bromide, and especially an uniform distribution of these elements in the copolymer was confirmed (**Figure 3**).
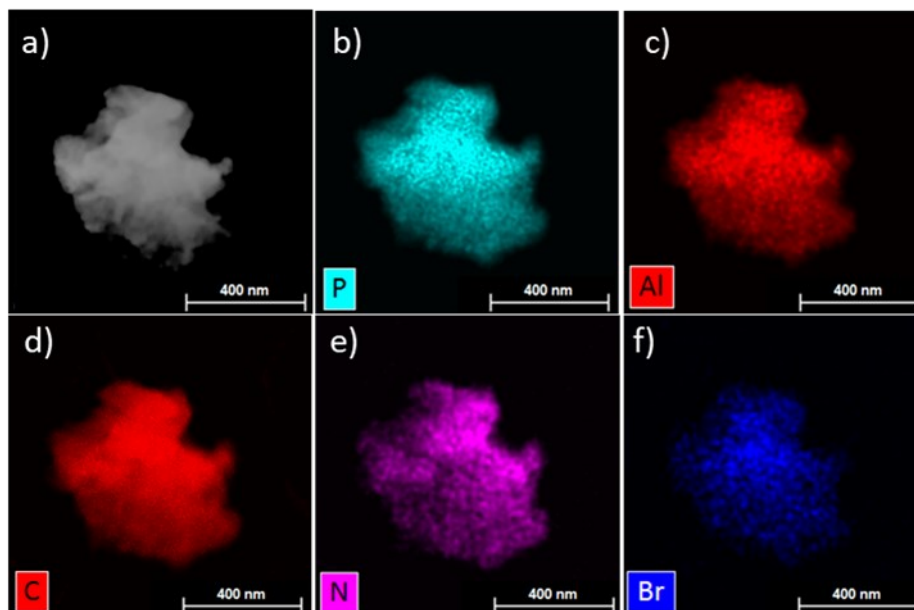
Figure 3. TEM micrographs of **TSP-AlCl-PhospBr** (a) and EDX elemental-mapping images (b-f).

The textural property of the material was explored by means of N_2 adsorption/desorption measurements. The specific surface area (SSA), estimated by the Brunauer-Emmett-Teller (BET) method, and the pore size distribution analysed by applying the Barrett-Joyner-Halenda (BJH) method, were calculated to be 212 m^2/g and 0.17 cm^3/g, respectively. Based on the IUPAC classification, the N_2 physisorption isotherm of the hybrid copolymeric material exhibits typical type II isotherms with H4 hysteresis loop (**Figure 4**).
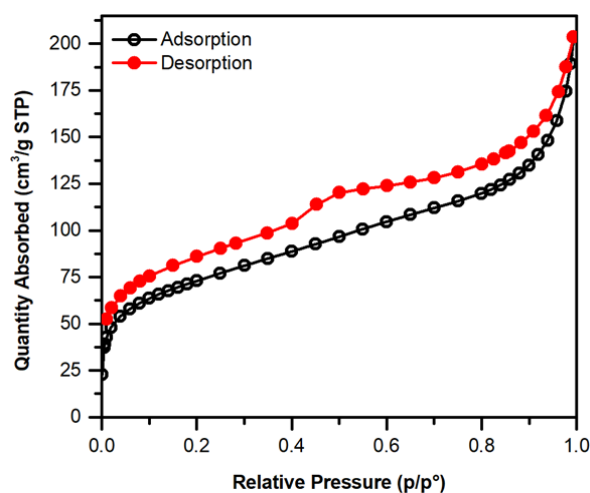
Figure 4. Nitrogen adsorption-desorption isotherms of **TSP-AlCl-PhospBr**.

The first proof of the copolymerization process has been provided by Fourier-transform infrared (FT-IR) spectroscopy (**Figure 5**). FT-IR spectrum of **TSP-AlCl-**

PhospBr was compared with those of its precursors. In particular, some characteristics IR bands of both aluminium porphyrin (blue line) and phosphonium salt (red line) can be clearly identified in the spectrum of the copolymeric material (black line) as highlighted in **Figure 5**.
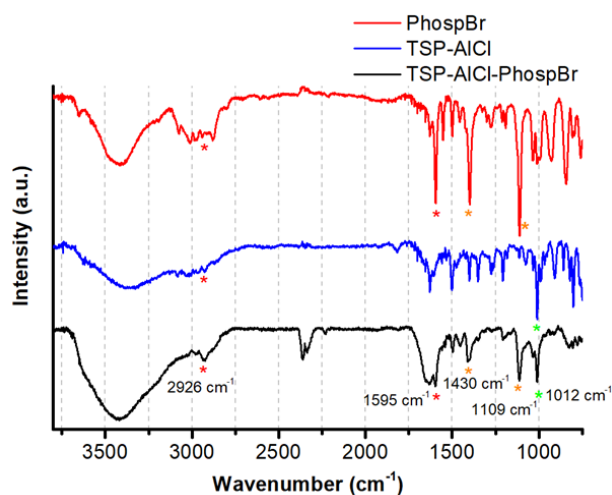
Figure 5. FT-IR spectra of Phosphonium salt (red line), TSP-AlCl (blue line) and **TSP-AlCl-PhospBr** (KBr pellet; green line).

The typical vibration of the metalloporphyrin ring around 1012 cm^{-1} as well as the intense absorptions at 1430 and 1109 cm^{-1} associated with the stretching and bending vibration modes of the P–C bond in the phosphonium moieties are revealed.[1-4] The copolymer spectrum also shows the band at 1595 cm^{-1} attributed to the stretching vibration mode of C=C–C bond of the phenyl units along with the symmetrical C–H stretching present in the aromatic core located in the region below 3000 cm^{-1}. Furthermore, the high hygroscopicity of the copolymer results in a large and strong absorption band at 3200-3800 cm^{-1} and a medium absorption band at 1628 cm^{-1}, arising from O–H stretching and H–O–H bending of water, respectively.

To further characterize **TSP-AlCl-PhospBr**, solid state ^{13}C NMR was employed by means of the Cross-Polarization Magic Angle Spinning Total Suppression of spinning side bands technique (CP-MAS-TOSS ^{13}C NMR). ^{13}C NMR spectrum, in **Figure 6a**, shows the signals attributed to the carbon atoms of the porphyrin ring along with the phenyl moieties of the phosphonium salt in the δ = 115–160 ppm range, whereas the aliphatic ones are located in the range between δ = 6–50 ppm. The highly shielded

signal at δ = 6 ppm corresponds to the -CH$_3$ of the ethyl chain in the phosphonium salt structure.

The ^{31}P NMR MAS analysis of the hybrid material was performed to verify the stability of phosphorus during the polymerization process. The spectrum in **Figure 6b** displays a single peak at 25 ppm, which is in accordance with the literature; indeed, the typical signals of (R)$_4$P$^+$ resonate in the 22-26 ppm range. This analysis allowed to corroborate the preservation of phosphonium salt moieties in the copolymer skeleton.[5-7]
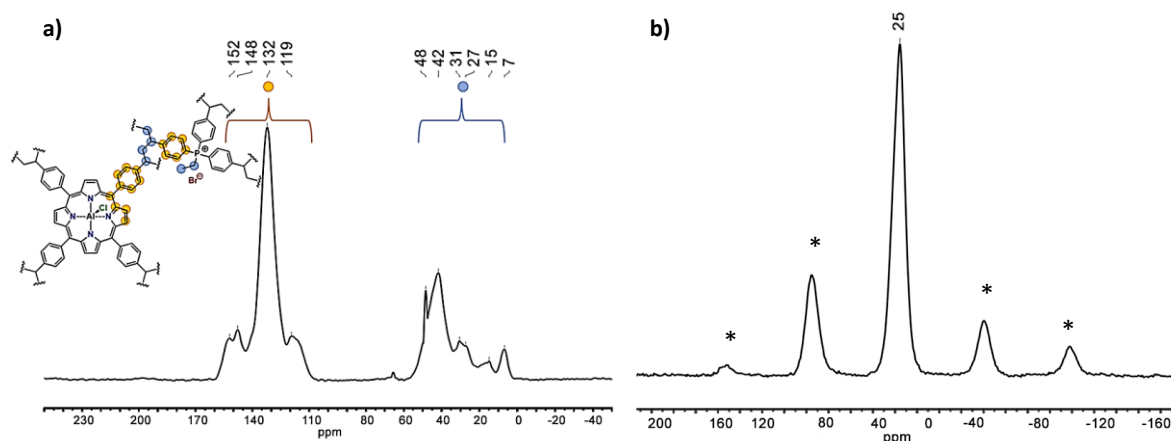
Figure 6. a) ^{13}C CP-MAS-TOSS NMR of **TSP-AlCl-PhospBr** and b) ^{31}P CP-MAS-NMR of **TSP-AlCl-PhospBr**. Asterisks indicate spinning side bands.

By X-ray photoelectron spectroscopy (XPS), the chemical composition of the outer surface of the material was analysed (**Figure 7**). The survey spectrum shows the presence of the peaks relative to the Lewis acid (Al) and those of the nucleophile (Br$^-$).

Consequently, the possibility of including both catalytic active sites in the structure of a bifunctional catalyst is confirmed. Furthermore, through the analysis of the high resolution XPS spectrum of the N1s region it was possible to verify the total complexation of the porphyrin ring with the metal. Indeed, the spectrum displays only a signal at 399.1 eV corresponding to the nitrogen atoms of the porphyrin ring coordinated with the metal. Indeed, the spectrum displays only a signal at 399.1 eV corresponding to the nitrogen atoms of the porphyrin ring coordinated with aluminium (Al–N). Finally, the amount of aluminium in **TSP-AlCl-PhospBr** was determined by inductively coupled plasma atomic emission spectroscopy (ICP-OES) analysis (0.36 mmol/g).
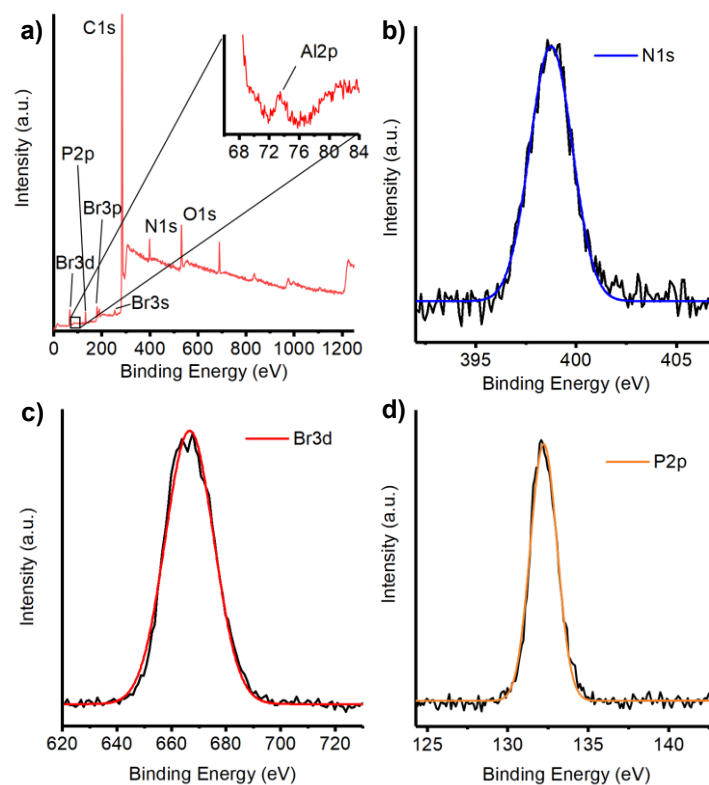
Figure 7. a) XPS survey spectrum of **TSP-AlCl-PhospBr**, b) N1s region, c) Br3d region and d) P2p region.

The copolymerized phosphonium-based salt was tested as heterogeneous catalyst for the conversion of CO_2 into cyclic carbonates under solvent-free reaction conditions. The formation of epichlorohydrin carbonate was chosen as benchmark reaction to verify the catalytic behaviour and the reusability of the catalyst. The recycling tests were carried out at non-quantitative conversion of epichlorohydrin. As illustrated in **Figure 8**, the catalytic material was employed for four consecutive runs at 60 °C without any considerable decrease of the performance. After each catalytic cycle, the copolymer was recovered by filtration and washed several times with toluene, ethanol and ethyl ether and dried under vacuum at 60 °C overnight. These results demonstrated the robustness of the catalyst in being used in several cycles.

Based on these preliminary results, our focus has been on the catalytic activity of the material under different reaction conditions and using other substrates such as glycidol, styrene oxide and cyclohexene oxide (**Table 1**, Entries 1-10). The catalytic performances of the solids were evaluated in terms of turnover number (TON_{Al}, defined as moles of epoxide converted/moles of Al active sites), turnover frequency (TOF_{Al}; TON_{Al}/reaction time in hours) and productivity (P, calculated as grams of cyclic carbonates obtained *per* grams of catalyst).
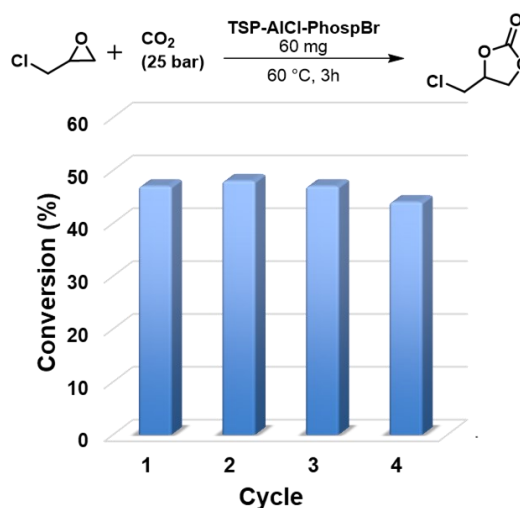
Figure 8. Recycling tests of **TSP-AlCl-PhospBr**. Reaction conditions: epichlorohydrin (307 mmol), 60 mg of catalyst (0.021 mmol Al) 25 bar of CO_2, 3 h, 60 °C, 500 rpm.

As shown in **Table 1**, some of the catalytic experiments were performed using reused **TSP-AlCl-PhospBr**, reflecting the versatility and good robustness of the material under different reaction conditions during catalysis between CO_2 and different epoxides (entries 2, 5, 7). Deeper investigations on epichlorohydrin conversion have been conducted (entries 1-6). It is worth mentioning that the catalyst can be employed at room temperature, achieving a conversion of 16% into the corresponding epichlorohydrin carbonate in only 3 hours with a TON_{Al} value of 2300 (entry 1). Nevertheless, the extension of the reaction time to 24 hours resulted in an increased conversion with a higher TON_{Al} value (entry 2). The same conversion value is obtained by reducing the reaction time to 3 hours and operating at a slightly higher temperature (entry 3). Higher conversion values and TON_{Al} are obtained when the reaction temperature is raised up to 80 °C (entries 4-6). These additional tests were carried out under the same conditions except for the amount of CO_2 used. When the system is filled with an initial pressure of 25 bar or a constant pressure of 10 bar is maintained, similar conversion values of 88% and 90% are obtained (entries 4 and 5). The analysis of the pressure/temperature *vs.* time graph (**Figure 9a**) of entry 4 revealed that a very low final pressure was reached indicating the plausible total consumption of CO_2. Conversely, a complete conversion and a corresponding TON_{Al} value of 14500 were reached when the system was charged and maintained at the CO_2 operating pressure of 25 bar (entry 6 and **Figure 9b**).
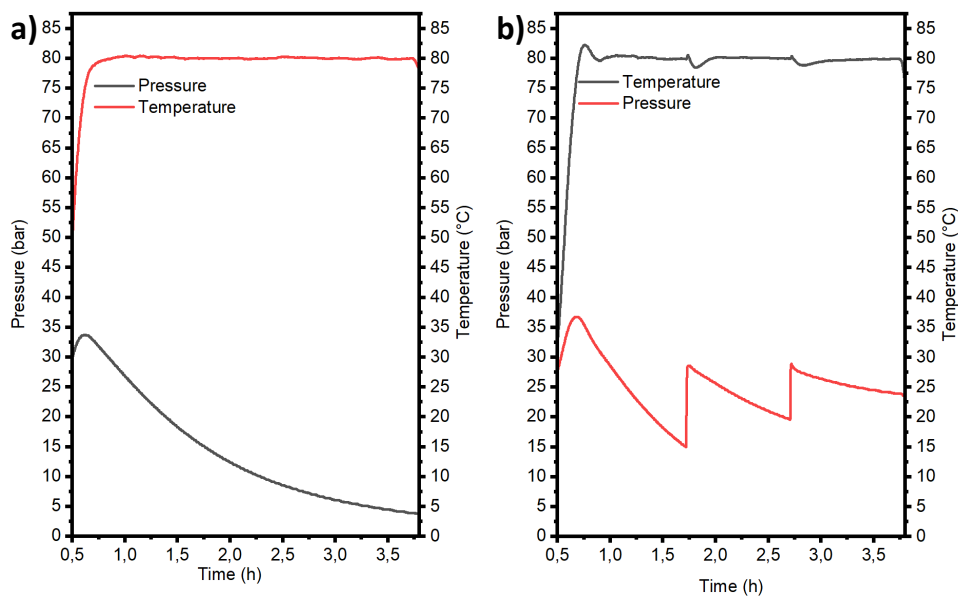
Figure 9. Pressure/Temperature *vs.* Time plot of the reaction between epichlorohydrin and CO_2 at 80 °C for 3h a) with an initial pressure of 25 bar (**Table 1**, entry 4) and b) with a constant pressure of 25 bar (**Table 1**, entry 6).

The reactivity of glycidol was studied at two different temperatures, 30 and 50 °C (entries 7-8). Once again, the catalyst is shown to be active at room temperature, achieving a good conversion value of 21% in 6 hours, with a TON_{Al} value of 3550. In addition, decreasing the reaction time from 6 to 3 hours and operating at 50 °C clearly leads to an improvement in terms of conversion and TON_{Al}, 65% and 1100, respectively. With the more challenging styrene oxide, 34% conversion was achieved when the reaction was conducted at 100 °C for 3 h (entry 9). Cyclohexene oxide exhibited a conversion of 31% when the reaction was run at 150 °C for 24 hours (entry 10). *Cis*-cyclohexene carbonate was not the only product. In addition to *cis*-cyclohexene carbonate, the presence of poly(cyclohexene carbonate) and *trans*-cyclohexene carbonate can also be observed. The formation of the *trans* isomer was attributed to a back-biting reaction, which can take place at the terminal end of the developing polymer chain. Indeed, through ^{1}H NMR a *cis/trans*-cyclohexene carbonate ratio of 70:30 and a selectivity toward the corresponding cyclic carbonate of 80% can be observed.[8-9]

As previously reported, the use of the co-catalyst enables a cooperativity effect during the CO_2 conversion with the epoxide to generate cyclic carbonates.

Table 1. Cyclic carbonates synthesis catalyzed by **TSP-AlCl-PhospBr**.

Entry	Test	Substrate	t (h)	T (°C)	Conv. (%)[a]	TON$_{Al}$[b]	TOF$_{Al}$ (h^{-1})[b]	Productivity[c]
1[d]	fresh		3	30	16	2300	800	111
2[e,f]	recycled		24	30	49	7000	300	340
3[d]	fresh	Cl, 230 or 307 mmol	3	60	47	6900	2300	327
4[d]	fresh		3	80	88	12900	4300	612
5[e,f,g]	recycled		3	80	90	12900	4300	625
6[d,h]	fresh		3	80	>99	14500	4900	688
7[e,i]	recycled	HO, 362 or 271 mmol	6	30	21	3600	600	149
8[h,j]	fresh		3	50	65	1100	3700	462
9	fresh	210 mmol	3	100	34	3400	1100	285
10[k,l]	fresh	237 mmol	24	150	31	1200	50	171

Reaction conditions: CO_2 (25 bar), catalyst 60 mg (0.021 mmol Al), 500 rpm [a] Determined by ^{1}H NMR; [b] TON and TOF values calculated on the basis of the Al content obtained from ICP analysis; [c] Productivity: grams of product/grams of catalyst; [d] 307 mmol of epichlorohydrin were used; [e] Catalyst 45 mg (0.016 mmol Al); [f] 230 mmol of epichlorohydrin were used; [g] CO_2 constant pressure 10 bar; [h] CO_2 constant pressure 25 bar; [i] 271 mmol of glycidol were used; [j] 362 mmol of glycidol were used; [k] Catalyst 170 mg (0.059 mmol Al); [l] Selectivity toward cyclic carbonates 80 % (cis/trans ratio 70:30).

To further corroborate this phenomenon, three additional tests were conducted as described in **Scheme 2**. These experiments involved the use of different catalytic systems under homogeneous conditions: the tetrastyrylporphyrin-aluminium chloride complex (**TSP-AlCl**) as Lewis acid, **TSP-AlCl** combined with ethyltriphenylphosphonium bromide as source of Br$^-$ ions (**EthylPhospBr**), and the employment of **EthylPhospBr** alone. Consistently, the amount of aluminium introduced for the reactions in the homogeneous setup corresponded to that of the **TSP-AlCl-PhospBr** (0.021 mmol).
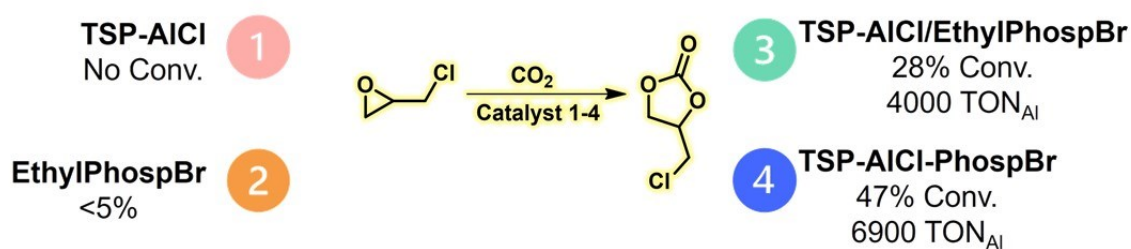
Scheme 2. Comparison of the activity between the heterogenous bifunctional catalyst **TSP-AlCl-PhospBr** and the homogeneous systems **TSP-AlCl**, **EthylPhospBr** and **TSP-AlCl/EthylPhospBr** in the reaction between CO_2 and epichlorohydrin. Reaction conditions: epichlorohydrin (307 mmol), catalyst (0.021 mmol Al) 25 bar CO_2, 60 °C, 3 h, 500 rpm.

Interestingly, the heterogeneous material, **TSP-AlCl-PhospBr**, showed higher activity than the homogeneous **TSP-AlCl/EthylPhospBr** combination, with conversion values of 47% and 30%, respectively. The reaction catalyzed by the Lewis base species alone (**EthylPhospBr**) showed lower activity, with a conversion <5%, while the Lewis acid species alone does not lead to any conversion. These results demonstrate the importance of the presence of co-catalytic species in the system, but also the remarkable performance of the bifunctional heterogeneous material. The possible explanation for this result could be attributed to the spatial arrangement of the two distinct catalytic sites (aluminium and bromide ions) in the **TSP-AlCl-PhospBr** material. Actually, in the material the two active sites are directly linked, unlike the homogeneous **TSP-AlCl/EthylPhospBr** combination, which represents a relatively more disordered system. In particular, the structure of the polymeric network allows a close proximity between aluminium porphyrin core (Lewis acid) and phosphonium salt (bromide anion), resulting in a synergistic effect between the two active sites (**Figure 10**).
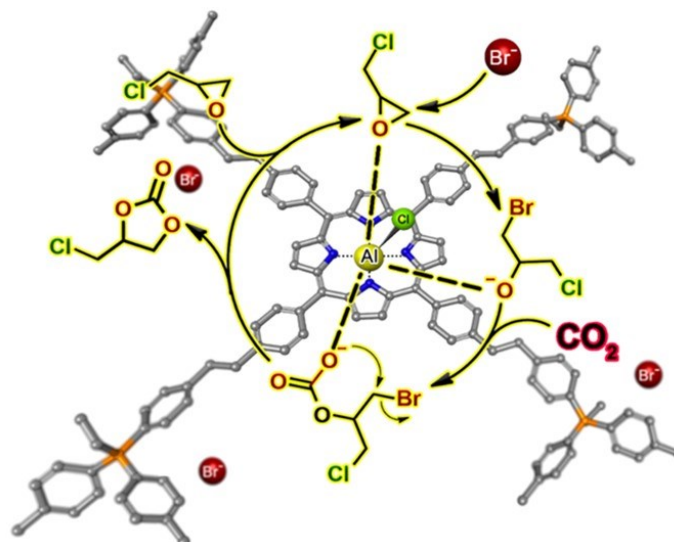
Figure 10. Representation of the synergistic effect between Al-porphyrin and phosphonium salt in the synthesis of cyclic carbonates.

5.3 Conclusions

A copolymerized phosphonium cross-linked networks was prepared by using aluminium chloride tetrastyrylporphyrin and vinyl-functionalized quaternary phosphonium salt monomer as molecular building blocks. A simple one-pot method of AIBN-mediated radical polymerization was followed for the synthesis of **TSP-AlCl-PhospBr** containing aluminium as Lewis acid species and bromide as nucleophilic species. Several spectroscopic and analytical methods were used to fully describe the cross-linked material including TGA, ICP-OES, FT-IR, XPS, TEM, solid-state NMR and porosimetry. The novel material was employed as heterogeneous bifunctional catalyst in the cycloaddition reaction of CO_2 with epoxides to obtain the corresponding cyclic carbonates under solvent-free conditions. Performance evaluation of the hybrid material was carried out taking into account some critical requirements, such as recyclability of the catalyst, turnover number (TON_{Al}) turnover frequency (TOF_{Al}) and productivity values. The catalyst was easily recyclable for four consecutive cycles in the reaction between CO_2 and epichlorohydrin. Moreover, its robustness was also confirmed after consecutive uses under different reaction conditions, making it a useful material for transforming CO_2 into cyclic carbonate. Remarkably, the catalyst could be successfully employed at room temperature, achieving excellent TON_{Al} value of 2339 in only three hours. The cross-linked material showed high catalytic activity and versatility with different epoxides, reaching high TON_{Al} and TOF_{Al} values. This outstanding

catalytic performance can be attributed to the close proximity between the metal centres and the bromide ions due to the direct covalent bonding, which allows for the cooperative effect during the catalytic cycle enabling the obtainment of the desired cyclic carbonate in a short time as highlighted through the comparison experiment under homogeneous conditions. Recently Dai *et al.*[10] demonstrate synergy in similar bifunctional systems based on a series of porous organic catalysts in which the two active sites are phosphonium chloride and magnesium porphyrin. In this report, the catalytic tests were carried out at 1 atm in a temperature range between 40 and 80 °C, using 10 mmol of epoxide with a loading of 0.05 mol% for long reaction times. Conversely, we applied higher pressures (25 bar) in a temperature range between 30 and 150 °C, to a significantly larger amount of epoxide (230 to 362 mmol). In addition, catalytic loadings were substantially lower, ranging from 0.02 mol% to 0.006 mol%, with shorter reaction times, allowing obtaining high TON and TOF values. These conditions acquire substantial relevance since they are similar to those often used on an industrial scale. As a result, only modest changes would be required to scale the cyclic carbonate synthesis described here on a large scale. [11]

5.4 Experimental Sections

Materials and methods. Ethyl bromide (98%), diethylaluminium chloride (25 wt% in toluene), 1,2-dibromoethane (98%), magnesium turnings (98%), phosphorus(III) chloride (99%), 2,2'-Azobis(2-methylpropionitrile) (AIBN) (98%), magnesium sulphate (>99.5%) were purchased from Sigma Aldrich and used as received. Ethyltriphenylphosphonium bromide (>98%), pyrrole (>99%), 4-bromostryrene (>95%), styrene oxide (98%), epichlorohydrin (99%), cyclohexene oxide (98%) and glycidol (96%) were bought from TCI chemicals and used without any purification. Solvents (HPLC grade) were purchased from commercial suppliers without any further purification.

Solid state ^{13}C spectrum was recorded at room temperature on a JEOL ECZ-R spectrometer operating at 14.1 T using a 3.2 mm automas probe and spinning frequencies of 10 kHz. 31P-NMR spectrum was recorded at room temperature on a VARIAN Avance 400 at 9.1 T using a 4 mm probe and spinning frequencies of 10 kHz. 1H-NMR spectra were collected on a JEOL 400 spectrometer or on a Bruker Avance 400 spectrometer. Thermogravimetric analysis (TGA) was performed in a

Mettler Toledo TGA STAR system with a heating rate of 10 °C/min, under nitrogen flow from 25 to 900 °C or under oxygen flow from 100 to 1000 °C. N_2 adsorption-desorption measurement was carried out at 77 K by using a volumetric adsorption analyser (Micromeritics ASAP 2420). Before starting the analysis, the sample was pre-treated at 150 °C for 8 h under reduced pressure (0.1 mbar). The BET technique was used to calculate the specific surface area in the range p/p_0=0.05-0.30, while the BJH method was used to estimate pore size distributions from the adsorption isotherm.[12] TEM micrographs were taken on a Philips TECNAI 10 at 80–100 kV. Inductively coupled plasma optical emission spectroscopy (ICP-OES) was performed in an Optima 8000 spectrometer. Analyses of X-ray photoelectron spectroscopy (XPS) were conducted in a ThermoFisher ESCALAB 250Xi instrument equipped with a monochromatic Al Kα X-ray source (1486.6 eV) and a hemispherical deflector analyser (SDA) working at constant pass energy (CAE), allowing for constant energy resolution across the whole spectrum. The experiments were carried out using a 200 μm diameter X-ray spot. The charge neutralization of the sample was achieved with a flood gun using low energy electrons and argon ions. The pressure in the analysis chamber was in the range of 10-8 Torr during data collection. Survey spectra were recorded with a 200 eV pass energy, whereas high-resolution individual spectra were collected with a 50 eV pass energy. Analyses of the peaks were carried out with the Thermo Avantage software, based on the non-linear squares fitting program using a weighted sum of Lorentzian and Gaussian component curves after background subtraction according to Shirley and Sherwood.

Synthetic procedures

Synthesis of tristyrylphosphine. Tristyrylphosphine was synthesized according to a reported procedure.[13] In a 250 mL two-neck round-bottom flask, under Ar atmosphere, Mg (944 mg, 38.94 mmol) and dry THF (54 mL) were transferred. The mixture was allowed to stir at 30 °C for 30 min before the addition of 1,2-dibromoethane (130 μL). Hence, the mixture was cooled to 0 °C by an ice bath and a solution of 4-bromostryrene (4.6 mL, 32.54 mmol) in THF (2.6 mL) was added. Then, the mixture was allowed to reach room temperature and stirred for 4 hours. A solution of PCl_3 (700 μL) in THF (2.6 mL) was slowly added at 0 °C and stirred at room temperature overnight. The reaction mixture was quenched with a saturated NH_4Cl solution (40 mL), filtered to remove any insoluble residue, and extracted with hexane. The

combined organic layers were dried over MgSO$_4$, filtered, concentrated under vacuum (at room temperature to avoid any polymerization), and purified by column chromatography on silica gel (hexane). Tristyrylphosphine was obtained as a white solid (1.55 g; 57 %). ^{1}H NMR (400 MHz, DMSO, δ): 7.49 (dd, J = 8.1, 1.2 Hz, 1H), 7.21 (t, J = 7.8 Hz, 1H), 6.73 (dd, J = 17.7, 11.0 Hz, 1H), 5.86 (dd, J = 17.7, 0.8 Hz, 1H), 5.30 (dd, J = 11.0, 0.6 Hz, 1H). FT-IR (film): 3076, 3004, 1627, 1488, 1399, 1186, 1090, 1015, 986, 910, 833.

Synthesis of and ethyl-tris(4-vinylphenyl)phosphonium bromide. Ethyl-tris(4-vinylphenyl)phosphonium bromide was synthesized according to a reported procedure, with a few minor adjustments.[14] In a 10 mL Schlaker tube, under argon atmosphere, tristyrylphosphine (1.5 mmol; 530 mg) and ethyl bromide (20.2 mmol; 1.5 mL) were charged and the reaction mixture was stirred at 42 °C for 26 h. After cooling to room temperature, a white mixture was formed and was transferred to a round-bottom flask with chloroform and concentrated under vacuum. Phosphonium salt was obtained as white crunchy solid (650 mg, 97%). ^{1}H NMR (400 MHz, CDCl$_3$, δ): 7.74 (ddd, J = 11.2, 10.2, 5.6 Hz, 1H), 6.76 (dd, J = 17.6, 10.9 Hz, 1H), 5.96 (d, J = 17.6 Hz, 1H), 5.52 (d, J = 10.9 Hz, 1H), 3.85 (m, J = 14.8, 7.4 Hz, 1H), 1.38 (m, J = 20.1, 7.4 Hz, 1H) ppm. FT-IR (film): 3420, 2926, 2885, 1595, 1430, 1109, 1026, 995, 921, 839 cm^{-1}.

 Synthesis of TSP-AlCl-PhospBr. In a two-neck round-bottom flask, tetrastyrylporphyrin aluminium chloride[15] (0.13 mmol; 100 mg) and ethyl tris(4-vinylphenyl)phosphonium bromide (0.51 mmol; 230 mg) were transferred and dissolved in dry dimethylformamide (DMF) (5.1 mL). The reaction mixture was sonicated for 20 min, under argon atmosphere. After the addition of AIBN (10 mol%), the system was degassed by bubbling argon for 20 min and the temperature was gradually increased up to 160 °C. The reaction mixture was allowed to react at this temperature for 72 h. The solid was recovered by centrifugation and washed several times with DMF, methanol and diethyl ether. Before each centrifugation, the catalyst was sonicated for 10 min in the washing solvent. After drying under vacuum at 60 °C, **TSP-AlCl-PhospBr** was obtained as a brown solid (320 mg, 96%). FT-IR (KBr pellet): 3420, 2926, 1643, 1595, 1430, 1109, 1012, 823, 771 cm^{-1}.

Catalytic Tests. Catalytic experiments were carried out in a Cambridge Design Bullfrog batch reactor, with temperature control, pressure monitoring and mechanical stirring.

In each run, a fine dispersion of the catalyst and the right amount of the selected epoxide was added to a Teflon vial. Then, the reactor was closed, and the mechanical stirring speed was set to 500 rpm. The system was purged with N_2 for 10 min, before the addition of 25 or 10 bar of CO_2. Subsequently, the temperature was gradually raised with a ramp of 5 °C/min and maintained at the required temperature during the proper reaction time. At the end of the reaction time, the reactor was cooled to room temperature and slowly depressurized. The separation of the catalyst from the reaction mixture was performed by filtration (Millipore filtration using a 0.45 μm PTFE membrane). The supernatant was analysed by ^{1}H NMR spectroscopy in $(CD_3)_2SO$.

Recycling Tests. The recyclability of the materials was verified in the reaction between epichlorohydrin and CO_2. After each catalytic test, the hybrid was recovered by filtration (Millipore filtration with 0.45 μm PTFE membrane) and washed several times with toluene, ethanol and diethyl ether. The catalyst was then dried overnight in a vacuum oven at 60 °C before being used in the next cycle. To maintain the ratio between moles of catalyst and moles of epoxide, the amount of epoxide was adjusted according to the recovered catalyst. The conversion of epichlorohydrin into cyclic carbonate was estimated by ^{1}H NMR analysis.

5.5 References

1. Chang, L.; Zhang, X.; Shi, X.; Zhao, L.; Liu, X. M., Synthesis and characterization of a novel fibrous antibacterial fiber with organophorsphor functional groups. *J. Appl. Polym. Sci.* **2014**, *131*, 40935.

2. Daasch, L.; Smith, D., Infrared Spectra of Phosphorus Compounds. *Anal. Chem.* **1951**, *23*, 853-868.

3. Patel, H. A.; Somani, R. S.; Bajaj, H. C.; Jasra, R. V., Preparation and characterization of phosphonium montmorillonite with enhanced thermal stability. *Appl. Clay Sci.* **2007**, *35*, 194-200.

4. Tait, S.; Osteryoung, R. A., Infrared study of ambient-temperature chloroaluminates as a function of melt acidity. *Inorg. Chem.* **1984**, *23*, 4352-4360.

5. Rivera-Barrera, D.; Poveda-Jaramillo, J. C., Thermal desorption of trimethylphosphine (TMP) on the HY zeolite followed by FT-IR and 31P MAS NMR. *J. Solid State Chem.* **2021**, *294*, 121862.

6. Haw, J. F.; Zhang, J.; Shimizu, K.; Venkatraman, T. N.; Luigi, D.-P.; Song, W.; Barich, D. H.; Nicholas, J. B., NMR and Theoretical Study of Acidity Probes on Sulfated Zirconia Catalysts. *J. Am. Chem. Soc.* **2000**, *122*, 12561-12570.

7. Merat, L. M. O. C.; Gil, R. A. S. S.; Guerra, S. R.; Dieguez, L. C.; Caldarelli, S.; Eon, J. G.; Ziarelli, F.; Pizzala, H., A spectroscopic probe for combined acid and redox properties in acid catalysts. *J. Mol. Catal. A Chem.* **2007**, *272*, 298-305.

8. Pescarmona, P. P.; Taherimehr, M., Challenges in the catalytic synthesis of cyclic and polymeric carbonates from epoxides and CO2. *Catal. Sci. Technol.* **2012**, *2*, 2169-2187.

9. Cozzolino, M.; Melchionno, F.; Santulli, F.; Mazzeo, M.; Lamberti, M., Aldimine-Thioether-Phenolate Based Mono- and Bimetallic Zinc Complexes as Catalysts for the Reaction of CO2 with Cyclohexene Oxide. *Eur. J. Inorg. Chem.* **2020**, *2020*, 1645-1653.

10. Dai, Z.; Tang, Y.; Zhang, F.; Xiong, Y.; Wang, S.; Sun, Q.; Wang, L.; Meng, X.; Zhao, L.; Xiao, F.-S., Combination of binary active sites into heterogeneous porous polymer catalysts for efficient transformation of CO2 under mild conditions. *Chinese J. Catal.* **2021**, *42*, 618-626.

11. J-P., L. Process for the preparation of propylene carbonate US7728164B2, 2010.

12. Barrett, E. P.; Joyner, L. G.; Halenda, P. P., The Determination of Pore Volume and Area Distributions in Porous Substances. I. Computations from Nitrogen Isotherms. *J. Am. Chem. Soc.* **1951**, *73*, 373-380.

13. Cai, R.; Ye, X.; Sun, Q.; He, Q.; He, Y.; Ma, S.; Shi, X., Anchoring Triazole-Gold(I) Complex into Porous Organic Polymer To Boost the Stability and Reactivity of Gold(I) Catalyst. *ACS Catal.* **2017**, *7*, 1087-1092.

14. Wang, W.; Wang, Y.; Li, C.; Yan, L.; Jiang, M.; Ding, Y., State-of-the-Art Multifunctional Heterogeneous POP Catalyst for Cooperative Transformation of CO2 to Cyclic Carbonates. *ACS Sustain. Chem. Eng.* **2017**, *5*, 4523-4528.

15. Campisciano, V.; Valentino, L.; Morena, A.; Santiago-Portillo, A.; Saladino, N.; Gruttadauria, M.; Aprile, C.; Giacalone, F., Carbon nanotube supported aluminum porphyrin-imidazolium bromide crosslinked copolymer: A synergistic bifunctional catalyst for CO2 conversion. *J. CO2 Util.* **2022**, *57*, 101884.

CHAPTER VI

Polymerizable Deep Eutectic Solvents: Convenient Reactive Dispersion Media for the Production of Novel Multi-Walled Carbon Nanotubes-Based Functional Materials
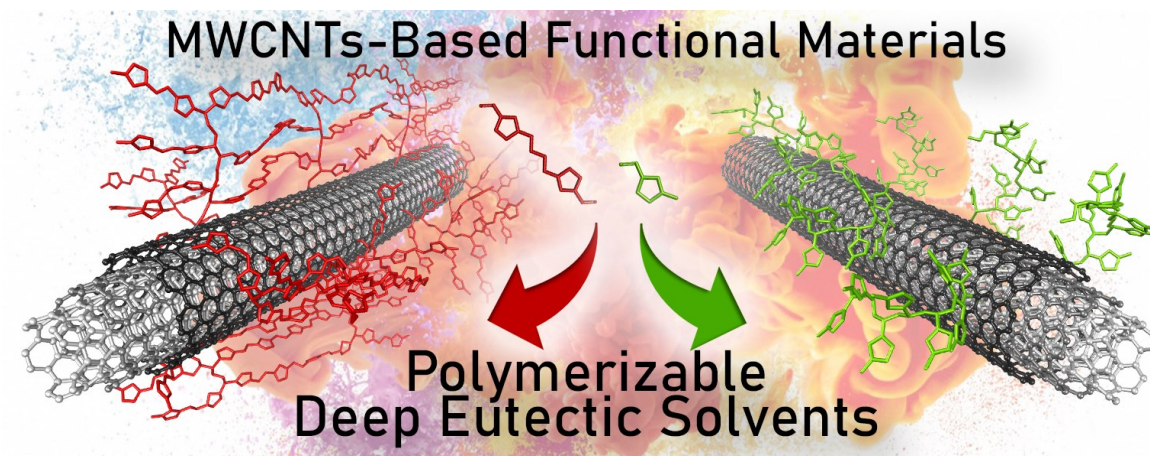
A manuscript based on this chapter has been submitted for publication

CHAPTER VI

Polymerizable Deep Eutectic Solvents: Convenient Reactive Dispersion Media for the Production of Novel Multi-Walled Carbon Nanotubes-Based Functional Materials

6.1 Abstract

A new straightforward and green approach for the covalent functionalization of multi-walled carbon nanotubes (MWCNTs) was developed. This carbon nanostructure was efficiently derivatized by polymerizing proper deep eutectic monomers (DEM), a subclass of deep eutectic solvents (DES), based on a series of mono- and bis-vinyl imidazolium salts endowed with different functional groups ($-OH$, $-NH_2$, $-NH_3^+Br^-$) in the side chain or in the spacer. Herein, DEM systems played a triple role as convenient dispersion media for MWCNTs, efficient reactive systems, and also as structure-directing agents for the radical-initiated polymerization process onto the surface of MWCNTs. In addition, the new methodology allowed obtaining highly functionalized hybrid materials, as shown by thermogravimetric analyses, in short reaction times (<1 h). Transmission electron microscopy (TEM) revealed that the polymeric network orderly develops along the surface of the nanotubes, which act as templating agent for both mono- and bis-vinyl imidazolium salts, despite the random nature of the process for the latter species. This new functionalization strategy of MWCNTs stands out for its environmentally friendly and time-saving nature leading to the formation of materials with significant potential for applications in a plethora of research fields. As a proof of their possible application, we tested these new hybrid materials as recoverable and recyclable catalysts for the conversion of CO_2 into cyclic carbonates under solvent-free conditions, showing good catalytic performances, even in the absence of additional co-catalysts.

6.2 Introduction

In the field of nanomaterials science and nanotechnology, multi-walled carbon nanotubes (MWCNTs) are gaining increasing importance due to their adaptability to meet specific requirements for various applications.[1-4] The remarkable electronic, mechanical, and thermal properties exhibited by this allotropic form of carbon make them highly desirable materials in a wide range of application fields, including energy conversion and storage, electronics, catalysis, optoelectronics, sensing, drug delivery systems, biomedicine, and the formation of high-performance materials such as films and fibers.[5-12] Despite their outstanding properties, carbon nanotubes usually exhibit poor solubility and dispersibility in common solvents. Indeed, pristine CNTs typically aggregate in bundles due to van der Waals and $\pi-\pi$ stacking interactions between the tube walls, resulting in the formation of highly entangled 3D networks that make it difficult to achieve stable and fine dispersions in both aqueous and organic media, limiting their potential. To enhance the dispersibility of CNTs and broaden their potential applications, a key strategy involves chemical modifications of their structures.[13-14] Chemical surface functionalization has the dual purpose of preventing nanotubes aggregation and promoting the synthesis of innovative materials in which the intrinsic properties of MWCNTs are combined with those of the functionalization units, resulting in hybrid systems with vast potential for various applications. One way to obtain the chemical modification of CNTs is represented by the use of corrosive acids, oxidizing agents, and/or other hazardous chemicals often leading to the permanent deep damage of the sidewalls of carbon nanotubes.[14-16] An alternative method is represented by non-covalent interactions of CNTs with suitable dispersing agents. In this context, in 2003, Fukushima et *al.* discovered that when mixed with imidazolium-based ionic liquids (ILs), pristine carbon nanotubes gave rise to physical gel, the so-called bucky gels.[17-18] The mere combination of ILs with carbon nanotubes resulted in the dispersion and separation of the entangled nanotubes. The excellent processability of pristine CNTs within these gels was attributed to a sort of shielding effect that ILs, with their high dielectric constants, exert onto the strong $\pi-\pi$ stacking interaction among CNTs.[19] ILs can be deemed inherently superior to conventional organic solvents for dispersing CNTs owing to their characteristics, such as reduced flammability, minimal or absent volatility, exceptional thermal stability, and notable ionic conductivity. Moreover, the unique interactions between ILs and nanocarbons confer distinctive properties to these nanocomposites, improving their dispersibility in various environments and expanding their field of use.[18,20-21] ILs have also been used for the covalent modification of the surface of carbon nanoforms (CNFs) such as single- and multi-walled carbon nanotubes and carbon

nanohorns. In particular, different bis-vinyl imidazolium salts have been exploited to achieve CNFs-functionalization with highly cross-linked polymer networks, through a radical polymerization process. More in depth, a good degree of functionalization variability was explored by changing the identity of the spacer and/or the anion[22-25] or by co-polymerizing bis-vinyl imidazolium salts with different vinyl building block species.[26-27] Another viable alternative for achieving optimal results in nanotube dispersion involves the use of a class of solvents that shares some of the advantageous characteristics of ILs, the deep eutectic solvents (DESs).[28-31] DESs have gained significant interest over the last twenty years as a new category of environment friendly solvents, but their low cost makes them more desirable in the large-scale synthesis of novel functional materials. This heightened attention follows a study by Abbott et al.,[32-33] who observed an unusually pronounced reduction in melting point of the eutectic mixture of specific hydrogen bond donors (HBDs) and acceptors (HBAs) with respect to the parent compounds. DESs are valued for their eco-friendliness and sustainability due to their minimal toxicity, biodegradability and ease of synthesis.[34] In addition they can be tailored to suit specific applications by selecting appropriate components and adjusting their molar ratio, making them versatile and promising in a wide range of applications.[35] However, the role of DESs is not only limited to that of a green reaction medium for CNTs dispersion, and in this context, interesting examples are reported by Gutiérrez and co-workers that have successfully used DESs as convenient dispersion media of MWCNTs and for dissolution of polymerizable monomer/s (furfuryl alcohol or resorcinol-formaldehyde pair) for nanocomposite preparation.[36-39] In fact, if one component of the DES is involved in the functionalization of the carbon nanostructure, then DES can act as both dispersion medium of CNTs and reactant.[40] Specifically, this particular class of deep eutectic solvents, characterized by the inclusion of polymerizable units within either HBD or HBA components has been pioneered and defined as deep eutectic monomers (DEMs) by Mota-Morales et al. who applied the so-called frontal polymerization in deep eutectic solvents by employing combinations of "classic monomers" such as acrylic acid or methacrylic acid with choline chloride.[41] These DEMs were characterized by the inclusion of a polymerizable acrylate group within the hydrogen bond donor unit. Furthermore, they explored the frontal polymerization using DEMs consisting of various ammonium salts and hydrogen bond donors containing acrylic acids and acrylamides.[42] DEMs can represent a very intriguing solution to reduce the dependence on classical volatile organic solvents in the production of polymers. The high flexibility in the DEMs formation by changing both the nature and the molar ratio of the constituent species close to the eutectic point to meet specific requirements allow to expand the conditions in which polymerization takes place. Moreover, in the light of the above, the

advantageous features of DEMs pave the way for the optimization of a convenient methodology for covalent anchoring of the polymerizable component of DEM onto the CNTs surface with the production of novel functional materials. However, during the polymerization process, the depletion of the polymerizable component of the DEM, causes the change of the starting HBD/HBA molar ratio inducing the eutectic rupture and a phase segregation by means of a spinodal decomposition and the formation of a polymer-depleted solid phase, mainly consisting of the inert component of the DEM.[43-44] The formation of this solid phase could have significant consequences on the morphology of the resulting material. However, although some alkyl imidazolium salts as HBA have been used to obtain a classic DES system,[45-51] conversely, to date no imidazolium salts with mono- or bis-vinyl moieties used as polymerizable HBA have been employed in the formation of DEMs. Therefore, herein, a new synthetic method employing deep eutectic monomers as environmentally friendly reaction media and reactive agents for the functionalization of multi-walled carbon nanotubes (MWCNTs) is reported. In particular, the radical polymerization of mono- or bis-vinyl imidazolium salts used for the first time as HBA components of DEMs systems in the presence of CNTs structures was investigated. Interestingly, the CNTs outer walls acted as template for the growth of highly compact polymeric imidazolium networks for both mono- and bis-vinyl imidazolium salts, despite the random nature of the polymerization process for the latter species. The resulting materials were employed as heterogeneous and recyclable catalysts for the conversion of CO_2 into epoxides to generate cyclic carbonates.

6.3 Results and discussion

The preparation of novel DEM systems containing polymerizable HBA species, namely mono- and bis-vinyl imidazolium salts, was conducted by selecting urea and dimethylurea (DMU) as hydrogen bond donors. Two different HBA/HBD ratios of 1:2 and 1:4 with respect to bromide ions were chosen. In the proposed methodology, the pivotal component of the eutectic mixture is the hydrogen bond acceptor, as it is the active agent directly involved in the polymerization reaction. In order to achieve structural variability of the final hybrid material, different mono- and bis-vinyl imidazolium bromide monomers **1a-e**, endowed with hydroxyl or amine groups, included in the spacer or side chain, were synthetized (*vide infra* **Scheme 1**).
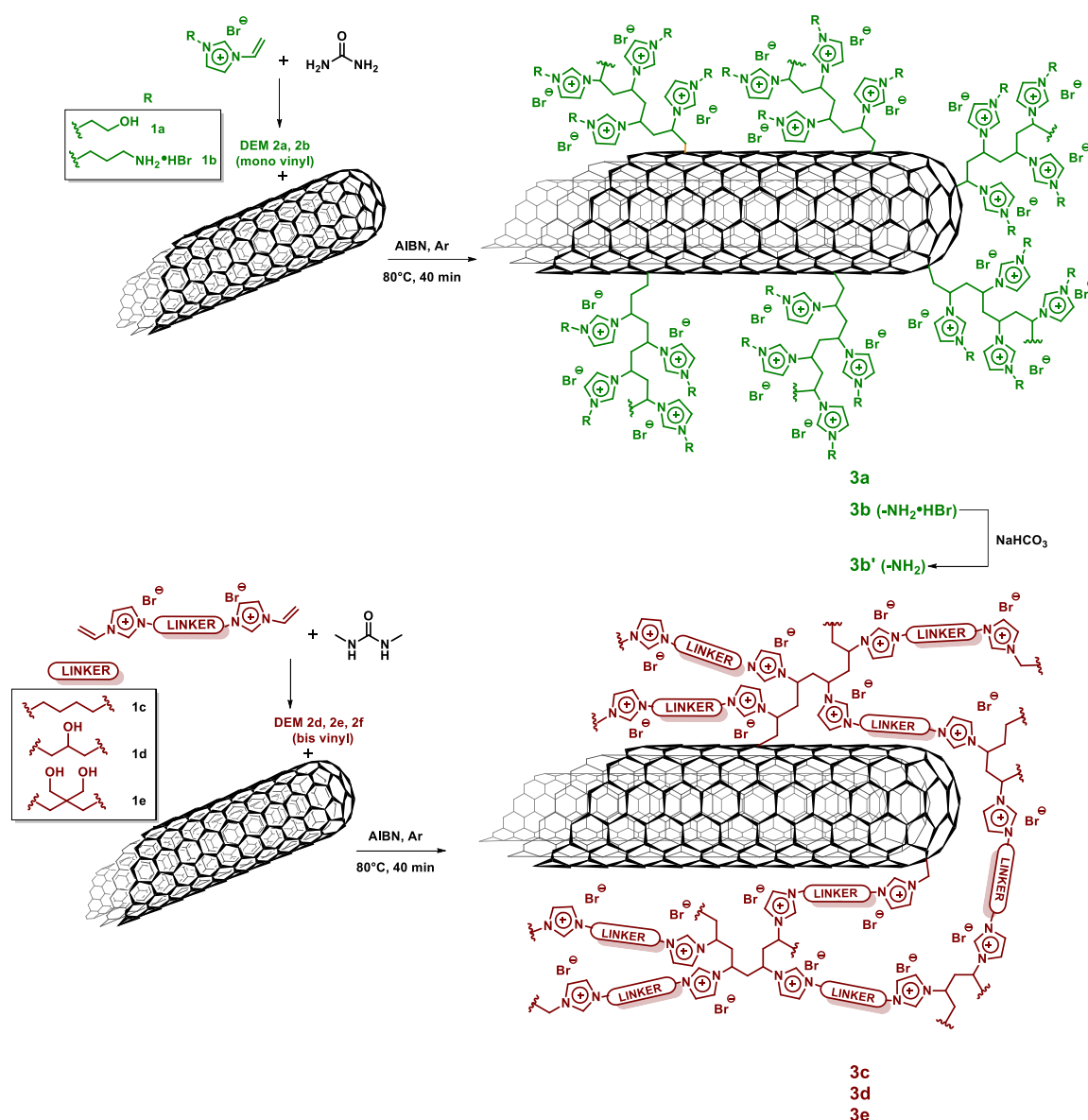
Scheme 1. Synthetic procedure for the preparation of materials **3a-e**.

As shown in **Figure 1**, the eutectic mixture is generated after two hours at 80 °C from the two solid components.
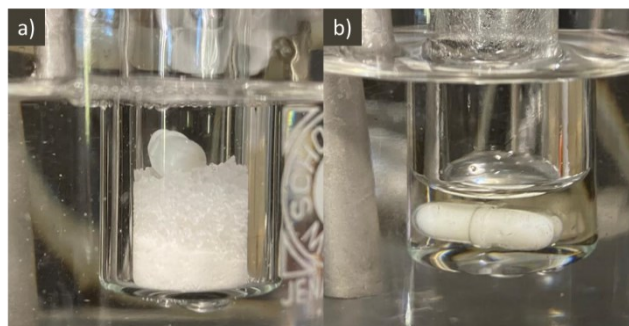

Figure 1. Formation of deep eutectic monomers, in detail DEM **2c**: from the solid starting components bis-vinyl imidazolium salt **1c** and dimethylurea (a) to DEM (b), respectively.

Differential Scanning Calorimetry (DSC) was performed to investigate the thermal behaviour of the prepared DEM systems (**Figure 2a-b**). Each sample was analyzed with a heating and

cooling temperature ramp of 10 °C min^{-1}. DSC analysis confirms the successful formation of the DEM systems (solid lines) since their melting temperatures were lower than both the parent imidazolium salts (dashed lines **1a-e**) and the hydrogen bond donors (urea and DMU, red lines). Except for DEM **2a,** which is liquid at room temperature and shows no crystallization peak until -40 °C, and DEM **2b** that displays only a melting peak, DEMs **2c-e** showed a reproducible behaviour for three cycles, with the presence of melting and crystallization peaks (not showed in **Figure 2**). Moreover, bis-vinyl imidazolium salt **1e** (dashed yellow line) exhibits no melting peak in the range of temperature examined (up to 120 °C).
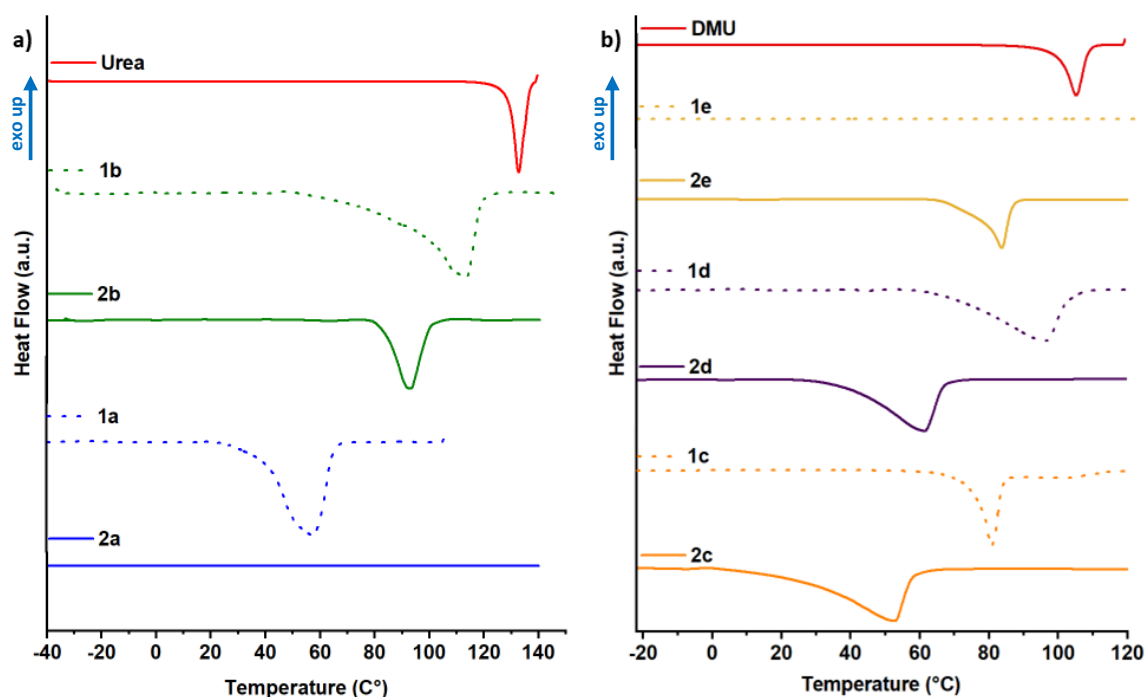
Figure 2. Differential scanning calorimetry (DSC) thermograms of (a) vinyl imidazolium salts **1a-b**, DEM system **2a-b**, and urea; (b) vinyl imidazolium salts **1c-e**, DEM systems **2c-e**, and dimethylurea.

Once established that DEMs were formed, they were exploited as efficient and reactive dispersing media for carbon nanotubes. In such a way, a series of novel hybrid materials based on MWCNT/polyimidazolium salts **3a-e** were prepared through a convenient and straightforward methodology. The radical polymerization initiated by the thermal decomposition of 2,2'-azobis(isobutyronitrile) (AIBN) at 80 °C within the different DEM media **2a-e**, based on mono- or bis-vinyl imidazolium salts **1a-e**, in the presence of MWCNTs, resulted in highly functionalized hybrid materials in just 40 minutes (**Scheme 1**). This strategy represents a versatile approach to get easy access to functionalized carbon nanotubes with different functional groups, which can be in turn post-modified. Thermogravimetric analysis

under a nitrogen flow was employed to analyze the thermal profiles of the resulting hybrids MWCNT/polyimidazolium salts **3a-e** (**Figure 3a-b**). All the materials proved to be very stable up to 270 °C, a temperature beyond which they start to decompose, except for material **3b'**, endowed of amino-groups in the side chains, which starts to degrade at a lower temperature of *ca.* 160 °C, and shows a marked decomposition process above 200 °C. The good thermal stability of the final hybrids is promising for their possible use under heating regimes. Thermogravimetric profile of pristine MWCNTs (*p*-MWCNTs, black line) showed very low weight loss (1 wt%) up to 700 °C. The functionalization loadings of materials **3a-e** were then estimated by evaluating their weight losses at 700 °C. The following values were obtained: **3a** 3.6, **3b** 2.3, **3b'** 2.9, **3c** 4.2, **3d** 3.6, and **3e** 3.1 mmol/g of imidazolium units. The estimation of specific surface areas (SSA) was carried out using the Brunauer–Emmett–Teller (BET) method.[52-53] The resulting SSA values were relatively low, falling within the range of less than 15 m²/g, in agreement with those previously obtained for analogue CNFs/polyimidazolium salts hybrids.[23-24,54-55]
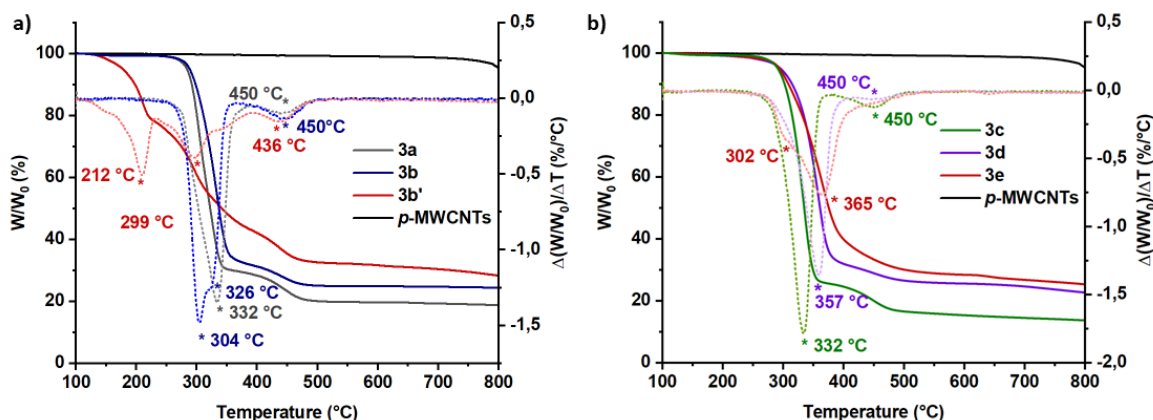
Figure 3. TGA under N_2 flow and derivative thermogravimetric (DTG) curves (dotted lines) of a) *p*-MWCNT (black line), **3a** (grey line), **3b** (blue line) and **3b'** (red line), and b) *p*-MWCNT (black line), **3c** (green line), **3d** (violet line) and **3e** (red line).

Solid state ^{13}C-cross-polarization magic angle spinning NMR (^{13}C-CPMAS NMR) spectra of all hybrid materials **3a-e** were collected and reported in **Figure 4**. In the spectra, the signals of the aromatic carbon atoms of imidazolium moieties can be observed in the region between 115-150 ppm. Meanwhile, the signals associated with aliphatic carbon atoms are in the upfield region of the spectrum, ranging from 20 to 70 ppm. Additionally, the successful outcome of the polymerization process was confirmed by the absence of any signals in the 100–115 ppm region, where carbon atoms of the vinyl group typically resonate.
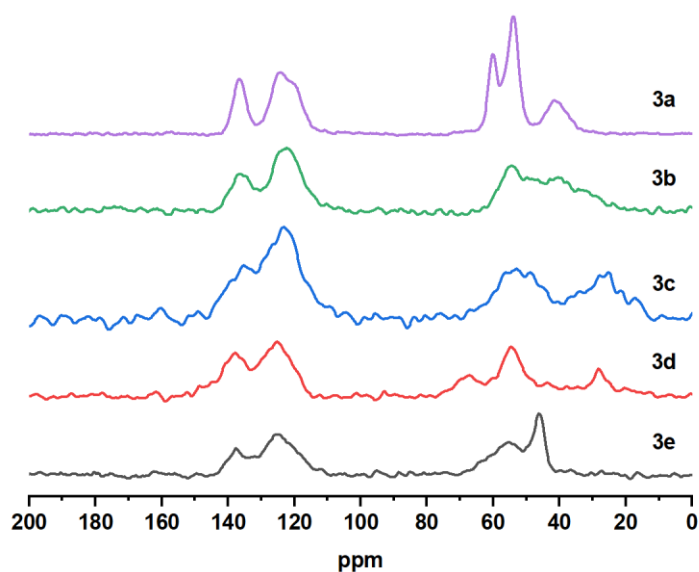
Figure 4. ^{13}C-CPMAS-TOSS NMR solid state of hybrid materials **3a-e**.

The evidence of the good outcome of the polymerization process was also confirmed by Fourier-transform infrared (FT-IR) spectroscopy, comparing the spectra of the imidazolium salts precursors with the spectra of the corresponding final hybrid materials (**Figure 5**). FT-IR spectra of monomers **1a-e** (**Figure 5,** red lines) show the typical bands associated with the C=C stretching of vinyl group of the imidazolium functionalities centred at 1620-1690 cm^{-1} and two bands at 920-960 cm^{-1} corresponding to the C–H bending. As expected, these peaks disappear in the spectra of the hybrid materials **3a-e** (black lines), confirming the successful polymerization. Furthermore, the highly hygroscopic nature of the polymerized imidazolium salt results in the presence of a wide absorption peak between 3200-3500 cm^{-1}, attributable to the stretching of O–H bonds, and a moderate absorption at 1550 cm^{-1} arising from the bending of H–O–H bonds of the adsorbed water.
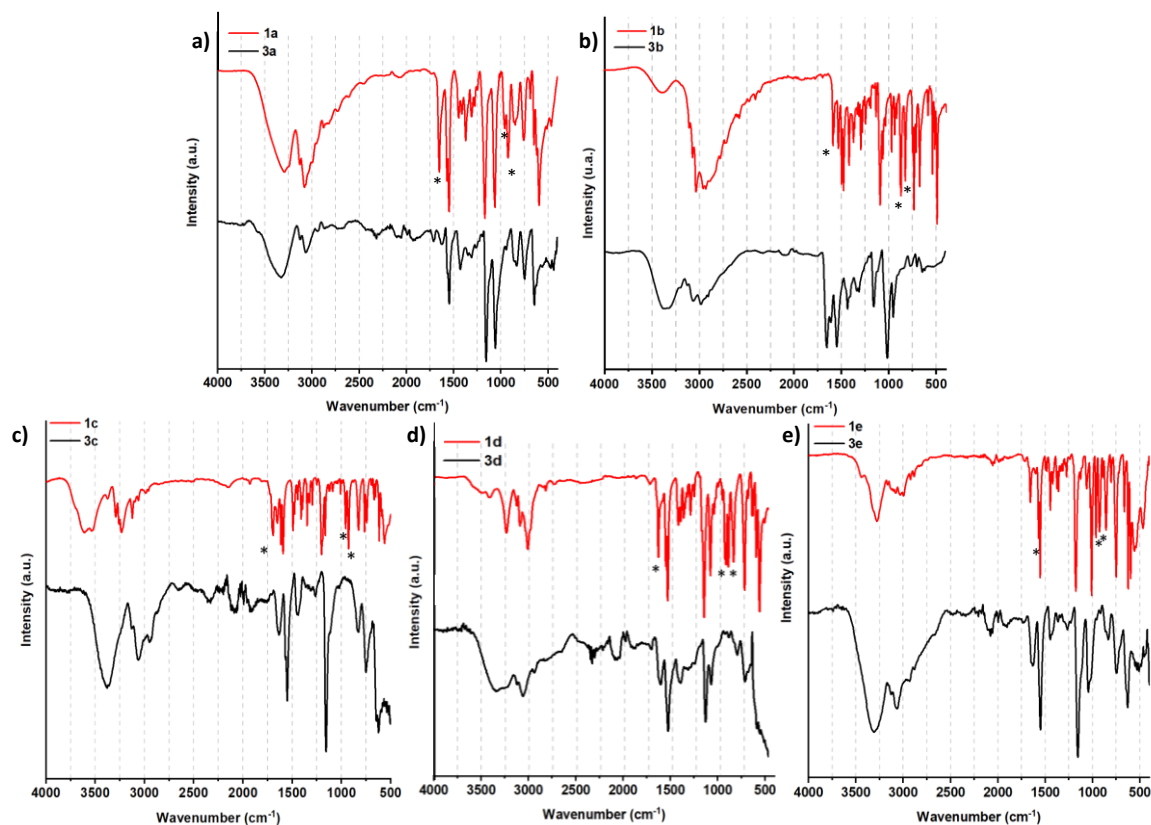
Figure 5. FT-IR spectra of a) monomer **1a** (red line) and the polymer **3a** (black line), b) monomer **1b** (red line) and the polymer **3b** (black line), c) monomer **1c** (red line) and the polymer **3c** (black line), d) monomer **1d** (red line) and the polymer **3d** (black line) and e) monomer **1e** (red line) and the polymer **3e** (black line).

All the prepared hybrid materials were subjected to Raman spectroscopic analysis (**Figure 6**), which made it possible to assess the covalent functionalization of carbon nanotubes through the change in the intensity ratio of the D band to the G band (I_D/I_G) compared to I_{D0}/I_{G0} ratio in the pristine CNTs. In particular in the material **3a**, an increased normalized I_D/I_G ratio from the I_{D0}/I_{G0} ratio of 1.16 was found, proving the attachment onto the CNTs surface. Raman spectra of materials **3b**, **3b'**, and **3c** revealed no remarkable differences from Raman spectrum of p-MWCNTs. In order to interpret these results, it is necessary to take into account both the nature of the support material, being MWCNTs, and the functionalization process involved, namely radical polymerization. Indeed, despite the high degree of functionalization of the obtained materials, minimal disruption of the π-system of the outermost nanotube layer and thus minimal changes in the corresponding Raman spectra are obtained. Unfortunately, materials **3d** and **3e** gave rise to intense fluorescence emissions, upon excitation with all the laser wavelengths used (532, 633, and 785 nm), which hindered the acquisition of the Raman spectra.
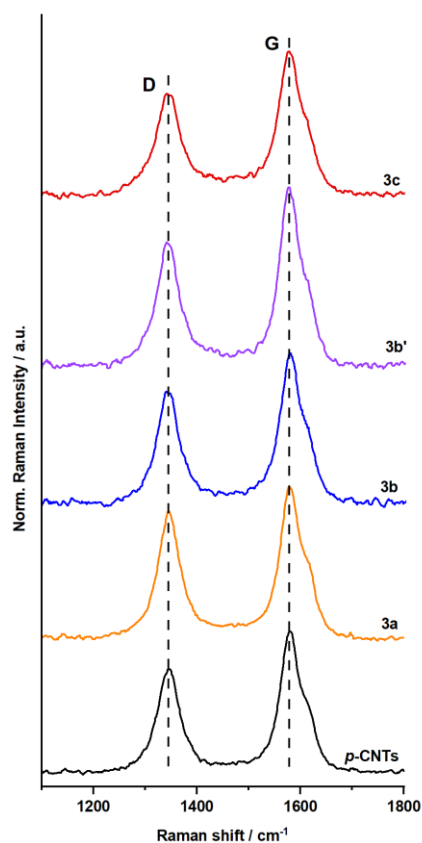
Figure 6. Raman spectra of *p*-MWCNTs (black line), polymer **3a** (orange line), polymer **3b** (blu line), polymer **3b'** (violet line) and the polymer **3c** (red line) irradiated with 532 nm laser.

Transmission electron microscopy (TEM) was used to investigate the morphology of the prepared hybrid materials. The micrographs of these hybrids (**Figure 7**) were compared with those of *p*-MWCNTs (**Figure 7a**). It was observed that in all cases, regardless of the nature of the monomer (mono- or bis-vinyl imidazolium salt), the polymerization led to the formation of hybrid materials in which the carbonaceous skeleton, consisting of MWCNTs, was surrounded by a tightly compacted polymeric coating. It is worth to note that despite the random nature of the polymerization nature, the templating effect exerted by CNTs on the growth of the polymeric network has been previously observed by us in some of our previous works where CNTs were functionalized with different bis-vinyl imidazolium salts.[22-23,26-27,54-55]
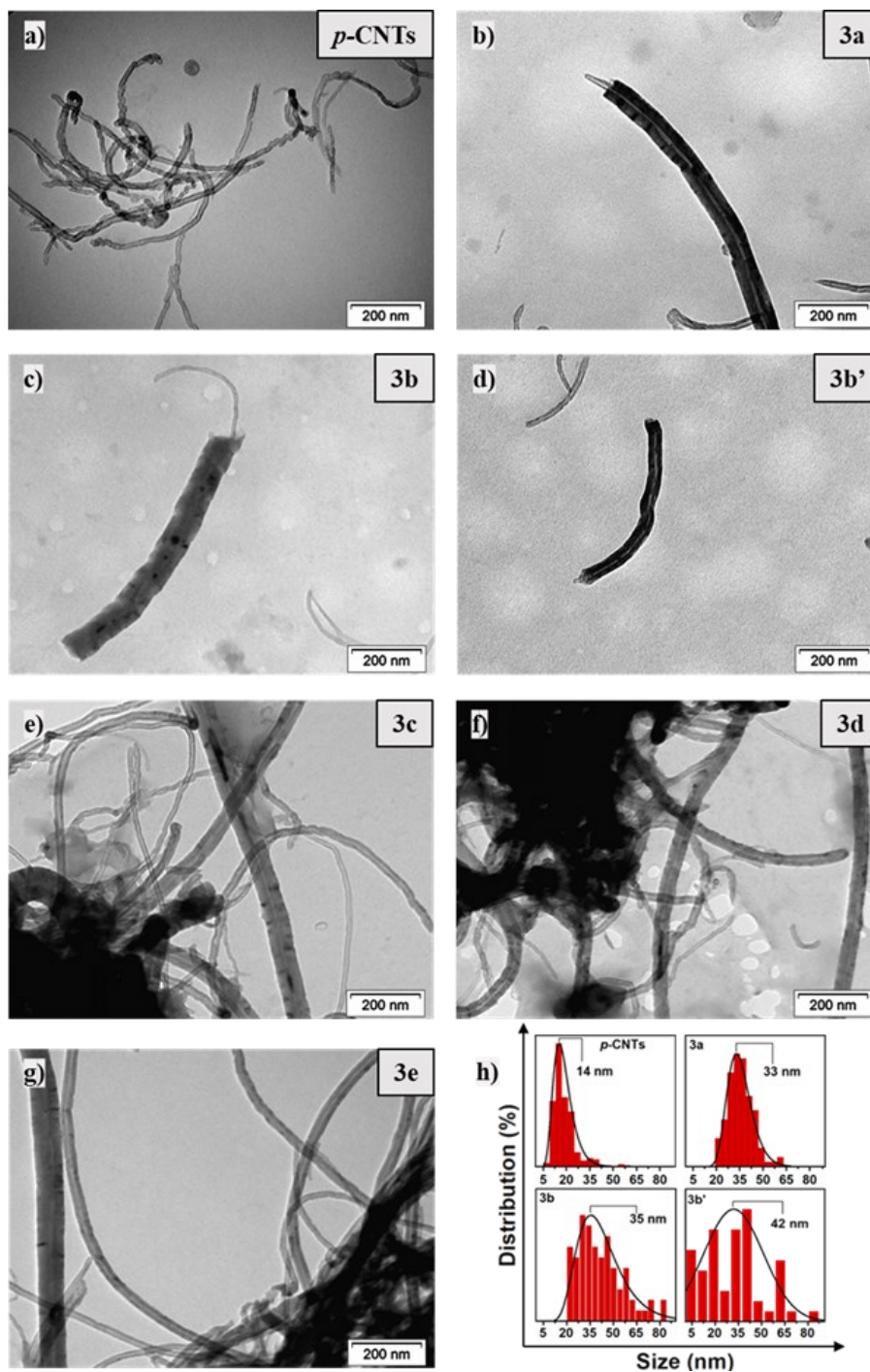
Figure 7. Transmission electron microscopy images of: (a) *p*-MWCNTs; (b) **3a**; (c) **3b**; (d) **3b'**; (e) **3c**;(f) **3d**; (g) **3e** and size distribution histograms of *p*-MWCNTs, **3a**, **3b** and **3b'**.

The polymerization in DEM media formed from mono-vinyl monomers as HBA species led to the formation of well-dispersed and individualized nano-objects having mean diameters larger than that of *p*-MWCNTs. The size distribution histograms of *p*-MWCNTs and materials **3a**, **3b**, and **3b'**, shown in **Figure 7h**, highlight this increase in average size since *p*-MWCNTs have a mean diameter of 14 ± 7 nm (n = 150 counts), whereas materials **3a**, **3b**, and **3b'** show bigger diameters of 35 ± 8 (n = 160 counts), 33 ± 8 (n = 155 counts), and 42 ± 10 (n = 55

counts), respectively. Once again, the use of bis-vinyl monomers as polymerizable HBA species resulted in the covering of CNTs skeleton, although the possibility of cross-linking led to the formation of numerous aggregates that significantly lowered the number of individualized nano-objects hampering and making statistically not significant the construction of a size distribution curve. However, no objects with diameter bigger than 50 nm have been identified. Regarding this last observation, it is noteworthy to compare material **3c** (4.2 mmol/g) obtained by DEM-mediated functionalization with the same material previously obtained by us with conventional method dissolving the bis-vinyl imidazolium salt **1c** in ethanol (4.5 mmol/g).[23] Despite the two synthetic strategies gave rise to materials with similar functionalization degrees, significant differences in means diameters were obtained. Specifically, the conventional methodology resulted in a thicker polymeric coating of *ca.* 150 nm against a more compact layer of 50 nm in the case of DEM-mediated functionalization (**Figure 8**). This outcome can be explained by considering the different nature of the two reaction media, namely ethanol and the DEM system, in which polymerization takes place. Indeed, the concentration of the monomer **1c** is lower in ethanol with respect to that in DEM system **2c** (**1c**/DMU). Therefore, when ethanol was used as solvent, the low monomer concentration could cause a lower number of anchored vinyl moieties on the surface of MWCNT which, consequently, polymerize in a less compact manner giving a material with a large radius around the MWCNT; conversely the higher monomer concentration in the DEM **2c**, along with the eutectic rupture and phase segregation, could result in a greater number of anchored vinyl moieties that leads to a higher compact structure with a much lower radius (*ca.* 50 nm). In the light of the above, in addition to act as a dispersing medium for CNTs and reactant for the CNTs-templated polymerization process, DEM plays a third role since it can actively affect the morphology of the obtained material. The sustainability of the whole process is further increased considering the possible recovery and reuse of the inert HBD component at the end of the reaction.
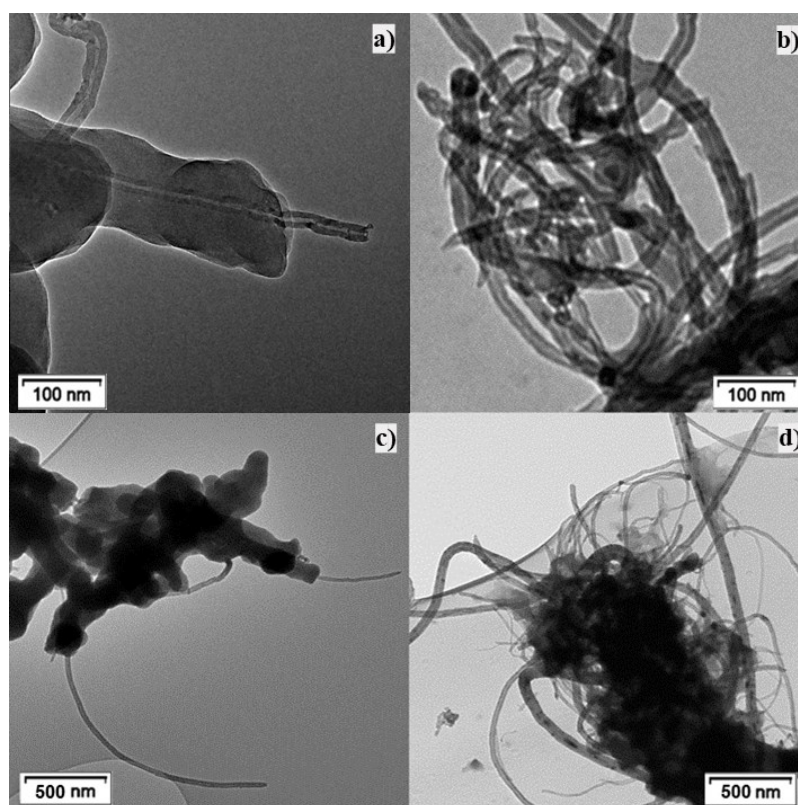
Figure 8. Transmission electron microscopy images of: (a and c) hybrid material obtained in diluted solvent conditions (2.6 mg/mL of MWCNTs in ethanol)[23] and (b and d) hybrid material **3c**.

Furthermore, when we carried out the conventional polymerization of the bis-vinyl imidazolium salt **1c,** a dispersion of 2.6 mg/mL of MWCNTs in ethanol was used.[23] In this case, a homogeneous material with a good degree of functionalization was obtained. Herein, we have been interested in investigating whether it was possible to reduce the amount of organic solvent using a concentration of 10 mg/mL of MWCNTs, namely the higher achievable suitable to ensure both a good dispersion of the nanotubes and the solubilization of the bis-vinyl imidazolium salt **1c**. Such conditions led to the obtainment of a physical mixture of CNTs supported and homopolymerized poly-imidazolium salt (**Figure 9**) indicating that higher dilutions are needed to avoid the heterogeneity of the material.

This evidence further corroborates the green aspects of DEM-mediated functionalization of MWCNTs since it allows reducing the amounts of organic solvents used. Furthermore, regarding the functionalization with mono-vinyl salts, although a couple of examples have been reported,[56-59] when ethanol was used as dispersing medium, no polymerization was initiated under all the conditions tested by us. This emphasizes another advantage of DEM-mediated polymerization, which enables the preparation of new materials that would otherwise not be accessible.
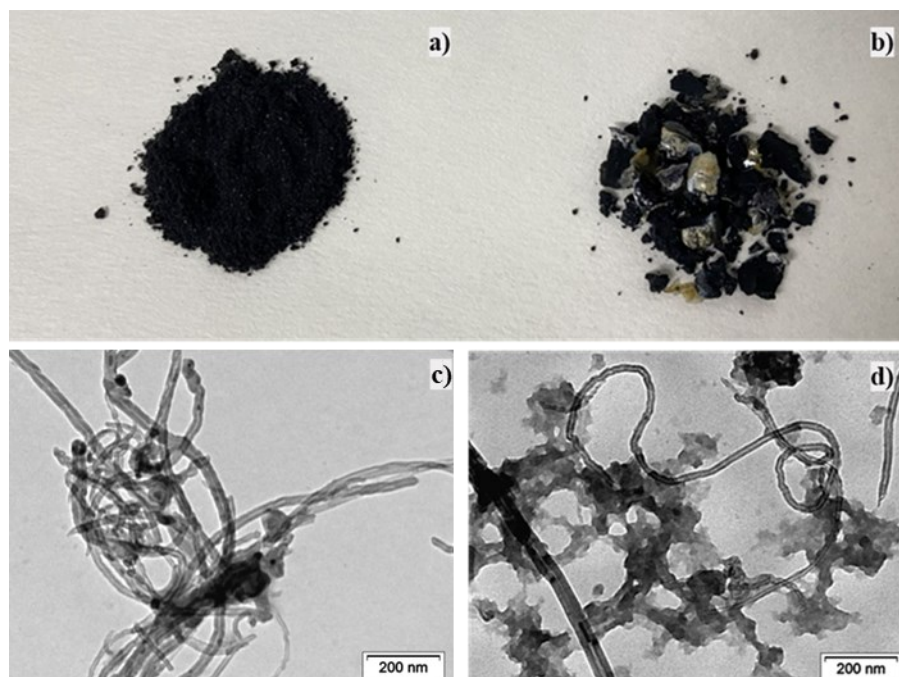
Figure 9. Hybrid material **3c** (a) and hybrid material prepared with a concentration of 10 mg/mL of MWCNTs in ethanol (b). Transmission electron microscopy images of: (c) material **3c** and (d) material obtained in concentrated solvent conditions (10 mg/mL of MWCNTs in ethanol).

Once characterized, all the hybrid materials **3a-e** were applied as heterogeneous catalysts for the conversion of CO_2 into cyclic carbonates. The catalytic performance of the hybrids was evaluated in terms of conversion, turnover number (TON, defined as moles of epoxide converted/moles of supported imidazolium bromide), turnover frequency (TON/time (h)) and recyclability. In order to study the effect of the different linear and cross-linked polymer supported onto MWCNTs, six catalytic tests were carried out in the reaction between carbon dioxide and epichlorohydrin under solvent free conditions, at 150 °C, and without using any co-catalytic species (**Table 1**).

Table 1. Conversion of epichlorohydrin and CO_2 into the cyclic carbonate.[a]
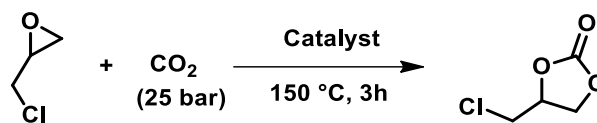
Entry	Catalyst	Conversion(%)[b]	TON[c]	TOF[c]
1	3a	70	1020	340
2	3b	56	640	210
3	3b'	57	970	320
4	3c	70	850	280
5	3d	47	650	210
6	3e	25	430	145

[a] Reaction conditions: epichlorohydrin (306 mmol), catalyst 60 mg (**3a** 0.21 mmol Br⁻; **3b** 0.27 mmol Br⁻; or **3b'** 0.18 mmol Br⁻; **3c** 0.25 mmol Br⁻; **3d** 0.22 mmol Br⁻; or **3e** 0.18 mmol Br⁻), 25 bar CO_2, 150 °C, 3 h, 500 rpm. [b] Determined by ¹HNMR. [c] TON and TOF values calculated based on the bromide content in the hybrid materials.

From this preliminary investigation, **3a** resulted the more active material. This behaviour can be ascribed to the different structures of the hybrids. The better catalytic activity of **3a** could be explained by the linear morphology of the polymer supported on the MWCNTs, leading to a higher accessibility of the imidazolium units to the substrates. This hybrid material was chosen for further investigation. Again, the reaction between CO_2 and epichlorohydrin was selected as benchmark reaction to study the recyclability of the hybrid material. Three consecutive cycles were performed without significant loss in catalytic activity (**Figure 10**). After each cycle, the material was recovered through centrifugations Subsequently, it was washed with toluene, ethanol, and diethyl ether, requiring no further activation treatments.
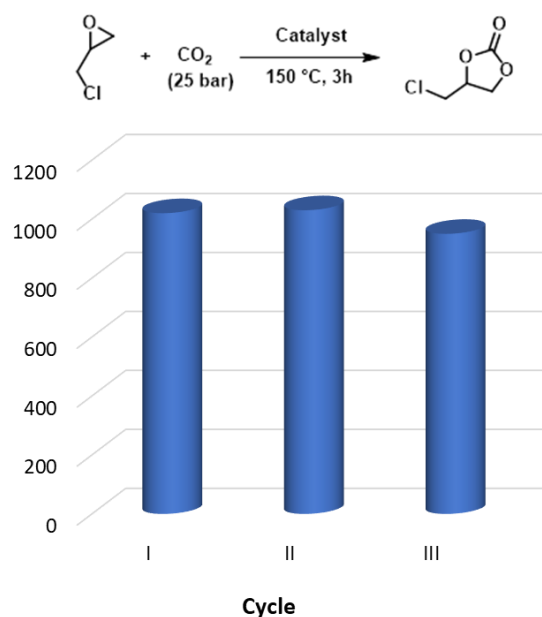
Figure 10. Recycling test of **3a**. Reaction conditions: epichlorohydrin (306 mmol), 60 mg **3a** (0.21 mmol Br$^-$), 25 bar CO_2, 3 h, 500 rpm.

6.4 Conclusion

In conclusion, we reported a novel synthetic strategy based on the triple role of DEMs able to act as convenient dispersion media for MWCNTs, efficient reactive systems, and also as structure-directing agents for the polymerization process. This methodology was exploited for the functionalization of MWCNTs by means of the radical polymerization of mono- or bis-vinyl imidazolium salts endowed with different functional groups (–OH, –NH_2, –$NH_3^+Br^-$) used as HBA species of the eutectic mixtures. The new hybrid materials were fully characterized by means of TGA, ^{13}C-CPMAS TOSS NMR, FT-IR, SSA, Raman, and TEM analyses. This latter technique revealed the effective coverage of the CNTs structure by the polymeric matrix. Whereas CNTs acted as template for the growth of the polymeric network, the DEM systems played a complementary role on the morphology of the hybrid materials, which were characterized by the presence of a compact polymeric matrix around the CNTs structure. The hybrids were successfully applied as heterogeneous catalysts for the conversion of carbon dioxide and epichlorohydrin into the corresponding cyclic carbonate and the best performing material was further investigated to carry out recycling studies for three consecutive runs. This promising and eco-friendly strategy paves the way for the obtainment of different functional materials in which both the identity of DEM and that of support material can be varied. In addition, the use of these hybrids both for the immobilization of metal nanoparticles and for the generation of N-doped carbon nanotubes is currently underway.

6.5 Experimental Part

Materials and methods. Chemicals and solvents were purchased from commercial suppliers to be used without further purification. Thermogravimetric analysis (TGA) was performed in a Mettler Toledo TGA STAR system with a heating rate of 10 °C/min, either under oxygen flow from 100 to 1000 °C or under nitrogen flow from 25 to 900 °C. Differential scanning calorimetry (DSC) measurements were carried out with a TA Instruments mod. 2920 differential scanning calorimeter (TA Instrument Inc., New Castle, DE, USA) equipped with a TA Instruments refrigerated cooling system. Samples (~4 mg) were weighed in aluminium TA Tzero hermetic pans, which were subsequently sealed with aluminium lids. The analyses were performed with heating and cooling rates of 10 °C min^{-1} under a N_2 atmosphere of 60 mL min^{-1}. Raman spectra were acquired using Horiba LabRam HR Evolution equipment with a 532 nm laser line, using a spectral resolution of about 7 cm^{-1} and a laser intensity that does not interfere with the signal. Transmission electron microscopy (TEM) images were recorded using a Philips Tecnai 10 microscope operating at 80-100 kV. Nitrogen adsorption-desorption analyses were carried out at 77 K in a Micromeritics ASAP 2420 volumetric adsorption analyzer. Before the analysis the sample was pre-treated at 150 °C for 8 h under reduced pressure (0.1 mbar). The Brunauer-Emmett-Teller (BET) method was applied in the 0.05-0.30 p/p_0 range to calculate the specific surface area. ^1H NMR spectra were recorded on a Bruker 400 MHz spectrometer. Solid state ^{13}C NMR spectra were recorded at room temperature on a JEOL ECZ-R spectrometer operating at 11.7 T using a 3.2 mm AUTOMAS probe and spinning frequencies of 10 kHz. FT-IR measurements were performed in absorbance mode using a Perkin Elmer two DEP.

Synthetic procedures

Synthesis of 1-hydroxyethyl-3-vinyl imidazolium bromide (1a). 1-Hydroxyethyl-3-vinylimidazolium bromide (**1a**) was prepared according to a procedure reported in the literature.[60] In a 50 mL two-necked round-bottomed flask, 1-vinylimidazole (34.61 mmol, 3.2 mL) and 2-bromoethanol (34.83 mmol, 2.6 mL) were added in 17.5 mL of ethanol. The mixture was then stirred at 80 °C under an inert argon atmosphere for 48 h. After cooling at room temperature, the mixture was stirred was washed with diethyl ether several times to remove any traces of reagents. Once dried at 40 °C under vacuum, a highly viscous yellow

compound was obtained. (6.6 g; 86%). ^{1}H NMR (400 MHz, DMSO-D6, δ): 9.50 (s, 1H), 8.22 (s, 1H), 7.89 (s, 1H), 7.34 (dd, J = 15.7, 8.8 Hz, 1H), 5.98 (dd, J = 15.6, 2.3 Hz, 1H), 5.42 (dd, J = 8.7, 2.3 Hz, 1H), 4.39 – 4.17 (m, 2H), 3.91 – 3.66 (m, 2H); ^{13}C NMR (101 MHz, DMSO-D6, δ): 136.21, 129.36, 124.19, 119.33, 109.08, 59.61, 52.58.

Synthesis of 3-ammoniopropyl-1-vinyl imidazolium bromide (1b). The procedure was similar to that reported previously with minor changes.[61] A solution of 3-bromopropylamine hydrobromide (15.9 mmol, 3.55 mL) and 1-vinylimidazole (15.9 mmol, 1,47 mL) in acetonitrile (7.95 mL) was heated for 24 h in an oil bath at 75 °C, with magnetic stirring. After cooling at room temperature, the mixture was washed several times with diethyl ether. The solid product was dissolved in methanol and dried under vacuum obtaining a white solid. (4.72 g; 95 %). ^{1}H NMR (400 MHz, DMSO-D6, δ): 9.63 (s, 1H), 8.26 (s, 1H), 7.99 (s, 2H), 7.34 (dd, J = 15.6, 8.8 Hz, 1H), 5.99 (dd, J = 15.6, 2.0 Hz, 1H), 5.43 (dd, J = 8.7, 2.0 Hz, 1H), 4.35 (t, J = 6.8 Hz, 1H), 2.86 (d, J = 6.1 Hz, 2H), 2.27 – 1.78 (m, 2H). ^{13}C NMR (101 MHz, DMSO-D6, δ): 136.25, 129.51, 123.75, 119.81, 109.29, 46.93, 36.27, 27.82.

Synthesis of bis(vinyl)imidazolium bromide (1c). Bis(vinyl)imidazolium bromide was obtained through the reaction of 1-vinylimidazole (1.5 mL, 16 mmol) and 1,2-dibromoethane (950 μL, 7.88 mmol) in methanol (2 mL) according to the procedure reported in the literature.[62] The system was stirred at 65 °C overnight, under Ar atmosphere and in the dark. Then the mixture was transferred in a 100 mL round bottom flask and the volume was reduced under vacuum before adding with Et₂O (70 mL). After sonication and vigorous stirring, a white precipitate was obtained and the supernatant was removed by simple decantation. Afterwards, methanol (2 mL) was added and gently warmed to solubilize the solid obtaining a yellowish viscous oil, which again after the addition of diethyl ether and sonication gave rise to a white precipitate. The procedure was repeated several times. Once purified, the compound appeared as a white solid. Finally, the compound was dried under vacuum at 60 °C overnight. (3.1 g; 98%). ^{1}H NMR (400 MHz, CD₃OD, δ): 9.41 (s, 1H), 8.01 (t, J = 1.8 Hz, 1H), 7.81 (d, J = 1.8 Hz, 1H), 7.26 (dd, J = 15.6, 8.7 Hz, 1H), 5.93 (dd, J = 15.6, 2.7 Hz, 1H), 5.44 (dd, J = 8.7, 2.7 Hz, 1H), 4.35 (t, J = 6.7 Hz, 2H), 2.02 (dd, J = 6.6, 3.4 Hz, 2H).^{13}C NMR (101 MHz, DMSO-D6, δ): 136.00, 129.42, 123.78, 119.69, 109.21, 48.91, 26.24.

Synthesis of 1,3-bis(3-vinylimidazolium)propan-2-ol bromide (1d). Compound **1d** was synthesized following the procedure reported in the literature.[22] In a 50 mL round-bottomed flask, 1,3-dibromopropan-2-ol (5 mmol, 1.09 g), 1-vinylimidazole (16 mmol, 1.44 mL), and 15

mL acetonitrile were mixed. The system underwent sonication for 10 minutes with simultaneous argon bubbling. Subsequently, the reaction mixture was refluxed at 80 °C for 5 days in the absence of light. Then the solvent was removed under vacuum, and the residue was dissolved in a small amount of methanol and precipitated with diethyl ether. This solubilization and precipitation process was repeated several times. After purification, the compound presented as a white solid. Finally, the compound was dried under vacuum at 60 °C overnight.1.967 g, 97 %) ^{1}H NMR (400 MHz, DMSO-D6, δ): 9.75 (s, 1H), 8.45 (s, 1H), 8.13 (s, 1H), 7.56 (dd, J = 15.7, 8.8 Hz, 1H), 6.19 (dd, J = 15.6, 2.4 Hz, 1H), 5.62 (dd, J = 8.8, 2.4 Hz, 1H), 4.69 (dd, J = 13.7, 3.0 Hz, 1H), 4.38 (dd, J = 13.7, 8.1 Hz, 1H), 3.66 – 3.44 (m, 1H).^{13}C NMR (101 MHz, DMSO-D6, δ): 136.56, 129.35, 124.47, 119.46, 109.38, 67.84, 52.67.

Synthesis of 1,3-bis(1-vinyl-imidazolium)(2,2-bis(hydroxymethyl)propane bromide (1e). Compound **1e** was obtained through the reaction of 2,2'-bisbromethyl-1,3-propanediol (3.74 mmol, 1g) and 1-vinylimidazole (11.22 mmol, 1.02 mL) in DMF (1 mL). The system was stirred at 120 °C for 120 hours, under Ar atmosphere and in the dark. Due to the formation of a precipitate, 1 mL of DMF was added to the mixture after 24 h and a further 2 mL of DMF after 48 h. Then the mixture was transferred in a 50 mL falcon with the minimum volume of methanol and washed with Et$_2$O. The procedure was repeated several times. Afterwards, the precipitate was transferred into a screw-cap vial and cold methanol (6 mL) was added; the vial was placed in the freezer for 10 minutes before centrifugation (3 minutes, 3000 rpm). The operation was repeated twice with methanol and once with ether. A brown precipitate was obtained. (1.23 g; 73.2 %) ^{1}H NMR (400 MHz, DMSO-D6, δ): 9.51 (s, 1H), 8.31 (s, 1H), 7.84 (s, 1H), 7.38 (dd, J = 15.5, 8.7 Hz, 1H), 6.03 (dd, J = 15.6, 2.3 Hz, 1H), 5.46 (dd, J = 8.8, 2.2 Hz, 1H), 4.34 (s, 1H), 3.22 (s, 2H). ^{13}C NMR (101 MHz, DMSO-D6, δ): 136.75, 128.82, 124.78, 118.70, 108.82, 58.49, 49.18, 45.38.

General procedure for the synthesis of DEM systems (2a-e). In a 5 mL glass vial, mono or bis-vinyl imidazolium salt **1a-e** (HBA) and urea or dimethylurea (HBD) were added in 1:2 or 1:4 ratio with respect to bromide ions. The two solid components were allowed to mix at 80 °C for 2 h with a stirring speed of 500 rpm. HBA species **1a-c** always gave rise to homogeneous liquids when mixed in all investigated ratios with HBD species, namely urea or dimethylurea in the 1:2 and 1:4 ratios. In the case of HBA species **1d-e**, a homogeneous liquid was formed only by using a 1:4 ratio with dimethylurea as HBD.

General procedure for the synthesis of hybrid materials (3a-e). Once the DEM formed, MWCNTs were added and the mixture was stirred for 30 min at 80 °C to achieve a homogeneous dispersion. Then, AIBN was added under Ar atmosphere and the reaction mixture was allowed to react at 80 °C for 40 min. The dark residue obtained was transferred into a centrifuge tube by adding methanol. The residue was subjected to centrifugation, three times with methanol and once with Et_2O. The washings were combined and dried under vacuum to recover the corresponding HBD. The residue was recovered and dried under vacuum at 40 °C.

Synthesis of hybrid material 3a. In a 5 mL glass vial, imidazolium salt **1a** (2 mmol, 438.1 mg) and urea (8 mmol, 485.3 mg) were added and mixed at 80 °C for 2 h in ratio 1:4 with respect to bromide ions. After complete dissolution, the MWCNTs (50 mg) were transferred into the systems and the mixture was stirred for 30 min at 80 °C until a homogeneous dispersion was obtained. Then, AIBN (5 mol%, 18 mg) was added under Ar atmosphere and the reaction mixture was allowed to react at 80 °C for 40 min. The dark residue obtained was transferred into a centrifuge tube by adding methanol. The residue was subjected to centrifugation, washed once with DMSO, three times with methanol and once with Et_2O. The washings were combined and dried under vacuum to recover the corresponding HBD. The residue was recovered and dried under vacuum at 40 °C (450 mg; 92%).

Synthesis of hybrid material 3b. In a 5 mL glass vial, imidazolium salt **1b** (1 mmol, 313 mg) and urea (4 mmol, 240 mg) were added and mixed at 80 °C for 2h in ratio 1:2 with respect to bromide ions. After complete dissolution, the MWCNTs (25 mg) were transferred into the systems and the mixture was stirred for 30 min at 80 °C until a homogeneous dispersion was obtained. Then, AIBN (5 mol%, 9 mg) was added under Ar atmosphere and the reaction mixture was allowed to react at 80 °C for 40 min. The dark residue obtained was transferred into a centrifuge tube by adding methanol. The residue was subjected to centrifugation, washed once with DMSO, three times with methanol and once with Et_2O. The washings were combined and dried under vacuum to recover the corresponding HBD. The residue was recovered and dried under vacuum at 40 °C (198 mg; 59%).

Synthesis of hybrid material 3b'. Hybrid material **3b'** was prepared through the deprotonation of hybrid **3b**. Solid **3b** was washed with a saturated solution of sodium bicarbonate (3x40 mL), methanol (2x40 mL) and one with ether (1x40 mL). The black solid obtained was dried under vacuum (100 mg).

Synthesis of hybrid material 3c. In a 5 mL glass vial, imidazolium salt **1c** (1 mmol, 404 mg) and dimethylurea (8 mmol, 720 mg) were added and mixed at 80 °C for 2h in ratio 1:4 with respect to bromide ions. After complete dissolution, the MWCNTs (50 mg) were transferred into the systems and the mixture was stirred for 30 min at 80 °C until a homogeneous dispersion was obtained. Then, AIBN (2.5 mol%, 9 mg) was added under Ar atmosphere and the reaction mixture was allowed to react at 80 °C for 40 min. The dark residue obtained was transferred into a centrifuge tube by adding methanol. The residue was subjected to centrifugation, three times with methanol and once with Et$_2$O. The washings were combined and dried under vacuum to recover the corresponding HBD. The residue was recovered and dried under vacuum at 40 °C (435 mg; 95%).

Synthesis of hybrid material 3d. In a 5 mL glass vial, imidazolium salt **1d** (0.5 mmol, 203 mg) and dimethylurea (4 mmol, 360 mg) were added and mixed at 80 °C for 2h in ratio 1:4 with respect to bromide ions. After complete dissolution, the MWCNTs (25 mg) were transferred into the systems and the mixture was stirred for 30 min at 80°C until a homogeneous dispersion was obtained. Then, AIBN (5 mol%, 9 mg) was added under Ar atmosphere and the reaction mixture was allowed to react at 80 °C for 40 min. The dark residue obtained was transferred into a centrifuge tube by adding methanol. The residue was subjected to centrifugation, three times with methanol and once with Et$_2$O. The washings were combined and dried under vacuum to recover the corresponding HBD. The residue was recovered and dried under vacuum at 40 °C (182 mg; 83%).

Synthesis of hybrid material 3e. In a 5 mL glass vial, imidazolium salt **1e** (0.5 mmol, 225 mg) and dimethylurea (4 mmol, 360 mg) were added and mixed at 80 °C for 2h in ratio 1:4 with respect to bromide ions. After complete dissolution, the MWCNTs (25 mg) were transferred into the systems and the mixture was stirred for 30 min at 80°C to achieve a homogeneous dispersion of the carbonaceous skeleton. Then, AIBN (5 mol%, 9 mg) was added under Ar atmosphere and the reaction mixture was allowed to react at 80 °C for 40 min. The dark residue obtained was transferred into a centrifuge tube by adding methanol. The residue was subjected to centrifugation, three times with methanol and once with Et$_2$O. The washings were combined and dried under vacuum to recover the corresponding HBD. The residue was recovered and dried under vacuum at 40 °C (233 mg; 93%).

Conventional polymerization of MWCNTs in solvent conditions. In a two-neck round-bottom flask, a suspension of MWCNTs (50 mg) and imidazolium salt **1c** (1 mmol, 404 mg) in absolute ethanol (5ml) was sonicated for 20 min. Afterwards, AIBN (2.5 mol%, 9 mg) was

added and argon was bubbled in the reaction mixture for 20 min. The mixture was then heated at 80 °C. After 20 h the solid washed with methanol and diethyl ether. The residue was recovered and dried under vacuum at 40 °C (425 mg; 94%).

Catalytic experiments. Catalytic experiments were carried out in a Cambridge Design Bullfrog batch reactor with temperature control and mechanical stirring. Before each experiment, the material was dried overnight in a vacuum oven at 60 °C. In each test, the catalyst was added to 24 mL of epoxide in a Teflon vial under solvent free conditions. After closing the reactor, the mixture was stirred at 500 rpm. The system was then purged for 10 min with N_2 before the addition of 25 bar of CO_2. After this, the system was heated at 150 °C temperature with a rate of 5 °C/min. The reaction mixture was stirred at 150 °C for 3 h. After this time, the reactor was cooled down to room temperature and then it was depressurized. The separation of the catalyst from the reaction mixture was easily performed by centrifugation (15 min at 4500 rpm). The supernatant was analyzed by ^{1}H NMR.

Recycling test. The recyclability of the materials was checked in the reaction between epichlorohydrin and CO_2. At the end of the reaction, the material was recovered by centrifugation and washed several times with toluene, ethanol and one time with diethyl ether. Moreover, the catalyst was previously sonicated in the washing solvent up to get a good dispersion. After drying at 60 °C under vacuum, the catalyst was reused in the same reaction maintaining the ratio between moles of catalyst and moles of epoxides.

6.6 References

1.   Su, D. S.; Perathoner, S.; Centi, G., Nanocarbons for the Development of Advanced Catalysts. *Chem. Rev.* **2013**, *113*, 5782-5816. https://doi.org/10.1021/cr300367d.

2.   Lehman, J. H.; Terrones, M.; Mansfield, E.; Hurst, K. E.; Meunier, V., Evaluating the characteristics of multiwall carbon nanotubes. *Carbon* **2011**, *49*, 2581-2602. https://doi.org/10.1016/j.carbon.2011.03.028.

3.   Campisciano, V.; Gruttadauria, M.; Giacalone, F., Modified Nanocarbons for Catalysis. *ChemCatChem* **2019**, *11*, 90-133. https://doi.org/10.1002/cctc.201801414.

4.   Rümmeli, M. H.; Ayala, P.; Pichler, T., Carbon Nanotubes and Related Structures: Production and Formation. In *Carbon Nanotubes and Related Structures*, Dirk M. Guldi; Martín, N., Eds. Wiley-VCH Weinheim, Germany, **2010**; pp 1-21.

5.   Jariwala, D.; Sangwan, V. K.; Lauhon, L. J.; Marks, T. J.; Hersam, M. C., Carbon nanomaterials for electronics, optoelectronics, photovoltaics, and sensing. *Chem. Soc. Rev.* **2013**, *42*, 2824-2860. https://doi.org/10.1039/C2CS35335K.

6.   Melchionna, M.; Marchesan, S.; Prato, M.; Fornasiero, P., Carbon nanotubes and catalysis: the many facets of a successful marriage. *Catal. Sci. Technol.* **2015**, *5*, 3859-3875. https://doi.org/10.1039/C5CY00651A.

7.   Yang, Y.; Yang, X.; Yang, Y.; Yuan, Q., Aptamer-functionalized carbon nanomaterials electrochemical sensors for detecting cancer relevant biomolecules. *Carbon* **2018**, *129*, 380-395. https://doi.org/10.1016/j.carbon.2017.12.013.

8.   Yang, Z.; Ren, J.; Zhang, Z.; Chen, X.; Guan, G.; Qiu, L.; Zhang, Y.; Peng, H., Recent Advancement of Nanostructured Carbon for Energy Applications. *Chem. Rev.* **2015**, *115*, 5159-5223. https://doi.org/10.1021/cr5006217.

9.   Kumar, S.; Sidhu, H. K.; Paul, A. K.; Bhardwaj, N.; Thakur, N. S.; Deep, A., Bioengineered multi-walled carbon nanotube (MWCNT) based biosensors and applications thereof. *Sens. Diagn.* **2023**, *2*, 1390-1413. https://doi.org/10.1039/D3SD00176H.

10.   Bianco, A.; Kostarelos, K.; Partidos, C. D.; Prato, M., Biomedical applications of functionalised carbon nanotubes. *Chem. Commun.* **2005**, 571-577. https://doi.org/10.1039/B410943K.

11.   Bianco, A.; Kostarelos, K.; Prato, M., Applications of carbon nanotubes in drug delivery. *Curr. Opin. Chem. Bio.* **2005**, *9*, 674-679. https://doi.org/10.1016/j.cbpa.2005.10.005.

12.   Barrejón, M.; Marchesan, S.; Alegret, N.; Prato, M., Carbon nanotubes for cardiac tissue regeneration: State of the art and perspectives. *Carbon* **2021**, *184*, 641-650. https://doi.org/10.1016/j.carbon.2021.08.059.

13.   Hirsch, A., Functionalization of Single-Walled Carbon Nanotubes. *Angew. Chem. Int. Ed.* **2002**, *41*, 1853-1859. https://doi.org/10.1002/1521-3773(20020603)41:11<1853::AID-ANIE1853>3.0.CO;2-N.

14.   Tasis, D.; Tagmatarchis, N.; Bianco, A.; Prato, M., Chemistry of Carbon Nanotubes. *Chem. Rev.* **2006**, *106*, 1105-1136. https://doi.org/10.1021/cr050569o.

15.   Singh, P.; Campidelli, S.; Giordani, S.; Bonifazi, D.; Bianco, A.; Prato, M., Organic functionalisation and characterisation of single-walled carbon nanotubes. *Chem. Soc. Rev.* **2009**, *38*, 2214-2230. https://doi.org/10.1039/B518111A.

16.   Ziegler, K. J.; Gu, Z.; Peng, H.; Flor, E. L.; Hauge, R. H.; Smalley, R. E., Controlled Oxidative Cutting of Single-Walled Carbon Nanotubes. *J. Am. Chem. Soc.* **2005**, *127*, 1541-1547. https://doi.org/10.1021/ja044537e.

17.   Fukushima, T.; Kosaka, A.; Ishimura, Y.; Yamamoto, T.; Takigawa, T.; Ishii, N.; Aida, T., Molecular Ordering of Organic Molten Salts Triggered by Single-Walled Carbon Nanotubes. *Science* **2003**, *300*, 2072-2074. https://doi.org/10.1126/science.1082289.

18.   Fukushima, T.; Aida, T., Ionic Liquids for Soft Functional Materials with Carbon Nanotubes. *Chem. Eur. J.* **2007**, *13*, 5048-5058. https://doi.org/10.1002/chem.200700554.

19.   Wang, J.; Chu, H.; Li, Y., Why Single-Walled Carbon Nanotubes Can Be Dispersed in Imidazolium-Based Ionic Liquids. *ACS Nano* **2008**, *2*, 2540-2546. https://doi.org/10.1021/nn800510g.

20.   Tunckol, M.; Durand, J.; Serp, P., Carbon nanomaterial–ionic liquid hybrids. *Carbon* **2012**, *50*, 4303-4334. https://doi.org/10.1016/j.carbon.2012.05.017.

21.   Polo-Luque, M. L.; Simonet, B. M.; Valcárcel, M., Functionalization and dispersion of carbon nanotubes in ionic liquids. *Trends Anal. Chem.* **2013**, *47*, 99-110. https://doi.org/10.1016/j.trac.2013.03.007.

22.   Morena, A.; Campisciano, V.; Comès, A.; Liotta, L. F.; Gruttadauria, M.; Aprile, C.; Giacalone, F., A Study on the Stability of Carbon Nanoforms–Polyimidazolium Network Hybrids in the Conversion of CO2 into Cyclic Carbonates: Increase in Catalytic Activity after Reuse. *Nanomaterials* **2021**, *11*, 2243. https://doi.org/10.3390/nano11092243.

23.   Campisciano, V.; Calabrese, C.; Liotta, L. F.; La Parola, V.; Spinella, A.; Aprile, C.; Gruttadauria, M.; Giacalone, F., Templating effect of carbon nanoforms on highly cross-linked imidazolium network: Catalytic activity of the resulting hybrids with Pd nanoparticles. *Appl. Organomet. Chem.* **2019**, *33*, e4848. https://doi.org/10.1002/aoc.4848.

24.   Calabrese, C.; Liotta, L. F.; Carbonell, E.; Giacalone, F.; Gruttadauria, M.; Aprile, C., Imidazolium-Functionalized Carbon Nanohorns for the Conversion of Carbon Dioxide: Unprecedented Increase of Catalytic Activity after Recycling. *ChemSusChem* **2017**, *10*, 1202-1209. https://doi.org/10.1002/cssc.201601427.

25.   Buaki-Sogó, M.; Vivian, A.; Bivona, L. A.; García, H.; Gruttadauria, M.; Aprile, C., Imidazolium functionalized carbon nanotubes for the synthesis of cyclic carbonates: reducing the gap between homogeneous and heterogeneous catalysis. *Catal. Sci. Technol.* **2016**, *6*, 8418-8427. https://doi.org/10.1039/C6CY01068G.

26.   Valentino, L.; Campisciano, V.; Célis, C.; Lemaur, V.; Lazzaroni, R.; Gruttadauria, M.; Aprile, C.; Giacalone, F., Highly cross-linked bifunctional magnesium porphyrin-imidazolium bromide polymer: Unveiling the key role of co-catalysts proximity for CO2 conversion into cyclic carbonates. *J. Catal.* **2023**, *428*, 115143. https://doi.org/10.1016/j.jcat.2023.115143.

27.   Campisciano, V.; Valentino, L.; Morena, A.; Santiago-Portillo, A.; Saladino, N.; Gruttadauria, M.; Aprile, C.; Giacalone, F., Carbon nanotube supported aluminum porphyrin-imidazolium bromide crosslinked copolymer: A synergistic bifunctional catalyst for CO2 conversion. *J. CO2 Util.* **2022**, *57*, 101884. https://doi.org/10.1016/j.jcou.2022.101884.

28.   Le, C. M. Q.; Cao, X. T.; Tu, T. T. K.; Lee, W.-K.; Lim, K. T., Facile covalent functionalization of carbon nanotubes via Diels-Alder reaction in deep eutectic solvents. *Applied Surface Science* **2018**, *450*, 122-129. https://doi.org/10.1016/j.apsusc.2018.04.173.

29.   Chen, L.; Deng, J.; Song, Y.; Hong, S.; Lian, H., Highly Stable Dispersion of Carbon Nanotubes in Deep Eutectic Solvent for the Preparation of CNT-Embedded Carbon

Xerogels for Supercapacitors. *ChemElectroChem* **2019**, *6*, 5750-5758. https://doi.org/10.1002/celc.201901611.

30. Brandão, A. T. S. C.; Rosoiu, S.; Costa, R.; Silva, A. F.; Anicai, L.; Enachescu, M.; Pereira, C. M., Characterization of Carbon Nanomaterials Dispersions: Can Metal Decoration of MWCNTs Improve Their Physicochemical Properties? *Nanomaterials* **2022**, *12*, 99. https://doi.org/10.3390/nano12010099.

31. Patiño, J.; López-Salas, N.; Gutiérrez, M. C.; Carriazo, D.; Ferrer, M. L.; Monte, F. d., Phosphorus-doped carbon–carbon nanotube hierarchical monoliths as true three-dimensional electrodes in supercapacitor cells. *J. Mater. Chem. A* **2016**, *4*, 1251-1263. https://doi.org/10.1039/C5TA09210H.

32. Abbott, A. P.; Boothby, D.; Capper, G.; Davies, D. L.; Rasheed, R. K., Deep Eutectic Solvents Formed between Choline Chloride and Carboxylic Acids: Versatile Alternatives to Ionic Liquids. *J. Am. Chem. Soc.* **2004**, *126*, 9142-9147. https://doi.org/10.1021/ja048266j.

33. Abbott, A. P.; Capper, G.; Davies, D. L.; Rasheed, R. K.; Tambyrajah, V., Novel solvent properties of choline chloride/urea mixtures. *Chem. Commun.* **2003**, 70-71. https://doi.org/10.1039/B210714G.

34. Płotka-Wasylka, J.; de la Guardia, M.; Andruch, V.; Vilková, M., Deep eutectic solvents vs ionic liquids: Similarities and differences. *Microchemical Journal* **2020**, *159*, 105539. https://doi.org/10.1016/j.microc.2020.105539.

35. Smith, E. L.; Abbott, A. P.; Ryder, K. S., Deep Eutectic Solvents (DESs) and Their Applications. *Chem. Rev.* **2014**, *114*, 11060-11082. https://doi.org/10.1021/cr300162p.

36. Gutiérrez, M. C.; Rubio, F.; del Monte, F., Resorcinol-Formaldehyde Polycondensation in Deep Eutectic Solvents for the Preparation of Carbons and Carbon−Carbon Nanotube Composites. *Chem. Mater.* **2010**, *22*, 2711-2719. https://doi.org/10.1021/cm9023502.

37. Carrasco-Huertas, G.; Jiménez-Riobóo, R. J.; Gutiérrez, M. C.; Ferrer, M. L.; del Monte, F., Carbon and carbon composites obtained using deep eutectic solvents and aqueous dilutions thereof. *Chem. Commun.* **2020**, *56*, 3592-3604. https://doi.org/10.1039/D0CC00681E.

38. Gutiérrez, M. C.; Carriazo, D.; Tamayo, A.; Jiménez, R.; Picó, F.; Rojo, J. M.; Ferrer, M. L.; del Monte, F., Deep-Eutectic-Solvent-Assisted Synthesis of Hierarchical Carbon Electrodes Exhibiting Capacitance Retention at High Current Densities. *Chem. Eur. J.* **2011**, *17*, 10533-10537. https://doi.org/10.1002/chem.201101679.

39. Mota-Morales, J. D.; Gutiérrez, M. C.; Ferrer, M. L.; Jiménez, R.; Santiago, P.; Sanchez, I. C.; Terrones, M.; Del Monte, F.; Luna-Bárcenas, G., Synthesis of macroporous poly(acrylic acid)–carbon nanotube composites by frontal polymerization in deep-eutectic solvents. *J. Mater. Chem. A* **2013**, *1*, 3970-3976. https://doi.org/10.1039/C3TA01020A.

40. del Monte, F.; Carriazo, D.; Serrano, M. C.; Gutiérrez, M. C.; Ferrer, M. L., Deep Eutectic Solvents in Polymerizations: A Greener Alternative to Conventional Syntheses. *ChemSusChem* **2014**, *7*, 999-1009. https://doi.org/10.1002/cssc.201300864.

41. Mota-Morales, J. D.; Gutiérrez, M. C.; Sanchez, I. C.; Luna-Bárcenas, G.; del Monte, F., Frontal polymerizations carried out in deep-eutectic mixtures providing both the monomers and the polymerization medium. *Chem. Commun.* **2011**, *47*, 5328-5330. 10.1039/C1CC10391A.

42. Mota-Morales, J. D.; Gutiérrez, M. C.; Ferrer, M. L.; Sanchez, I. C.; Elizalde-Peña, E. A.; Pojman, J. A.; Monte, F. D.; Luna-Bárcenas, G., Deep eutectic solvents as both active

fillers and monomers for frontal polymerization. *J. Polym. Sci.* **2013**, *51*, 1767-1773. https://doi.org/10.1002/pola.26555.

43.   Paraknowitsch, J. P.; Thomas, A., Functional Carbon Materials From Ionic Liquid Precursors.   *Macromol.   Chem.   Phy.*   **2012**,   *213*,   1132-1145. https://doi.org/10.1002/macp.201100573.

44.   Gutiérrez, M. C.; Carriazo, D.; Ania, C. O.; Parra, J. B.; Ferrer, M. L.; del Monte, F., Deep eutectic solvents as both precursors and structure directing agents in the synthesis of nitrogen doped hierarchical carbons highly suitable for CO2 capture. *Energy Environ. Sci.* **2011**, *4*, 3535-3544. 10.1039/C1EE01463C.

45.   Yang, X.; Zhang, Y.; Liu, F.; Chen, P.; Zhao, T.; Wu, Y., Deep eutectic solvents consisting of EmimCl and amides: Highly efficient SO2 absorption and conversion. *Sep. Purif. Technol.* **2020**, *250*, 117273. https://doi.org/10.1016/j.seppur.2020.117273.

46.   Ren, Z.; Wu, X.; Yu, H.; Zhang, F.; Tian, S.; Zhou, Z., Effective separation of toluene from n-heptane with imidazolium-based deep eutectic solvents. *Fuel* **2022**, *326*, 124992. https://doi.org/10.1016/j.fuel.2022.124992.

47.   Liu, Y.; Cao, Z.; Zhou, Z.; Zhou, A., Imidazolium-based deep eutectic solvents as multifunctional catalysts for multisite synergistic activation of epoxides and ambient synthesis of   cyclic   carbonates.   *J.   CO2   Util.*   **2021**,   *53*,   101717. https://doi.org/10.1016/j.jcou.2021.101717.

48.   Huang, W.; Wang, H.; Hu, W.; Yang, D.; Yu, S.; Liu, F.; Song, X., Degradation of polycarbonate to produce bisphenol A catalyzed by imidazolium-based DESs under metal-and solvent-free   conditions.   *RSC   Adv.*   **2021**,   *11*,   1595-1604. https://doi.org/10.1039/D0RA09215K.

49.   Chen, T.; Xu, Y., The Effect of DBU on Microstructure and CO2 Absorption of EmimCl-TEG and BmimCl-TEG Deep Eutectic Solvents. *ChemistrySelect* **2023**, *8*, e202301413. https://doi.org/10.1002/slct.202301413.

50.   Kabane, B.; Redhi, G. G., Thermodynamic properties and activity coefficients at infinite dilution for different solutes in deep eutectic solvent: 1-butyl-3-methylimidazolium chloride + glycerol.   *J.   Mol.   Liq.*   **2020**,   *311*,   113216. https://doi.org/10.1016/j.molliq.2020.113216.

51.   Choudhury, S.; Mahanta, U.; Prasanna Venkatesh, R.; Banerjee, T., Ionic liquid derived novel deep eutectic solvents as low viscous electrolytes for energy storage. *J. Mol. Liq.* **2022**, *366*, 120245. https://doi.org/10.1016/j.molliq.2022.120245.

52.   Thommes, M.; Kaneko, K.; Neimark, A. V.; Olivier, J. P.; Rodriguez-Reinoso, F.; Rouquerol, J.; Sing, K. S. W., Physisorption of gases, with special reference to the evaluation of surface area and pore size distribution (IUPAC Technical Report). *Pure Appl. Chem.* **2015**, *87*, 1051-1069. https://doi.org/10.1515/pac-2014-1117.

53.   Brunauer, S.; Emmett, P. H.; Teller, E., Adsorption of Gases in Multimolecular Layers. *J. Am. Chem. Soc.* **1938**, *60*, 309-319. https://doi.org/10.1021/ja01269a023.

54.   Ziccarelli, I.; Mancuso, R.; Giacalone, F.; Calabrese, C.; La Parola, V.; De Salvo, A.; Della Ca, N.; Gruttadauria, M.; Gabriele, B., Heterogenizing palladium tetraiodide catalyst for carbonylation   reactions.   *J.   Catal.*   **2022**,   *413*,   1098-1110. https://doi.org/10.1016/j.jcat.2022.08.007.

55.   Campisciano, V.; Burger, R.; Calabrese, C.; Liotta, L. F.; Lo Meo, P.; Gruttadauria, M.; Giacalone, F., Straightforward preparation of highly loaded MWCNT–polyamine hybrids and

their application in catalysis. *Nanoscale Adv.* **2020**, *2*, 4199-4211. https://doi.org/10.1039/D0NA00291G.

56. Wang, Y.; Ma, Z.; Liu, P.; He, W., Flexible conductive energetic film based on energetic ionic liquids and carbon nanotubes for information security transient electronics. *Chem. Eng. J.* **2023**, *473*, 144981. https://doi.org/10.1016/j.cej.2023.144981.

57. Ding, Y.; Klyushin, A.; Huang, X.; Jones, T.; Teschner, D.; Girgsdies, F.; Rodenas, T.; Schlögl, R.; Heumann, S., Cobalt-Bridged Ionic Liquid Polymer on a Carbon Nanotube for Enhanced Oxygen Evolution Reaction Activity. *Angew. Chem. Int. Ed.* **2018**, *57*, 3514-3518. https://doi.org/10.1002/anie.201711688.

58. Feng, X.; Gao, W.; Zhou, S.; Shi, H.; Huang, H.; Song, W., Discrimination and simultaneous determination of hydroquinone and catechol by tunable polymerization of imidazolium-based ionic liquid on multi-walled carbon nanotube surfaces. *Anal. Chim. Acta* **2013**, *805*, 36-44. https://doi.org/10.1016/j.aca.2013.10.044.

59. Wu, B.; Hu, D.; Kuang, Y.; Liu, B.; Zhang, X.; Chen, J., Functionalization of Carbon Nanotubes by an Ionic-Liquid Polymer: Dispersion of Pt and PtRu Nanoparticles on Carbon Nanotubes and Their Electrocatalytic Oxidation of Methanol. *Angew. Chem. Int. Ed.* **2009**, *48*, 4751-4754. https://doi.org/10.1002/anie.200900899.

60. Li, N.; Qu, R.; Han, X.; Lin, W.; Zhang, H.; Zhang, Z. J., The Counterion Effect of Imidazolium-Type Poly(ionic liquid) Brushes on Carbon Dioxide Adsorption. *ChemPlusChem* **2019**, *84*, 281-288. https://doi.org/10.1002/cplu.201800636.

61. Tan, Y.; Li, M.; Ye, X.; Wang, Z.; Wang, Y.; Li, C., Ionic liquid auxiliary exfoliation of WS2 nanosheets and the enhanced effect of hollow gold nanospheres on their photoelectrochemical sensing towards human epididymis protein 4. *Sens. Actuators B Chem.* **2018**, *262*, 982-990. https://doi.org/10.1016/j.snb.2018.02.066.

62. Campisciano, V.; Valentino, L.; Morena, A.; Santiago-Portillo, A.; Saladino, N.; Gruttadauria, M.; Aprile, C.; Giacalone, F., Carbon nanotube supported aluminum porphyrin-imidazolium bromide crosslinked copolymer: A synergistic bifunctional catalyst for CO2 conversion. *J. CO2 Util.* **2022**, *57*, 101884. https://doi.org/10.1016/j.jcou.2022.101884.

CHAPTER VII

Highly Functionalized SWCNTs with a Dopamine Derivative as a Support for Pd Nanoparticles: A Recyclable Catalyst for the Reduction of Nitro Compounds and the Heck Reaction
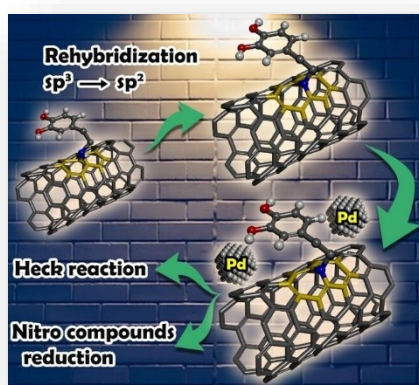
This chapter is based on:

CHAPTER VII

Highly Functionalized SWCNTs with a Dopamine Derivative as a Support for Pd Nanoparticles: A Recyclable Catalyst for the Reduction of Nitro Compounds and the Heck Reaction

7.1 Abstract

Single-walled carbon nanotubes (SWCNTs) were functionalized with a dopamine derivative in which the amine group was converted to azide (dopamine azide). The direct reaction of SWCNTs and dopamine azide in *o*-dichlorobenzene at high temperature (160 °C) led to very highly functionalized CNTs (≈60 wt%). Surprisingly, despite this high degree of functionalization, Raman spectroscopy detected a low disruption of the π-network of the carbonaceous support. This finding was justified by the rehybridization from sp^3 to sp^2 of the sidewall carbon atoms of CNTs involved in the functionalization process. Further characterization by means of different techniques such as X-ray photoelectron spectroscopy (XPS) analysis and transmission electron microscopy (TEM) allowed to shed some light on the chemical composition and morphology of the obtained material. Moreover, the estimation of the total content of phenolic units and their reducing potential after CNTs functionalization was also assessed using Folin and Ciocalteu and 2,2-diphenyl-1-picryl hydrazide (DPPH) assays. The functionalization of CNTs was exploited to immobilize palladium(II) species that were subsequently reduced with $NaBH_4$ leading to the formation of Pd nanoparticles (NPs). The so obtained hybrid material was used as a recyclable heterogeneous catalyst for the reduction of nitro compounds and the Heck reaction.

7.2 Introduction

Carbon nanoforms (CNFs) and especially carbon nanotubes (CNTs) benefit from great popularity due to their widespread use for a plethora of applications in different research areas such as electronics, photonics, nanomedicine or their use for the production of high-performance composite materials.

All of these applications are due to their peculiar electronic properties, high thermal stability, and mechanical resistance, which can hardly be found in other materials. However, the full exploitation of such unique properties is hampered by a lack of compatibility and poor processability of the pristine CNFs in commonly used solvents due to their hydrophobicity and tendency to agglomerate because of the strong Van der Waals interactions.

The covalent functionalization of CNTs with specific moieties represents a valuable solution to this issue to improve their affinity with different solvents[1-2] and impart peculiar properties, which are fundamental in many fields, such as catalysis.[3] Certainly, the most widely used functionalization technique consists in the oxidative acid treatment of CNTs with the generation of defects onto their surface with the introduction of different oxygenated functions such as carbonyl, carboxyl, and hydroxyl[4-5] or even, under the most harsh conditions, with formation of severe damage to the nanotube structure that can cause their shortening.[6]

The alternative is to proceed with the direct covalent functionalization of pristine CNTs by means of different routes, avoiding any oxidative pre-treatment.[7-18] However, any kind of nanotube modification, except for supramolecular modification, leads to the more or less severe disruption of the π-network with the rehybridization from sp^2 to sp^3 of the sidewall carbon atoms involved in the functionalization process. The partial loss of the π-conjugation constitutes a detrimental event that can affect the mechanical, electronic and thermal properties of CNTs.

Attempts to retain the native properties of CNTs have been pursued, for example, by using mild oxidation conditions with the purpose of introducing carboxyl groups only at initial defects that already exist in the CNTs sidewall.[4] Furthermore, some theoretical studies have identified [2+1] cycloadditions onto CNTs sidewall as a potential route to preserve the π-conjugated electronic structure of CNTs by cleaving bond between adjacent sidewall carbons, recovering the sp^2 hybridization and the properties of the pristine CNTs.[19-21] The experimental proof of such hypothesis was provided by Adeli, Haag, Reich *et al.*,[22] and very recently by Donskyi and co-workers,[23] who covalently functionalized SWCNTs by means of nitrene [2+1] cycloaddition reaction using the electron-poor monoazido-dichloro-triazine that allows the introduction of stable functionalities onto single-walled carbon nanotubes (SWCNTs) sidewall while preserving the aromaticity.

Here we have chosen dopamine as a precursor for the corresponding dopamine azide,[24] which in turn was used for the functionalization of SWCNTs. The conversion of amine to the azide group in dopamine has considerable consequences on the course of oxidative polymerization of this catechol derivative as the cyclization routes leading to indole units are clearly suppressed and consequently the possibility to generate melanin like pigments commonly referred to as polydopamine.[25-27] Mrówczyński *et al.*[28] investigated the polymerization process of dopamine azide, which requires stronger oxidation conditions ($NaIO_4$) compared to native dopamine. Furthermore, the obtained polymers result soluble in organic solvents due to the lack of cross-linkage between building blocks consisting of dopamine azide monomers.

Several reports have described the properties of CNTs coated with polydopamine as obtained by exposure of the CNTs to dopamine solution under oxidative conditions. Though, under these conditions, the structure of the CNTs is not affected at all, deposition of the pigmented material cannot be controlled and excess can be formed assembling together the CNTs.[29-34]

On this basis, the functionalization of SWCNTs with dopamine azide could represent a valuable route to get a selective controlled modification of SWCNTs avoiding the pigment formation that takes place when amino groups are present. It is also expected that this functionalization can both modify surface properties of the CNF and reduce to a minimum the disrupting of π-network responsible of unique properties of carbon nanotubes.

The presence of catechol moieties onto SWCNTs allowed their surface properties to be tailored, resulting in a material with high compatibility towards polar solvents and with the possibility to exploit the *o*-diphenol functionalities as binding sites for different metal species.

A high degree of functionalization of SWCNTs ($\approx$60 wt%) with catechol moieties was obtained with a relatively low increase in the D band intensity (I_D) with respect to the G band (I_G) as detected by Raman spectroscopy, indicating that there was only a partial loss of the original π-network of pristine SWCNTs. This result could have interesting implications in certain application fields of CNFs that require both high electrical conductivity and specific surface properties such as in the case of SWCNTs-based sensors.[35]

The catechol functionalized SWCNTs were used as support and stabilizer for palladium nanoparticles (Pd NPs) and the resulting hybrid material was tested for two catalytic applications, namely the reduction of nitro compounds and the Heck reaction.

7.3 Results and discussion

The diazotransfer reaction allowed to convert dopamine **1** into the corresponding dopamine azide **2**,[24] which was reacted in refluxing *o*-dichlorobenzene (oDCB) and under an argon atmosphere in the presence of pristine SWCNTs. Under these conditions, the direct functionalization of SWCNTs was achieved resulting in material **5** (**Scheme 1**). The use of dopamine azide was initially selected with the aim of exploiting the well-established functionalization route of CNTs via in situ generated reactive nitrenes.[36-39]
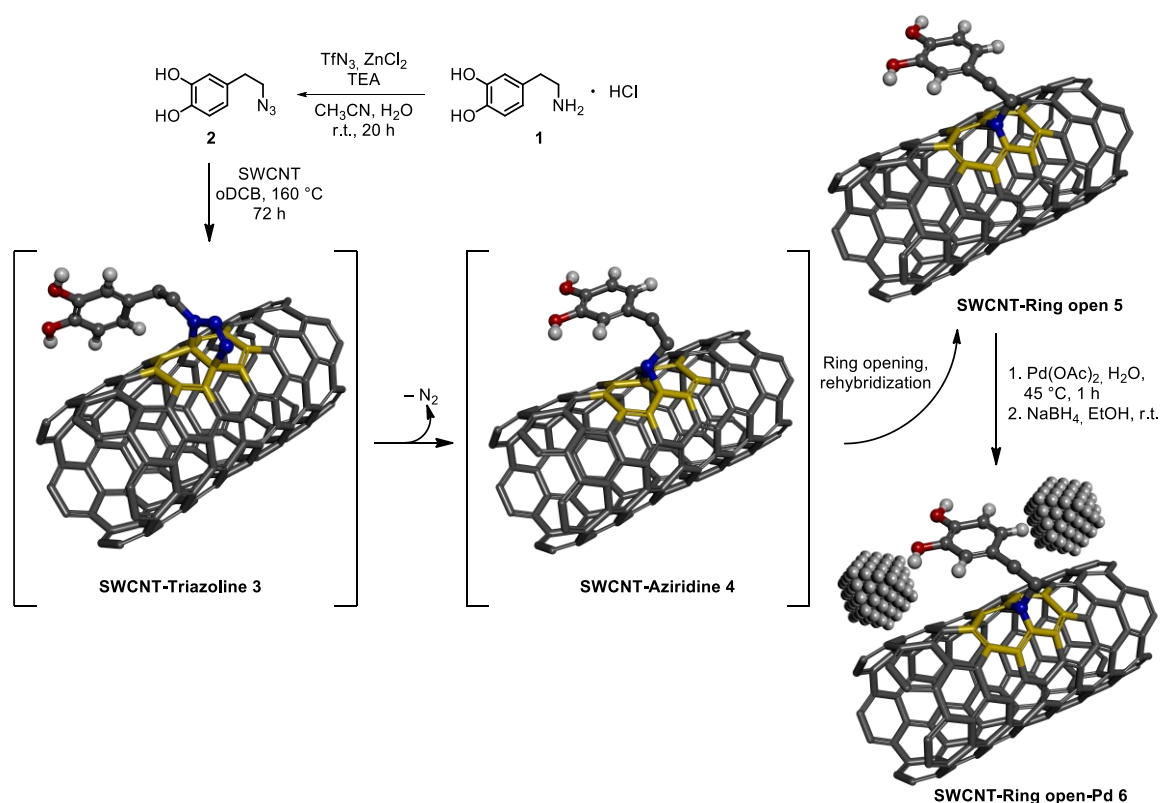
Scheme 1. Preparation of the functionalized SWCNTs material **5** by means of the formation of the proposed 1,2,3-triazoline adduct **3** and immobilization of Pd NPs to obtain hybrid **6**.

Surprisingly, thermogravimetric analysis (TGA) under air flow (**Figure 1**), showed an unusually high functionalization degree of material **5**. A 59.5 wt% loading was estimated taking into account the weight loss at 530 °C, at which temperature pristine SWCNTs are still stable with only 1 wt% loss. We therefore questioned the reasons for this result.
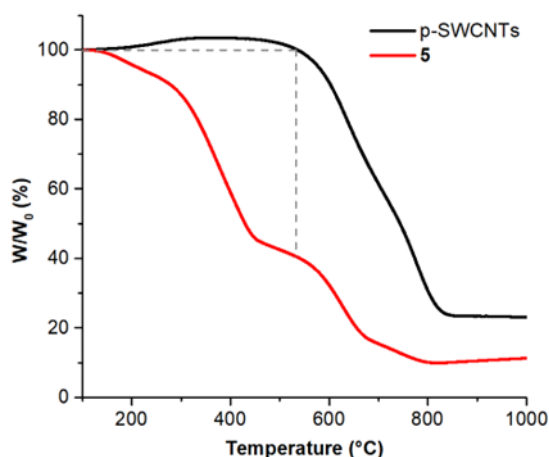
Figure 1. Thermogravimetric analysis under air flow of p-SWCNTs and **5**.

Recently, Mrówczyński *et al.*[28] have shown that the polymerization of dopamine azide can only be achieved under highly oxidizing conditions (NaIO$_4$), producing polymers soluble in organic solvents.

Herein no oxidant was used and the reaction of functionalization of SWCNTs was carried out under inert atmosphere in refluxing oDCB. Therefore, it can be assumed that oxidation and polymerization process of dopamine azide (**2**) under the reaction conditions herein adopted play a marginal role in the functionalization process of SWCNTs, although some oxidation due to the presence of adventitious oxygen and the high temperature adopted cannot be ruled out at all.

To obtain further evidence and shed some light on why such a high functionalization degree of SWCNTs was obtained, in an additional blank test the dopamine azide was refluxed in oDCB under inert atmosphere for 72 h without the presence of SWCNTs. If thermal decomposition of the organic azide takes place, initial extrusion of nitrogen occurs with the formation of the nitrene species, which can undergo stabilization through different reactions leading to consumption of the starting azide, such as isomerization to imines, dimerization to azo compounds, hydrogen abstraction followed by ring closure to heterocyclic compounds, among others.[40] The result of this experiment was quite interesting, indeed, it was possible to recover the starting dopamine azide (**2**) along with traces of a residue, probably generated as a result of oxidation and polymerization of catechol moieties, slightly soluble in dimethyl sulfoxide. FTIR analysis of this residue (**Figure 2**) was in accordance with that shown by Mrówczyński and co-workers still confirming the presence of both azido group (2100 cm^{-1}) and a network of H-bonded hydroxyl groups (3500-3200 cm^{-1}).
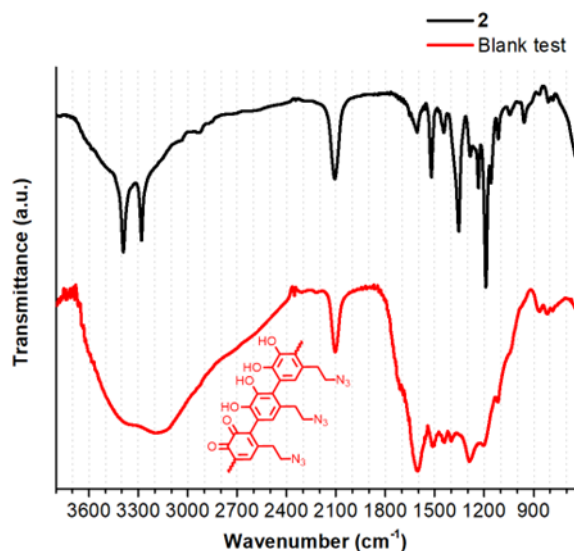
Figure 2. FT-IR spectra of dopamine azide **2** and the residue recovered from the blank test.

These results allowed us to draw some preliminary conclusions: 1) dopamine azide **2** has a very high thermal stability that can probably undergo classical azide decomposition with the formation of nitrene moiety only under very harsh conditions; 2) the oxidation/polymerization process of the catechol moiety is a secondary path that can nevertheless contribute to the functionalization of SWCNTs by means of the reactive azide moieties 3) as a consequence of the first observation, it is proposed that dopamine azide, in analogy to fullerene C_{60} reactivity with aryl azides,[41] reacts with SWCNTs by means of an azide-alkene [3+2] cycloaddition to form 1,2,3-triazoline adduct **3**, which evolves to the formation of aziridine derivative **4** as a result of nitrogen extrusion at high temperature (**Scheme 1**). There are some aspects in favour of this hypothesis. First of all, the thermal stability of organic azides is strongly dependent on the nature of substituent and the temperature of decomposition with the generation of nitrene intermediate decreases in the order alkyl/aryl azides>azidoformates and sulfonyl azides>acyl azides.[41-43] This means that if at high temperature the chosen azide does not decompose with the extrusion of nitrogen and the formation of nitrene derivative, then, the [3+2] cycloaddition of azide to the sidewall of CNTs will be favoured over [2+1] route. Thermogravimetric/differential scanning calorimetry analysis (TGA/DSC) under nitrogen atmosphere of the dopamine azide **2** (**Figure 3**) proved that it was stable up to 200 °C, quite above 160 °C adopted in the reaction conditions for the functionalization of SWCNTs. In particular, dopamine azide decomposes with an exothermic process between 190 and 265 °C. The onset temperature of exothermic decomposition (T_{on} exo) is 200 °C and the maximum heat flow of 1.62 W/g was reached at 236 °C.
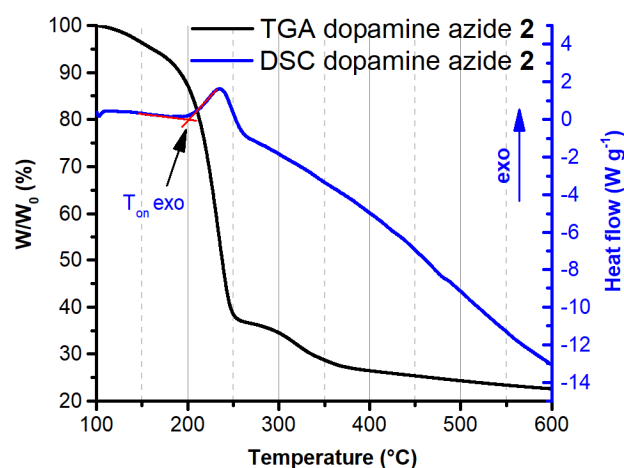
Figure 3. TGA/DSC analyses of dopamine azide **2** recorded under nitrogen flow (10 °C/min).

Further investigations about structural changes of SWCNTs in material **5** were carried out by means of Raman spectroscopy (**Figure 4**), which represents a powerful technique to assess the covalent functionalization of SWCNTs by the change in the intensity ratio of the D band to the G band (I_D/I_G) compared to I_{D0}/I_{G0} ratio in the pristine SWCNTs. Despite the very high functionalization degree of 59.5 wt% (see above) a relatively low normalized I_D/I_G ratio from the I_{D0}/I_{G0} ratio of 1.85 was detected, leading one to wonder how such high functionalization degree was eventually reached.
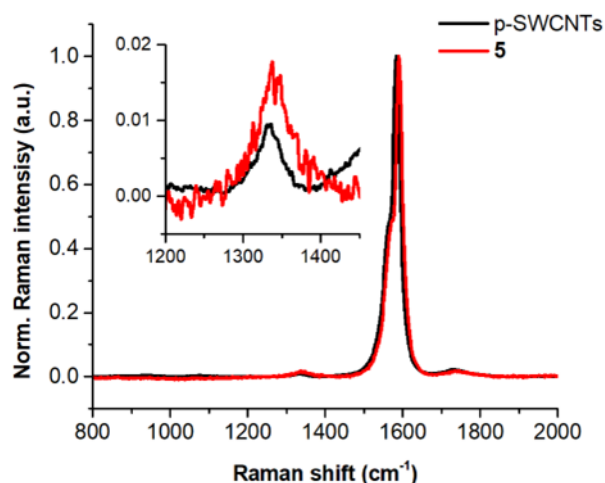
Figure 4. Raman spectra of p-SWCNTs and **5**. The inset shows the increase of the intensity of the D band of material **5**.

A plausible explanation of such results could have been provided by Adeli, Haag, Reich *et al.*,[7] and very recently by Donskyi and co-workers,[23] who obtained high degree of functionalization up to one functional moiety per 25 carbon atoms and proved experimentally what until then had only been theorized,[19-21] namely that the covalent functionalization of SWCNTs with an

electron-poor aromatic azide led to a non-destructive covalent functionalization still maintaining the electronic and optoelectronic properties of SWCNTs preserving the π-network of the pristine carbon nanoform. An initial in situ generation of a nitrene that can undergo to [2+1] cycloaddition to form an aziridine derivative, whose strained ring opens to the final rehybridized structure with the recovering of the π-network of SWCNTs has been hypothesised. Quantum chemical calculations predict that the entire reaction proceeds without activation barrier at room temperature.[7]

In the present work, if the thermal stability of dopamine azide (**2**) is taken into account, the same conclusions can be drawn when the initial stage is constituted by the [3+2] cycloaddition of the azide derivative onto SWCNTs sidewalls with the generation of the corresponding triazoline **3**, which after nitrogen extrusion can evolve in the formation of the aziridine derivative **4** and eventually in the open form **5** (**Scheme 1**) in analogy to the reaction of fullerene C_{60} with alkyl azides leading to the preferential formation of the [5,6]-open isomer.[44-45] However, it should be emphasized that the distinction between the direct (formation of nitrene) and the indirect ([3+2] cycloaddition) method for the formation of aziridines from organic azides and alkenes remains a hard task. One way to discriminate between the two routes is to perform a blank experiment in the reaction conditions in absence of any olefin (see above) to assess the thermal stability of the chosen organic azide.

All the evidences gathered on the high functionalization degree of material **5** despite the small modification of the π-conjugate network lead to conclude that the modification of the nanotubes is mainly due to a [3+2] cycloaddition mechanism of dopamine azide **2** onto the nanotube sidewalls to obtain triazoline derivative **3** and the subsequent extrusion of nitrogen to form the aziridine derivative **4**, which subsequently undergoes partial rehybridization (the incomplete rearrangement could be due to the high functionalization degree reached: one functional moiety per *ca*. 10 carbon atoms) restoring the conjugate network of the nanotube in the material **5**.

The presence of intact phenolic units onto material **5** and their reducing potential was also assessed by use of chemical assays namely the Folin and Ciocalteu and the 2,2-diphenyl-1-picryl hydrazide (DPPH), measuring the presence of phenol groups and the hydrogen donor ability of a given material, respectively. Data in **Table 1** confirm the presence of phenolic functionalities in material **5** that also exhibit a good hydrogen donor ability as indicated by the EC_{50} value. For comparative purposes, and as a control that the observed activity was indeed due to the free catechol groups of the dopamine derivative linked to the SWCNT, a derivative of dopamine azide having the catechol groups protected as acetyl derivative was used for functionalization of the SWCNT. As expected, the resulting material **5Ac** gave a very low response to both assays.

Table 1. Results of the Folin-Ciocalteu assay and DPPH assay on the material **5** and its acetylated derivative **5Ac**.

Material	FOLIN-CIOCALTEU ASSAY (Gallic acid equivalents)	DPPH ASSAY (EC$_{50}$ (mg/mL))
5	$4.17 \times 10^{-04} \pm 1.2 \times 10^{-05}$	$0.81 \pm 8.5 \times 10^{-03}$
5Ac	$5.07 \times 10^{-05} \pm 1 \times 10^{-05}$	$1.8 \pm 5 \times 10^{-02}$

Material **5** was used as support for palladium species by means of exposure to palladium acetate in distilled water at a SWCNT/Pd ratio of 9 : 1 over 1 h at 45 °C. After repeated washings, the material was subjected to a reduction treatment with sodium borohydride to obtain material **6** (**Scheme 1**). The palladium content of **6** was found to be of 1.27 wt%, as determined by means of inductively coupled plasma optical emission spectroscopy (ICP-OES).

Both materials **5** and **6** were subjected to X-ray photoelectron spectroscopy (XPS) analysis (**Figure 5 and Table 2**). In **Figure 5** high resolution XPS spectra of C1s, N1s regions for materials **5** and **6**, and Pd3d region for material **6** are shown. The C1s peak of both **5** and **6** shows the presence of five components at 284.6, 285.6, 286.4, and 287.4 eV characteristic of sp^2 and, sp^3 carbon atoms, C–O and C–N, and C=O bonds, respectively. Furthermore, the peak centred at 290.6 eV is attributed to the shake-up satellite (π→π*) process,[46-47] clearly visible in the C1s peak of pristine SWCNTs (**Figure 5a and Table 2**). N1s peak of both materials **5** and **6** show two contributions associated with aziridine at 399.0 eV (close structure)[48-49] and open structure nitrogen atoms at higher binding energies.[50-51] The atomic ratio between the two types of nitrogen atoms in material **5**, open and closed form, respectively, of about 78 : 22 (**Table 2**) confirms the preliminary results obtained by Raman spectroscopy, which showed a relatively low perturbation of the conjugated network of SWCNTs despite of the high functionalization degree. Since, as mentioned above, the oxidation/polymerization process of the catechol moieties does not affect the azido groups, the absence of any azide-attributable peaks in the N1s region shows how all these functional groups totally reacted with the SWCNTs. The Pd3d spectrum of material **6** shows the presence of two doublets due to the typical spin-orbit splitting (Pd3d$_{5/2}$ and Pd3d$_{3/2}$ components) and the concomitant presence of two species of palladium, namely Pd(0) and Pd(II). The relative amount of the components due to Pd(0) and Pd(II) species allowed to estimate a degree of reduction of 56 % after treatment with NaBH$_4$.
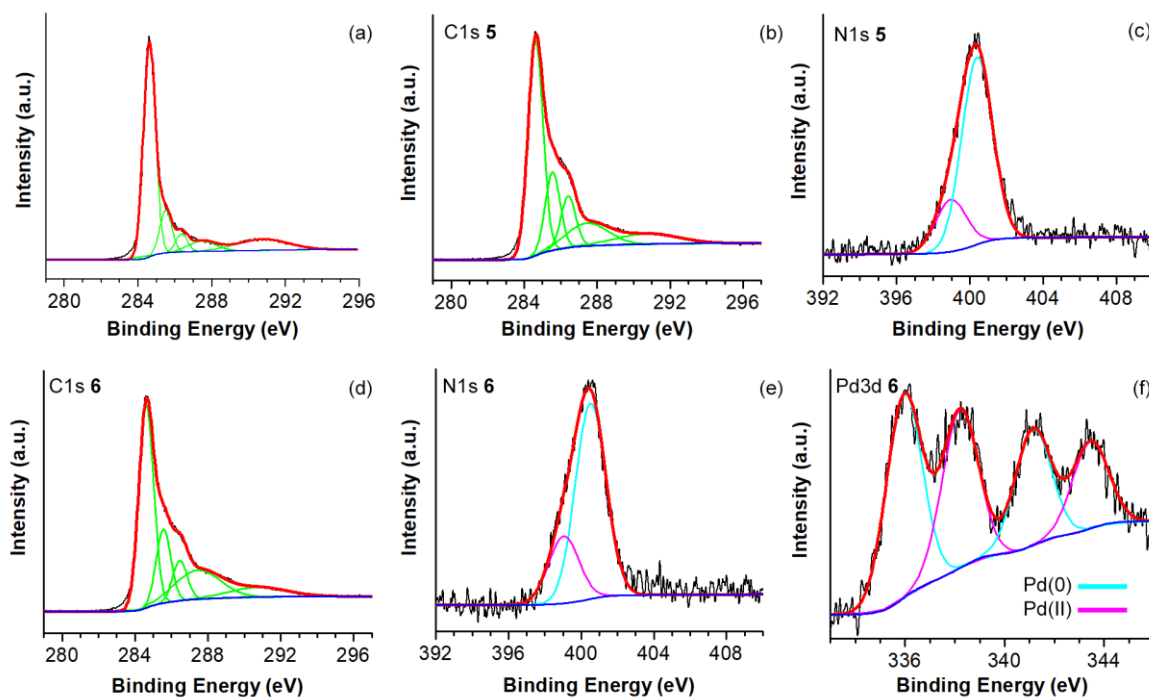
Figure 5. High resolution XPS spectra of C1s for *p*-SWCNTs (a), for materials **5** (b) and **6** (d), N1s regions for materials **5** (c) and **6** (e) and Pd3d region for material **6** (f).

Table 2. Binding energies of the deconvoluted peaks of XPS spectra of *p*-SWCNTs, **5** and **6** (the relative percentages are given in square brackets).

Compound	C1s (eV)	N1s (eV)	Pd3d$_{5/2}$ (eV)
5	284.6 [47.5%] C–C sp^2 285.6 [17.4%] C–C sp^3 286.4 [11.5%] C–O/C-N 287.5 [14.1%] C–O 290.7 [9.5%] $\pi\rightarrow\pi^*$	399.0 [21.7%] N aziridine 400.4 [78.3%] N ring open	-
6	284.6 [45.7%] C–C sp^2 285.6 [16.6%] C–C sp^3 286.5 [9.1%] C–O/C-N 287.4 [19.9%] C–O 290.7 [8.7%] $\pi\rightarrow\pi^*$	399.0 [25.5%] N aziridine 400.5 [74.5%] N ring open	335.9 [56.2%] Pd(0) 338.2 [43.8%] Pd(II)
***p*-SWCNTs**	284.6 [61.7%] C–C sp^2 285.5 [12.3%] C–C sp^3 286.4 [5.2%] C–O 287.5 [6.9%] C=O 290.7 [13.9%] $\pi\rightarrow\pi^*$		

Transmission electron microscopy (TEM) was used to investigate the morphology of materials **5** and **6** (**Figure 6**). Pristine SWCNTs are arranged to form a highly entangled network of long carbonaceous structures (**Figure 6a**). Their functionalization with dopamine azide to obtain material **5** did not result in the dispersion of individual nanotubes, but rather in the presence of a dense network of rough filaments, probably due to both the establishment of numerous hydrogen bonds between the functionalized CNTs and the presence of a polymeric matrix

arising from the partial oxidation of catechol moieties as stated above (**Figure 6b**). TEM micrograph of material **6** (**Figure 6c**) showed how the network of functionalized CNTs served as support for the stabilization of palladium nanoparticles, which are all clearly visible and uniformly dispersed throughout the material.
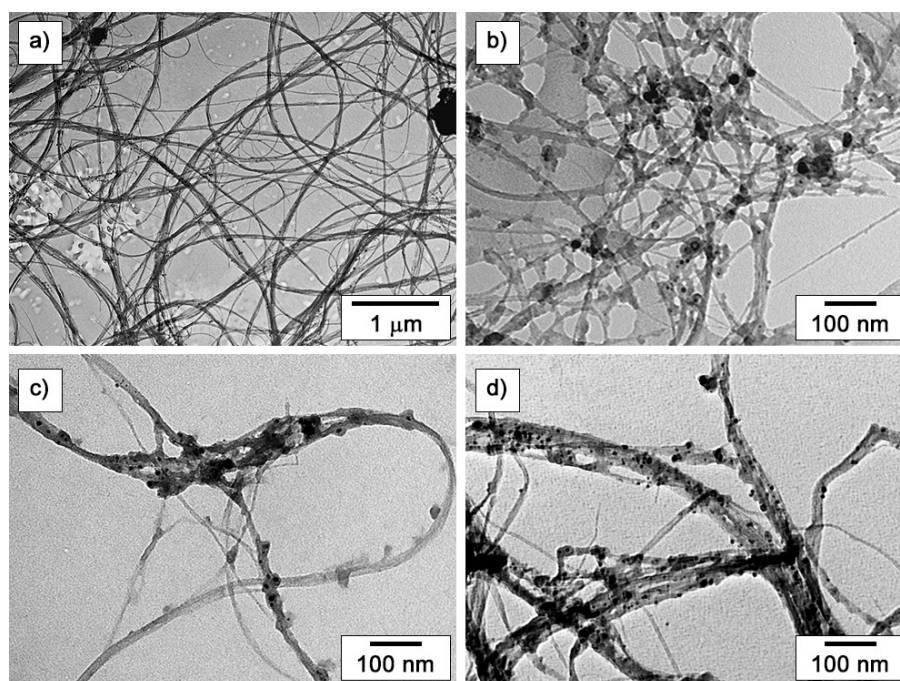
Figure 6. TEM images of a) pristine SWCNTs, b) materials **5**, c) **6**, and d) **6** after recycling tests in the Heck reaction.

The catalytic activity of **6** was investigated in the reduction of nitrobenzene derivatives to the corresponding anilines. The catalytic performances were evaluated in terms of conversion, yield, selectivity, turnover number (TON, calculated as moles of nitrobenzene converted/moles of Pd), turnover frequency (TOF) and recyclability. Firstly, *p*-nitroaniline was picked out as the model substrate in the screening studies to improve reaction conditions. Preliminary tests were performed in water by employing sodium borohydride as the hydrogen source. In one hour, with a catalytic loading of 0.02 mol % and using a molar ratio of 1 : 4 (substrate/hydrogen source), 72% conversion to the corresponding aniline was achieved (**Table 3**, entry 1). When the reaction was run in 2 h the conversion into the desired product was almost complete (entry 2). By increasing the amount of $NaBH_4$ a full conversion was recorded in only one hour (entry 3). An identical result was also obtained by doubling the amount of catalyst with a lower substrate/$NaBH_4$ ratio of 1 : 2.5 (entry 4). Still a good conversion value (73%) and a very high TON value was reached when **6** was decreased to 0.005 mol % (entry 5). Notably, by conducting the reaction in the absence of the catalyst, using only sodium borohydride as the reducing agent,

less than 5 % conversion to the corresponding aniline occurred (entry 6) whereas in the presence of pristine SWCNTs a *ca.* 8 % conversion was obtained (entry 7).

Table 3. Screening of reaction conditions for the reduction of 4-nitroaniline.[a]
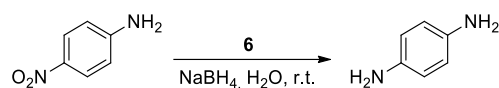
Entry	Catalyst (mol%)	NaBH$_4$ (mmol)	Time (h)	Conv. (%)[b]	TON[c]/ TOF (h^{-1})[c]	Selectivity (%)
1	0.02	4	1	72	3600/3600	>99
2	0.02	4	2	98	4900/2450	>99
3	0.02	8	1	>99	5000/5000	>99
4	0.04	2.5	0.5	>99	2500/5000	>99
5[d]	0.005	4	2	73	14600/7300	>99
6[e]	-	8	1	<5	-/-	>99
7[f]	SWCNT	8	1	8	-/-	>99

[a] Reaction conditions: 4-nitroaniline (1 mmol), sodium borohydride (2.5, 4 or 8 mmol), catalyst (0.005 or 0.02 or 0.04 mol%; 0.42 or 1.68 or 3.36 mg), water (5 mL), 30 °C, 1600 rpm. [b] Determined by ^{1}H NMR; isolated yield: ≥95% of conversion. [c] TON and TOF values calculated based on the Pd content obtained from ICP. [d] Water (2 mL). [e] Without catalyst, water (5 mL). [f] In the presence of pristine SWCNT (0.8. mg).

Considering the high catalytic activity of **6**, reaction conditions reported in **Table 3**, entry 3, were selected to explore the versatility of the hybrid material in the reduction of different aromatic nitro compounds, including aryl halides, phenols, and nitroarenes with aliphatic chain. Some of the catalytic tests were repeated, thus confirming the good reproducibility of the experiments. As mentioned in **Table 4**, in all the catalytic tests, a full selectivity toward the corresponding aniline was reached together with excellent TON and TOF values, without the noticeable influence of functional groups on the reaction.

Table 4. Nitro-reduction reactions catalyzed by **6**.[a]

Entry	Substrate	Time (h)	Conv. (%)[b]	TON[c]/ TOF (h⁻¹)[c]	Selectivity (%)
1		1	>99	5000/5000	>99
2		1	>99	5000/5000	>99
3		0.5	>99	5000/10000	>99
4		0.5	>99	5000/10000	>99
5		2	>99	5000/2500	>99
6		2	95	4750/2375	97
7[d]		3	90	4500/1500	>99
8		1	>99	5000/5000	>99
9		2	>99	5000/2500	>99
10		1	>99	5000/5000	>99
11[e]		4	80	4000/1000	>99

[a] Reaction conditions: nitro compounds (1 mmol), sodium borohydride (8 mmol), catalyst (0.02 mol %), water (5 mL), 30 °C, 1600 rpm. [b] Determined by ¹H NMR; isolated yield: ≥95 % of conversion. [c] TON and TOF values calculated on the basis of the Pd content obtained from ICP. [d] Isolated yield 60 %. [e] Dehalogenation occurred with the formation of aniline; selectivity, TON, and TOF values refer to the obtained aniline.

In particular, the reduction of nitroarenes with strong electron-donating substituents in both ortho, meta and, para occurred quite rapidly, though reaction times were not optimized (entry 1–4). Less electro-donating alkyl chains gave the corresponding anilines in two hours (entry 5

and 6). The reduction of halogen-substituted nitroarene was effective within 1–4 h and selectively produced the corresponding anilines without any observable dehalogenation except for iodo as a substituent (entry 7–11). Indeed, in this case, dehalogenation occurred, which can be explained as a function of the less strong C–I bond (entry 11).

To thoroughly investigate the catalytic behavior and robustness of the solid, recycling experiments were conducted. The recyclability of the heterogeneous hybrid material **6** in the *p*-nitroaniline reduction was studied. As illustrated in **Figure 7**, **6** was reused for six consecutive runs without any considerable decrease of the catalytic performance. Overall, TON of 30,000 is achieved.
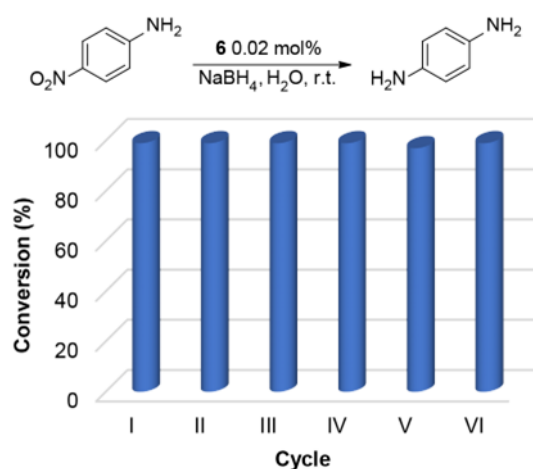
Figure 7. Recycling test of **6**. Reaction conditions: 4-nitroaniline (1 mmol), sodium borohydride (8 mmol), catalyst (0.02 mol%), water (5 mL), 30 °C, 1 h, 1600 rpm

More in-depth studies on the recyclability of **6** have been carried out by changing substrates (**Figure 8**). In the first cycle 1-isopropyl-4-nitrobenzene was used (green), changing from the second cycle to 1-ethyl-4-nitrobenzene (orange). A decrease in catalytic activity in the second cycle was evident. The decrease in conversion at the second cycle is due to the poor dispersion of the catalyst. This was attributed to the fact that, in this case, the nitro derivative was added first and then the solvent. The catalyst, being hydrophilic, aggregates strongly on contact with the liquid hydrophobic reactant and remains in that aggregated form even after the addition of water. But the situation turned out to be reversible. After recovering the used catalyst and changing the order of addition, conversion returns quantitatively without further treatment. Once again, the catalyst was shown to be versatile, robust and reusable for multiple runs.
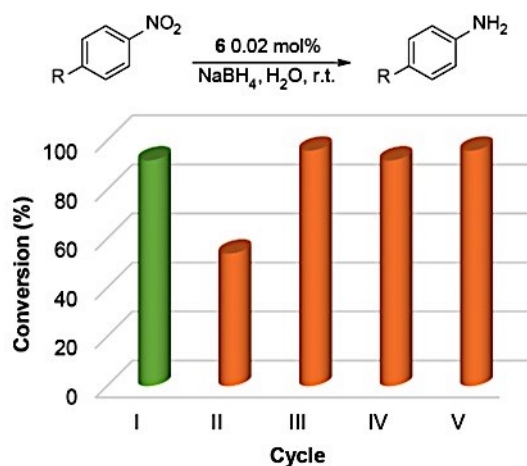
Figure 8. Recycling test of **6**. Reaction conditions: 1-isopropyl-4-nitrobenzene (green) or 1-ethyl-4-nitrobenzene (orange) (1 mmol), sodium borohydride (8 mmol), catalyst (0.02 mol%), water (5 mL), 30 °C, 1 h, 1600 rpm.

Finally, the remarkable catalytic activity of **6** was compared with several reported catalytic systems. **Table 5** shows that **6** is highly competitive with other systems used in the nitro reduction reaction. Even if some of these systems require lower amount of reducing agent or shorter reaction times, usually a larger amount of catalyst was used, up to 50–60 mg per mmol. Among these examples, a similar material was prepared by polymerization of catechol with terephthalaldehyde under basic condition (Pd@MOPOH).[52]

Palladium was immobilized from a $Pd(NO_3)_2$ solution followed by reduction with $NaBH_4$. Pd@MOPOH was used for the reduction of 4-nitrophenol at r.t. by using a 100-fold excess of $NaBH_4$ and a very high catalytic loading following the reaction spectroscopically (UV). Recycling tests were carried out on 6 mmol scale with 10 mg of catalyst. The reaction was complete in a short time (6 min), but no other substrates were investigated.

Table 5. Comparison of catalytic performance of different heterogeneous catalysts based on palladium nanoparticles in the nitro reduction of p-nitroaniline.

Entry	Catalyst	Conv.(%)	TON/ TOF (h⁻¹)	mol%	Reaction conditions[a]	Ref.
1	**6**	99	5000/5000	0.02	1:8; 60min; 30 °C; H_2O	Chapter VII
2	**6**	98	4900/2450	0.02	1:4; 120min; 30 °C; H_2O	Chapter VII
3	Pd@NC	95/	95/3166	1	1:2; 2min; r.t.; H_2O/EtOH	53
4	PdNi-G2-Fe_3O_4-GO	93	465/1409	0.21	1:2; 20min; r.t.; H_2O	54
5	Fe_3O_4@ Guanidine-Pd	96	738/1119	0.13	1:2; 40min; r.t.; H_2O	55
6	$PdCl_2(Bbtb-H)_2$	80	80/40	1	1:4; 120min; r.t.; EtOH	56
7	$Ti_{0.97}Pd_{0.03}O_{1.97}$	91	541/2164	0.17	1:4; 15min; r.t.; MeOH	57
8	Pd@CQD@ Fe_3O_4	90/	11250/2812	0.008	1:2; 240min; r.t.; H_2O/EtOH	58
9	Pd@PANI	90	3300/5000	0.026	1:2.5; 40min; r.t.; H_2O	59
10	Pd@CNx	94/	82/628	1.15	1:3 (H_3B-NH_3); 8min; r.t.; H_2O	60
11	$Pd_{1.4}$/TB-COF	69	386/162	0.2	H_2; 180min; 40 °C; EtOH	61
12	Pd/COF-BASU2	99	58/72	1.71	H_2; 50min; 75 °C; H_2O/EtOH	62

a Substrate/$NaBH_4$ or substrate/ H_3B-NH_3 ratio; time; temperature; solvent. In entries 11 and 12, H_2 was used.

Material **6** was also tested as catalyst for the Heck reaction. As first approach, recyclability was investigated. The probe reaction was the C–C coupling between 4-iodoanisole and methyl acrylate (**Table 6**). The reaction was carried out in the presence of triethylamine (TEA) and DMF as solvent at 105 °C. A blank test with pristine SWCNTs gave no product. In the first two runs, catalyst was used in 0.125 mol % for 3 h giving complete conversion and almost quantitative isolated yield. Then, we halved the amount of catalyst (0.062 mol %) maintaining the reaction time. Conversion was complete (entry 3). In the following runs we continued decreasing the amount of catalyst down to 0.025 mol %. After 6 runs, complete conversions were observed after 3 h of reaction (entries 4–6). Decreasing the reaction time to 1 h (entries 7–10) still high conversions were observed, albeit in two runs the reaction was not complete. A final run, the 11th, was carried out under the same condition but at lower temperature, also in this case conversion was still good. This investigation clearly showed two important aspects i. e. recyclability and optimization. The material appears to be recoverable and reusable, at least for 11 cycles with a total TON of 33,000.

Table 6. Recycling test of **6** in the reaction between 4-iodoanisole and methyl acrylate.[a]
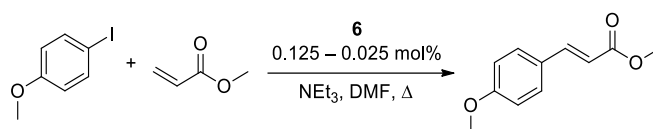
Cycle	Catalyst (mol%)	4-Ar-I (mmol)	t (h)	T (°C)	Conv. (%)[b]	TON[c]/ TOF (h⁻¹)[c]
1	0.125	0.5	3	105	>99	800/267
2	0.125	0.5	3	105	>99	800/267
3	0.062	0.5	3	105	>99	1613/538
4	0.031	1	3	105	>99	3226/1075
5	0.025	1	3	105	>99	4000/1333
6	0.025	1	3	105	>99	4000/1333
7	0.025	1	1.5	105	97	3880/2587
8	0.025	1	1.5	105	97	3880/2587
9	0.025	1	1	105	>99	4000/4000
10	0.025	1	1	105	>99	4000/4000
11	0.025	1	1	80	70	2800/2800

ᵃ Reaction conditions: 4-iodoanisole (1 equiv.), methyl acrylate (1.1 equiv.), triethylamine (1.2 equiv.), DMF (1 mL). ᵇ Determined by ¹H NMR with a yield of 98 % of the conversion. ᶜ TON and TOF values calculated based on the Pd content obtained from ICP

In addition, TEM micrographs of catalyst **6** after recycling showed no remarkable differences with respect to fresh catalyst (**Figure 6d**).

Furthermore, we have found that the reaction can be carried out under mild conditions being the catalyst used only at 0.025 mol % in a short reaction time. These reaction conditions (catalyst: 0.025 mol %; 105 °C; 1 h) were used in the reaction between methyl acrylate and a small set of iodobenzene compounds (**Table 7**). Products were obtained in excellent conversions and yields. In the case of reaction between 4-iodoanisole and styrene, a lower conversion was obtained (77%, entry 7).

Table 7. Heck reactions catalyzed by **6**.[a]

Entry	Product	Conversion (%)[b]	TON[c]	TOF (h⁻¹) [c]
1		>99	4000	4000
2		>99	4000	4000
3		>99	4000	4000
4		>99	4000	4000
5		>99	4000	4000
6		>99	4000	4000
7[d]		77	3080	1026

[a] Reaction conditions: aryl iodide (1 mmol), methyl acrylate (1.1 mmol), triethylamine (1.2 mmol), DMF (1 mL), catalyst (0.025 mol %), 105 °C, 1 h. [b] Determined by ^{1}H NMR with a yield of 98 % of the conversion. [c] TON and TOF values calculated based on the Pd content obtained from ICP. [d] Styrene (1.1 mmol), 3 h.

7.4 Conclusions

Single-walled carbon nanotubes were efficiently functionalized with a dopamine derivative, namely dopamine azide in which the amine group was converted to azide. Despite the high degree of functionalization of CNTs, Raman spectroscopy showed only a minor disruption of the π-network of the carbonaceous support. This finding was justified by taking into account the rehybridization process from sp^3 to sp^2 of the sidewall carbon atoms of CNTs after functionalization. The obtained material was thoroughly characterized, and the presence of the catechol units was exploited to immobilize palladium nanoparticles. The hybrid material was then used as active and recyclable catalyst for the reduction of nitro compounds and the Heck reaction.

7.5 Experimental Sections

Materials and methods. Chemicals and solvents were purchased from commercial suppliers (TCI chemicals, Sigma Aldrich) and used as received without further purification. SWCNTs were provided by TUBALL™. UV-vis spectra were recorded on a Jasco V-730 Spectrophotometer. Transmission electron microscopy (TEM) images were recorded using a Philips Tecnai 10 microscope operating at 80–100 kV. Thermogravimetric analyses (TGA) were performed under air flow from 100 to 1000°C with a heating rate of 10 °C min^{-1} with a Mettler Toledo TGA/DSC STAR System. All samples were maintained at 100 °C for 30 min to remove the adsorbed water. The X-ray photoelectron spectroscopy (XPS) analyses were carried out with a VG Microtech ESCA 3000 Multilab, equipped with a dual Mg/Al anode. As excitation source was used the Al Kα radiation (1486.6 eV). The sample powders were mounted on a double-sided adhesive tape. The pressure in the analysis chamber was in the range of 10^{-8} Torr during data collection. The constant charging of the samples was removed by referencing all the energies to the C 1s binding energy set at 285 eV. Raman spectra were acquired using Horiba LabRam HR Evolution equipment with a 532 nm laser line, using a spectral resolution of about 7 cm and a laser intensity that does not interfere with the signal. IR spectra (film for compound 2 and KBr pellet for blank test) were recorded on an Agilent Technologies Cary 630 FTIR spectrometer. ^{1}H NMR spectra were recorded on a Bruker 300, 400 or 600 MHz spectrometers using CDCl$_3$, CD$_3$OD or (CD$_3$)$_2$SO as solvent. Mass spectra were obtained using a GC-MS apparatus (Agilent technologies 7000 C GC/MS Triple Quad – 7890B GC System) at 70 eV ionization voltage. Inductively coupled plasma optical emission spectroscopy (ICP-OES) was carried out with an Optima 8000 Spectrometer.

Synthesis of dopamine azide 2. Dopamine azide **2** was prepared following a procedure previously reported in literature.[24] In a 50 mL two-necked round bottom flask, TfN$_3$ was freshly prepared by means of the slow addition of Tf$_2$O (1.6 mL, 9.54 mmol, 1.2 equiv.) to an ice-cooled suspension of NaN$_3$ (1.879 g, 28.62 mmol, 3.0 equiv.) in CH$_3$CN (10mL). The mixture was stirred at 0 °C for 2h under an argon atmosphere. In another 100 mL two-necked round bottom flask, a solution of dopamine hydrochloride salt **1** (1.538 g, 7.95 mmol, 1.0 equiv.) and ZnCl$_2$ (112 mg, 0.80 mmol, 0.1 equiv.) in 37.5 mL H$_2$O:CH$_3$CN (3 : 7) were taken. Then Et$_3$N (4.1 mL, 28.62 mmol, 3.0 equiv.) and freshly prepared TfN$_3$ were added. The reaction was stirred at rt overnight under an argon atmosphere. The reaction mixture was filtered and washed with CH$_3$CN. The filtrate was concentrated under vacuum and then extracted with EtOAc (3 x 20 mL). The organic layers were collected, dried over Na$_2$SO$_4$ and concentrated. The crude product

was purified by flash column chromatography (hexane/ethyl acetate 2 : 1 v/v) to give desired azide **2** in quantitative yield (1.424 g). ^{1}H NMR (400 MHz, CDCl$_3$, δ) :6.81 (d, *J*=8.1 Hz, 1H), 6.74 (d, *J*=2.0 Hz, 1H), 6.66 (dd, *J*=8.1, 2.0 Hz, 1H), 5.28 (sbr, 2H), 3.45 (t, *J*=7.2 Hz, 2H), 2.78 (t, *J*=7.2 Hz, 2H) ppm; ^{13}C NMR (150 MHz, CDCl$_3$, δ): 143.6, 142.2, 131.1 (quat.), 121.3, 115.9, 115.6 (aromatic *C*H), 52.6 (*C*H$_2$N$_3$), 34.6 (Ar*C*H$_2$) ppm.

Preparation of material 5. In a two-necked round bottom flask, 125 mg of SWCNTs were dispersed in 120 mL of oDCB by means sonication (4 x 20 min) followed by vigorous stirring (3 x 20 min). The dispersion was then stirred under argon atmosphere at 40 °C overnight. After that a solution of dopamine azide **2** (344 mg, 1.92 mmol) in 5 mL of oDCB was added and argon was bubbled in the reaction mixture for 30 min before increasing the temperature up to 160 °C and allowing it to react at this temperature and under argon atmosphere for 72 h. Afterwards, the reaction mixture was filtered under reduced pressure through a PTFE membrane filter (pore size 0.45 μm) and washed with dimethylformamide. The black residue was then collected from the filter, suspended in dimethylformamide, sonicated and filtered again. The washings with DMF were repeated several times until a light-yellow filtrate was obtained. The washings were continued with diethyl ether and the residue was finally dried at 60 °C under reduced pressure to give 320 mg of a black solid.

Preparation of material 6 from 5 by Pd loading. The SWCNT/Pd catalyst was prepared as previously described with slight modifications.[63-64] Briefly, **5** (200 mg) was dispersed in a solution of Pd(OAc)$_2$ (22 mg, 98 μ mol) in distilled water (7 mL) and stirred vigorously for 1 h at 45 °C. The material was then collected by centrifugation at 7000 rpm at 4 °C, washed times with acetone (3×10 mL) and distilled water (3×10 mL) and lyophilized to give a black powder (yield 95 % w/w).

The material was then suspended in 20 mL of absolute ethanol and put under vigorous stirring before a solution of NaBH$_4$ (30 mg, 0.75 mmol) in 3 mL of absolute ethanol was added dropwise. The resulting mixture was stirred at room temperature for 15 h and then filtered under reduced pressure through a PTFE membrane filter (pore size 0.45 μm). The material was washed with water, methanol and Et$_2$O, and finally dried at 40 °C under reduced pressure (180 mg of a black solid). 1.27 wt% Pd was measured by ICP-OES analysis.

Synthesis of acetylated dopamine azide 2Ac. The compound **2Ac** was synthesized by adapting a procedure reported elsewhere.[65] In a two-necked round bottom flask, and under

argon atmosphere, a solution of **2** (1.002 g, 5.59 mmol) in acetic anhydride (5.4 mL) and dry pyridine (270 μ L) was transferred. The reaction mixture was kept in an ultrasound bath at 200 W for 40 min, then evaporated under reduced pressure and the crude was purified by flash column chromatography (hexane/ethyl acetate 3 : 1 v/v) to afford **2Ac** as a yellow oil (855 mg, 58%). Spectroscopic data are in accordance with those reported in literature.[66] ^{1}H NMR (300 MHz, CDCl$_3$, δ): 7.15-7.05 (m, 3H), 3.53 (t, J=7.3 Hz, 2H), 2.9 (t, J=7.3 Hz, 2H), 2.29 (s, 3H), 2.28 (s, 3H) ppm; ^{13}C NMR (150 MHz, CDCl$_3$, δ): 168.3, 168.2 (*C*=O), 142.0, 140.8, 136.9 (quat.), 126.9, 123.7, 123.5 (aromatic *C*H), 52.0 (*C*H$_2$N$_3$), 34.6 (Ar*C*H$_2$), 20.6 (*C*H$_3$CO) ppm. GC-MS (EI, 70 ev) m/z (%)=263 ([M]+, 1), 179(22), 151(51), 123(100), 136(11), 43(88).

Preparation of material 5Ac. In a two-necked round bottom flask, 100 mg of SWCNTs were dispersed in 95 mL of oDCB by means sonication (4×20 min) followed by vigorous stirring (3 x 20 min). The dispersion was then stirred under argon atmosphere at 40 °C overnight. After that a solution of **2Ac** in 5 mL of oDCB was added and argon was bubbled in the reaction mixture for 30 min before increasing the temperature up to 160 °C and allowing it to react at this temperature and under argon atmosphere for 72 h. Afterwards, the reaction mixture was filtered under reduced pressure through a PTFE membrane filter (pore size 0.45 μm) and washed with dimethylformamide. The black residue was then collected from the filter, suspended in dimethylformamide, sonicated and filtered again. The washings with DMF were repeated several times until a light-yellow filtrate was obtained. The washings were continued with diethyl ether and the residue was finally dried at 60 °C under reduced pressure to give 153 mg of a black solid.

Blank test. In a 100 mL two-necked round bottom flask, dopamine azide **2** (225 mg; 1.26 mmol) and 50 mL of oDCB were charged. The flask was connected to a reflux condenser under the protection of an argon atmosphere. Argon was bubbled in the solution for 20 min before raising the temperature up to 160 °C. The reaction was maintained under stirring at this temperature for 72 h. The solvent was removed under vacuum and the residue was taken with diethyl ether and transferred in a centrifuge tube. After centrifugation at 4000 rpm, the supernatant was recovered and the residue was subjected to a further treatment with diethyl ether and subsequent centrifugation. The brown/black residue was collected and dried under vacuum (29 mg; partially soluble in DMSO), whereas the combined organic washings gave rise to unreacted dopamine azide **2** after solvent removal under vacuum.

Total phenolic content assay. The Folin and Ciocalteu assay was performed by adapting a procedure currently used to quantify the total phenolic content.[67] Briefly, **5** and **5Ac** were added at a final dose of 1–10 mg/mL to a solution consisting of Folin-Ciocalteu reagent, 75 g/L Na_2CO_3, and distilled water in a 1 : 3 : 16 v/v/v ratio. After 2 h incubation at room temperature, the absorbance at 760 nm was measured. Results were expressed as gallic acid equivalents (GAE). Experiments were run in triplicate.

DPPH assay. DPPH assay was performed as previously described with slight modifications.[68-70] To a 100 µM ethanolic solution of DPPH (2 mL) **5** and **5Ac** were added (final dose 0.5–2 mg/mL) and after 10 min under stirring at room temperature the absorbance of the solution at 515 nm was measured. Data are expressed as EC50, which is the concentration of the sample at which a 50 % DPPH reduction is observed. Experiments were run in triplicate.

General procedure for the reduction of nitroarenes. In a glass vial 1 mmol of nitroarene, 1.68 mg of **6** (0.02 mol %), and 5 mL of water were added. Before the addition of 8 mmol of sodium borohydride, the suspension was sonicated for a short time. The mixture was then stirred at 30 ° C for the specified time. After that it was filtered to remove the catalyst and extracted with ethyl acetate. The organic layer was dried with magnesium sulphate, filtered, and evaporated under vacuum. The conversion into the corresponding aniline derivative was estimated by ^{1}H NMR spectroscopy in $CDCl_3$, CD_3OD or $(CD_3)_2SO$.

General recycling procedure for reduction of nitroarenes. Catalyst reusability was verified in the reduction of *p*-nitroaniline to *p*-phenylenediamine in one hour at 30 °C. After each catalytic test, the catalyst was recovered by filtration under vacuum using a membrane (0.2 µm PTFE Membrane) and washed several times with water, ethyl acetate, ethanol and diethyl ether. Once recovered, the solid was reused for the next catalytic cycle. The conversions into the products were estimated by ^{1}H NMR analysis.

General procedure for the Heck reactions. The catalytic tests were performed in a 3 mL glass vial with screw cap, in which 2 mg of **6** (0.025 mol %), 1 mmol of aryl iodide, 1.1 mmol of alkene, 1.2 mmol of triethylamine and 1 mL of DMF were added. The reaction mixture was heated at 105°C under stirring for the required time. Then, it was allowed to cool down to room temperature and extracted with diethyl ether. The combined organic layers were dried over

MgSO$_4$, filtered and evaporated under reduced pressure. The conversions of the products were estimated by ^{1}H NMR analysis.

General recycling procedure for the Heck reaction. Recycling tests were carried out in a 3 mL glass vial with screw cap, using 4-iodoanisole as aryl iodide and methyl acrylate as alkene source. After each catalytic cycle the reaction mixture was centrifuged in order to remove the supernatant and recover the catalyst. The solid was washed by sonication and centrifugation with methanol (3×3 mL) and diethyl ether. The recovered catalyst was dried at 50 °C under vacuum before being used in the next cycle. All the combined supernatants were extracted with diethyl ether and then dried over MgSO$_4$. Once evaporated under reduced pressure the products of the recycling tests were analysed by ^{1}H NMR analysis.

7.6 References

1.   Banerjee, S.; Hemraj-Benny, T.; Wong, S. S., Covalent Surface Chemistry of Single-Walled Carbon Nanotubes. *Adv. Mater.* **2005**, *17*, 17-29.

2.   Bahr, J. L.; Tour, J. M., Covalent chemistry of single-wall carbon nanotubes. *J. Mater. Chem.* **2002**, *12*, 1952-1958.

3.   Campisciano, V.; Gruttadauria, M.; Giacalone, F., Modified Nanocarbons for Catalysis. *ChemCatChem* **2019**, *11*, 90-133.

4.   Zhang, J.; Zou, H.; Qing, Q.; Yang, Y.; Li, Q.; Liu, Z.; Guo, X.; Du, Z., Effect of Chemical Oxidation on the Structure of Single-Walled Carbon Nanotubes. *J. Phy. Chem. B* **2003**, *107*, 3712-3718.

5.   Singh, P.; Campidelli, S.; Giordani, S.; Bonifazi, D.; Bianco, A.; Prato, M., Organic functionalisation and characterisation of single-walled carbon nanotubes. *Chem. Soc. Rev.* **2009**, *38*, 2214-2230.

6.   Ziegler, K. J.; Gu, Z.; Peng, H.; Flor, E. L.; Hauge, R. H.; Smalley, R. E., Controlled Oxidative Cutting of Single-Walled Carbon Nanotubes. *J. Am. Chem. Soc.* **2005**, *127*, 1541-1547.

7.   Tasis, D.; Tagmatarchis, N.; Bianco, A.; Prato, M., Chemistry of Carbon Nanotubes. *Chem. Rev.* **2006**, *106*, 1105-1136.

8.   Syrgiannis, Z.; La Parola, V.; Hadad, C.; Lucío, M.; Vázquez, E.; Giacalone, F.; Prato, M., An Atom-Economical Approach to Functionalized Single-Walled Carbon Nanotubes: Reaction with Disulfides. *Angew. Chem. Int. Ed.* **2013**, *52*, 6480-6483.

9.   Syrgiannis, Z.; Bonasera, A.; Tenori, E.; La Parola, V.; Hadad, C.; Gruttadauria, M.; Giacalone, F.; Prato, M., Chemical modification of carbon nanomaterials (SWCNTs, DWCNTs, MWCNTs and SWCNHs) with diphenyl dichalcogenides. *Nanoscale* **2015**, *7*, 6007-6013.

10.   Vázquez, E.; Giacalone, F.; Prato, M., Non-conventional methods and media for the activation and manipulation of carbon nanoforms. *Chem. Soc. Rev.* **2014**, *43*, 58-69.

11.   Campisciano, V.; Calabrese, C.; Liotta, L. F.; La Parola, V.; Spinella, A.; Aprile, C.; Gruttadauria, M.; Giacalone, F., Templating effect of carbon nanoforms on highly cross-linked imidazolium network: Catalytic activity of the resulting hybrids with Pd nanoparticles. *Appl. Organomet. Chem.* **2019**, *33*, e4848.

12.   Mercadante, A.; Campisciano, V.; Morena, A.; Valentino, L.; La Parola, V.; Aprile, C.; Gruttadauria, M.; Giacalone, F., Catechol-Functionalized Carbon Nanotubes as Support for Pd Nanoparticles: a Recyclable System for the Heck Reaction. *Eur. J. Org. Chem.* **2022**, e202200497.

13.   Ziccarelli, I.; Mancuso, R.; Giacalone, F.; Calabrese, C.; La Parola, V.; De Salvo, A.; Della Ca, N.; Gruttadauria, M.; Gabriele, B., Heterogenizing palladium tetraiodide catalyst for carbonylation reactions. *J. Catal.* **2022**, *413*, 1098-1110.

14.   Campisciano, V.; Valentino, L.; Morena, A.; Santiago-Portillo, A.; Saladino, N.; Gruttadauria, M.; Aprile, C.; Giacalone, F., Carbon nanotube supported aluminum porphyrin-imidazolium bromide crosslinked copolymer: A synergistic bifunctional catalyst for CO_2 conversion. *J. CO2 Util.* **2022**, *57*, 101884.

15.   Morena, A.; Campisciano, V.; Comès, A.; Liotta, L. F.; Gruttadauria, M.; Aprile, C.; Giacalone, F., A Study on the Stability of Carbon Nanoforms–Polyimidazolium Network Hybrids in the Conversion of CO_2 into Cyclic Carbonates: Increase in Catalytic Activity after Reuse. *Nanomaterials* **2021**, *11*, 2243.

16.   Campisciano, V.; Burger, R.; Calabrese, C.; Liotta, L. F.; Lo Meo, P.; Gruttadauria, M.; Giacalone, F., Straightforward preparation of highly loaded MWCNT–polyamine hybrids and their application in catalysis. *Nanoscale Adv.* **2020**, *2*, 4199-4211.

17.   Giacalone, F.; Campisciano, V.; Calabrese, C.; La Parola, V.; Syrgiannis, Z.; Prato, M.; Gruttadauria, M., Single-Walled Carbon Nanotube–Polyamidoamine Dendrimer Hybrids for Heterogeneous Catalysis. *ACS Nano* **2016**, *10*, 4627-4636.

18.   Buaki-Sogó, M.; Vivian, A.; Bivona, L. A.; García, H.; Gruttadauria, M.; Aprile, C., Imidazolium functionalized carbon nanotubes for the synthesis of cyclic carbonates: reducing the gap between homogeneous and heterogeneous catalysis. *Catal. Sci. Technol.* **2016**, *6*, 8418-8427.

19.   Lee, Y.-S.; Marzari, N., Cycloaddition Functionalizations to Preserve or Control the Conductance of Carbon Nanotubes. *Phy. Rev. Lett.* **2006**, *97*, 116801.

20.   Chen, Z.; Nagase, S.; Hirsch, A.; Haddon, R. C.; Thiel, W.; Schleyer, P. v. R., Side-Wall Opening of Single-Walled Carbon Nanotubes (SWCNTs) by Chemical Modification: A Critical Theoretical Study. *Angew. Chem. Int. Ed.* **2004**, *43*, 1552-1554.

21.   Li, J.; Jia, G.; Zhang, Y.; Chen, Y., Bond-Curvature Effect of Sidewall [2+1] Cycloadditions of Single-Walled Carbon Nanotubes: A New Criterion To the Adduct Structures. *Chem. Mater.* **2006**, *18*, 3579-3584.

22.   Setaro, A.; Adeli, M.; Glaeske, M.; Przyrembel, D.; Bisswanger, T.; Gordeev, G.; Maschietto, F.; Faghani, A.; Paulus, B.; Weinelt, M.; Arenal, R.; Haag, R.; Reich, S., Preserving π-conjugation in covalently functionalized carbon nanotubes for optoelectronic applications. *Nature Commun.* **2017**, *8*, 14281.

23.   Nickl, P.; Radnik, J.; Azab, W.; Donskyi, I. S., Surface characterization of covalently functionalized carbon-based nanomaterials using comprehensive XP and NEXAFS spectroscopies. *Appl. Surf. Sci.* **2023**, *613*, 155953.

24.   Pagoti, S.; Dutta, D.; Dash, J., A Magnetoclick Imidazolidinone Nanocatalyst for Asymmetric 1,3-Dipolar Cycloadditions. *Adv. Synth. Catal.* **2013**, *355*, 3532-3538.

25.   Alfieri, M. L.; Micillo, R.; Panzella, L.; Crescenzi, O.; Oscurato, S. L.; Maddalena, P.; Napolitano, A.; Ball, V.; d'Ischia, M., Structural Basis of Polydopamine Film Formation: Probing 5,6-Dihydroxyindole-Based Eumelanin Type Units and the Porphyrin Issue. *ACS Appl. Mater. Interfaces* **2018**, *10*, 7670-7680.

26.   Alfieri, M. L.; Panzella, L.; Oscurato, S. L.; Salvatore, M.; Avolio, R.; Errico, M. E.; Maddalena, P.; Napolitano, A.; Ball, V.; d'Ischia, M., Hexamethylenediamine-Mediated Polydopamine Film Deposition: Inhibition by Resorcinol as a Strategy for Mapping Quinone Targeting Mechanisms. *Front. Chem.* **2019**, *7*.

27.   Alfieri, M. L.; Panzella, L.; Oscurato, S. L.; Salvatore, M.; Avolio, R.; Errico, M. E.; Maddalena, P.; Napolitano, A.; D'Ischia, M., The Chemistry of Polydopamine Film Formation: The Amine-Quinone Interplay. *Biomimetics* **2018**, *3*, 26.

28.   Szukowska, M.; Popenda, Ł.; Coy, E.; Filip, C.; Grajewski, J.; Kempiński, M.; Kim, Y.; Mrówczyński, R., Replacing amine by azide: dopamine azide polymerization triggered by sodium periodate. *Polym. Chem.* **2022**, *13*, 3325-3334.

29.   Zhu, J.; Shen, J.; Guo, S.; Park, C. B., Poly (vinylidene fluoride)-based microcellular dielectrics filled with polydopamine coated carbon nanotubes for achieving high permittivity and ultralow dielectric loss. *Compos. A: Appl. Sci. Manuf.* **2022**, *163*, 107222.

30.   Li, Q.; Lin, G.; Zhang, S.; Wang, H.; Borah, J.; Jing, Y.; Liu, F., Conducting and stretchable emulsion styrene butadiene rubber composites using SiO2@Ag core-shell particles and polydopamine coated carbon nanotubes. *Polym. Test.* **2022**, *115*, 107722.

31.   Weng, Z.; Zou, F.; Li, D.; Yao, Y., A high-sensitivity thin-film MWNT@PDA-AgNP nanocomposite sensor for acquiring microscopic deformations. *Compos. Sci. Technol.* **2022**, *229*, 109689.

32.   Feng, J.; Rohaizat, R. E. B.; Qian, S., Polydopamine@carbon nanotube reinforced and calcium sulphoaluminate coated hydrogels encapsulating bacterial spores for self-healing cementitious composites. *Cem. Conc. Comp.* **2022**, *133*, 104712.

33.   Demirci, S.; Sahiner, M.; Suner, S. S.; Sahiner, N., Improved Biomedical Properties of Polydopamine-Coated Carbon Nanotubes. *Micromachines* **2021**, *12*, 1280.

34.   Esmaeilzadeh, Z.; Karimi, M.; Mousavi Shoushtari, A.; Javanbakht, M., The effect of polydopamine coated multi-walled carbon nanotube on the wettability of sulfonated poly(ether ether ketone) nanocomposite as a proton exchange membrane. *J. Appl. Pol. Sci.* **2022**, *139*, 52142.

35.   Schroeder, V.; Savagatrup, S.; He, M.; Lin, S.; Swager, T. M., Carbon Nanotube Chemical Sensors. *Chem. Rev.* **2019**, *119*, 599-663.

36.   Holzinger, M.; Abraham, J.; Whelan, P.; Graupner, R.; Ley, L.; Hennrich, F.; Kappes, M.; Hirsch, A., Functionalization of Single-Walled Carbon Nanotubes with (R-)Oxycarbonyl Nitrenes. *J. Am. Chem. Soc.* **2003**, *125*, 8566-8580.

37.   Holzinger, M.; Vostrowsky, O.; Hirsch, A.; Hennrich, F.; Kappes, M.; Weiss, R.; Jellen, F., Sidewall Functionalization of Carbon Nanotubes. *Angew. Chem. Int. Ed.* **2001**, *40*, 4002-4005.

38.   Leinonen, H.; Rintala, J.; Siitonen, A.; Lajunen, M.; Pettersson, M., New nitrene functionalizations onto sidewalls of carbon nanotubes and their spectroscopic analysis. *Carbon* **2010**, *48*, 2425-2434.

39.   Yinghuai, Z.; Peng, A. T.; Carpenter, K.; Maguire, J. A.; Hosmane, N. S.; Takagaki, M., Substituted Carborane-Appended Water-Soluble Single-Wall Carbon Nanotubes: New Approach to Boron Neutron Capture Therapy Drug Delivery. *J. Am. Chem. Soc.* **2005**, *127*, 9875-9880.

40.   L'abbé, G., Decomposition and addition reactions of organic azides. *Chem. Rev.* **1969**, *69*, 345-363.

41.   Averdung, J.; Mattay, J., Exohedral functionalization of [60]fullerene by [3+2] cycloadditions: Syntheses and chemical properties of triazolino-[60]fullerenes and 1,2-(3,4-dihydro-2H-pyrrolo)-[60]fullerenes. *Tetrahedron* **1996**, *52*, 5407-5420.

42.   Evano, G., Organic Azides. Syntheses and Applications. Edited by Stefan Bräse and Klaus Banert. *Angew. Chem. Int. Ed.* **2010**, *49*, 6025-6025.

43.   Henery-Logan, K. R.; Clark, R. A., The reaction of phenyl azide with olefins. *Tetrahedron Lett.* **1968**, *9*, 801-806.

44.   Hirsch, A.; Brettreich, M., Cycloadditions. In *Fullerenes*, Hirsch, A.; Brettreich, M., Eds. Wiley-VCH: Weinheim, Germany, **2004**; pp 101-183.

45.   Schick, G.; Grösser, T.; Hirsch, A., The transannular bond in [5,6]-NCO2R-bridged monoadducts of [60]fullerene is open. *J. Chem. Soc., Chem. Commun.,* **1995**, 2289-2290.

46.   Manna, K.; Srivastava, S. K., Contrasting Role of Defect-Induced Carbon Nanotubes in Electromagnetic Interference Shielding. *J. Phy. Chem. C* **2018**, *122*, 19913-19920.

47.   Munaiah, Y.; Suresh, S.; Dheenadayalan, S.; Pillai, V. K.; Ragupathy, P., Comparative Electrocatalytic Performance of Single-Walled and Multiwalled Carbon Nanotubes for Zinc Bromine Redox Flow Batteries. *J. Phy. Chem. C* **2014**, *118*, 14795-14804.

48.   Sannasi, V.; Jeyakumar, D., Synthesis of Aziridinofullerene-Porphyrin Mediated by Triethyl Phosphite: Physicochemical and Electrochemical Properties. *ChemistrySelect* **2017**, *2*, 9130-9135.

49.   Wang, P.-C.; Liao, Y.-C.; Lai, Y.-L.; Lin, Y.-C.; Su, C.-Y.; Tsai, C.-H.; Hsu, Y.-J., Thermally induced variation in redox chemical bonding structures of single-walled carbon nanotubes exposed to hydrazine vapor. *Carbon* **2012**, *50*, 1650-1658.

50.   Paoletti, C.; He, M.; Salvo, P.; Melai, B.; Calisi, N.; Mannini, M.; Cortigiani, B.; Bellagambi, F. G.; Swager, T. M.; Di Francesco, F.; Pucci, A., Room temperature amine sensors enabled by sidewall functionalization of single-walled carbon nanotubes. *RSC Adv.* **2018**, *8*, 5578-5585.

51.   Mendoza, J. J.; Ledezma, R.; Gallardo, C. A.; Elias, A.; Elizalde, L. E., Covalent surface functionalization of carbon nanostructures via [2 + 1] cycloaddition microwave-assisted reactions. *J. Mater. Sci.* **2021**, *56*, 13524-13539.

52.   Qian, H.; He, Q.; Zheng, J.; Li, S.; Zhang, S., Catechol-functionalized microporous organic polymer as supported media for Pd nanoparticles and its high catalytic activity. *Polymer* **2014**, *55*, 550-555.

53.   Chowhan, B.; Gupta, M.; Sharma, N., Designing of Ultrafine PdNPs Immobilized Pyridinic-N Doped Carbon and Evaluation of its Catalytic Potential for Konevenagel Condensation, Synthesis of 4H-pyran Derivatives and Nitroreduction. *ChemistrySelect* **2019**, *4*, 12689-12700.

54.   Niakan, M.; Masteri-Farahani, M., Ultrafine and well-dispersed Pd-Ni bimetallic catalyst stabilized by dendrimer-grafted magnetic graphene oxide for selective reduction of toxic nitroarenes under mild conditions. *J. Hazard. Mater.* **2022**, *424*, 127717.

55.   Halligudra, G.; Paramesh, C. C.; Mudike, R.; Ningegowda, M.; Rangappa, D.; Shivaramu, P. D., PdII on Guanidine-Functionalized Fe3O4 Nanoparticles as an Efficient Heterogeneous Catalyst for Suzuki–Miyaura Cross-Coupling and Reduction of Nitroarenes in Aqueous Media. *ACS Omega* **2021**, *6*, 34416-34428.

56.   Jia, W.-G.; Gao, L.-L.; Wang, Z.-B.; Sun, L.-Y.; Han, Y.-F., Synthesis, Characterization, and Catalytic Activities of Palladium Complexes with Phenylene-Bridged Bis(thione) Ligands. *Organometallics* **2019**, *38*, 1946-1954.

57.   Prasanna; Usha, K. M., Highly recyclable palladium ion substituted TiO2 as the versatile ligand-free catalyst for the selective oxidation of alcohols and the reduction of nitroarenes. *J. Chem. Sci.* **2022**, *134*, 96.

58.   Gholinejad, M.; Zareh, F.; Nájera, C., Nitro group reduction and Suzuki reaction catalysed by palladium supported on magnetic nanoparticles modified with carbon quantum dots generated from glycerol and urea. *Appl. Organomet. Chem.* **2018**, *32*, e3984.

59.   Wang, G.; Yuan, S.; Wu, Z.; Liu, W.; Zhan, H.; Liang, Y.; Chen, X.; Ma, B.; Bi, S., Ultra-low-loading palladium nanoparticles stabilized on nanocrystalline Polyaniline (Pd@PANI): A efficient, green, and recyclable catalyst for the reduction of nitroarenes. *Appl. Organomet. Chem.* **2019**, *33*, e5159.

60.   Bhowmik, T.; Sadhukhan, M.; Kempasiddaiah, M.; Barman, S., Highly dispersed palladium nanoparticles supported on graphitic carbon nitride for selective hydrogenation of nitro compounds and Ullmann coupling reaction. *Appl. Organomet. Chem.* **2022**, *36*, e6613.

61.   Li, C.; Ren, X.; Guo, M.; Li, W.; Li, H.; Yang, Q., Highly active ultrafine Pd NPs confined in imine-linked COFs for nitrobenzene hydrogenation. *Catal. Sci. Technol.* **2021**, *11*, 3873-3879.

62.   Kouhdareh, J.; Keypour, H.; Alavinia, S.; Maryamabadi, A., Immobilization of Ag and Pd over a novel amide based covalent organic framework (COF-BASU2) as a heterogeneous reusable catalyst to reduce nitroarenes. *Inorg. Chim. Acta* **2023**, *545*, 121251.

63.   Kunfi, A.; May, Z.; Németh, P.; London, G., Polydopamine supported palladium nanoparticles: Highly efficient catalysts in Suzuki cross-coupling and tandem Suzuki cross-coupling/nitroarene reductions under green reaction conditions. *J. Catal.* **2018**, *361*, 84-93.

64.   Kunfi, A.; Szabó, V.; Mastalir, Á.; Bucsi, I.; Mohai, M.; Németh, P.; Bertóti, I.; London, G., Palladium on Polydopamine: Its True Potential in Catalytic Transfer Hydrogenations and Heck Coupling Reactions. *ChemCatChem* **2017**, *9*, 3236-3244.

65.   Capelli, L.; Manini, P.; Pezzella, A.; Napolitano, A.; d'Ischia, M., Efficient Synthesis of 5,6-Dihydroxyindole Dimers, Key Eumelanin Building Blocks, by a Unified o-Ethynylaniline-Based Strategy for the Construction of 2-Linked Biindolyl Scaffolds. *J. Org. Chem.* **2009**, *74*, 7191-7194.

66.   Tassano, E.; Alama, A.; Basso, A.; Dondo, G.; Galatini, A.; Riva, R.; Banfi, L., Conjugation of Hydroxytyrosol with Other Natural Phenolic Fragments: From Waste to Antioxidants and Antitumour Compounds. *Eur. J. Org. Chem.* **2015**, *2015*, 6710-6726.

67.   Moreno-Rojas, J. M.; Velasco-Ruiz, I.; Lovera, M.; Ordoñez-Díaz, J. L.; Ortiz-Somovilla, V.; De Santiago, E.; Arquero, O.; Pereira-Caro, G., Evaluation of Phenolic Profile and Antioxidant Activity of Eleven Pistachio Cultivars (Pistacia vera L.) Cultivated in Andalusia. *Antioxidants* **2022**, *11*, 609.

68.   Alfieri, M. L.; Pilotta, G.; Panzella, L.; Cipolla, L.; Napolitano, A., Gelatin-Based Hydrogels for the Controlled Release of 5,6-Dihydroxyindole-2-Carboxylic Acid, a Melanin-Related Metabolite with Potent Antioxidant Activity. *Antioxidants* **2020**, *9*, 245.

69.   Alfieri, M. L.; Panzella, L.; Arntz, Y.; Napolitano, A.; Ball, V.; d'Ischia, M., A Clean and Tunable Mussel-Inspired Coating Technology by Enzymatic Deposition of Pseudo-Polydopamine (ψ-PDA) Thin Films from Tyramine. *Int. J. Mol. Sci.* **2020**, *21*, 4873.

70.   El Yakhlifi, S.; Alfieri, M.-L.; Arntz, Y.; Eredia, M.; Ciesielski, A.; Samorì, P.; d'Ischia, M.; Ball, V., Oxidant-dependent antioxidant activity of polydopamine films: The chemistry-morphology interplay. *Colloids Surf. A: Physicochem. Eng. Asp.* **2021**, *614*, 126134.

CHAPTER VIII

General Conclusions

CHAPTER VIII

General Conclusions

This PhD dissertation has been focused on the design and development of novel hybrid materials as heterogeneous catalysts for CO_2 conversion with epoxides into cyclic carbonates, for C–C cross-coupling reactions such as the Heck-Mizoroki reaction and in the reduction of nitro compounds. The catalytic performance of all the hybrids were extensively evaluated in terms of recyclability, productivity, turnover number (TON) and turnover frequency (TOF) values. Several techniques were used to characterize the solids, including thermogravimetric analysis, multinuclear solid-state NMR, transmission electron microscopy, scanning electron microscopy, N_2 physisorption, chemical combustion analysis, X-ray photoelectron spectroscopy, among others. In particular, CO_2 conversion was performed under solvent-free reaction conditions. The first part of the thesis involved the development of bifunctional materials designed to contain both nucleophilic and Lewis acid sites simultaneously. These hybrid materials were prepared employing a simple one-step procedure based on the radical polymerization of bis-vinyl imidazolium salt and aluminium porphyrin (Chapter III) or magnesium porphyrin (Chapter IV) in the presence or absence of the MWCNTs used as support material. Both materials were shown to be highly active in CO_2 conversion and, surprisingly, to possess better catalytic activity than reference homogeneous catalytic systems. Interestingly, the materials under consideration exhibit variations in the choice of metal. Despite this subtle distinction, the two materials demonstrate distinct characteristics from both a synthetic and catalytic perspective. Notably, it has been demonstrated that for the material incorporating magnesium porphyrin, an adjustment of the Mg/Br^- ratio from 1:8 to 1:12 was necessary to achieve both an optimal coverage of the nanotube walls and the best catalytic performances. In contrast, the material with aluminium porphyrin exhibited flawless nanotube coverage at a 1:8 ratio. This disparity extends to the catalytic realm, with the **MWCNTs-TSP-AlCl-imi** material proving superior to its unsupported counterpart, **TSP-AlCl-imi**. The distinction between the supported **MWCNTs-TSP-Mg-imi 1:12** material and the unsupported **TSP-Mg-imi** material is not prominently discernible in the case of the magnesium porphyrin-containing material. Interestingly, **TSP-Mg-imi** proves to be more economically and environmentally appealing. This bifunctional catalyst was deliberately designed and prepared with only two components, resulting in no waste during the process. The significant catalytic activity observed in bifunctional materials provided the impetus for

the development of a third bifunctional material, as discussed in Chapter V. In this exploration, the choice was made to maintain aluminium porphyrin as the co-catalyst while introducing a change in the nucleophile counterion from imidazolium to a phosphonium salt. Despite the differences in the materials, it is crucial to conduct a comprehensive comparison between **MWCNTs-TSP-AlCl-imi**, **TSP-Mg-imi**, and **TSP-AlCl-PhospBr**. All three materials demonstrated the capability to convert epichlorohydrin at 80°C within 3 hours, with TON values of 16800, 10500, and 12900, respectively. The remarkably high TON values can be ascribed to the close proximity of the two catalytic active sites, which effectively cooperate. Notably, the **MWCNTs-TSP-AlCl-imi** material outperforms the other two unsupported materials, and this superiority can be attributed to its larger surface area, facilitating fully accessible catalytic sites. With the continuation of research into CO_2 conversion, a new green methodology was developed to obtain imidazolium-based organic salts as heterogeneous catalytic systems (Chapter VI). Carbon nanostructures were functionalized via a straightforward one-step procedure based on the radical polymerization of DEM systems, composing of a mono- or bis-vinyl imidazolium salts, in the presence of the pristine support leading to a broad series of hybrid materials. The catalytic activity of poly-imidazolium modified carbon nanotubes was preliminary explored in the synthesis of cyclic carbonates from carbon dioxide and epoxides by studying the influence of a linear or cross-linked poly-imidazolium. In terms of TON values, the results showed that linear materials have a higher catalytic activity compared to the cross-linked materials. This outcome was ascribed to the better availability of catalytic active sites. Then, single-walled carbon nanotubes was modified with a dopamine derivative through the [3+2] cycloaddition reaction (Chapter VII). The obtained solids were prepared to be employed as stabilizing supports for palladium nanoparticles. The corresponding hybrid was successfully tested as heterogeneous catalysts in Mizoroki-Heck couplings and the reduction of nitro compounds.

In this PhD thesis, all materials were observed to be easily recoverable and recyclable. They exhibited high activity in facilitating the formation of desired products, along with notable thermal stability and outstanding performance in turnover number, productivity, and selectivity. The synthetic pathways chosen for developing our hybrids offer opportunities for a wide range of new materials in future catalytic applications. It's worth highlighting that the conditions used for CO_2 conversion are notably significant, closely aligning with those commonly employed on an industrial scale. Consequently, only minor adjustments would be needed to upscale the cyclic carbonate synthesis reported to a larger production scale.